

# Lithium-Ion Batteries: Modelling and State of Charge Estimation

Lithium-Ion Batteries:  
Modelling and State of Charge Estimation

By  
Mohammed Sayed Mohammed Farag, B.Sc.

A THESIS  
Submitted to the School of Graduate Studies  
in Partial Fulfillment of the Requirements  
for the Degree  
Master of Applied Science  
McMaster University  
© Copyright by Mohammed Farag, June 2013, all rights reserved.

# **PERMISSION TO USE**

In presenting this thesis in partial fulfillment of the requirements for a Postgraduate degree from McMaster University, I agree that the Libraries of this University may make it freely available for inspection. I further agree that the permission for copying this thesis in any manner, in whole or in part for scholarly purposes, may be granted by the professors who supervised my thesis work or, in their absence, by the Head of the Department or the Faculty Dean in which my thesis work was conducted. It is understood that any copying or publication or use of this thesis or parts thereof for financial gain shall not be allowed without my written permission. It is also understood that due recognition shall be given to me and McMaster University in any scholarly use which may be made of any material in my thesis. Requests for permission to copy or to make other use of material in this thesis, in whole or part, should be addressed to:

Head of the Department of Mechanical Engineering  
McMaster University  
Faculty of Engineering  
1280 Main Street West  
Hamilton, Ontario L8S 4L6  
Canada

## MASTER OF APPLIED SCIENCE (2013)

### (Department of Mechanical Engineering)

McMaster University  
Hamilton, Ontario, Canada

BACHELOR OF SCIENCE (2008)  
(Department of Mechanical Engineering)

Ain Shams University  
Cairo, Egypt

# Lithium-Ion Batteries: Modelling and State of Charge Estimation

AUTHOR: Mohammed Farag, M.A.Sc (McMaster University)

SUPERVISOR: Dr. Saeid Habibi, Professor  
Department of Mechanical Engineering

NUMBER OF PAGES: 169,xx

“To my parents, Awatef and Sayed Farag, who provided me with their endless love, encouragement, support and absolute confidence in me throughout my life. You will always be the source of inspiration to all what I do in my life “

---

## ABSTRACT

---

Lithium-ion (Li-ion) cells are increasingly used in many applications affecting our daily life, such as laptops computers, cell phones, digital cameras, and other portable electronic devices. Lithium-ion batteries are increasingly being considered for their use in Electric Vehicles (EV), Hybrid Electric Vehicles (HEV) and Plug-in Hybrid Electrical Vehicles (PHEV) due to their high energy density, slow loss of charge when not in use, and for lack of hysteresis effect. New application domains for these batteries has placed greater emphasis on their energy management, monitoring and control strategies.

In this thesis, a comparative study between different models and state of charge (SOC) estimation strategies is performed. Battery models range from black-box representation to detailed electro-chemical reaction models that consider the underlying physics. The state of charge is estimated using the Extended Kalman filter (EKF) and the Smooth Variable Structure Filter (SVSF). The models and SOC estimation strategies are applied to experimental results from BMW Electrical and Hybrid Research and Development center and validated using a simulation model from AVL CRUISE software.

Overall, different models and SOC estimation scenarios were studied. An average improvement of 30% in the estimation accuracy was shown by the SVSF SOC method when compared with the EKF SOC strategy. In general, the SVSF SOC estimation technique demonstrates excellent capability and a fast speed of convergence.

---

## ACKNOWLEDGEMENTS

---

The author would like to express his gratitude to his supervisor, Dr. S.R. Habibi, for his supervision, advice, and guidance from the very early stage of this research until the end.

Financial support provided by the McMaster University School of Graduate Studies, the Department of Mechanical Engineering, and the Ontario Government's Graduate Scholarship Program is acknowledged.

I convey special acknowledgement to BMW AG Munich Germany. I was surrounded by knowledgeable and friendly people who helped me on a daily basis. I would like to thank all of my colleagues at BMW for being supportive during my stay in Germany. I would like to thank Dr. Matthias Fleckenstein for his assistance, technical expertise, and support during my internship.

I would like to thank my friends providing me with the support and friendship that I needed.

Most of all I would like to thank my family, my father Sayed, my mother Awatef, my brother Ahmed and my sister Maii for their endless love, encouragement, support and absolute confidence in me throughout my life. Without them I could not have finished this thesis.

---

# TABLE OF CONTENTS

---

PERMISSION TO USE.....	III
ABSTRACT.....	VI
ACKNOWLEDGEMENTS.....	VII
TABLE OF CONTENTS.....	VIII
LIST OF FIGURES .....	XI
NOMENCLATURE.....	XVII
INTRODUCTION.....	1
1.1. THESIS MOTIVATION .....	2
1.2. THESIS SCOPE AND OBJECTIVES .....	3
1.3. THESIS ORGANIZATION.....	3
LITERATURE REVIEW.....	5
2.1. CURRENT AND FUTURE ENERGY SITUATION.....	5
2.2. EV BATTERIES ENERGY-POWER TRADE-OFF.....	7
2.3. OVERVIEW OF BATTERY TERMINOLOGIES AND DEFINITIONS .....	9
2.4. GENERAL OPERATING PRINCIPLES OF LI-ION BATTERY.....	12
2.5. BATTERY MODELLING.....	15
2.5.1. Ideal Models .....	16
2.5.2. Behavioral and Black-box Models .....	16
2.5.3. Equivalent-Circuit Models .....	17
2.5.4. Electro-Chemical Models .....	18
2.6. STATE OF CHARGE (SOC) DETERMINATION.....	19
2.6.1. Discharge Test.....	20
2.6.2. Ampere-Hour Counting.....	20
2.6.3. Measurement of the Electrolyte Physical Properties .....	21
2.6.4. Open Circuit Voltage (OCV).....	21
2.6.5. Artificial Neural Network.....	22
2.6.6. Impedance Spectroscopy.....	23
2.6.7. State Estimation Techniques.....	23
2.7. THERMAL MANAGEMENT SYSTEMS.....	23

2.8. BATTERY AGING MECHANISMS FOR LI-ION.....	23
2.9. SUMMARY.....	24
<b>STATE OF CHARGE ESTIMATION.....</b>	<b>25</b>
3.1. STATE AND PARAMETER ESTIMATION THEORY.....	25
3.1.1. The Kalman Filter (KF) .....	27
3.1.2. The Extended Kalman Filter (EKF) .....	30
3.1.3. The Smooth Variable Structure Filter (SVSF).....	32
3.2. STATE OF CHARGE ESTIMATION APPLICATION .....	35
3.3. SIMULATION AND EXPERIMENTAL CELL TESTING .....	36
3.3.1. Simulation Experiment.....	36
3.3.2. Experimental Testing Cycle .....	41
3.4. SUMMARY.....	43
<b>BEHAVIORAL MODELLING .....</b>	<b>44</b>
4.1. INTRODUCTION .....	44
4.2. EVOLUTION OF BEHAVIORAL CELL MODELS.....	45
4.2.1. Combined Model .....	45
4.2.2. Simple Model .....	46
4.2.3. Zero-State Hysteresis Model.....	48
4.2.4. One-State Hysteresis Model .....	50
4.2.5. Enhanced Self-Correcting Model (2-States).....	52
4.2.6. Enhanced Self-Correcting Model (4-States).....	54
4.3. MODEL PARAMETER TUNING .....	55
4.3.1. Simulation Results .....	59
4.3.2. Experimental Results .....	64
4.4. SOC ESTIMATION .....	69
4.4.1. Simulation Results .....	69
4.4.2. Experimental Results .....	74
4.5. SUMMARY.....	79
<b>EQUIVALENT CIRCUIT MODELLING .....</b>	<b>82</b>
5.1. INTRODUCTION .....	82
5.2. EVOLUTION OF EQUIVALENT CIRCUIT CELL MODELS.....	83
5.2.1. The 1 <sup>st</sup> Order RC Model.....	83
5.2.2. The 1 <sup>st</sup> Order RC Model with One-State Hysteresis .....	84
5.2.3. The 2 <sup>nd</sup> Order RC Model.....	85

5.2.4. The 2 <sup>nd</sup> Order RC Model with One-State Hysteresis.....	86
5.2.5. The 3 <sup>rd</sup> Order RC Model .....	88
5.2.6. The 3 <sup>rd</sup> Order RC Model with One-State Hysteresis .....	89
5.3. MODEL PARAMETER TUNING .....	90
5.3.1. Simulation Results .....	91
5.3.2. Experimental Results .....	96
5.4. SOC ESTIMATION .....	101
5.4.1. Simulation Results .....	101
5.4.2. Experimental Results .....	106
5.5. SUMMARY .....	111
<b>ELECTRO-CHEMICAL MODELLING .....</b>	<b>114</b>
6.1. OVERVIEW OF LI-ION BATTERY COMPOSITION AND OPERATION .....	115
6.2. THE FULL ORDER ELECTRO-CHEMICAL MODEL.....	118
6.2.1. Lithium Ion Conservation Equations.....	119
6.2.2. Charge Conservation Equations.....	122
6.2.3. Butler-Volmer Kinetics Equations: .....	125
6.2.4. Cell Potential Measurable Equation:.....	126
6.3. REDUCED ORDER MODEL - SINGLE PARTICLE MODEL (SPM).....	127
6.3.1. Butler-Volmer Current Calculation Subsystem.....	129
6.3.2. Spherical Particle Diffusion Sub-System.....	129
6.3.3. Calculate Terminal Voltage Subsystem: .....	131
6.3.4. SOC Calculation .....	133
6.4. SOC ESTIMATION .....	135
6.4.1. Simulation Test Procedure and Results .....	136
6.5. SUMMARY .....	145
<b>CONCLUSION AND RECOMMENDATIONS.....</b>	<b>146</b>
7.1. SUMMARY OF RESEARCH .....	146
7.2. RECOMMENDATIONS AND FUTURE WORK .....	148
APPENDIX A .....	150
APPENDIX B .....	153
BIBLIOGRAPHY.....	155
GLOSSARY.....	167

---

# LIST OF FIGURES

---

FIGURE 2.1 - HUBBERT CHART FOR OIL PEAK PRODUCTION [4] .....	6
FIGURE 2.2 - RAGONE PLOT OF ENERGY STORAGE DEVICES [5,6].....	8
FIGURE 2.3 - RELATIVE PERFORMANCE OF VARIOUS ELECTROCHEMICAL ENERGY-STORAGE DEVICES [9] .....	9
FIGURE 2.4 - ELECTRIC VEHICLE CELL, MODULE AND PACK.....	10
FIGURE 2.5 - IMAGINARY STATE OF CHARGE GAUGE INDICATOR.....	11
FIGURE 2.6 - ELECTROCHEMICAL FUNCTIONALITY OF A BATTERY DURING CHARGING (A), DISCHARGING (B) [13].....	13
FIGURE 2.7 - SCHEMATIC REPRESENTATION OF A LI-ION BATTERY DURING DISCHARGING [7] .....	14
FIGURE 2.8 - PYRAMID OF DETAILS SHOWING THE LEVEL OF DETAILS IN EACH MODELING CATEGORY .....	15
FIGURE 2.9 - DIAGRAM OF AN ARTIFICIAL NEURON [61] .....	22
FIGURE 3.1 - STATE ESTIMATION – OVERVIEW .....	26
FIGURE 3.2 - OVERVIEW OF PREDICTOR-CORRECTOR METHOD [84] .....	27
FIGURE 3.3 - SUMMARY OF KALMAN FILTER EQUATIONS.....	29
FIGURE 3.4 - SUMMARY OF EXTENDED KALMAN FILTER EQUATIONS.....	31
FIGURE 3.5 - SVSF ESTIMATION CONCEPT.....	33
FIGURE 3.6 - SUMMARY OF SMOOTH VARIABLE STRUCTURE FILTER EQUATIONS.....	34
FIGURE 3.7 - SCHEMATIC DIAGRAM OF STATE UPDATE .....	35
FIGURE 3.8 - AVL CRUISE ELECTRIC VEHICLE MODEL [96].....	37
FIGURE 3.9 – VEHICLE VELOCITY PROFILE [UDDS CYCLE] .....	38
FIGURE 3.10 – BATTERY CELL CURRENT PROFILE [UDDS CYCLE] .....	38
FIGURE 3.11 - SIMULATION TEST CYCLE SEQUENCE.....	39
FIGURE 3.12 - SOC vs. TIME [UDDS TEST SEQUENCE] .....	39

FIGURE 3.13 - BATTERY CELL CURRENT PROFILE [UDDS TEST SEQUENCE] .....	40
FIGURE 3.14 - BATTERY CELL TERMINAL VOLTAGE PROFILE [UDDS TEST SEQUENCE].....	40
FIGURE 3.15 - EXPERIMENTAL BATTERY CURRENT PROFILE .....	41
FIGURE 3.16 - EXPERIMENTAL BATTERY SOC vs. TIME PROFILE.....	42
FIGURE 3.17 - EXPERIMENTAL BATTERY TERMINAL VOLTAGE BEHAVIOR.....	42
FIGURE 4.1 – SIMULATION BATTERY CELL CURRENT PROFILE [UDDS TEST SEQUENCE] .....	57
FIGURE 4.2 – SIMULATION BATTERY CELL TERMINAL VOLTAGE PROFILE [UDDS TEST SEQUENCE] 57	57
FIGURE 4.3 - EXPERIMENTAL BATTERY CURRENT PROFILE .....	58
FIGURE 4.4 - EXPERIMENTAL BATTERY TERMINAL VOLTAGE BEHAVIOR.....	58
FIGURE 4.5 – SIMULATION RESULTS OF CELL MODELING WITH COMBINED MODEL SHOWING THE MODEL TERMINAL VOLTAGE VERSUS THE TRUE VOLTAGE [UDDS] .....	59
FIGURE 4.6 – SIMULATION RESULTS OF CELL MODELING WITH SIMPLE MODEL SHOWING THE MODEL TERMINAL VOLTAGE VERSUS THE TRUE VOLTAGE [UDDS] .....	60
FIGURE 4.7 – SIMULATION RESULTS OF CELL MODELING WITH ZERO STATE HYSTERESIS MODEL SHOWING THE MODEL TERMINAL VOLTAGE VERSUS THE TRUE VOLTAGE [UDDS].....	60
FIGURE 4.8 - SIMULATION RESULTS OF CELL MODELING WITH ONE STATE HYSTERESIS MODEL SHOWING THE MODEL TERMINAL VOLTAGE VERSUS THE TRUE VOLTAGE [UDDS].....	61
FIGURE 4.9 – SIMULATION RESULTS OF CELL MODELING WITH ENHANCED SELF CORRECTING MODEL – 2 STATES SHOWING THE MODEL TERMINAL VOLTAGE VERSUS THE TRUE VOLTAGE [UDDS]61	61
FIGURE 4.10 – SIMULATION RESULTS OF CELL MODELING WITH ENHANCED SELF CORRECTING MODEL – 4 STATES SHOWING THE MODEL TERMINAL VOLTAGE VERSUS THE TRUE VOLTAGE [UDDS].....	62
FIGURE 4.11 – EXPERIMENTAL RESULTS OF CELL MODELING WITH COMBINED MODEL SHOWING THE MODEL TERMINAL VOLTAGE VERSUS THE TRUE VOLTAGE.....	64
FIGURE 4.12 – EXPERIMENTAL RESULTS OF CELL MODELING WITH SIMPLE MODEL SHOWING THE MODEL TERMINAL VOLTAGE VERSUS THE TRUE VOLTAGE.....	65
FIGURE 4.13 – EXPERIMENTAL RESULTS OF CELL MODELING WITH ZERO STATE HYSTERESIS MODEL SHOWING THE MODEL TERMINAL VOLTAGE VERSUS THE TRUE VOLTAGE .....	65
FIGURE 4.14 - EXPERIMENTAL RESULTS OF CELL MODELING WITH ONE STATE HYSTERESIS MODEL SHOWING THE MODEL TERMINAL VOLTAGE VERSUS THE TRUE VOLTAGE .....	66
FIGURE 4.15- EXPERIMENTAL RESULTS OF CELL MODELING WITH ENHANCED SELF CORRECTING MODEL – 2 STATES SHOWING THE MODEL TERMINAL VOLTAGE VERSUS THE TRUE VOLTAGE.66	66
FIGURE 4.16 – EXPERIMENTAL RESULTS OF CELL MODELING WITH ENHANCED SELF CORRECTING MODEL – 4 STATES SHOWING THE MODEL TERMINAL VOLTAGE VERSUS THE TRUE VOLTAGE.67	67

FIGURE 4.17 – SIMULATION RESULTS OF SOC ESTIMATION WITH COMBINED MODEL SHOWING THE EKF AND SVSF ESTIMATED VERSUS MODEL SOC. ....	69
FIGURE 4.18 – SIMULATION RESULTS OF SOC ESTIMATION WITH SIMPLE MODEL SHOWING THE EKF AND SVSF ESTIMATED VERSUS MODEL SOC.....	70
FIGURE 4.19 - SIMULATION RESULTS OF SOC ESTIMATION WITH ZERO STATE HYSTERESIS SHOWING THE EKF AND SVSF ESTIMATED VERSUS MODEL SOC.....	70
FIGURE 4.20 - SIMULATION RESULTS OF SOC ESTIMATION WITH ONE STATE HYSTERESIS SHOWING THE EKF AND SVSF ESTIMATED VERSUS MODEL SOC.....	71
FIGURE 4.21 - SIMULATION RESULTS OF SOC ESTIMATION WITH ENHANCED SELF CORRECTING MODEL – 2 STATES SHOWING THE EKF AND SVSF ESTIMATED VERSUS MODEL SOC.....	71
FIGURE 4.22 - SIMULATION RESULTS OF SOC ESTIMATION WITH ENHANCED SELF CORRECTING MODEL – 4 STATES SHOWING THE EKF AND SVSF ESTIMATED VERSUS MODEL SOC.....	72
FIGURE 4.23 - EXPERIMENTAL RESULTS OF SOC ESTIMATION WITH COMBINED MODEL SHOWING THE EKF AND SVSF ESTIMATED VERSUS MODEL SOC. ....	74
FIGURE 4.24 - EXPERIMENTAL RESULTS OF SOC ESTIMATION WITH SIMPLE MODEL SHOWING THE EKF AND SVSF ESTIMATED VERSUS MODEL SOC. ....	75
FIGURE 4.25 - EXPERIMENTAL RESULTS OF SOC ESTIMATION WITH ZERO STATE HYSTERESIS SHOWING THE EKF AND SVSF ESTIMATED VERSUS MODEL SOC.....	75
FIGURE 4.26 - EXPERIMENTAL RESULTS OF SOC ESTIMATION WITH ONE STATE HYSTERESIS SHOWING THE EKF AND SVSF ESTIMATED VERSUS MODEL SOC.....	76
FIGURE 4.27 - EXPERIMENTAL RESULTS OF SOC ESTIMATION WITH ENHANCED SELF CORRECTING MODEL – 2 STATES SHOWING THE EKF AND SVSF ESTIMATED VERSUS MODEL SOC.....	76
FIGURE 4.28 - EXPERIMENTAL RESULTS OF SOC ESTIMATION WITH ENHANCED SELF CORRECTING MODEL – 4 STATES SHOWING THE EKF AND SVSF ESTIMATED VERSUS MODEL SOC.....	77
FIGURE 4.29 – EXPERIMENTAL RESULTS FOR BEHAVIORAL MODELS COMPARISON OF AVERAGE MODELING RESULTS.....	79
FIGURE 4.30 - SIMULATION RESULTS FOR BEHAVIORAL MODELS COMPARISON OF AVERAGE MODELING RESULTS.....	80
FIGURE 4.31 - EXPERIMENTAL RESULTS FOR BEHAVIORAL MODELS COMPARISON OF SOC ESTIMATION ERROR USING EKF AND SVSF .....	81
FIGURE 4.32 – SIMULATION RESULTS FOR BEHAVIORAL MODELS COMPARISON OF SOC ESTIMATION ERROR USING EKF AND SVSF.....	81
FIGURE 5.1 - SCHEMATIC DIAGRAM FOR R-RC BATTERY MODEL.....	83
FIGURE 5.2 - SCHEMATIC DIAGRAM FOR R-RC_H BATTERY MODEL.....	84
FIGURE 5.3 - SCHEMATIC DIAGRAM FOR R-RC-RC BATTERY MODEL.....	85

FIGURE 5.4 - SCHEMATIC DIAGRAM FOR R-RC-RC_H BATTERY MODEL.....	87
FIGURE 5.5 - SCHEMATIC DIAGRAM FOR R-RC-RC-RC BATTERY MODEL .....	88
FIGURE 5.6 - SCHEMATIC DIAGRAM FOR R-RC-RC-RC BATTERY MODEL .....	89
FIGURE 5.7 - SIMULATION RESULTS OF CELL MODELING WITH R_RC MODEL SHOWING THE MODEL TERMINAL VOLTAGE VERSUS SIMULATED VOLTAGE .....	91
FIGURE 5.8 – SIMULATION RESULTS OF CELL MODELING WITH R_RC_H MODEL SHOWING THE MODEL TERMINAL VOLTAGE VERSUS SIMULATED VOLTAGE.....	92
FIGURE 5.9 - SIMULATION RESULTS OF CELL MODELING WITH R_RC_RC MODEL SHOWING THE MODEL TERMINAL VOLTAGE VERSUS SIMULATED VOLTAGE.....	92
FIGURE 5.10 - SIMULATION RESULTS OF CELL MODELING WITH R_RC_RC_H MODEL SHOWING THE MODEL TERMINAL VOLTAGE VERSUS SIMULATED VOLTAGE.....	93
FIGURE 5.11 - SIMULATION RESULTS OF CELL MODELING WITH R_RC_RC_RC MODEL SHOWING THE MODEL TERMINAL VOLTAGE VERSUS SIMULATED VOLTAGE.....	93
FIGURE 5.12 – SIMULATION RESULTS OF CELL MODELING WITH R_RC_RC_H MODEL SHOWING THE MODEL TERMINAL VOLTAGE VERSUS SIMULATED VOLTAGE.....	94
FIGURE 5.13– EXPERIMENTAL RESULTS OF CELL MODELING WITH R_RC MODEL SHOWING THE MODEL TERMINAL VOLTAGE VERSUS THE TRUE VOLTAGE.....	96
FIGURE 5.14– EXPERIMENTAL RESULTS OF CELL MODELING WITH R_RC_H MODEL SHOWING THE MODEL TERMINAL VOLTAGE VERSUS THE TRUE VOLTAGE.....	97
FIGURE 5.15– EXPERIMENTAL RESULTS OF CELL MODELING WITH R_RC_RC MODEL SHOWING THE MODEL TERMINAL VOLTAGE VERSUS THE TRUE VOLTAGE.....	97
FIGURE 5.16– EXPERIMENTAL RESULTS OF CELL MODELING WITH R_RC_RC_H MODEL SHOWING THE MODEL TERMINAL VOLTAGE VERSUS THE TRUE VOLTAGE .....	98
FIGURE 5.17 – EXPERIMENTAL RESULTS OF CELL MODELING WITH R_RC_RC_RC MODEL SHOWING THE MODEL TERMINAL VOLTAGE VERSUS THE TRUE VOLTAGE .....	98
FIGURE 5.18 - EXPERIMENTAL RESULTS OF CELL MODELING WITH R_RC_RC_RC_H MODEL SHOWING THE MODEL TERMINAL VOLTAGE VERSUS THE TRUE VOLTAGE .....	99
FIGURE 5.19 - SIMULATION RESULTS OF SOC ESTIMATION WITH R_RC MODEL SHOWING THE EKF AND SVSF ESTIMATED VERSUS MODEL SOC.....	101
FIGURE 5.20 - SIMULATION RESULTS OF SOC ESTIMATION WITH R_RC_H MODEL SHOWING THE EKF AND SVSF ESTIMATED VERSUS MODEL SOC. ....	102
FIGURE 5.21 - SIMULATION RESULTS OF SOC ESTIMATION WITH R_RC_RC MODEL SHOWING THE EKF AND SVSF ESTIMATED VERSUS MODEL SOC. ....	102
FIGURE 5.22 - SIMULATION RESULTS OF SOC ESTIMATION WITH R_RC_RC_H MODEL SHOWING THE EKF AND SVSF ESTIMATED VERSUS MODEL SOC.....	103

FIGURE 5.23 - SIMULATION RESULTS OF SOC ESTIMATION WITH R_RC_RC_RC MODEL SHOWING THE EKF AND SVSF ESTIMATED VERSUS MODEL SOC.....	103
FIGURE 5.24 - SIMULATION RESULTS OF SOC ESTIMATION WITH R_RC_RC_RC_H MODEL SHOWING THE EKF AND SVSF ESTIMATED VERSUS MODEL SOC.....	104
FIGURE 5.25 - EXPERIMENTAL RESULTS OF SOC ESTIMATION WITH R_RC MODEL SHOWING THE EKF AND SVSF ESTIMATED VERSUS MODEL SOC. ....	106
FIGURE 5.26 - EXPERIMENTAL RESULTS OF SOC ESTIMATION WITH R_RC_H MODEL SHOWING THE EKF AND SVSF ESTIMATED VERSUS MODEL SOC. ....	107
FIGURE 5.27 - EXPERIMENTAL RESULTS OF SOC ESTIMATION WITH R_RC_RC MODEL SHOWING THE EKF AND SVSF ESTIMATED VERSUS MODEL SOC.....	107
FIGURE 5.28 - EXPERIMENTAL RESULTS OF SOC ESTIMATION WITH R_RC_RC_H MODEL SHOWING THE EKF AND SVSF ESTIMATED VERSUS MODEL SOC.....	108
FIGURE 5.29 - EXPERIMENTAL RESULTS OF SOC ESTIMATION WITH R_RC_RC_RC MODEL SHOWING THE EKF AND SVSF ESTIMATED VERSUS MODEL SOC.....	108
FIGURE 5.30 - EXPERIMENTAL RESULTS OF SOC ESTIMATION WITH R_RC_RC_RC_H MODEL SHOWING THE EKF AND SVSF ESTIMATED VERSUS MODEL SOC.....	109
FIGURE 5.31- EXPERIMENTAL RESULTS FOR EQUIVALENT CIRCUIT MODELS COMPARISON OF AVERAGE MODELING RESULTS.....	111
FIGURE 5.32 - SIMULATION EXPERIMENTAL RESULTS FOR EQUIVALENT CIRCUIT MODELS COMPARISON OF AVERAGE MODELING RESULTS.....	112
FIGURE 5.33 - EXPERIMENTAL RESULTS FOR EQUIVALENT CIRCUIT MODELS COMPARISON OF SOC ESTIMATION ERROR USING EKF AND SVSF .....	113
FIGURE 5.34 - EXPERIMENTAL RESULTS FOR EQUIVALENT CIRCUIT MODELS COMPARISON OF SOC ESTIMATION ERROR USING EKF AND SVSF .....	113
FIGURE 6.1 - FULLY CHARGED BATTERY (100%) .....	115
FIGURE 6.2 - FULLY DISCHARGED BATTERY (0%) .....	115
FIGURE 6.3 - SIMPLIFIED SCHEMATIC DIAGRAM SHOWING CONCENTRATION GRADIENTS DURING HIGH RATE DISCHARGE.....	117
FIGURE 6.4 - SCHEMATIC DIAGRAM SHOWING THE INTERCALATION APPROACH FOR A BATTERY CELL [15] .....	118
FIGURE 6.5 - SCHEMATIC SIMPLIFICATION OF LITHIUM CONSERVATION EQUATIONS IN ELECTRODE SPHERICAL PARTICLE, RED LINE EQUATIONS REPRESENT BOUNDARY CONDITIONS, BLUE LINE REPRESENT THE LITHIUM ION GOVERNING EQUATION .....	120
FIGURE 6.6 - SCHEMATIC SIMPLIFICATION OF LITHIUM CONSERVATION EQUATIONS IN ELECTROLYTE, RED LINE REPRESENT BOUNDARY CONDITIONS EQUATIONS, BLUE LINE REPRESENT THE GOVERNING EQUATION.....	121

FIGURE 6.7 - SIMPLIFIED SCHEMATIC DIAGRAM SHOWING ALL BOUNDARY CONDITIONS FOR CHARGE CONSERVATION EQUATIONS.....	124
FIGURE 6.8 - SCHEMATIC REPRESENTATION OF SINGLE PARTICLE MODEL .....	127
FIGURE 6.9 - SIMPLIFIED REDUCED ORDER MODEL FOUR MAIN SUBSYSTEMS .....	128
FIGURE 6.10 - RELATION BETWEEN SOC AND SOLID SURFACE CONCENTRATION STOICHIOMETRY..	134
FIGURE 6.11 - SOC ESTIMATION USING SVSF .....	135
FIGURE 6.12 - CHARGING/DISCHARGING PULSE TRAIN CYCLE CURRENT PROFILE .....	137
FIGURE 6.13 – BATTERY FULL ORDER MODEL SOC BEHAVIOR [UDDS] .....	137
FIGURE 6.14 – BATTERY FULL-ORDER MODEL OUTPUT VOLTAGE PROFILE [UDDS] .....	138
FIGURE 6.15 - BATTERY FULL ORDER MODEL SOC BEHAVIOR [PULSE TRAIN CYCLE] .....	138
FIGURE 6.16 - BATTERY FULL-ORDER MODEL OUTPUT VOLTAGE PROFILE [PULSE TRAIN CYCLE] ...	139
FIGURE 6.17 - LITHIUM CONCENTRATION IN SOLID PARTICLE FULL-ORDER MODEL VS. SPM WITH EKF AND SVSF.....	140
FIGURE 6.18 - CRITICAL SURFACE CONCENTRATION IN SOLID PARTICLE FULL-ORDER MODEL VS. SPM WITH EKF AND SVSF .....	141
FIGURE 6.19 - SOC ESTIMATION USING SPM WITH EKF AND SVSF VS. FULL ORDER MODEL.....	141
FIGURE 6.20 - TERMINAL VOLTAGE COMPARISON FULL ORDER MODEL VS. SPM WITH EKF AND SVSF .....	142
FIGURE 6.21 - LITHIUM CONCENTRATION IN SOLID PARTICLE FULL-ORDER MODEL VS. SPM WITH EKF AND SVSF [PULSE TRAIN CYCLE].....	143
FIGURE 6.22- CRITICAL SURFACE CONCENTRATION IN SOLID PARTICLE FULL-ORDER MODEL VS. SPM WITH EKF AND SVSF [PULSE TRAIN CYCLE] .....	143
FIGURE 6.23 - SOC ESTIMATION USING SPM WITH EKF AND SVSF VS. FULL ORDER MODEL [PULSE TRAIN CYCLE].....	144
FIGURE 6.24 – TERMINAL VOLTAGE COMPARISON FULL ORDER MODEL VS. SPM WITH EKF AND SVSF [PULSE TRAIN CYCLE].....	144
FIGURE 6.25 – SIMULATION ELECTRO-CHEMICAL MODEL ESTIMATION COMPARISON OF SOC ESTIMATION ERROR USING EKF AND SVSF .....	145

---

## NOMENCLATURE

---

Symbol	Name	Unit
$a_s$	Active surface area per electrode unit volume	$\text{cm}^2 \text{cm}^{-3}$
$A$	Electrode plate area	$\text{cm}^2$
$c_e$	Electrolyte concentration	$\text{mol cm}^{-3}$
$c_s$	Solid concentration	$\text{mol cm}^{-3}$
$c_{se}$	Solid concentration at electrolyte interface	$\text{mol cm}^{-3}$
$F$	Faraday's number	$\text{C mol}^{-1}$
$i_0$	Exchange current density of an electrode reaction	$\text{A cm}^{-2}$
$i_e$	Electrolyte current density	$\text{A cm}^{-2}$
$i_s$	Solid current density	$\text{A cm}^{-2}$
$I$	Battery applied current	$\text{A}$
$j^{Li}$	Butler–Volmer current density	$\text{A cm}^{-3}$
$Q$	capacity	$\text{A s}$

$r$	Radial coordinate	cm
$R$	Universal Gas constant	J K <sup>-1</sup> mol <sup>-1</sup>
$R_f$	Film resistance on an electrode surface	Ω cm <sup>2</sup>
$R_s$	Radius of solid active material particles	cm
$s$	Laplace variable	rad s <sup>-1</sup>
$t$	time	s
$t^0$	transference number of lithium ion with respect to the velocity of solvent	-
$T$	Temperature	K
$T_s$	time step	s
$U$	Open circuit voltage	V
$U_P$	Cathode open circuit voltage	V
$U_n$	Anode open circuit voltage	V
$x$	spatial coordinate	cm

Greek symbol	Name	Unit
$\eta$	overpotential	V
$\phi_e$	electrolyte potential	V
$\phi_s$	solid potential	V
$\theta_n$	normalized solid concentration at anode	-
$\theta_p$	normalized solid concentration at cathode	-
$k^{eff}$	effective electrolyte phase ionic conductivity	Ω <sup>-1</sup> cm <sup>-1</sup>
$k_D^{eff}$	effective electrolyte phase diffusion conductivity	
$\sigma^{eff}$	effective conductivity of solid active material	
$\alpha_a$	anodic transfer coefficients of electrode reaction	-

$\alpha_c$  cathodic transfer coefficients of electrode reaction -

Matrix/Vector	Name	Unit
A,B,C,D	state variable model matrices	
L	Kalman filter (state estimator) gain matrix	
p, q	left eigenvector, right eigenvector	
r	residue vector	
u	state variable model input vector	
x	state vector	
y	state variable model output vector	
z	steady-state response vector	

Subscript	Name	Unit
K	sampling time step	
e	electrolyte phase	
s	solid phase	
s, avg	average, or bulk solid phase	
s, e	solid phase at solid/electrolyte interface	
s, max	solid phase theoretical maximum limit	
sep	separator region	
-	negative electrode region	
+	positive electrode region	
K	sampling time step	

---

Superscript	Name	Unit
T	Transpose	
eff	effective	
Li	Lithium species	

---

---

# Introduction

---

Recently, Lithium-ion (Li-ion) cells are increasingly used in many application affecting our daily life, such as laptops computers, cell phones, digital cameras, and other portable electronic devices. Lithium-ion batteries have gained attention in the past 10 years due to their high energy density, slow loss of charge when not in use, and for lack of hysteresis. Nowadays they are being used in new second generation Hybrid Electric (HEV) and Plug-in Hybrid Electrical (PHEV) Vehicles. As battery applications and usage increase, accurate management, monitoring and control strategies are needed to improve the performance, efficiency, safety, reliability and longevity of battery packs. Especially, in the case of Hybrid and electrical vehicles Battery management systems (BMS) play an important role as the battery operating conditions are subjected to fast transients and frequent charging and discharging cycles due to sudden acceleration or regenerative braking system maneuvers. Battery Management Systems (BMS) must be able to provide an accurate real-time estimate for the Battery State of Charge (SOC),

State of Health (SOH), cell aging, and Remaining Useful Life (RUL). The Battery SOC value is so critical also for the driver's point of view especially if the battery is the only source of power because SOC roughly speaking provide the driver with how much energy left within the battery. The main challenge with SOC is that it cannot be measured hence requiring state and parameter estimation strategies.

This chapter, provides an overview of research motivations answering the question of why there is a need for accurate battery modelling and reliable SOC estimation strategies. Also a brief summary about previous work found in literature is presented. The scope of the research, goals and contributions are described.

## 1.1. Thesis Motivation

The motivation for this research is driven by the world's need to reduce emissions and use sustainable and renewable energy sources. Important considerations for Hybrid and Electric vehicles are energy storage and battery management are considered in this research.

In conventional vehicles, the gasoline remaining in the tank can readily be measured by using a fluid level sensor. However, in the electric vehicles, it is not easy to measure the amount of useful energy remaining, known as SOC. This specifically the case when the battery is subjected to fast transients in terms of charging and discharging due to the driving cycle. Since SOC cannot be measured, an accurate mathematical model along with a robust estimation technique is necessary [1].

In Electric vehicles, another important consideration is the Remaining Useful Life (RUL) of the battery. Battery operation and management are important factors in extending battery life and Remaining Useful Life. Model based strategies are often used [2].

## 1.2. Thesis Scope and Objectives

In this thesis, different battery modelling techniques and SOC estimations strategies are considered and compared with respect to their performances. The research objectives can be stated as follows:

- Lithium ion battery cell models are selected, refined, implemented and validated using measured and simulated test data. The models considered can be categorized as: Behavioural, Equivalent circuit, and Electro-chemical models. Experimental data used for model validation were obtained from BMW AG Research and Development center (Munich, Germany).
- Estimation strategies were used for obtaining the SOC. These included the Extended Kalman Filter (EKF) and Smooth Variable Structure Filter (SVSF)

A performance comparative study of the battery models in conjunction with estimation strategies for obtaining SOC is presented.

## 1.3. Thesis Organization

This thesis is divided into 7 chapters:

**Chapter 1:** Thesis Motivation, Scope and Objectives are discussed.

**Chapter 2:** A literature review of battery modelling techniques and SOC estimation strategies is presented.

**Chapter 3:** Estimation algorithms are introduced and used for SOC estimation. The experimental and simulation test procedures used for model validation are described.

**Chapter 4:** Behavioral modelling techniques categorized as Black-box are described and used for SOC estimation.

**Chapter 5:** Equivalent circuit modelling techniques also known as Impedance-based modelling are introduced and used for SOC estimation.

**Chapter 6:** Electro-Chemical modelling techniques are described and used for SOC estimation.

**Chapter 7:** The performance of the SOC estimation using the three categories of models and the two types of estimation algorithms considered in this research are compared and discussed. Conclusion based on performance measurements and complexity analysis are presented. Recommendations for future research are also provided.

---

# Literature Review

---

Li-ion batteries are increasingly used in Hybrid and Electric Vehicles. However, for higher efficiency and longer life, special considerations must be given to their operating conditions for preventing thermal runaways, aging, and physical damage. Therefore, there is an important and fundamental need for a Battery Management System (BMS). These need to be able to accurately assess, estimate and control the Battery State of charge (SOC), State of Health (SOH) and core temperature. These three parameters allow the BMS to determine the optimal operating strategy such that the battery pack lifetime is maximized [3]. This chapter presents the basic battery terminologies, the basic operating principles and the different approaches to Li-Ion battery modelling and SOC Estimation.

## 2.1. Current and Future Energy Situation

Presently, our societies rely heavily on fossil fuels, coal and oil for our energetic needs. However, there is a worldwide concern about these sources of energy due to factors associated with their geopolitical, economic and environmental impact. Even though,

fossil fuels are naturally produced, their consumption rate is higher than their production rate, causing strain on available reserves. Over reliance on fossil fuels is unsustainable and the reserves are diminishing rapidly as shown by the Association for the Study of Peak Oil and Gas (ASPO), who predicts that the oil extraction peak will be reached before 2020 (as shown in Figure 2.1). Thus, consideration of alternative sources of energy and in particular electrification is a necessity.

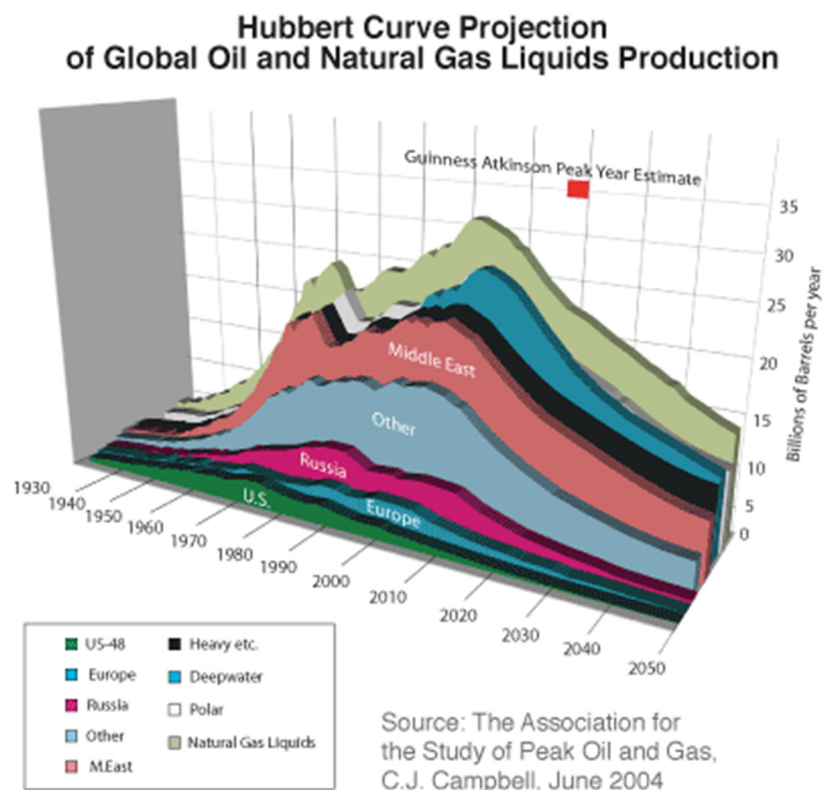


Figure 2.1 - Hubbert chart for oil peak production [4]

A requirement of electrification is energy storage that in turn relies on electro-chemical batteries. They convert chemical energy to electrical energy and are widely used in all sectors of industry (automotive, aerospace, medical, military, etc.) as well as in consumer goods (e.g. low current applications, home appliances, cell phones, and laptop computers).

Batteries are a key element in hybrid and Electric vehicles. Lithium-based batteries are specifically of interest due to their high energy density. Furthermore, they are less toxic than nickel cadmium or lead acid cells, and after use they can be recycled posing fewer environmental concerns.

## 2.2. EV Batteries Energy-Power Trade-Off

The Ragone<sup>1</sup> plot in Figure 2.2 shows the difference between the power and energy densities for different energy supply systems. As shown the Internal Combustion Engine (ICE) remains the most desirable choice due to the high specific power and specific energy of fossil fuels. Ultracapacitors have a high power density, which enables them to supply a very high peak power in a very short period (milliseconds). Alternatively, fuel cells possess high energy density but need long time period (hours) to be charged or discharged. This limits their applications in the automotive industry where both high power as well as energy density are required.

Lithium-based batteries provide a reasonable compromise between energy density and power density, making them an attractive choice for the next generation of Hybrid Electric Vehicles (HEVs), (PHEVs) and Electric Vehicles (EVs).

---

<sup>1</sup> A Ragone plot is a 2- axis chart used for performance comparison of various energy storing devices. On such a chart, the energy density (in Wh/kg) is plotted versus power density (in W/kg). Both axes are logarithmic, which allows comparing performance of very different devices (for example extremely high, and extremely low power densities).

Conceptually, the vertical axis describes how much energy is available, while the horizontal axis shows how quickly that energy can be delivered. Sloping lines on the Ragone plot indicate the required time to get the charge in or out of the device.

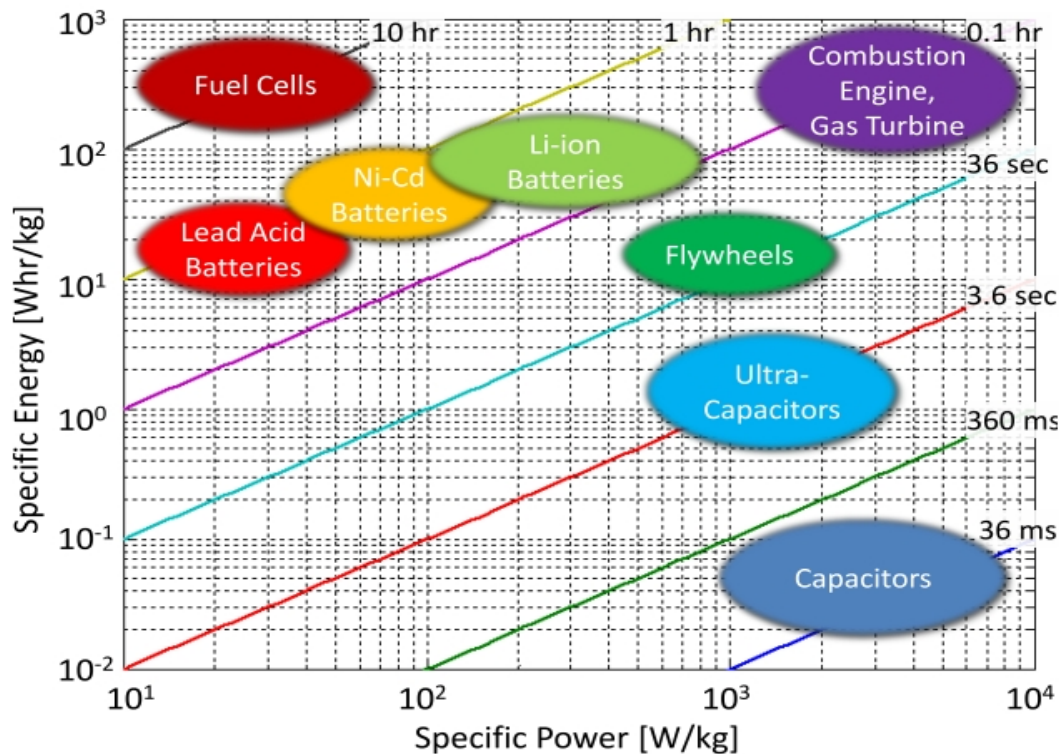


Figure 2.2 - Ragone Plot of Energy Storage Devices [5,6]

The Ragone plot shown in Figure 2.2 shows that lithium ion batteries are better by at least a factor of 2.5 compared to other technologies in terms of high specific power and energy [7]. The Li-Ion battery at this time, is the technology best suited to the needs of electric vehicles, due to their large specific energy density and specific power, and their ability to accommodate fast transients as shown in Figure 2.3 [3]. As shown in the Ragone plot of Figure 2.3 above, it can be seen that the Li-ion battery is the best match to the EV goal. As such considerable investment is being made to their development and to improve their performance, reliability, durability, safety and aging [3,8].

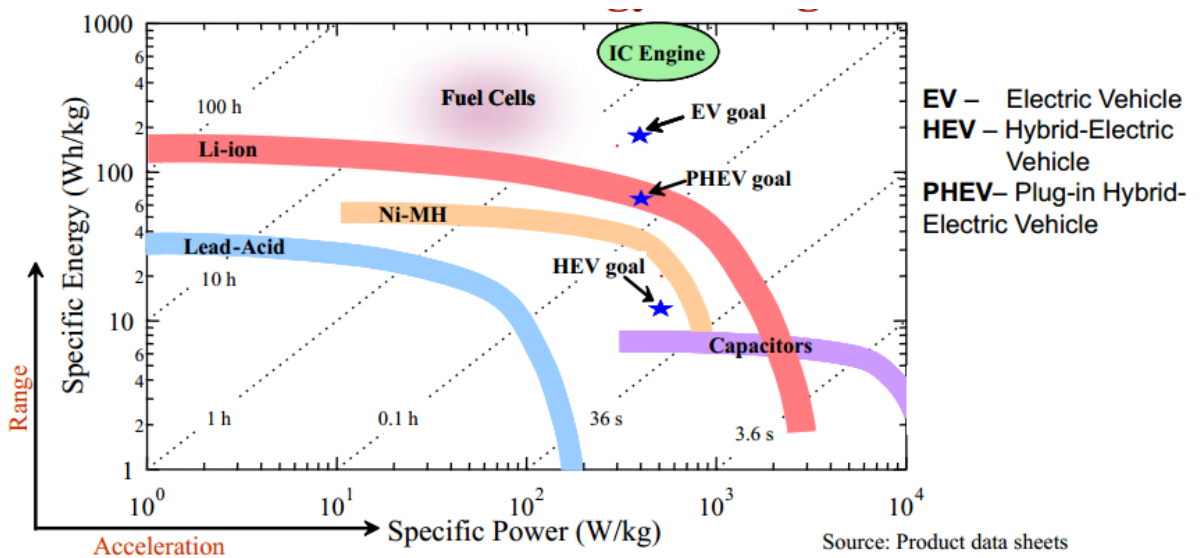


Figure 2.3 - Relative Performance of Various Electrochemical Energy-Storage Devices [9]

## 2.3. Overview of Battery Terminologies and Definitions

Battery terminologies used to describe the parameters, characteristics and properties of a battery cells are as follows.

- ***Rechargeable and Non-Rechargeable Battery Cells***

If a battery does not allow irreversible chemical reactions to take place, it cannot be recharged, such a battery is called the primary battery. If there is another battery that allows reversible chemical reaction to take place (which means it a rechargeable battery), this second battery is called the secondary battery [10,11].

- ***Cell, Modules and Packs***

Every Hybrid Electric Vehicles (HEVs), Plug-In Hybrid Electric Vehicles (PHEVs) and Electric Vehicles (EVs) contains a high voltage battery pack that consists of two or more modules; each module consists of two or more cells. A cell is the smallest unit connected in parallel or in series to form one module. A module is then connected in a parallel or series configuration to form one pack, as shown in Figure 2.4.

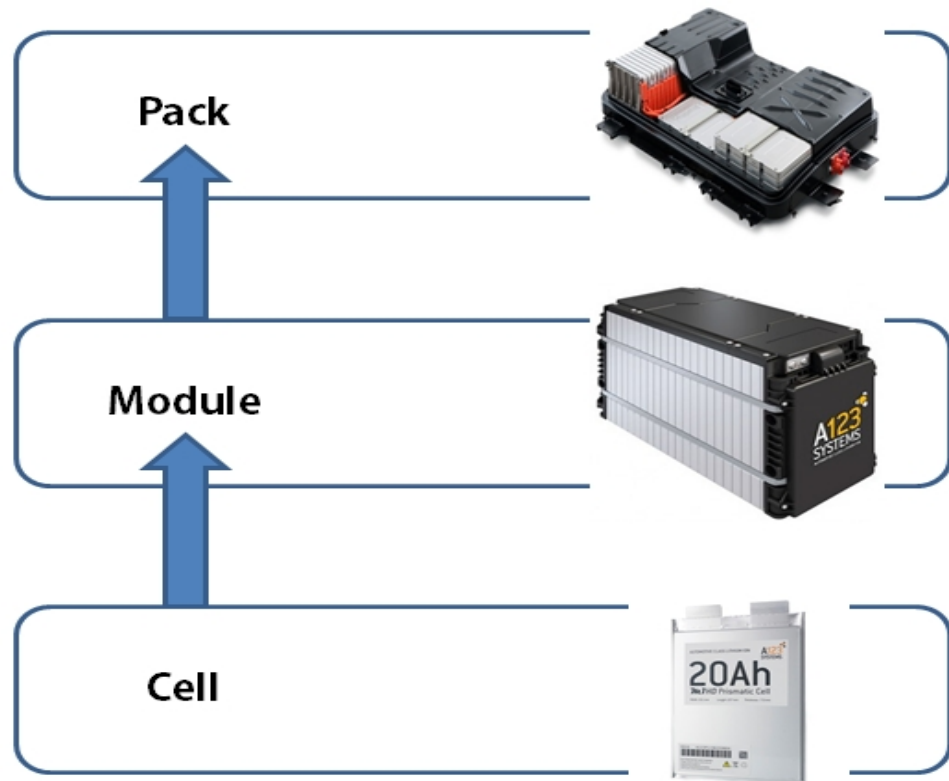


Figure 2.4 - Electric vehicle Cell, Module and Pack

- ***Charge Rate (C-Rate)***

Battery charge rate or as denoted by *C-rate* describes the rate at which the battery is charged or discharged relative to its maximum capacity. A 1C rate means that the applied discharge current will discharge a fully charged battery in 1 hour. For a battery with a capacity of 20 Amp-hours, this equals to a 20 Amps discharge current. A 5C rate for this battery would be  $20 \times 5 = 100$  Amps, and a C/2 rate would be  $20/2 = 10$  Amps.

- ***Terminal Voltage ( $V_t$ )***

The voltage measured between the battery terminals when a load is applied.

- ***Open-Circuit Voltage ( $V_{ocv}$ )***

The voltage measured between the battery terminals when no load is applied.

- ***Capacity or Nominal Capacity***

The coulometric capacity is the total Amp-hours that can be drawn from a battery when being fully discharged from 100% state-of-charge to its rated minimum cut-off voltage at a certain discharge current (specified as a C-rate). Capacity is calculated by multiplying the discharge current (in Amps) by the discharge time (in hours) [10].

- ***State Of Charge (SOC)***

In electric vehicles, parameter is the State of Charge (SOC) as it shows the current battery capacity as a percentage of maximum capacity. As such it provides a measure of the amount of electric energy stored in a battery. It is analogous to a fuel gauge on a conventional internal combustion engine vehicle [10,12]. State of Charge (SOC) is a dimensionless number between 0 and 1 representing a percentage. It is worth noting that a zero SOC does not mean that the battery is fully empty, only that the battery cannot be discharged anymore without causing some permanent damage (irreversible chemical reaction) to it [11].

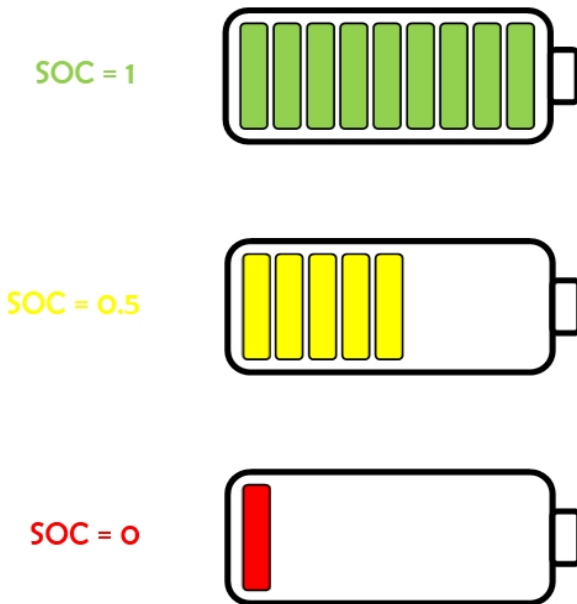


Figure 2.5 - Imaginary State of Charge Gauge Indicator

- ***Depth of Discharge (DOD)***

The Depth of Discharge (DOD) is the alternative method of indicating the Battery State of Charge (SOC), The DOD is the percentage of battery capacity that has been already discharged. In other words,  $DOD (\%) = 100 - SOC (\%)$ .

- ***Cut-Off Voltage***

The minimum allowable voltage at which the battery is known to be “*empty*”.

- ***Cycle Life***

This is the number of cycles that can be performed before the battery reaches End of Life (EoL).

- ***State Of Health (SOH)***

The State of Health (SOH) indicates a condition in the battery life between the beginning of life (BoL) and end of life (EoL) in percentages. The BoL of a battery is defined as the point in time when battery life begins. The EoL of a battery is reached when the battery cannot perform according to its predefined minimum requirements. For EV applications, the battery manufacturers define EoL, when one of the following conditions has been reached [13,14,15]:

- 80% drop in the battery capacity compared to its rated capacity under reference conditions. This is known as capacity fading.
- 80% drop in the battery's maximum power compared to the rated power. This is known as power fading.

## 2.4. General Operating Principles of Li-Ion Battery

In this section, the functionality of the lithium-ion battery using an electrolyte is discussed. A battery converts chemical energy into electrical energy and vice versa. The battery cell voltage is calculated by the energy of chemical reaction taking place inside the

cell. The basic setup of a battery consists of three main parts: the positive electrode, the separator, and the negative electrode. The positive and negative electrodes are referred to as the cathode and the anode, as shown in Figure 2.6. The battery is connected to an external load using current collector plates. In case of Li-ion cells, a copper collector is used in the negative electrode while an aluminum collector is used for the positive electrode [13,14,16,17].

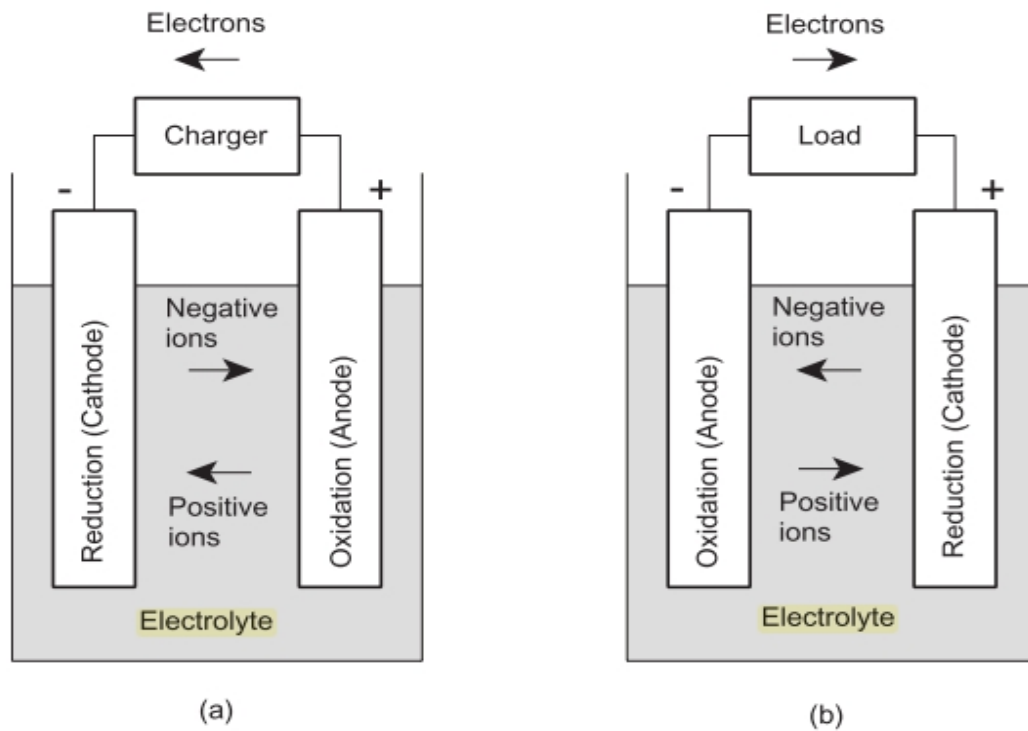


Figure 2.6 - Electrochemical functionality of a battery during charging (a), discharging (b) [13]

**The anode** is the electrode capable of supplying electrons to the load. The anode composite material defines the name of the Li-ion battery and is usually made up of a mixture of carbon (ex.  $\text{Li}_x\text{C}_6$ ), while the electrolyte can be made of liquid, polymer or solid materials (ex.  $\text{LiPF}_6$ ). In case of solid or polymer materials, the electrolyte will also act also as separator.

The separator is a porous membrane allowing the transfer of lithium ions *only*, thus serving as a barrier between electrodes. It prevent the occurrence of short-circuit and thermal run aways while at the same time offering negligible resistance.

The cathode is the electrode usually made of metal oxides (ex.  $\text{LiCoO}_2$  or  $\text{LiMn}_2\text{O}_4$ ) [13,14,16,17] as shown in Figure 2.7.

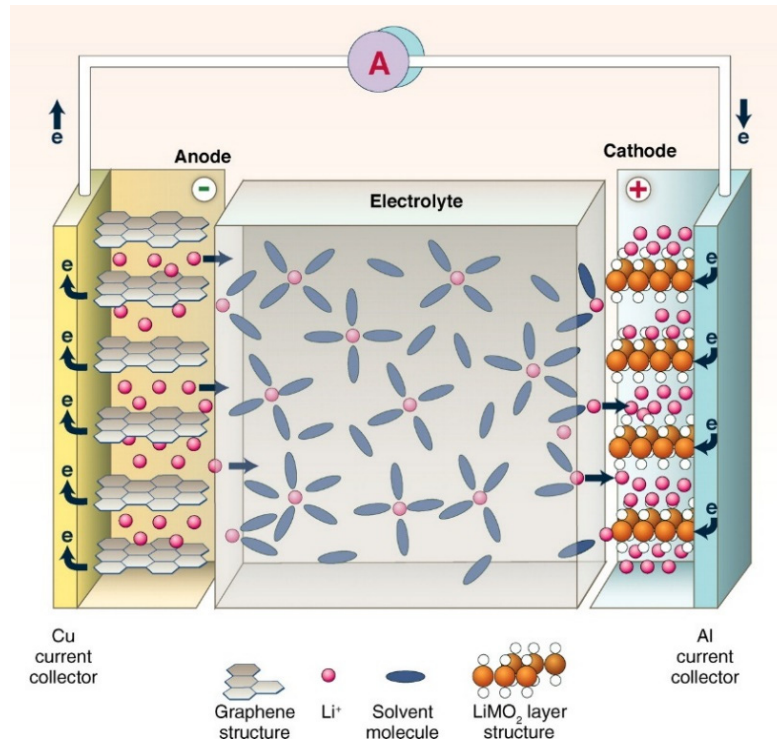


Figure 2.7 - Schematic representation of a Li-ion battery during discharging [7]

Under the presence of a load current, (Reduction – Oxidation) Redox reaction occurs. Oxidation reaction takes place at the anode where the trapped lithium particles start to deintercalate or diffuse toward the electrolyte-solid interface splitting lithium into ions and electrons. Lithium ions transfer through the solution due to the potential difference while the electrons moves through the current collector because the electrolyte solution acts as an electronic insulator [18]. Reduction reaction takes place at the cathode where the traveling lithium ions from the anode start to intercalate and react with the electrons coming from the positive collector. The process of lithium ion insertion into the electrode

happens without a change in the electrode crystal structure "intercalation" mechanism. The whole phenomenon of intercalation and deintercalation is reversible as lithium ions pass back and forth between the electrodes during charging and discharging [19,20,21]. In theory, this phenomenon could go on infinitely. Unfortunately, due to cell material degradation and other irreversible chemical reactions, the cell capacity and power degrades with the number of cycles and usage [5,14].

## 2.5. Battery Modelling

Battery modelling is an important and challenging consideration in battery management systems. In the literature, numerous battery models have been reported. The choice between these models is a trade-off between model complexity, accuracy, and parameterization effort. The models can be classified into four categories, starting from the most abstract to most detailed as shown in Figure 2.8. These categories are Ideal, Behavioral or Black-box, Equivalent circuit, and Electrochemical Models as follows.

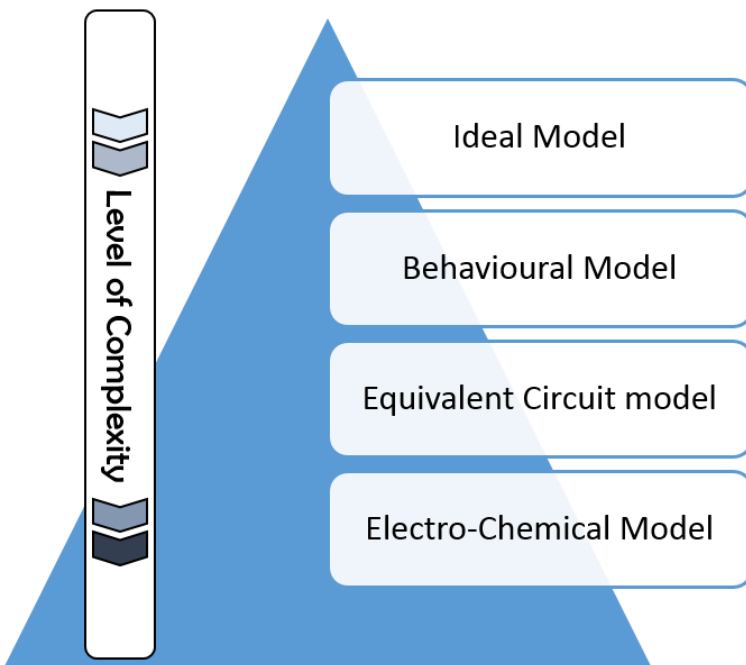


Figure 2.8 - Pyramid of details showing the level of details in each modeling category

### 2.5.1. Ideal Models

As the name suggests, the battery is represented as an ideal voltage source with unlimited power. These models are used only if the energy storage device (battery) is not of interest.

### 2.5.2. Behavioral and Black-box Models

Behavioral and Black-box Models simulate the terminal voltage behavior of the batteries without the need for the specification of the underlying physical or electrochemical behavior. These models consist of *phenomenological functions* that requires measured data to be used. Alternatively neural networks, empirical functions or look-up tables may be used. Peukert's law [22] is one of the first well-known examples of a behavioral model for batteries, where an empirical function is used to describe the dependence of the battery's remaining capacity on the discharge rate as follows.

$$I^{PC}t = \text{Constant} \quad (2.1)$$

Where,  $I$  is the discharge current,  $t$  is the maximum discharge time and  $PC$  is the Peukert's Coefficient which ranges from 1 to 2 [23]. The battery capacity can be calculated as follows [23]:

$$C_{n1} = C_n \left( \frac{I_n}{I_{n1}} \right)^{PC-1} \quad (2.2)$$

Where  $C_{n1}$  is the battery remaining capacity at the discharge current of  $I_{n1}$  [23].

Another form of behavioral model was introduced by Shepherd [24], to predict the terminal voltage during charging/discharging conditions as follows [25]:

$$E(t) = E_o + R_\alpha i(t) + \frac{K_1}{q_s(t)} \quad (2.3)$$

Where,  $E_o$  is the initial cell voltage,  $R_\alpha$  is the cell internal resistance,  $q_s(t)$  is the instantaneous stored charge, and  $K_1$  is a constant. A further modification was made to equation (2.3) by the Unnewehr model, [25]:

$$E(t) = E_o + R_\alpha i(t) + K_2 q_s(t) \quad (2.4)$$

Nernst introduced another two constants  $K_3$  and  $K_4$  which are used for curve fitting as follows [26]:

$$E(t) = E_o + R_\alpha i(t) + K_3 \ln\left(\frac{q_s(t)}{Q}\right) - K_4 \ln\left(\frac{Q - q_s(t)}{Q}\right) \quad (2.5)$$

Where,  $Q$  is the total charge capacity of the cell and the constants  $K_1$ ,  $K_2$ ,  $K_3$ , and  $K_4$  can be obtained by fitting experimental data [27].

Plett combined a series of behavioral models to simulate the battery operations [28,29,30]. Four models were discussed in his publication namely simple, zero-hysteresis, one-state hysteresis, and enhanced self-correcting (ESC). All of these were based on Peukert's and Shepherd's models. These models can account for cell hysteresis, polarization time constants, and ohmic loss effects [31]. Use of Artificial neural networks and fuzzy logic in modelling is discussed in [32]. Behavioral models can achieve accuracies of up to 2% [33,34].

### 2.5.3. Equivalent-Circuit Models

Lumped-element equivalent-circuit components such as resistors and capacitors can be used to represent the behavior of a battery cell [25]. They are widely applied because of their simplicity, low number of parameters to tune, and easy implementation [35,36]. They commonly consist of first-order, second-order, or third-order RC models in addition to the hysteresis effect [37]. The model parameters such as resistances and capacitances are calculated by system-identification using test data.

Present Battery Management Systems (BMS) rely on Equivalent circuit models due to their simplicity and robustness, which allow these models to be implemented in real time applications. However, they have limitations in providing insight into the electrochemical reactions that occur internally inside the cell. This limitation makes them unable to predict electrochemical phenomena like cell degradation, capacity fading, and power fading. In literature, these models also can be coupled or integrated with thermal models to predict the overall cell behavior as discussed in [38].

#### 2.5.4. Electro-Chemical Models

Electro-Chemical Models (ECM) or physics-based models can capture the electrochemical reactions using partial differential equations (PDE). This type of model links physical parameters to internal electrochemical dynamics of the cell allowing trade off analysis and high accuracy. A well-known early model with a high accuracy of 2% was originally developed by Doyle, Fuller and Newman [39,40]. Since electrochemical models use partial differential equations with typically numerous unknown parameters, they are significantly more complicated and computationally expensive than others, making their use in real-time applications for battery management systems (BMS) almost impractical. For real-time applications of ECM, model reduction is mandatory. Several approaches for ECM reduction have been proposed in literature. It was observed that much of the computational complexity involved in ECMs comes from solving PDEs for the lithium concentration in the solid particles of the electrodes (Spherical Diffusion). A common strategy is to make approximations and simplifications for this calculation [41]. Forman and Bashash in [42] have used the Padé approximation to match the power series representation of the solid diffusion equation to a desired order. This approach works well in matching the DC values, but does not perform well when the battery is subjected to high charging and discharging dynamic input currents existing due to sudden acceleration or regenerative braking action. Wang and Subramanian in [43,44] have used a parabolic profile to approximate the concentration throughout the solid particle, thus eliminating

the need for the spherical diffusion PDE. This approach works well at low discharge rates but does not perform well for high dynamic charge and discharge inputs such as those encountered in hybrid- and electric vehicle applications. Cai and White in [45] use *proper orthogonal decomposition*<sup>2</sup> at discrete locations within the solid particle and across the cell to find electrochemical variables. This approach works well at high currents. To generate an accurate Reduced Order Model (ROM) look-up tables with model parameters gathered from simulation or experimental data have been used [41]. However, a short coming of this approach is that model parameters supplied in look-up tables need to change as the battery ages, thus compromising model accuracy. In Kandler Smith's approach in [46,47], PDEs are used to model reductions for 2D-porous- electrodes. These are then linearized and a Laplace-domain transfer function is obtained. Optimization is then used for obtaining model parameters [48].

Electro-Chemical and thermal behavior are both considered in [49]. Here, the thermal energy equations are coupled to the electrochemical model by considering temperature-dependent physiochemical properties [50,51]. Electro-chemical models have also been used in literature to capture battery aging through SOH estimation as discussed in [52,53].

## 2.6. State of Charge (SOC) Determination

The Battery Management System (BMS) and the accurate estimation of State of Charge (SOC) have been researched extensively in the past decade. SOC estimation not only provides information on battery performance, but also reminds the user of the remaining useful energy in the battery. SOC estimation is considered in this section.

---

<sup>2</sup> Proper Orthogonal Decomposition (POD) is also named Principal component analysis (PCA), it is a mathematical procedure aims to obtain a compact representation from a set of data observations using the orthogonal transformation.

### 2.6.1. Discharge Test.

The Discharge test is the most reliable method for determining the State of Charge (SOC) of a battery cell. In this test, the cell is discharged under time and controlled conditions. The battery discharge time at controlled discharge rate indicates the value of SOC. This test requires consecutive recharging of the cell that is very time consuming. Also this test decreases the Remaining Useful Life (RUL) of the battery.

### 2.6.2. Ampere-Hour Counting

Ampere-hour counting technique is the most common technique for calculating the SOC. Since the battery discharge and recharge is directly related to the supplied and the withdrawn currents respectively, the idea of battery current balancing is applied as follows. If a starting ( $SOC_0$ ) is known, the value of the current integral is the direct indicator for the SOC. Such that:

$$SOC = SOC_0 - \frac{1}{C_n} \int_{t_0}^t I d\tau \quad (2.6)$$

Where  $C_n$  is the nominal capacity,  $I$  is the discharge current and  $SOC_0$  is the initial SOC value. Three main drawbacks of this method are:

1. Incorrect current measurement could result in a large error due to integration in equation (2.1).
2. Ampere-hour counting calculation is based on a predefined calibration point that may not always be available.
3. Not all of the current discharged from the battery can be taken into account because of losses.

The first drawback can be overcome by having an accurate sensor that is often expensive. The second drawback is solved by having a predefined calibration point. The third drawback can be eliminated by adding a constant correction charging factor ( $\eta_i$ ) to the

battery at each charge/discharge cycle, where the value of ( $\eta_i$ ) changes with the number of cycles to compensate for battery capacitance losses as follows:

$$SOC = SOC_0 - \frac{\eta_i}{C_n} \int_{t_0}^t I d\tau \quad (2.7)$$

The error in Ampere-hour counting can be maintained low by defining a correction factor and defining a re-calibration point [54].

The Ah counting (known as Coulomb counting) method [55] provides a higher accuracy than other SOC calculation methods. It is easy and reliable if the current measurement is accurate and if the re-calibration point is available.

### 2.6.3. Measurement of the Electrolyte Physical Properties

This method is used in lead-acid batteries. Here, a linear relationship between the electrolyte acid concentration and the SOC is established and used to determine the value of the SOC. A possible application of this method to batteries with liquid electrolyte is provided in [56].

### 2.6.4. Open Circuit Voltage (OCV)

This method is promising for applications where the battery is allowed to rest for long periods of time as the battery terminal voltage decays with time to the Open Circuit Voltage (OCV). SOC can then be inferred from the OCV via look-up tables. However, this method cannot be used for dynamic SOC estimation, and its accuracy is adversely affected by temperature variations and hysteresis. Since the rest periods occur from time to time; this technique can be used in addition to Ah counting. Such a combination allows the SOC to be calculated after a rest period using the OCV-SOC interrelation; this SOC can then be used as a re-calibration point for the Ah counting method [57].

## 2.6.5. Artificial Neural Network

SOC determination using Artificial Neural Networks (ANN) is discussed in details in [58,59,60]. Since artificial neural networks can establish an input/output relationship for non-linear complex systems, SOC and SOH can readily be obtained with ANNs. An ANN is composed of neurons that are interconnected together to form a relationship between the network's input and outputs as shown in Figure 2.9

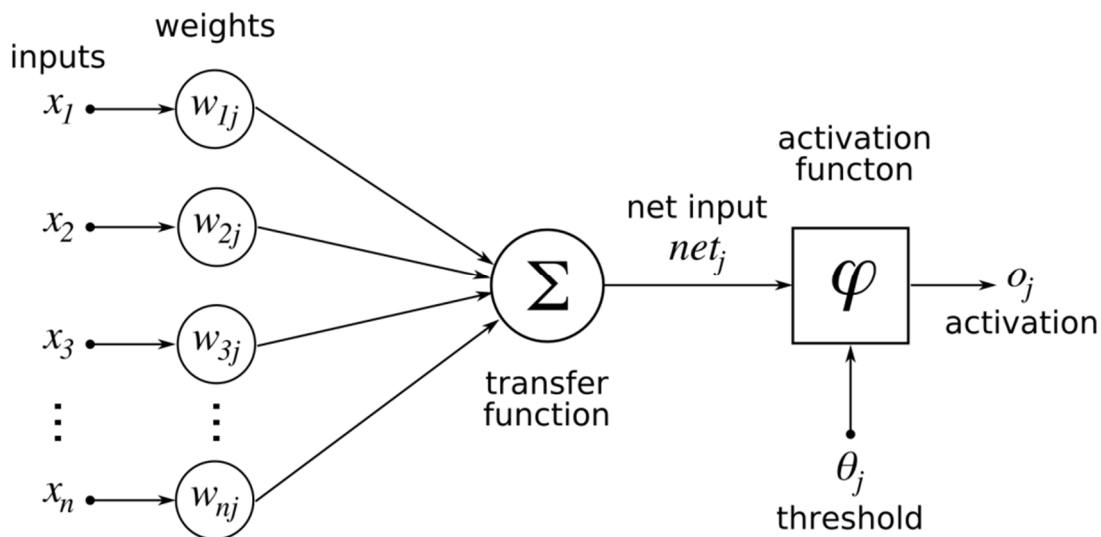


Figure 2.9 - Diagram of an Artificial Neuron [61]

$$net_j = x_1 w_{1j} + x_2 w_{2j} + x_3 w_{3j} + \dots + x_n w_{nj} + b \quad (2.8)$$

$$o_j = \varphi(net_j) \quad (2.9)$$

Where \$(x\_1, x\_2, x\_3, \dots, x\_n)\$ represent neuron inputs, their weights are \$(w\_{1j}, w\_{2j}, w\_{3j}, \dots, w\_{nj})\$, \$b\$ is bias and \$\varphi\$ denotes a nonlinear activation function.

ANN mimics the human brain and needs to be trained [62]. The techniques and algorithms used for training of the ANN are presented in [63]. A limitation of ANN is that it requires a large amount of data for training for all operating conditions and situations [64].

### 2.6.6. Impedance Spectroscopy

Electro-Chemical Impedance Spectroscopy (EIS) is widely discussed in literature [65,66,67]. It is based on establishing a baseline by measuring the cell impedances over a wide range of Alternating Current (AC) frequencies under different SOCs. SOC is inferred by measuring the cell impedance values and correlating them against baseline impedance for various SOC [68,69].

### 2.6.7. State Estimation Techniques

Any state estimation technique like Extended Kalman Filter (EKF) or smooth variable structure filter (SVSF) can be used to estimate the system's observable states. In the case of batteries, one of the system's states is the SOC. The above mentioned estimation methods require a model of the dynamic system. The EKF and the SVSF were applied to SOC estimation using six different battery models in [28,29,30,31] and delivered an estimation error of less than 5%.

## 2.7. Thermal Management Systems

Thermal management of lithium ion batteries is an important consideration. Battery overheating or thermal runaways could result in unsafe operating conditions with unwanted consequences. In order to keep the battery within its desired operating range the temperature of the cell core needs to be determined and monitored. Since the core temperature is difficult to measure, this temperature needs to be estimated [70]. Battery models also can be integrated with thermal models to form a more comprehensive approach to battery performance characterization [38,49].

## 2.8. Battery Aging Mechanisms for Li-Ion.

The phenomenon of battery aging is complex [71] and is affected by the battery operating conditions as shown in [72,73,74,75]. In literature, the aging has been mainly

defined as capacity or power fading to a predefined limit, where capacity fade is identified as loss of capacity [76] and power fade is identified as increase in the battery internal resistance [30]. The main reasons for aging are:

- Extreme Conditions: operating the battery under extreme conditions such as high temperature [72], high charging rates [77,78], or high SOC levels.
- Normal Conditions: aging can be caused due to battery storage (calendar aging) or usage (cycling aging). It is observed to be a result of several processes where performance degradation takes place due to irreversible chemical reactions [79].

## 2.9. Summary

Battery cell modeling and state of charge estimation are very important aspects that can improve the reliability of a vehicle is Battery Management System. This chapter provided an overview of battery terminologies and modeling strategies. A number of different battery modeling techniques were presented selecting between them is a trade-off between model complexity, accuracy, and parameterization. This chapter also discussed different SOC estimation techniques. The SOC determination using state estimation techniques is the focus of this thesis.

---

# State of Charge Estimation

---

In this chapter, estimation strategies for State of Charge (SOC) are discussed. A description of the evolution of SOC estimation techniques and strategies is considered. The application of various estimation techniques to estimate SOC in battery systems is presented. It is followed by simulation and experimental procedure used in model fitting and SOC estimation. Summary and conclusion are provided.

## 3.1. State and Parameter Estimation Theory

*“When the five senses fail to provide direct information, human beings rely on post-sensory cognitive function of the brain to interpret sensory inputs to derive new information. Fortunately for dynamic systems, this can be done more mathematically using modeling and state-estimation.” [1]*

Estimation is used to extract information from measurement signals. They are used in many fields such as target tracking, control, monitoring, filtering, signal/image processing, navigation, and communication [80].

Figure 3.1 depicts the estimation process, requiring access to input and output data.

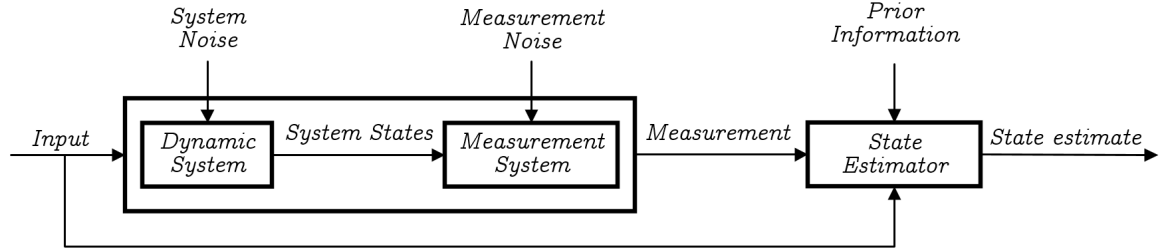


Figure 3.1 - State estimation – Overview

As shown in the above figure, in model-based estimations, information needed would typically include knowledge about:

- A dynamic model or functional representation.
- Probability distribution or upper bound for system and measurement noise.
- The prior information.

In any casual dynamic system (for example battery cell) as shown in Figure 3.1, the output (*Measurement*) is a function of the past and present *input*. The past input effect on the system are summarized in the *System States*. Measurements are typically a function of one or more state. In battery systems the system states may include SOC, hysteresis value, and value of polarization effects [28,29,30].

Discrete time state-space representation is commonly used in filtering for modelling of a system under consideration as follows:

$$x_{k+1} = A_k x_k + B_k u_k + \omega_k \quad (3.1)$$

$$y_k = C_k x_k + D_k u_k + v_k \quad (3.2)$$

Where  $x_k \in \mathbb{R}^{n \times 1}$  is the state vector,  $u_k \in \mathbb{R}^{p \times 1}$  is the input vector,  $y_k \in \mathbb{R}^{m \times 1}$  is the system output vector,  $\omega_k \in \mathbb{R}^{n \times 1}$  is the system noise, and  $v_k \in \mathbb{R}^{m \times 1}$  is the measurement noise.  $A_k \in \mathbb{R}^{n \times n}$ ,  $B_k \in \mathbb{R}^{n \times p}$ ,  $C_k \in \mathbb{R}^{m \times n}$ , and  $D_k \in \mathbb{R}^{m \times p}$  are the

system, input, measurement and feed through matrices. Equation (3.1) and (3.2) are the state and measurement equations. A commonly used method for obtaining the state vector from measurement is the Kalman Filter.

### 3.1.1. The Kalman Filter (KF)

R.E. Kalman first introduced Kalman Filter [81] in 1960 as an *optimal recursive model based data processing algorithm for linear filtering purposes*. Since then extensive research has been conducted on KF and its modified form for non-linear systems referred to as the Extended Kalman Filter (EKF). The Kalman filter is an optimal filter for linear Gaussian problems as it addresses the estimation problem through minimizing the Minimum Mean Square Error (MMSE) between the state estimate  $\hat{x}_k$  and the true state  $x_k$  given the measured input data and the observed output data. It's a model-based method derived in discrete time domain. The Kalman filter [82] can be summarized in two set of mathematical equations: time update equations (Predictor) and measurement update equations (Corrector) [80,81,83], as shown in Figure 3.2

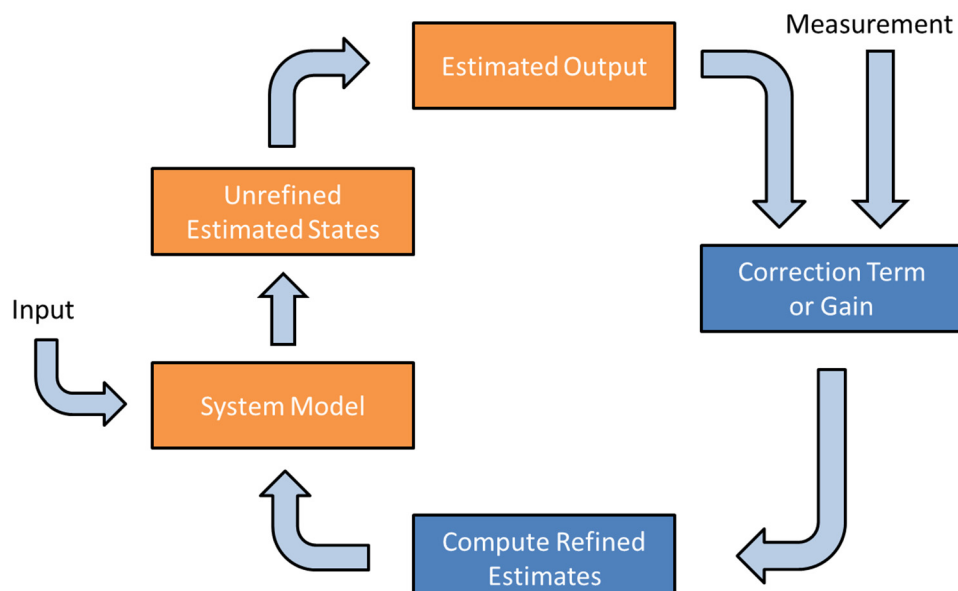


Figure 3.2 - Overview of Predictor-Corrector method [84]

Consider the discrete-time system defined by equation (3.1) and (3.2), where the variables  $\omega_k$  is the system noise, and  $v_k$  is the measurement noise. The KF assume that both  $\omega_k$  and  $v_k$  are independent of each other, and have zero mean Gaussian distribution as shown below:

$$p(\omega_k) \sim \mathcal{N}(0, Q_k) \quad (3.3)$$

$$p(v_k) \sim \mathcal{N}(0, R_k) \quad (3.4)$$

Where  $Q_k$  and  $R_k$  are the system and measurement noise covariance, respectively.

The KF is optimal if the system is linear, observable, and if  $\omega_k$  and  $v_k$  are white. The KF is a predictor corrector method that has two stages. The first stage involves a time update using the model for obtaining a prediction of the state vector referred to as the a priori state estimate  $\hat{x}_{k+1|k}$  such that:

$$\hat{x}_{k+1|k} = A\hat{x}_{k|k} + Bu_k \quad (3.5)$$

An error covariance estimate  $P_{k+1|k}$  for the a priori estimate is then calculated:

$$P_{k+1|k} = AP_{k|k}A^T + Q_k \quad (3.6)$$

Where k denotes the sample time.

The error covariance estimate provides an indication of the level of uncertainty in the state estimate and is used for error bounds calculation. “Large singular values” for  $P_{k+1|k}$  indicate a high level of uncertainty in our estimated state, while “small singular values” for  $P_{k+1|k}$  indicate a high level of confidence in our estimated state [30]. In the second stage, a corrective term is calculated using the measurement and what is referred to as the Kalman gain  $K_{k+1}$ , where:

$$K_{k+1} = P_{k+1|k} C^T (C P_{k+1|k} C^T + R_{k+1})^{-1} \quad (3.7)$$

A refined a posteriori state estimates  $\hat{x}_{k+1|k+1}$  is then calculated such that:

$$\hat{x}_{k+1|k+1} = \hat{x}_{k+1|k} + K_{k+1} (z_{k+1} - C \hat{x}_{k+1|k}) \quad (3.8)$$

The associated a posteriori error covariance estimate  $P_{k+1|k+1}$  is obtained as [85]:

$$P_{k+1|k+1} = (I - K_{k+1} C) P_{k+1|k} \quad (3.9)$$

The a posteriori state estimate  $\hat{x}_{k+1|k+1}$  effectively incorporates a knowledge of the measurement to correct or tune up the a priori estimate. A small value of Kalman gain  $K_{k+1}$  in equation (3.12) means a small error covariance matrix  $P_{k+1|k}$ , which means that more confidence should be placed on the a priori estimate. A high value on the other hand indicates that higher emphasis is placed on measurements. The Kalman Filter algorithm is summarized in Figure 3.3.

Time Update (Predictor)	Measurement Update (Corrector)
Predict the state ahead $\hat{x}_{k+1 k} = A \hat{x}_{k k} + B u_k$	Compute Kalman Gain $K_{k+1} = P_{k+1 k} C^T (C P_{k+1 k} C^T + R_{k+1})^{-1}$
Predict the error covariance ahead $P_{k+1 k} = A P_{k k} A^T + Q_k$	Update estimate with measurement $\hat{x}_{k+1 k+1} = \hat{x}_{k+1 k} + K_{k+1} (z_{k+1} - C \hat{x}_{k+1 k})$
	Update error covariance $P_{k+1 k+1} = (I - K_{k+1} C) P_{k+1 k}$

Figure 3.3 - Summary of Kalman Filter equations

Details about the optimality and derivation of the Kalman filter can be found in [81,86,80,83]. The assumption that the noise processes are white is rarely met in practical

applications. If this assumption is violated the Kalman filter will not be optimal and can become unstable [31,87,88].

### 3.1.2. The Extended Kalman Filter (EKF)

For non-linear systems the Extended Kalman Filter needs to be used. In the EKF the system model is linearized around the current a priori state estimate. The linearized model is then used for the calculation of the Kalman gain. In case of non-linear systems, let:

$$x_{k+1} = f(x_k, u_k) + \omega_k \quad (3.10)$$

$$y_k = g(x_k, u_k) + v_k \quad (3.11)$$

Where the first equation represents the state equation (3.15) and the second equation is the output equation (3.16), both  $\omega_k$  and  $v_k$  are assumed to be white noise, with zero mean and known covariance matrices ( $Q$ ) and ( $R$ ) respectively.

Similarly to the Kalman filter, the a priori estimates are obtained using the system model which in this case is as follows:

$$\hat{x}_{k+1|k} = f(\hat{x}_{k|k}, u_k) \quad (3.12)$$

$$P_{k+1|k} = F_k P_{k|k} F_k^T + Q_k \quad (3.13)$$

The system models is then linearized around  $\hat{x}_{k+1|k}$  such that:

$$F_k = \left. \frac{\partial f(x_k, u_k)}{\partial x_k} \right|_{x_k=\hat{x}_{k+1|k}} \quad (3.14)$$

$$H_k = \left. \frac{\partial g(x_k, u_k)}{\partial x_k} \right|_{x_k=\hat{x}_{k+1|k}} \quad (3.15)$$

The Kalman gain  $K_{k+1}$  is then calculated using the linearized model such that:

$$K_{k+1} = P_{k+1|k} G_{k+1}^T \left( G_{k+1} P_{k+1|k} G_{k+1}^T + R_{k+1} \right)^{-1} \quad (3.16)$$

The a posteriori estimates are then obtained as:

$$\hat{x}_{k+1|k+1} = \hat{x}_{k+1|k} + K_{k+1} \left( z_{k+1} - g(\hat{x}_{k+1|k}, u_k) \right) \quad (3.17)$$

$$P_{k+1|k+1} = (I - K_{k+1} G_{k+1}) P_{k+1|k} \quad (3.18)$$

The Extended Kalman Filter algorithm is summarized in Figure 3.4.

Time Update (Predictor)	Measurement Update (Corrector)
Predict the state ahead $\hat{x}_{k+1 k} = f(\hat{x}_{k k}, u_k)$	Compute Kalman Gain $K_{k+1} = P_{k+1 k} G_{k+1}^T \left( G_{k+1} P_{k+1 k} G_{k+1}^T + R_{k+1} \right)^{-1}$
Predict the error covariance ahead $P_{k+1 k} = F_k P_{k k} F_k^T + Q_k$	Update estimate with measurement $\hat{x}_{k+1 k+1} = \hat{x}_{k+1 k} + K_{k+1} \left( z_{k+1} - g(\hat{x}_{k+1 k}, u_k) \right)$
	Update error covariance $P_{k+1 k+1} = (I - K_{k+1} G_{k+1}) P_{k+1 k}$

Figure 3.4 - Summary of Extended Kalman Filter equations

The extended Kalman filter linearization may become unstable in the presence of uncertainties. A more robust estimation strategy for condition monitoring of batteries is the Smooth Variable Structure Filter (SVSF).

### 3.1.3. The Smooth Variable Structure Filter (SVSF)

Habibi proposed the smooth variable structure filter (SVSF) in 2007 [89]. The SVSF was initially inspired by the Variable Structure Filter (VSF) [90]. It is a model-based estimation strategy that is related to the sliding mode control (SMC) [89]. The SMC uses a discontinuous control signal to retain states on a desired trajectory while achieving robustness to disturbances and modeling uncertainties [91,92]. If a state is away from its desired trajectory, a switching gain is used to push the state again towards the desired trajectory in order to minimize the tracking errors. The SVSF can guarantee stability given bounded uncertainties [84].

The SVSF uses the same concept as SMC's switching action to correct state estimates [93]. The SVSF has a predictor-corrector structure as in KF. It can be applied to linear or non-linear systems and for both state and parameter estimation applications [89]. It is a model-based method that is robust to modelling uncertainties and noise [94,89]. The SVSF estimation concept is illustrated in Figure 3.5. It shows that the initial estimate is forced to converge to the actual state trajectory using the SVSF gain. The SVSF gain works by pushing the estimate back and forth along the actual state trajectory while retaining it in a region known as the existence subspace. The width of the existence subspace  $\beta$  is a time varying and is function of modeling uncertainties [89].

Given a non-linear system with a model given in equations (3.15) and (3.16). The a priori state estimate  $\hat{x}_{k+1|k}$  is obtained as:

$$\hat{x}_{k+1|k} = \hat{f}(\hat{x}_{k|k}, u_k) \quad (3.19)$$

The SVSF assumes that the measurement equation is linear such that:

$$z_k = C\hat{x}_{k+1|k} + v_k \quad (3.20)$$

An a priori estimate of the output vector  $\hat{z}_{k+1|k}$  is obtained from equation (3.20) as follows:

$$\hat{z}_{k+1|k} = C\hat{x}_{k+1|k} \quad (3.21)$$

The corresponding error is obtained as:

$$e_{z,k+1|k} = z_{k+1} - \hat{z}_{k+1|k} \quad (3.22)$$

Further to [89], the SVSF corrective term is:

$$K_{k+1}^{SVSF} = \hat{C}^+ (|e_{z,k+1|k}| + \gamma |e_{z,k|k}|) \circ \text{sat} \left( \frac{e_{z,k+1|k}}{\psi} \right) \quad (3.23)$$

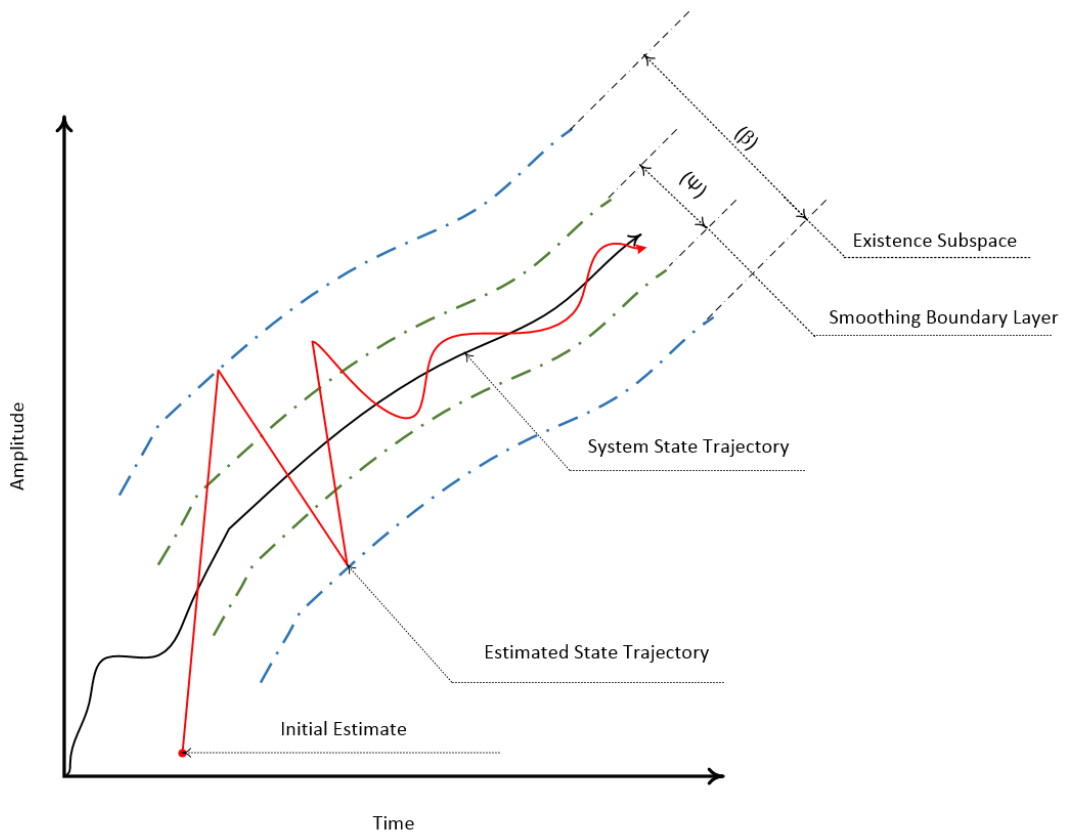


Figure 3.5 - SVSF estimation concept

The SVSF gain depends on: the a priori measurement errors  $e_{z,k+1|k}$ , the a posteriori measurement errors  $e_{z,k|k}$ , a smoothing boundary layer widths  $\psi$ , a constant  $\gamma$ , and an estimate of the measurement matrix  $\hat{C}$ . The SVSF gain is used for obtaining the a posteriori estimate as:

$$\hat{x}_{k+1|k+1} = \hat{x}_{k+1|k} + K_{k+1}^{SVSF} \quad (3.24)$$

The updated a posteriori measurement estimates  $\hat{z}_{k+1|k+1}$  and its corresponding error  $e_{z,k+1|k+1}$  are then calculated:

$$\hat{z}_{k+1|k+1} = C\hat{x}_{k+1|k+1} \quad (3.25)$$

$$e_{z,k+1|k+1} = z_{k+1} - \hat{z}_{k+1|k+1} \quad (3.26)$$

The SVSF process is summarized in Figure 3.6 and is repeated iteratively.

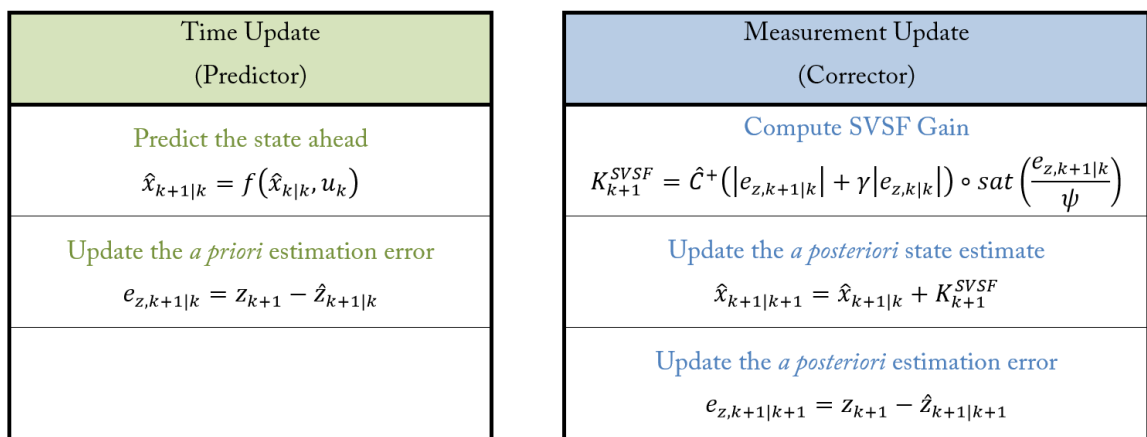


Figure 3.6 - Summary of Smooth Variable Structure Filter equations

According to [89], the SVSF estimation process is stable and will converge to the existence subspace during the reachability phase according to equation (3.27):

$$|e_{z_{k+1|k+1}}| < |e_{z_{k|k}}| \quad (3.27)$$

The SVSF proof yields the derivation of the SVSF gain from equation (3.27) as described in [89,95]. The proof of stability is discussed in [95].

### 3.2. State of Charge Estimation Application

An overview of two state and parameter estimation strategies that are used in this research (namely, the EKF and the SVSF) were presented. In this section, their use for condition monitoring of batteries is discussed. A battery condition monitoring system is depicted in Figure 3.7

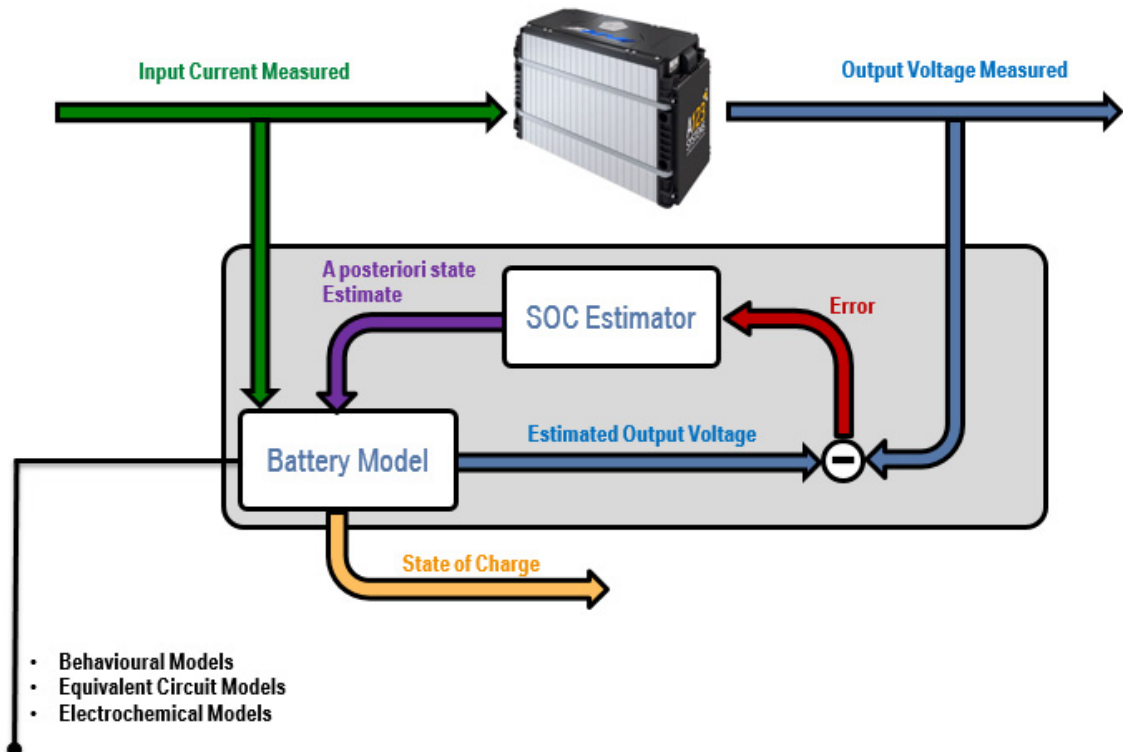


Figure 3.7 - Schematic diagram of state update

The battery has a single input (Current)  $u_k$ , and a measured output (Voltage)  $y_k$ . It has also has an internal states (such as SOC) represented by the state vector  $x_k$ . The condition monitoring systems proposed in this research were implemented by using both simulations and experimental studies conducted on lithium-ion battery cells.

### 3.3. Simulation and Experimental Cell Testing

In this research, a range of models for lithium-ion batteries and two estimation methods are used for state estimation. The models and the estimation strategies are then compared. Here a strategy and procedure for their fair comparison is defined. This comparison is made by using both simulated and experimental data. The advantage of including a simulated study is that all parameters are known and a known disturbance can be injected into the process for examining robustness to uncertainties.

#### 3.3.1. Simulation Experiment

Simulation data was gathered using the AVL CRUISE software platform. This software is a well-known vehicle and powertrain simulation tool. The electric vehicle model of Figure 3.8 was used. It consists of several blocks connected through a simulation algorithm. The simulated vehicle as published in [96] is shown in Figure 3.8 is a typical mid-size, front-wheel sedan with gross weight of 3500 lbs. and a top speed of 120 km/hr. The vehicle is powered by a 32kWh capacity lithium-ion battery pack which is liquid-cooled.

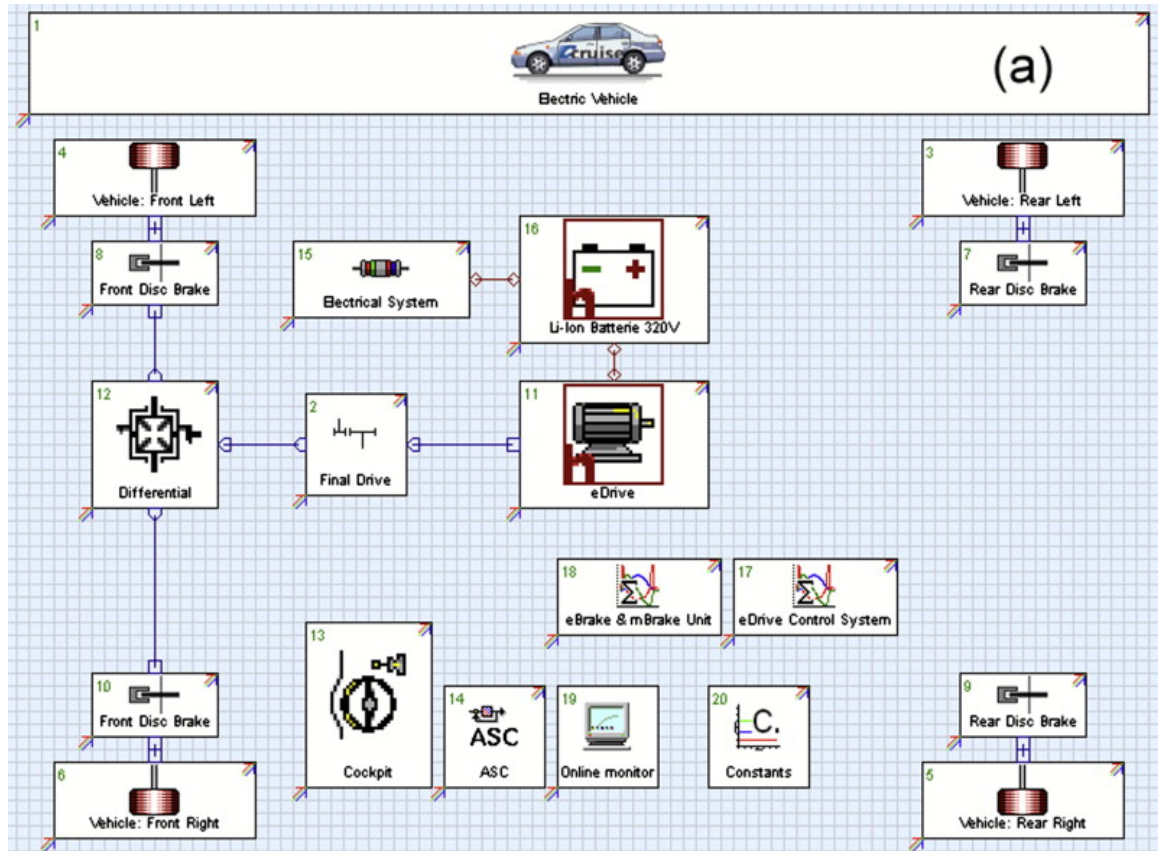


Figure 3.8 - AVL CRUISE Electric Vehicle model [96]

The drivetrain includes a traditional PID controller that maintains the speed of the vehicle at the desired speed and thus mapping the velocity profile to battery pack current supply requirement. Since all the models are designed for cell-level batteries, battery pack current is scaled down in order to obtain the applied current per cell. The AVL CRUISE vehicle model is equipped with regenerative braking capability so the battery is recharged on braking. The cell in the simulation has a nominal capacity of 7.5 Ah.

The driving cycle used in the simulation is the Urban Dynamometer Driving Schedule (UDDS). The vehicle components specifications are sized to meet the requirements of an Urban Dynamometer Driving Schedule (UDDS) cycle with maximum speed of 100 Km/hr. The vehicle speed profile is shown in Figure 3.9, and the battery scaled down cell current is shown in Figure 3.10.

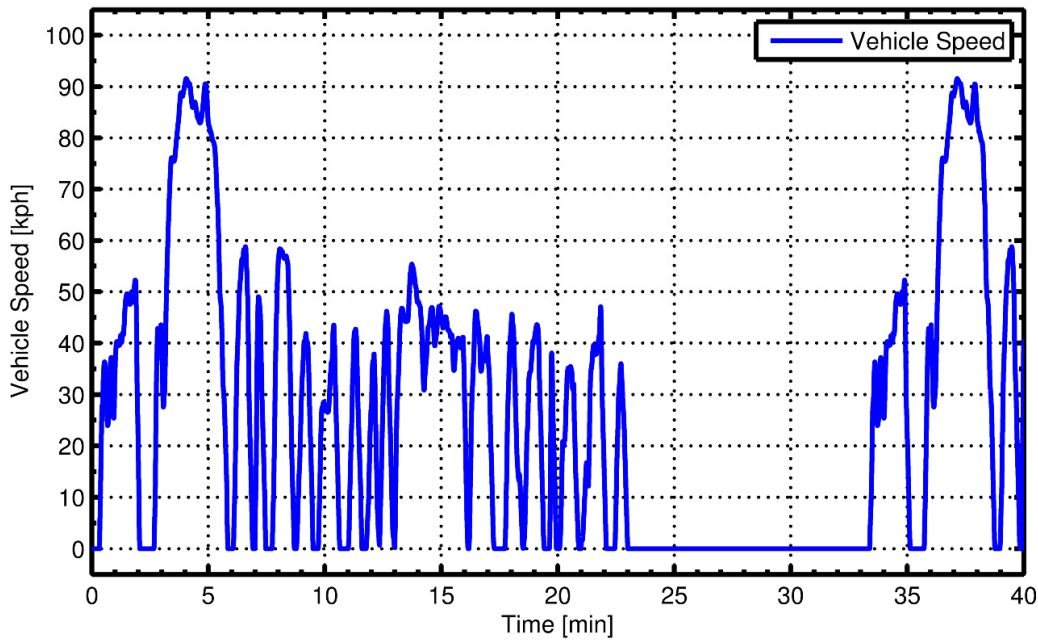


Figure 3.9 – Vehicle velocity profile [UDDS Cycle]

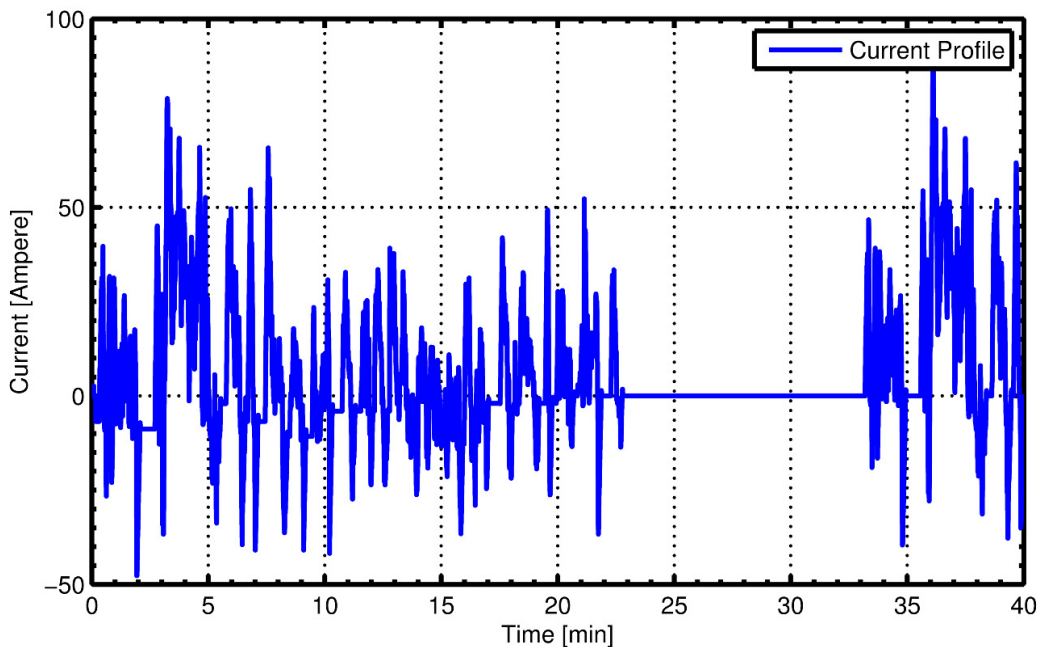


Figure 3.10 – Battery cell current profile [UDDS Cycle]

The simulation test cycle is a sequence of 2 urban dynamometer driving schedule (UDDS) cycles, separated by 0A (rest period) as shown in Figure 3.11. A relatively large operating range was selected for the battery testing (5% to 95% of the SOC) as shown in Figure 3.12.

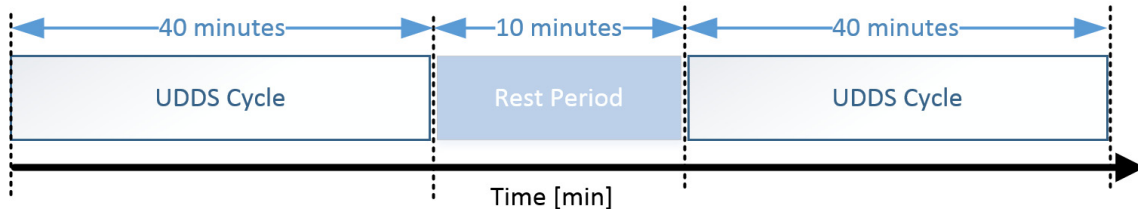


Figure 3.11 - Simulation test cycle sequence

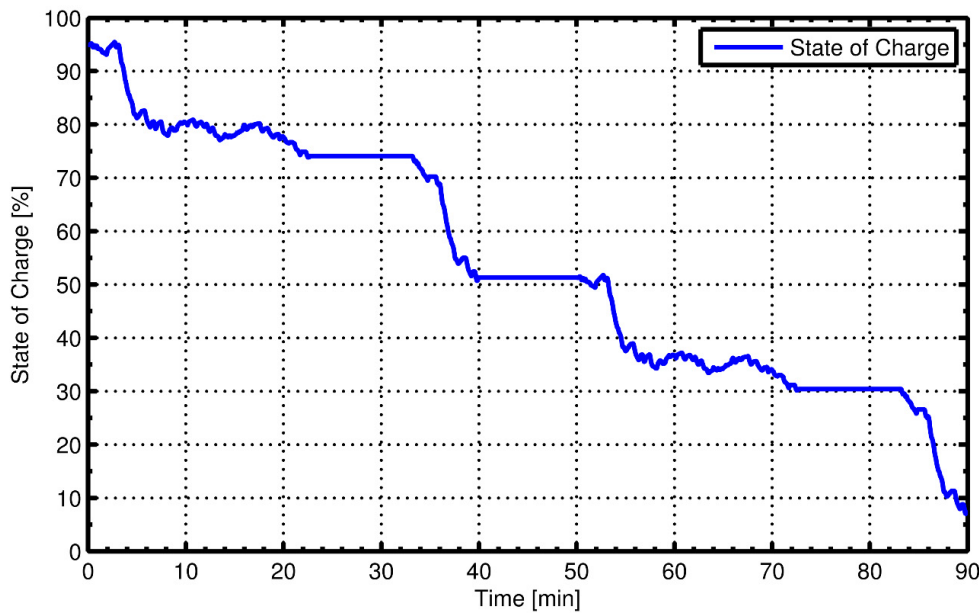


Figure 3.12 - SOC vs. Time [UDDS Test Sequence]

The overall current and terminal voltage for the test sequence can be seen in Figure 3.13 and Figure 3.14 respectively, where every peak in the current profile represent a sudden acceleration or declaration (regenerative breaking action) event.

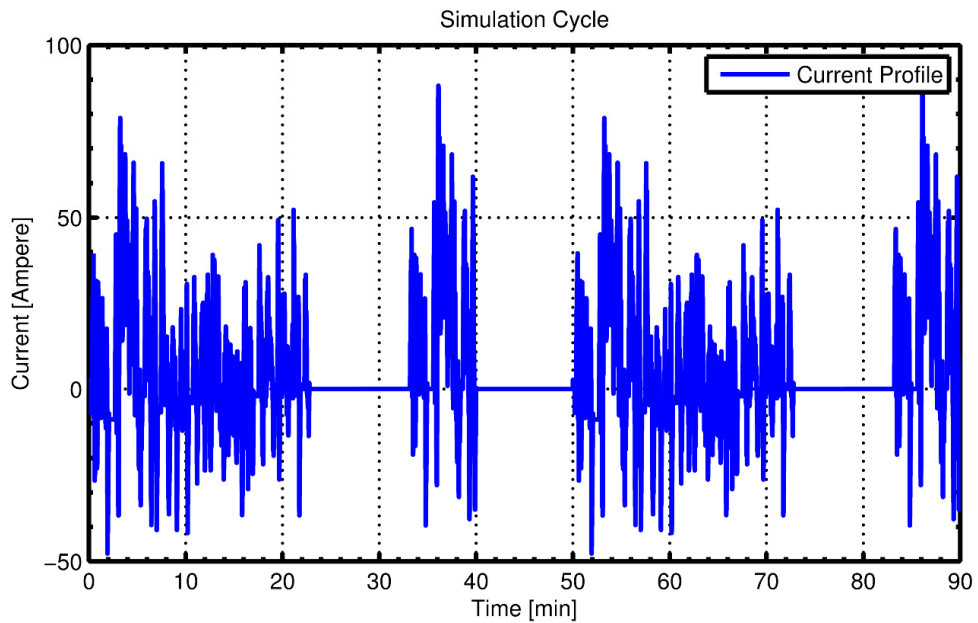


Figure 3.13 - Battery cell current profile [UDDS Test Sequence]

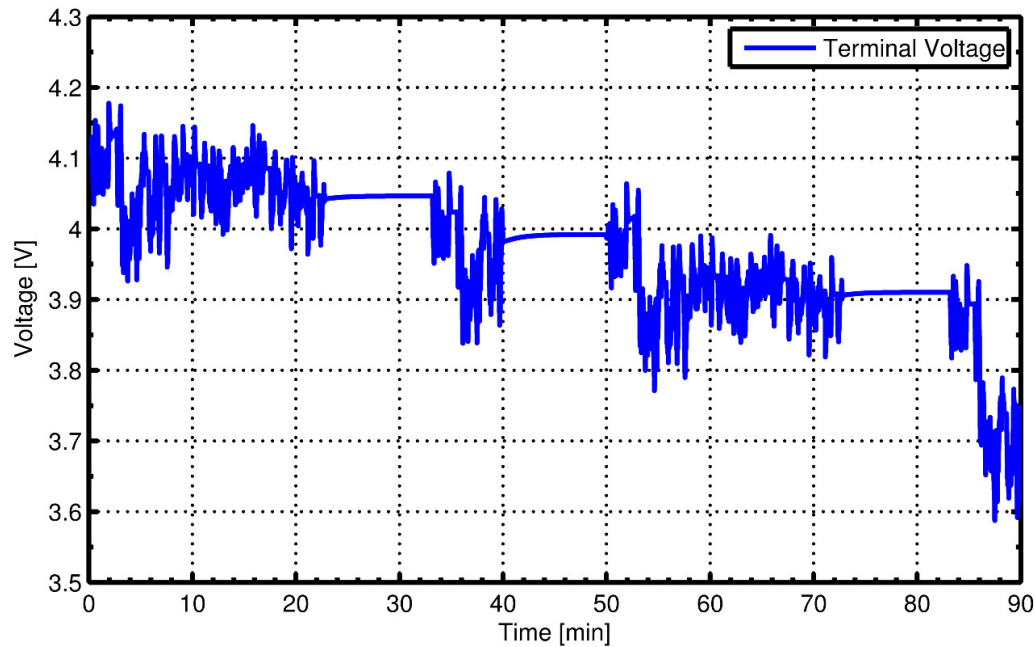


Figure 3.14 - Battery Cell terminal Voltage profile [UDDS Test Sequence]

Note that the decrease in the output voltage value overtime in Figure 3.14 is related to the discharging effect of the battery from 95% to 5% SOC.

### 3.3.2. Experimental Testing Cycle

An Experimental setup at the BMW<sup>3</sup> Electrical and Hybrid Research and Development Center Research and Development was used for battery testing. The battery was subjected to a full discharging cycle with the current profile shown in Figure 3.15. Battery cell nominal capacity was 20 Ah. The test were performed in a temperature controlled chamber at 25 degree celsius. The battery nominal voltage was 3.7 [V]. Due to proprietary nature of the experiment setup, some details are not provided.

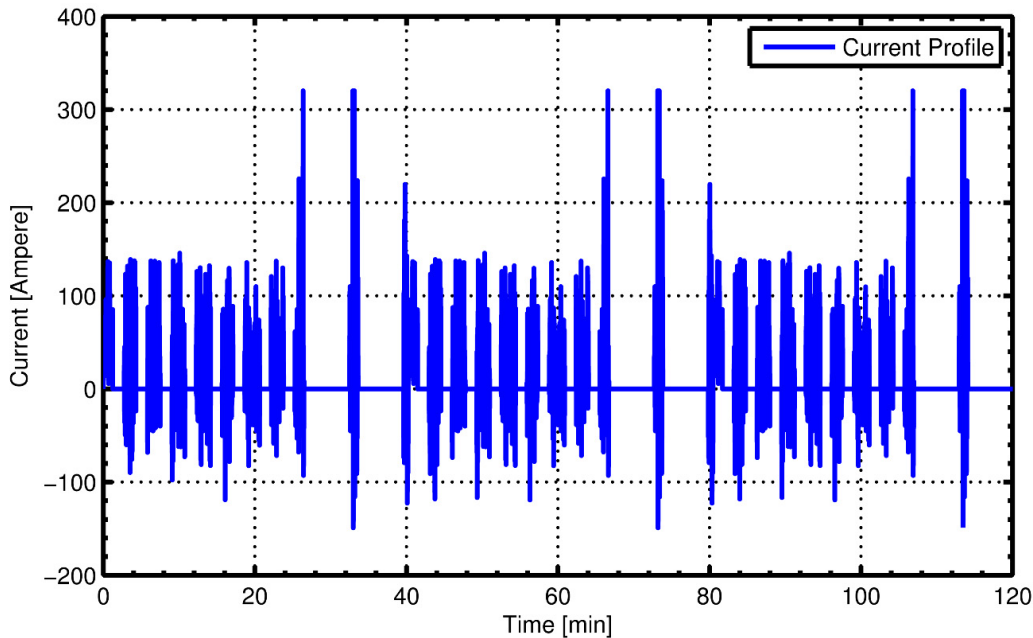


Figure 3.15 - Experimental battery current profile

Note that the degradation in output terminal voltage overtime is shown in Figure 3.17 and is related to the discharging of the battery from 100% to 0% SOC.

<sup>3</sup> BMW, Research and development center

Address: Dostlerstraße, 80809 Munich, Germany.

Website: [www.bmwgroup.com](http://www.bmwgroup.com)

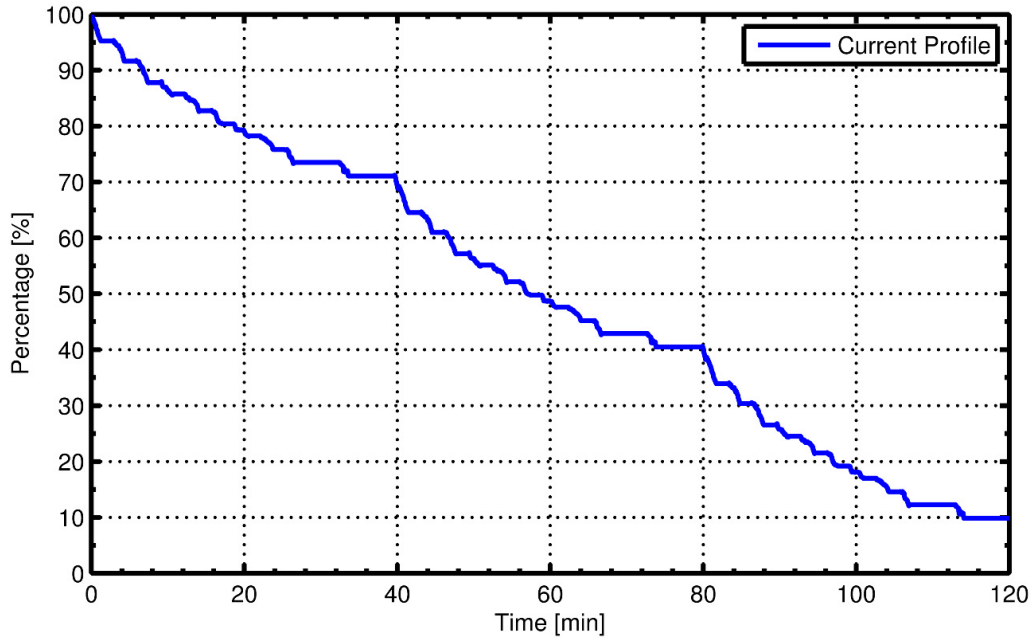


Figure 3.16 - Experimental battery SOC vs. Time profile

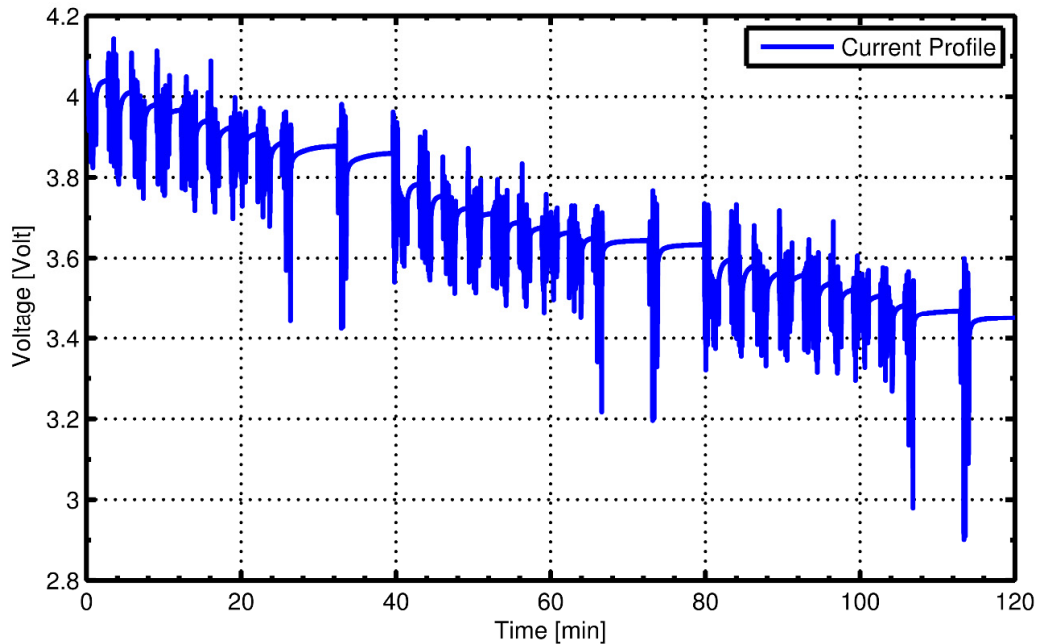


Figure 3.17 - Experimental Battery Terminal Voltage behavior

This simulation and Experimental data is used in the following chapters for comparing the models and estimations techniques. A quantitative measure used for comparison is the

root-mean-squared error (RMSE) for the estimated terminal voltage versus the measured or simulated battery voltage as given in equation (3.32)

$$RMSE = \sqrt{\frac{\sum_{t=0}^n ((y_t - \hat{y}_t)^2)}{n}} \quad (3.28)$$

### 3.4. Summary

Estimation theory is an important tool for SOC estimation. This chapter provided a comprehensive review of three estimation strategies (KF, EKF, and SVSF). The Kalman filter provides an optimal solution for linear problems under certain assumptions. If any of these assumption are violated, the KF yields sub-optimal results and can become unstable. The EKF is a modified version of the KF for non-linear system

This chapter also provided an overview of another methodology that is referred to as SVSF. The SVSF improves the robustness of the estimation process. The SVSF and the EKF implantations and comparisons with various battery models form the core of this thesis.

---

# **Behavioral Modelling**

---

In this chapter, Behavioral models of Lithium ion cell are reviewed. Introduction and a detailed discussion of the advantages and disadvantages of this modelling approach is provided. It is followed by an overview of battery modelling evolution and behavioral models of varying complexity. Summary and discussions are provided.

## **4.1. Introduction**

A number of Behavioral models for electrical batteries have been proposed with varying degrees of complexity. These models are empirical functions with parameters derived from measurements without any knowledge of the internal structure or material properties of batteries. This leads to very accurate models for the measured operating conditions, but with limited validity outside the measured conditions. Increasing the number of parameters makes it easier to fit the function output to battery measurements, but can result in over parameterization, that compromises the validity of the model beyond the regions considered, while increasing computational complexity.

## 4.2. Evolution of Behavioral Cell Models

In this section, several techniques available for Behavioral modelling of batteries are discussed. The models can range from having one state representing the SOC to models capable of capturing the battery hysteresis and relaxation effects during charging and discharging cycles.

### 4.2.1. Combined Model

The terminal voltage of the battery may be predicted in a number of different ways. One important method of predicting the voltage is based on the SOC. A number of models have been formulated and discussed in [97,98]. The following three are amongst the most popular [97,99]:

- Shepherd:  $y_k = E_0 - Ri_k - K_i/z_k$
- Unnewehr universal model:  $y_k = E_0 - Ri_k - K_i z_k$
- Nernst:  $y_k = E_0 - Ri_k + K_2 \ln(z_k) + K_3 \ln(1 - z_k)$

In these models,  $y_k$  is the cell terminal voltage,  $R$  is the cell internal resistance,  $K_i$  is the polarization resistance,  $z_k$  is the cell SOC, and  $K_1, K_2, K_3$  are constants chosen to fit the model to the data [97]. Note that all of these models may be used in a ‘combined model’ that performs better than individually models. A combined model proposed in [97] is defined by the following equations:

$$z_{k+1} = z_k - \left( \frac{\eta_i \Delta t}{C} \right) i_k \quad (4.1)$$

$$y_k = K_0 - Ri_k - \frac{K_1}{z_k} - K_2 z_k + K_3 \ln(z_k) + K_4 \ln(1 - z_k) \quad (4.2)$$

The unknown quantities in the model may be estimated using system identification [97]. For example, given a set of  $N$  cell input-output parameters  $(y_k, i_k, z_k)$ , the values may be solved by using least squares estimation [97]. A Simple offline (batch) processing method

for parameter calculation can be carried out as follows. Let the output vector  $Y$  be defined as:

$$Y = [y_1, y_2, y_3, \dots, \dots, y_N]^T \quad (4.3)$$

An output matrix  $H$  is then defined:

$$H = [h_1, h_2, h_3, \dots, \dots, h_N]^T \quad (4.4)$$

The rows in matrix  $H$  are:

$$h_j^T = \left[ 1, i_j^+, i_j^-, \frac{1}{z_j}, z_j, \ln(z_j), \ln(1 - z_j) \right] \quad (4.5)$$

Where  $i_j$  is the battery current,  $i_j^+$  is the charging current, and  $i_j^-$  is the discharging current and can be calculated as follows:

$$\begin{aligned} i_j^+ &= i_j & \text{if } i_j > 0 \\ i_j^- &= i_j & \text{if } i_j < 0 \\ \text{else } i_j^+ &= i_j^- = 0 \end{aligned} \quad (4.6)$$

Then  $Y = H\theta$ , where  $\theta^T = [k_0, R^+, R^-, k_1, k_2, k_3, k_4]$  is the parameter vector with unknown elements. By using least-squares estimation, the parameters in  $\theta$  are obtained as:

$$\theta = (H^T H)^{-1} H^T Y. \quad (4.7)$$

#### 4.2.2. Simple Model

As presented in [97], obtaining the parameters values for the combined model. The model may be divided into two additive parts: one depending only on the SOC ( $z_k$ ), and the other depending only on the current ( $i_k$ ). This yields two equations:

$$f(z_k) = K_0 - \frac{K_1}{z_k} - K_2 z_k + K_3 \ln(z_k) + K_4 \ln(1 - z_k) \quad (4.8)$$

$$f(i_k) = R i_k \quad (4.9)$$

Where,

$$y_k = f(z_k) - f(i_k) \quad (4.10)$$

As explained in [97], all the parameters in equation (4.8) are SOC dependent so decreasing the number of parameters in combined model for easier implementation can be as follows:

$$z_{k+1} = z_k - \left( \frac{\eta_i \Delta t}{C} \right) i_k \quad (4.11)$$

$$y_k = OCV(z_k) - R i_k \quad (4.12)$$

where  $OCV$  refers to the open circuit voltage, the OCV curve is assumed to be the average of the charge and discharge curves taken at low currents (C/20) or (C/25) from fully charged to fully discharged. Use of low charging and discharging minimize the cell dynamics. A Simple offline (batch) processing method for parameter calculation can be carried out as follows. Let the output vector  $Y$  be defined as:

$$Y = [y_1, y_2, y_3, \dots, y_N]^T \quad (4.13)$$

An output matrix  $H$  is then defined:

$$H = [h_1, h_2, h_3, \dots, h_N]^T \quad (4.14)$$

The rows in matrix H are:

$$h_j^T = [i_j^+, i_j^-] \quad (4.15)$$

Where  $i_j$  is the battery current,  $i_j^+$  is the charging current, and  $i_j^-$  is the discharging current and can be calculated as follows:

$$\begin{aligned} i_j^+ &= i_j \text{ if } i_j > 0 \\ i_j^- &= i_j \text{ if } i_j < 0 \\ \text{else } i_j^+ &= i_j^- = 0 \end{aligned} \quad (4.16)$$

Then  $Y = H\theta$ , where  $\theta^T = [R^+, R^-]$  is the parameter vector with unknown elements. By using least-squares estimation, the parameters in  $\theta$  are obtained as:

$$\theta = (H^T H)^{-1} H^T Y. \quad (4.17)$$

### 4.2.3. Zero-State Hysteresis Model

An important concept that is ignored by the previous two models is the hysteresis. The hysteresis affects the SOC estimation since after discharging, the cell voltage relaxes to a value less than the true OCV. Conversely, after charging, the cell voltage relax to a value higher than the true OCV. For improved SOC estimation, the hysteresis should be considered as described in [97]. In this model a term is added to the output equation to map the memory effect of the hysteresis. However, no extra state is added for the hysteresis. A basic model of hysteresis involves simply adding a term to the output equation (2.2.4) as follows:

$$z_{k+1} = z_k - \left( \frac{\eta_i \Delta t}{C} \right) i_k \quad (4.18)$$

$$y_k = OCV(z_k) - Ri_k - s_k M(z_k) \quad (4.19)$$

Where  $s_k$  represents the sign of the current (including a memory effect during a rest period). For some sufficiently small and positive value  $\varepsilon$ , one has:

$$s_k = \begin{cases} +1 & i_k > \varepsilon \\ -1 & i_k < -\varepsilon \\ s_k - 1 & |i_k| \leq \varepsilon \end{cases} \quad (4.20)$$

Also, note that  $M(z_k)$  is half the difference between the charge and discharge values (i.e., average between the discharging and charging curve) [97]. Typically, the value for  $M$  can be assumed constant. As per [97], the zero-state hysteresis model is an improvement over the simple model, but only crudely approximates the underlying phenomenon. Whereas the level of hysteresis slowly changes as the cell is charged or discharged, the model estimates hysteresis as immediately flipping between its maximum positive and negative values when the sign of current changes. A Simple offline (batch) processing method for parameter calculation can be carried out as follows. Let the output vector  $Y$  be defined as:

$$Y = [y_1, y_2, y_3, \dots, \dots, y_N]^T \quad (4.21)$$

An output matrix  $H$  is then defined:

$$H = [h_1, h_2, h_3, \dots, \dots, h_N]^T \quad (4.22)$$

The rows in matrix  $H$  are:

$$h_j^T = [i_j^+, i_j^-, s_j] \quad (4.23)$$

Using  $\mathbf{Y} = \mathbf{H}\theta$ , where  $\theta^T = [R^+, R^-, M]$  is the parameter vector with unknown elements. By using least-squares estimation, the parameters in  $\theta$  are obtained as:

$$\theta = (\mathbf{H}^T \mathbf{H})^{-1} \mathbf{H}^T \mathbf{Y}. \quad (4.24)$$

#### 4.2.4. One-State Hysteresis Model

One of the drawbacks in the Zero-State Hysteresis model is that the hysteresis effect is added as a constant in the output equation. However, the hysteresis has a slow transition which can be modelled by adding a ‘hysteresis state’ to the model to capture the change in the hysteresis value. Suppose that  $h(z, t)$  is the hysteresis voltage as a function of SOC and time, then as shown in [97]:

$$\frac{dh(z, t)}{dz} = \beta sgn(\dot{z})[M(z, \dot{z}) - h(z, t)] \quad (4.25)$$

Where  $M(z, \dot{z})$  is a function that gives the maximum hysteresis value as a function of SOC and the rate-of-change of SOC. The term  $M(z, \dot{z}) - h(z, t)$  states that the rate-of-change of hysteresis voltage is proportional to the distance away from the main hysteresis loop; leading to a type of voltage decay in the major loop. The term  $\beta$  is considered positive and constant; and affects the rate of voltage decay. The sign function forces the equation to be stable for both charging and discharging [97]. However to add the hysteresis effect to the model, equation (3.22) needs to be transferred from being a differential equation in SOC to be a differential equation in the time domain by multiplying both sides of the equation by  $\frac{dz}{dt}$ .

Equation (3.22) becomes:

$$\frac{dh(z, t)}{dz} \times \frac{dz}{dt} = \beta sgn(\dot{z})[M(z, \dot{z}) - h(z, t)] \times \frac{dz}{dt} \quad (4.26)$$

It should be noted that  $\frac{dz}{dt}$  can be calculated as the differentiation of equation (3.1):

$$\frac{dz}{dt} = -\left(\frac{\eta_i}{C}\right)i(t) \quad (4.27)$$

With:

$$\dot{z}sgn(\dot{z}) = |\dot{z}| \quad (4.28)$$

By substituting equations (3.24) and equations (3.25) to equations (2.23), then:

$$h(t) = -\left|\frac{\eta_i i(t)\beta}{C_n}\right| h(t) + -\left|\frac{\eta_i i(t)\beta}{C_n}\right| M(z, \dot{z}) \quad (4.29)$$

Equation (3.26) can then be discretized as shown in [97]:

$$h_{k+1} = \exp\left(-\left|\frac{\eta_i i(t)\beta}{C_n}\right|\right) h_k + \left(1 - \exp\left(-\left|\frac{\eta_i i(t)\beta}{C_n}\right|\right)\right) M(z, \dot{z}) \quad (4.30)$$

As shown above, this equation is a linear time varying model as the states and the input change with current  $i_k$  and hence with time. The overall state-space model for the one-state hysteresis model is obtained as [97]:

$$\begin{bmatrix} h_{k+1} \\ z_{k+1} \end{bmatrix} = \begin{bmatrix} F(i_k) & 0 \\ 0 & 1 \end{bmatrix} \begin{bmatrix} h_k \\ z_k \end{bmatrix} + \begin{bmatrix} 0 & 1 - F(i_k) \\ -\frac{\eta_i \Delta t}{C} & 0 \end{bmatrix} \begin{bmatrix} i_k \\ M(z, \dot{z}) \end{bmatrix} \quad (4.31)$$

$$y_k = OCV(z_k) - Ri_k + h_k \quad (4.32)$$

Where:

$$F(i_k) = \exp\left(-\left|\frac{\eta_i i(t)\beta}{C_n}\right|\right) \quad (4.33)$$

The parameters vector to be optimized for this model is  $\theta = [R^+, R^-, M^+, M^-, \gamma]^T$ .

#### 4.2.5. Enhanced Self-Correcting Model (2-States)

The enhanced self-correcting (ESC) battery model represents one of the most accurate currently being used models for battery SOC estimation. This model can accurately capture battery dynamics and can thus be implemented in a vehicle BMS as it accommodates for hysteresis, polarization time constants, and ohmic losses. One of its major drawbacks in the previous model considered in section 4.2.4 is the relaxation effect as described by Plett in [97]. Relaxation effect can be defined as the phenomena that takes place when the battery is subjected to pulsed input current, as it takes time for the voltage to completely settle to a steady state value, while the same phenomena happens when the battery is allowed to rest and the voltage takes time to converge to the rest voltage (OCV). These time constants should be included in our model to capture the dynamics that take place in an electric vehicle applications. This model is required to:

- Force the output voltage  $y_k$  to converge to  $OCV + h_k$  after a rest period.
- Force the output voltage  $y_k$  to converge to  $OCV + h_k - Ri_k$  after a period of constant charging or discharging

To meet these requirements while taking care of the hysteresis effect, the output equation of the model should be in a form that allows it to capture the dc gain (bias) and the fast variations also as shown in [28,97,30]:

$$y_k = OCV(z_k) + h_k + filt(i_k) - Ri_k \quad (4.34)$$

Where the filter '*filt(.)*' design must be enforced to satisfy the both requirements listed above. The first requirement could be fulfilled by implementing a stable linear filter, while the second one can be fulfilled by a linear filter with zero DC gain. A state space representation for a low-pass filter can be in the following form:

$$f_{k+1} = A_f f_k + B_f i_k \quad (4.35)$$

$$y_k^f = G f_k \quad (4.36)$$

Where  $f_k$  is the filter state vector at a discrete time steps k,  $i_k$  is the input vector,  $y_k^f$  is the filter output vector,  $A_f$  is the state transition matrix and it determines the poles and resonant modes (stability) of the dynamic system.

The filter stability is ensured if the poles of the  $\max|eig(A_f)| < 1$ . In other words, by considering  $A_f = diag(\alpha)$ , then stability is achieved if all  $-1 < \alpha_j < 1$ . However, the matrix  $B_f$  should be chosen with taking care of not having any zero entry [28,97,30]. After investigating the stability, it is guaranteed that  $y_k$  will tend to  $OCV(z_k) + h_k$  during rest conditions. The two constants  $g_1, g_2$  can be calculated by equation (3.33) as shown in [97] to ensure zero dc-gain of the filter, so that  $y_k$  will tend to  $OCV(z_k) - Ri_k + h_k$  during constant current profiles.

$$g_n = \sum_{k=1}^n g_k \frac{(1 - \alpha_n)}{(1 - \alpha_k)} \quad (4.37)$$

The ESC with two filter states model in the state space form is as follows [97]:

$$\begin{bmatrix} f_{1,k+1} \\ f_{2,k+1} \\ h_{k+1} \\ z_{k+1} \end{bmatrix} = \begin{bmatrix} \alpha_1 & 0 & 0 & 0 \\ 0 & \alpha_2 & 0 & 0 \\ 0 & 0 & F(i_k) & 0 \\ 0 & 0 & 0 & 1 \end{bmatrix} \begin{bmatrix} f_{1,k} \\ f_{2,k} \\ h_k \\ z_k \end{bmatrix} + \begin{bmatrix} 1 & 0 \\ 1 & 0 \\ 0 & (1 - F(i_k)) \\ -\frac{\eta_i \Delta t}{C} & 0 \end{bmatrix} \begin{bmatrix} i_k \\ M(z, \dot{z}) \end{bmatrix} \quad (4.38)$$

$$y_k = OCV(z_k) - Ri_k + h_k + g_1 f_{1,k} + g_2 f_{2,k} \quad (4.39)$$

Where  $z_k$  is the state of charge,  $f_k$  is the states of the low pass filter on  $i_k$  which is used to characterize the polarization time constants,  $h_k$  is the state representing charging or discharging hysteresis effect,  $OCV$  is the open circuit voltage,  $C$  is the battery nominal capacity,  $R$  is the battery internal resistance,  $G$  is the output matrix of the low pass filter, and  $\alpha_i$  are the poles of the low pass filter. This model contains two inputs as follows:  $i_k$  is the battery input current and  $M(z, \dot{z})$ , that is the maximum polarization due to hysteresis. The model has one output  $y_k$ , which is the terminal voltage. The parameters vector to be optimized for this model is  $\theta = [R^+, R^-, g_1, \beta_1, \beta_2, M^+, M^-, \gamma]^T$ . Where  $\beta_n = \tanh(\alpha_n)$  and  $\alpha_n$  is the vector of the filter pole locations. The tanhfunction is used to force the pole location to be within the unity circle of stability  $\pm 1$  (i.e. stable system).

#### 4.2.6. Enhanced Self-Correcting Model (4-States)

The enhanced self-correcting (ESC) model is a two states model. System dynamics can be captured better by increasing the number of states to four states [97]. The resulting ESC model in the state space form is as follows:

$$\begin{bmatrix} f_{1,k+1} \\ f_{2,k+1} \\ f_{3,k+1} \\ f_{4,k+1} \\ h_{k+1} \\ z_{k+1} \end{bmatrix} = \begin{bmatrix} \alpha_1 & 0 & 0 & 0 & 0 & 0 \\ 0 & \alpha_2 & 0 & 0 & 0 & 0 \\ 0 & 0 & \alpha_3 & 0 & 0 & 0 \\ 0 & 0 & 0 & \alpha_4 & 0 & 0 \\ 0 & 0 & 0 & 0 & F(i_k) & 0 \\ 0 & 0 & 0 & 0 & 0 & 1 \end{bmatrix} \begin{bmatrix} f_{1,k} \\ f_{2,k} \\ f_{3,k} \\ f_{4,k} \\ h_k \\ z_k \end{bmatrix} + \begin{bmatrix} 1 & 0 \\ 1 & 0 \\ 1 & 0 \\ 1 & 0 \\ 0 & (1 - F(i_k)) \\ -\frac{\eta_i \Delta t}{C} & 0 \end{bmatrix} \begin{bmatrix} i_k \\ M(z, \dot{z}) \end{bmatrix} \quad (4.40)$$

$$y_k = OCV(z_k) - Ri_k + h_k + g_1 f_{1,k} + g_2 f_{2,k} + g_3 f_{3,k} + g_4 f_{4,k} \quad (4.41)$$

Where the parameters vector to be optimized for this model is  $\theta = [R^+, R^-, g_1, g_2, g_3, \beta_1, \beta_2, \beta_3, \beta_4, M^+, M^-, \gamma]^T$ .

### 4.3. Model Parameter Tuning

The first three models (Combined Model, Simple Model, and Zero State Hysteresis Model) in this chapter are “linear with respect to their parameters”. This makes identifying the values of the model parameters straightforward using least squares estimation, where the parameters can be obtained by equation (4.7).

When the model is not linear in parameters as in (One State Hysteresis and Enhanced self-correcting models), the least squares estimation cannot be used. A Matlab Global Optimization Toolbox called the Generalized Pattern Search (GPS) algorithm is used to calculate the model parameters. GPS algorithm is a pattern search algorithms that computes a sequence of points that approach an optimal point. At each step, the

algorithm searches a set of points, called a mesh, around the current point—the point computed at the previous step of the algorithm. The mesh is formed by adding the current point to a scalar multiple of a set of vectors called a pattern. If the pattern search algorithm finds a point in the mesh that improves the objective function at the current point, the new point becomes the current point at the next step of the algorithm.

GPS algorithm is used to optimize model parameters by calculating the best value for the parametric vector  $\theta$  to minimize a cost function. The GPS cost function is the Root-Mean-Squared Error (RMSE) in predicting the terminal voltage. The stopping criterion adopted is based on the difference the fitness value of the cost function (i.e., RMSE between the measured and simulated voltage) at two consecutive steps (i.e., step  $t$  and  $t+1$ ). The threshold value of this change is chosen to be 1e-06. The number of iterations changes from one model to another. The GPS requires a lower bounds, upper bounds and initial starting point of the elements of the parametric vector  $\theta$ . The starting point is usually randomly selected. The GPS' output is the optimized parametric vector  $\theta$ .

The measured and simulated currents and voltages are the inputs. The simulation data are shown in Figure 4.1 and Figure 4.2 are used for calculating the model parameters. In case of experimental results the data are shown in Figure 4.3 and Figure 4.4. These date are used for model parameter identification and represent approximately 25%, the renaming 75% are used for validating the model.

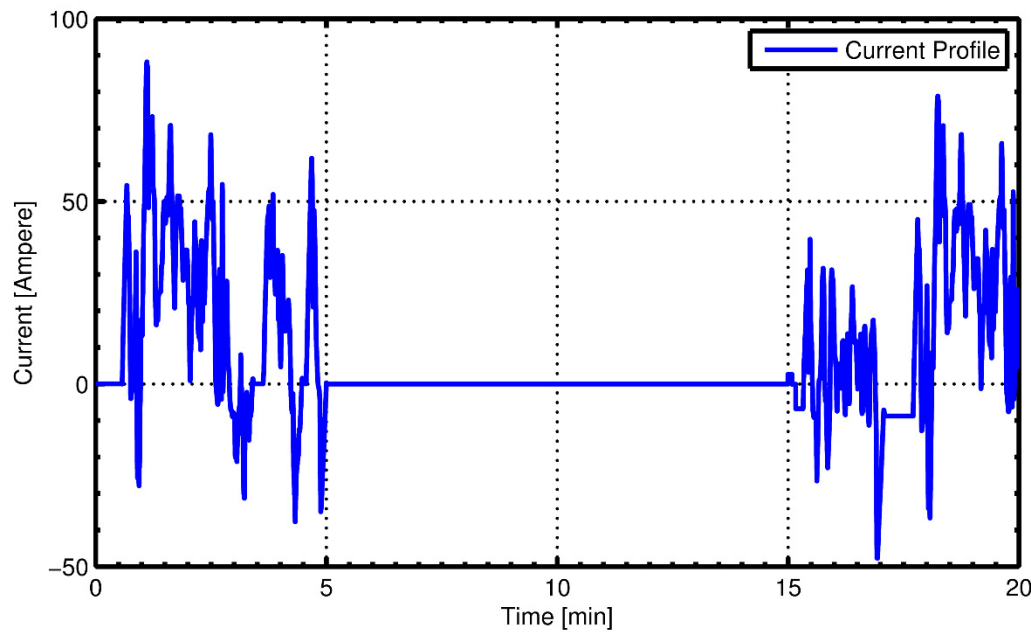


Figure 4.1 – Simulation battery cell current profile [UDDS Test Sequence]

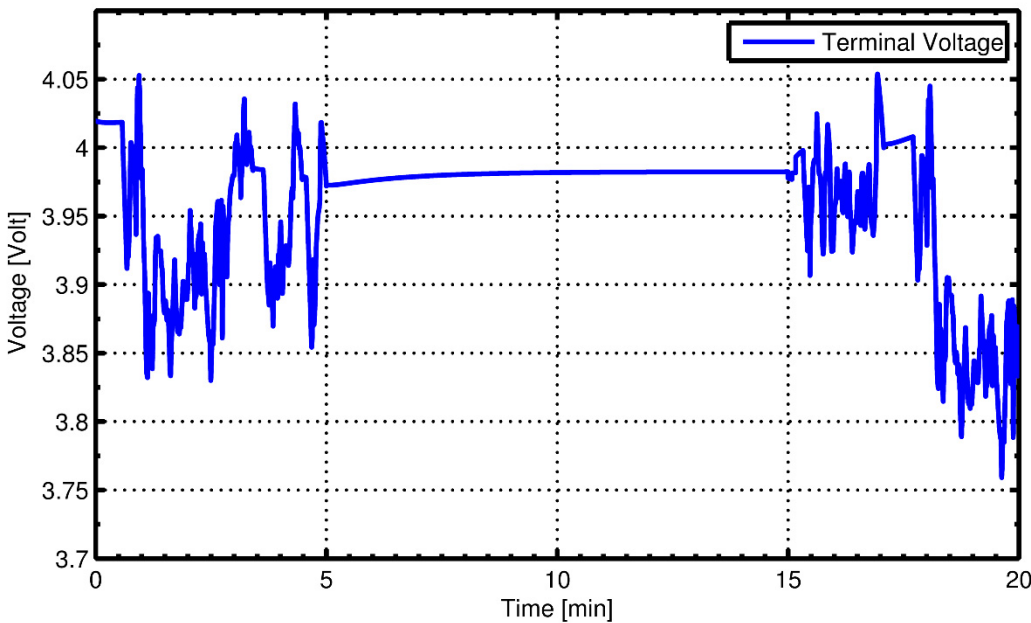


Figure 4.2 – Simulation battery Cell terminal Voltage profile [UDDS Test Sequence]

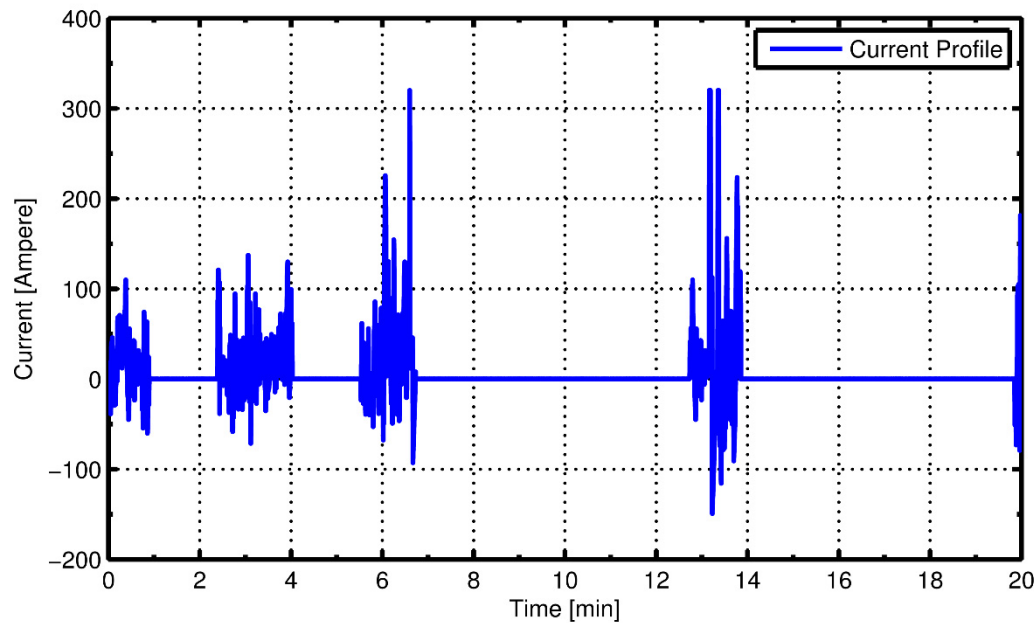


Figure 4.3 - Experimental battery current profile

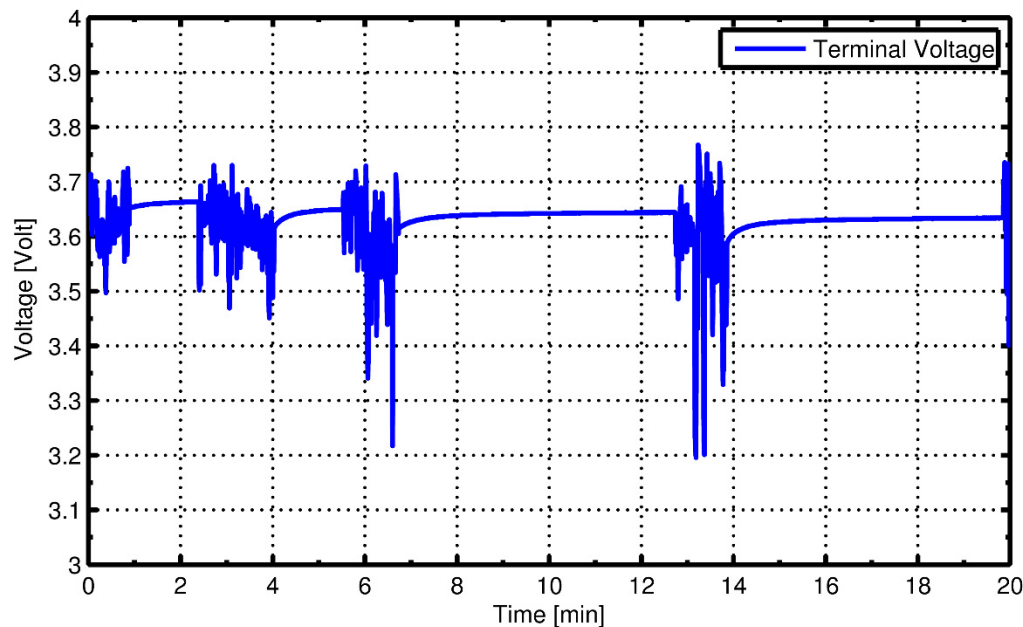


Figure 4.4 - Experimental Battery Terminal Voltage behavior

The parametric vector  $\theta$  for each of the models is obtained using the GPS to tune the model parameters.

### 4.3.1. Simulation Results

The simulation data set of Figure 3.13 and Figure 3.14 were used as input to all models, the output of the models compared to the cell terminal voltage under UDDS cycle is shown in Figure 4.5 - Figure 4.10. The parametric vector  $\theta$  for all the models was obtained as in Table 4.2 using GPS algorithm with data from Figure 4.1 and Figure 4.2.

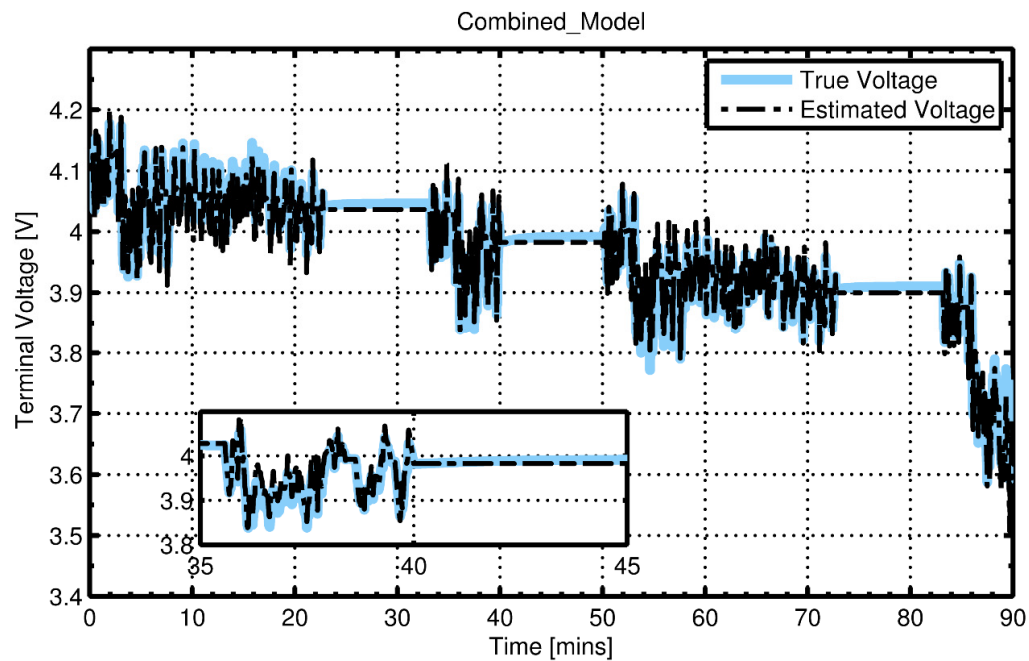


Figure 4.5 – Simulation Results of cell modeling with combined model showing the model Terminal Voltage versus the True Voltage [UDDS]

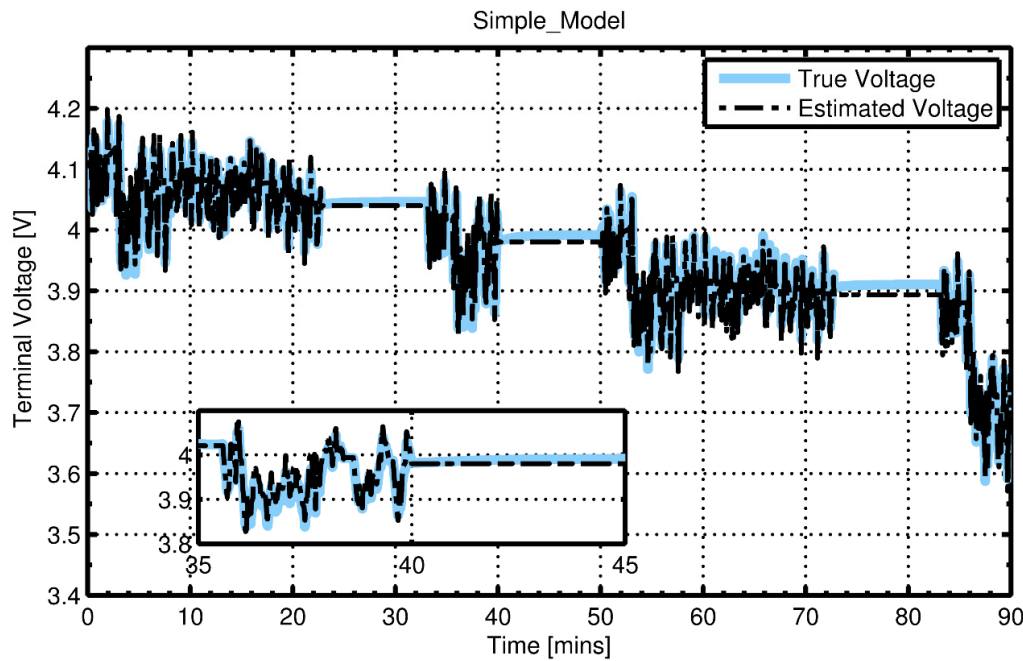


Figure 4.6 – Simulation Results of cell modeling with Simple model showing the model Terminal Voltage versus the True Voltage [UDDS]

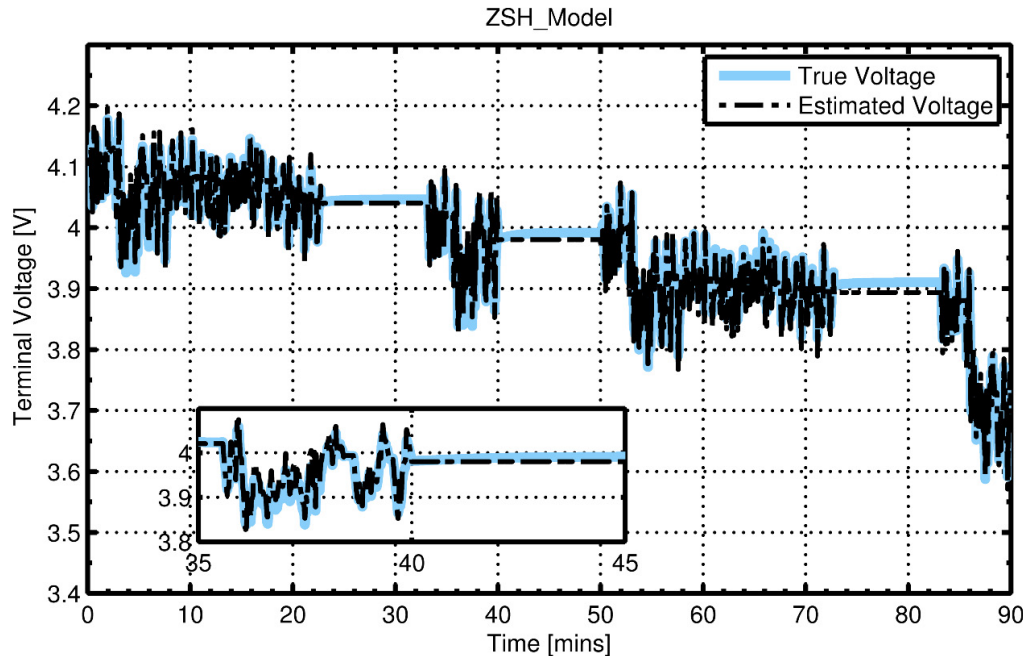


Figure 4.7 – Simulation Results of cell modeling with Zero State Hysteresis model showing the model Terminal Voltage versus the True Voltage [UDDS]

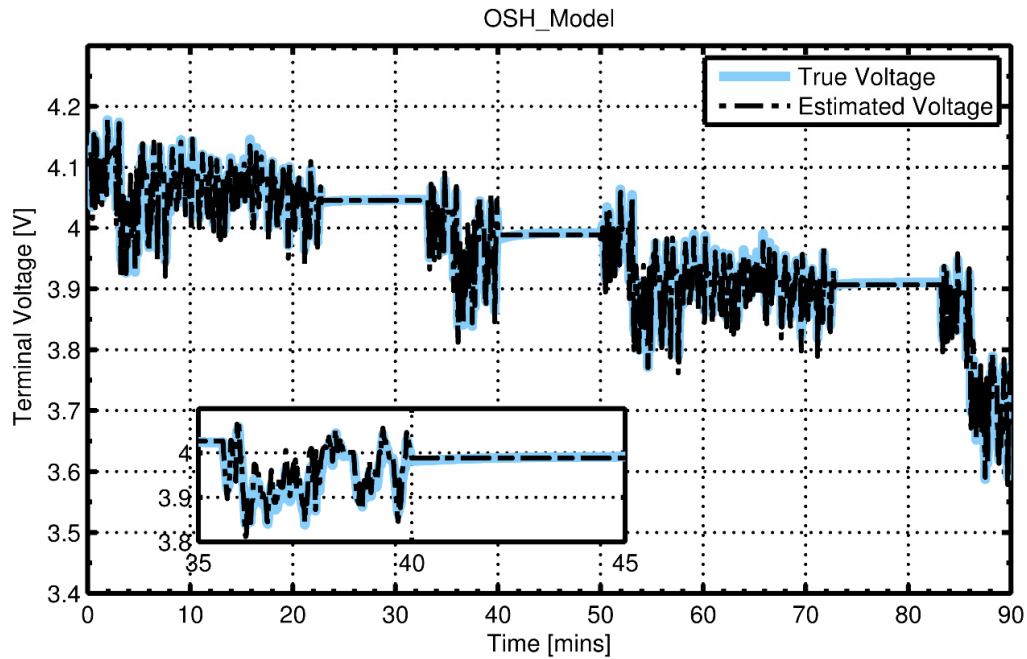


Figure 4.8 - Simulation Results of cell modeling with One State Hysteresis model showing the model Terminal Voltage versus the True Voltage [UDDS]

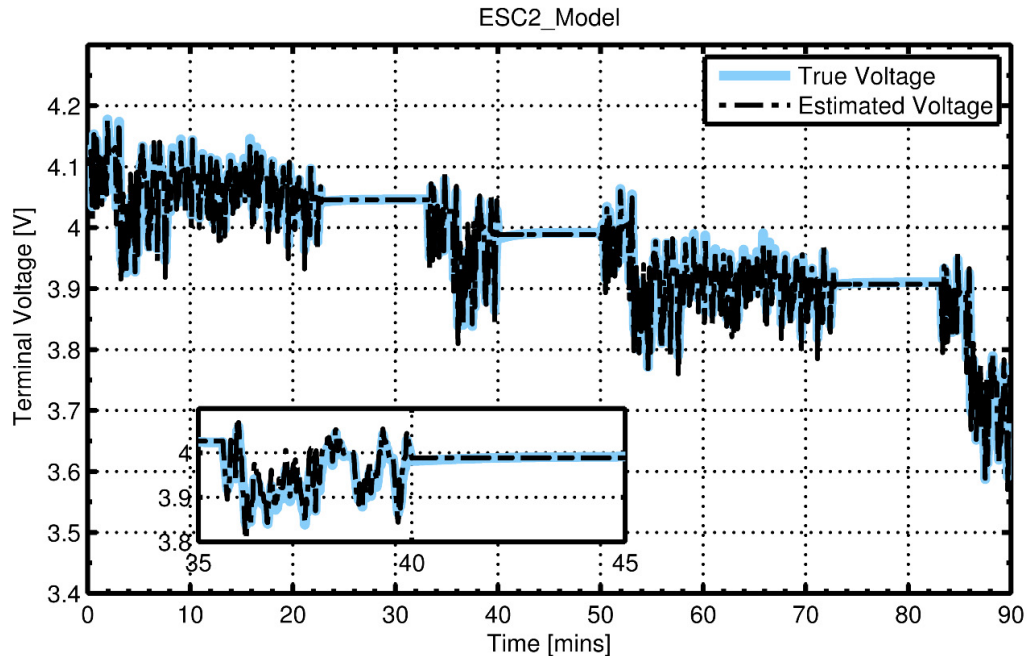


Figure 4.9 – Simulation Results of cell modeling with Enhanced Self Correcting model – 2 States showing the model Terminal Voltage versus the True Voltage [UDDS]

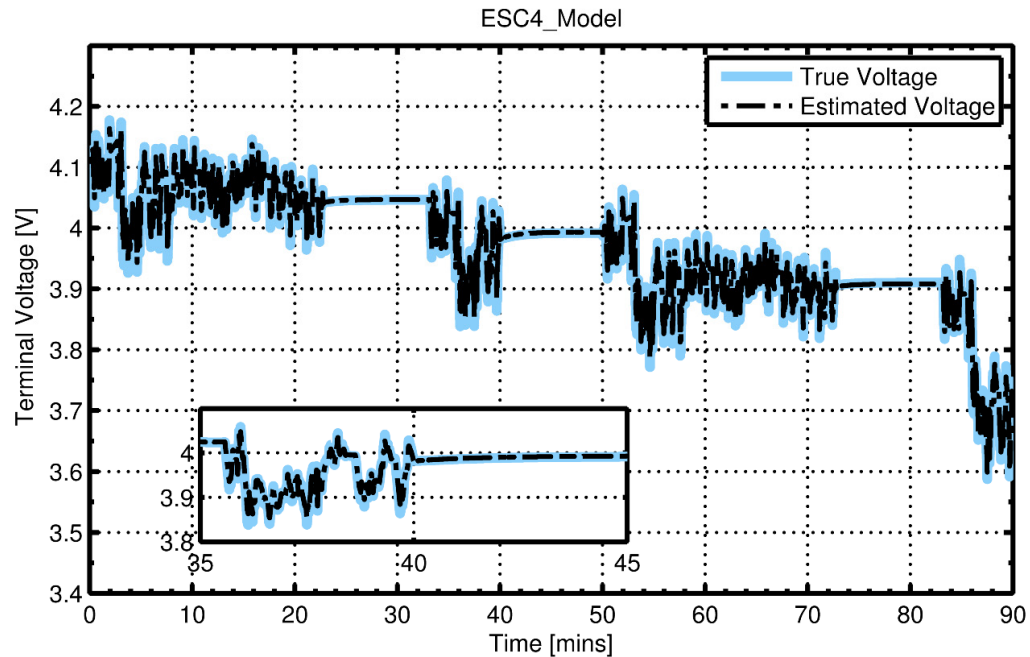


Figure 4.10 – Simulation Results of cell modeling with Enhanced Self Correcting model – 4 States showing the model Terminal Voltage versus the True Voltage [UDDS]

The associated root mean squared error between the cell voltage and the simulated voltage is shown in Table 4.1.

Model Parameters	Combined	Simple	Zero-State Hysteresis	One-State Hysteresis	ESC-2	ESC-4
RMSE	18.4	9.5	9.9	8.0	1.8	1.4

Table 4.1 – The RMSE for each model

Model Parameters	Combined	Simple	Zero-State Hysteresis	One-State Hysteresis	ESC-2	ESC-4
$k_0$	4.23	-	-	-	-	-
$k_1$	3.86E-05	-	-	-	-	-
$k_2$	0.24	-	-	-	-	-
$k_3$	0.22	-	-	-	-	-
$k_4$	-0.04	-	-	-	-	-
$R^+$	0.0022	0.0023	0.0022	0.0022	0.0017	0.00174
$R^-$	0.002	0.0018	0.0016	0.0016	0.0017	0.00174
$g_1$	-	-	-	-	-6.90E-06	-6.90E-04
$g_2$	-	-	-	-	-	3.21E-05
$g_3$	-	-	-	-	-	0
$\beta_1$	-	-	-	-	2.71	2.74
$\beta_2$	-	-	-	-	3.86	0.35
$\beta_3$	-	-	-	-	-	0.28
$\beta_4$	-	-	-	-	-	3.86
$M^+$	-	-	0.0041	0.0105	0.0105	0.0105
$M^-$	-	-	0.0041	-0.016	-0.016	-0.01
$\gamma$	-	-	-	0.1	0.1	0.1

Table 4.2 - The parametric Values for variable in all models

### 4.3.2. Experimental Results

The experimental data set of Figure 3.15 and Figure 3.17 were used as input to all models, the output of the models compared to the cell terminal voltage is shown in Figure 4.11- Figure 4.16. The parametric vector  $\theta$  for all the models was obtained as in Table 4.4 using GPS algorithm with data from Figure 4.3 and Figure 4.4.

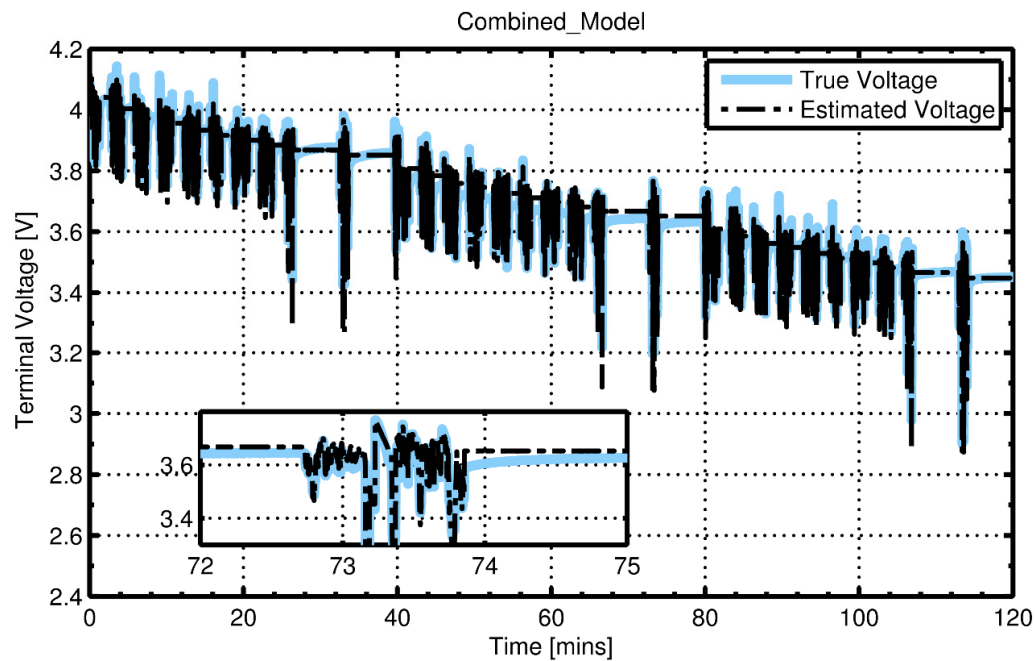


Figure 4.11 – Experimental Results of cell modeling with Combined model showing the model Terminal Voltage versus the True Voltage

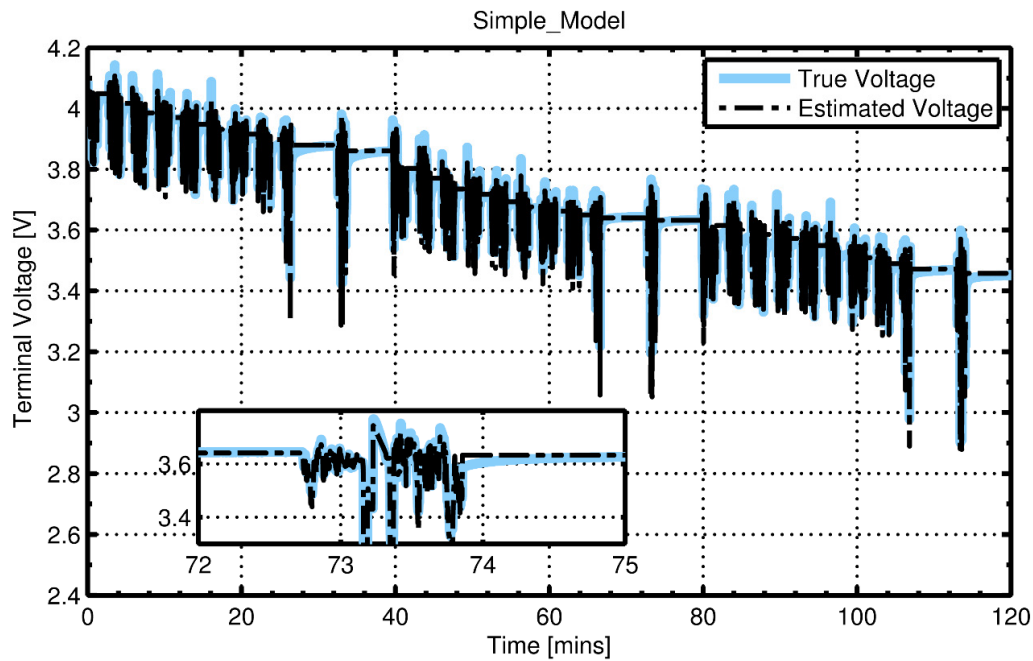


Figure 4.12 – Experimental Results of cell modeling with Simple model showing the model Terminal Voltage versus the True Voltage

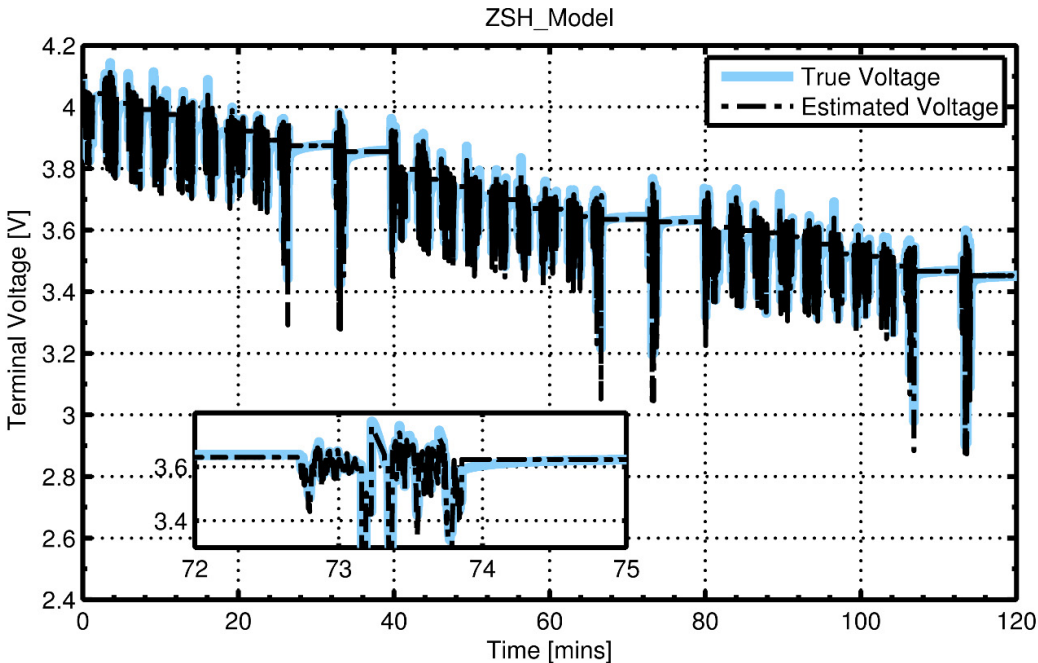


Figure 4.13 – Experimental Results of cell modeling with Zero State Hysteresis model showing the model Terminal Voltage versus the True Voltage

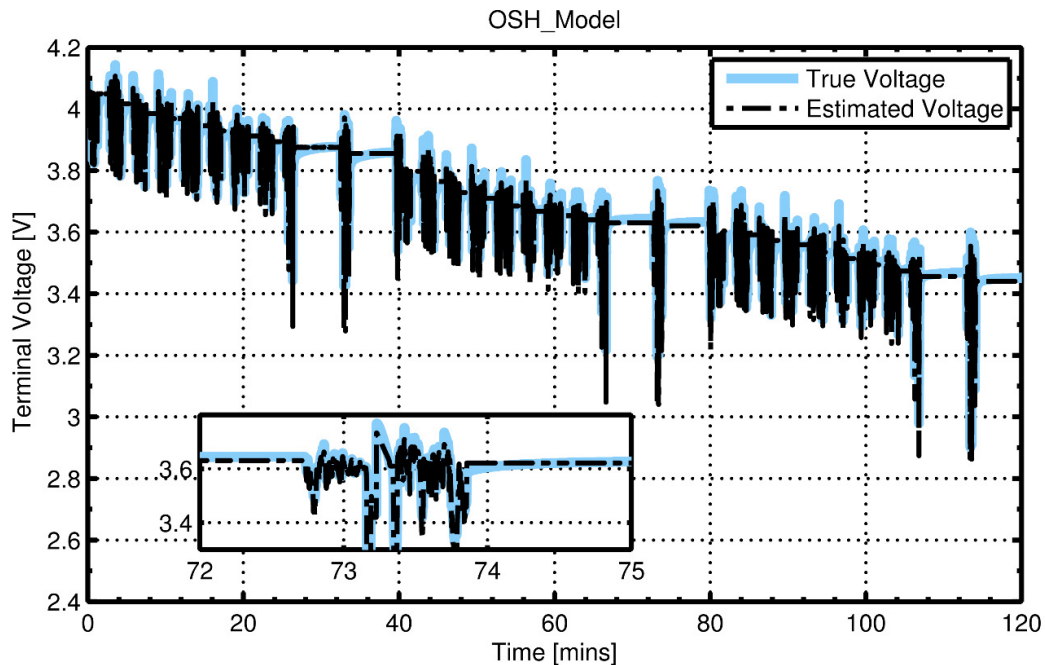


Figure 4.14 - Experimental Results of cell modeling with One State Hysteresis model showing the model Terminal Voltage versus the True Voltage

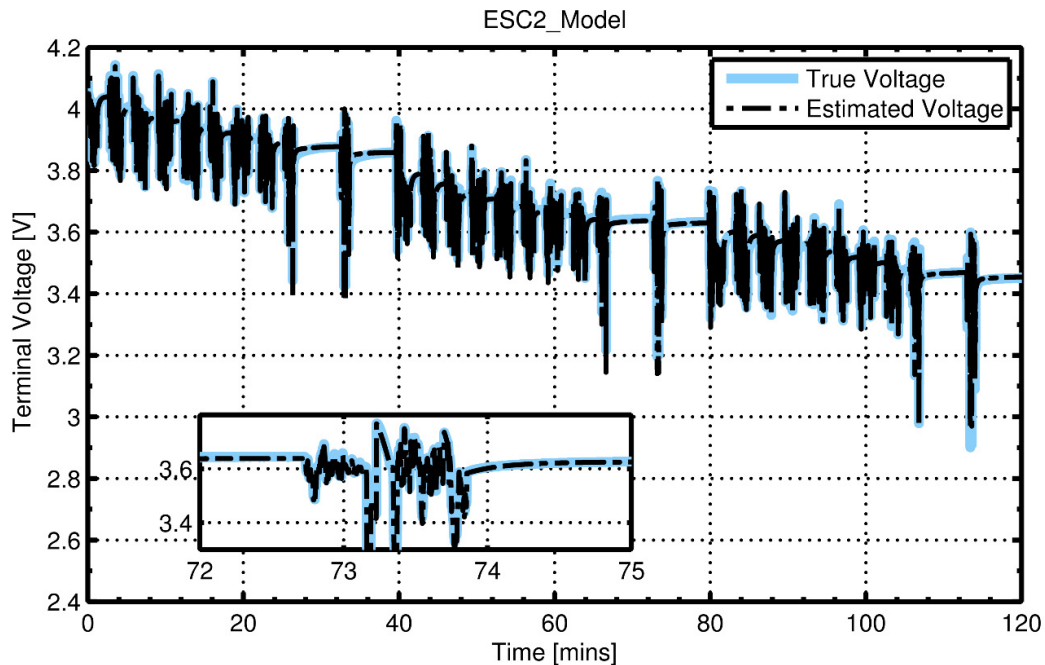


Figure 4.15 – Experimental Results of cell modeling with Enhanced Self Correcting model – 2 States showing the model Terminal Voltage versus the True Voltage

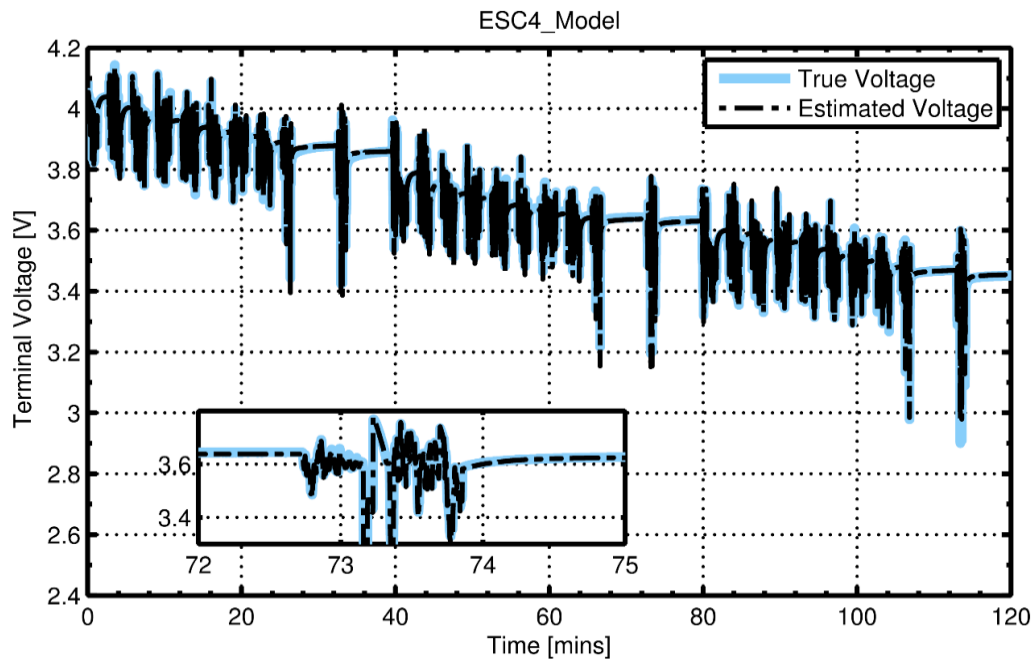


Figure 4.16 – Experimental Results of cell modeling with Enhanced Self Correcting model – 4  
States showing the model Terminal Voltage versus the True Voltage

The associated root mean squared error between the cell voltage and the simulated voltage is shown in Table 4.3

Model Parameters	Combined	Simple	Zero-State Hysteresis	One-State Hysteresis	ESC-2	ESC-4
RMSE	24.7	20.9	20.2	18.2	6.9	6.7

Table 4.3 – The RMSE for each model

Model Parameters	Combined	Simple	Zero-State Hysteresis	One-State Hysteresis	ESC-2	ESC-4
$k_0$	0.0018	-	-	-	-	-
$k_1$	0.0001	-	-	-	-	-
$k_2$	-0.565	-	-	-	-	-
$k_3$	0.012	-	-	-	-	-
$k_4$	-0.027	-	-	-	-	-
$R^+$	0.0018	0.0018	0.0018	0.0018	0.0013	0.00174
$R^-$	0.0007	0.0007	0.0007	0.0007	0.0012	0.00174
$g_1$	-	-	-	-	-6.90E-06	-6.90E-04
$g_2$	-	-	-	-	-	3.11E-05
$g_3$	-	-	-	-	-	0
$\beta_1$	-	-	-	-	2.81	2.84
$\beta_2$	-	-	-	-	4.13	0.14
$\beta_3$	-	-	-	-	-	0.28
$\beta_4$	-	-	-	-	-	4.11
$M^+$	-	-	0.005	0.032	0.032	0.032
$M^-$	-	-	0.005	-0.81	-0.81	-0.81
$\gamma$	-	-	-	0.12	0.12	0.12

Table 4.4 - The parametric Values for variable in all models

## 4.4. SOC Estimation

The SOC estimation results using the EKF and the SVSF for all of the six modeling techniques are presented in this section.

### 4.4.1. Simulation Results

In this section, the EKF SOC and SVSF SOC estimation results will be presented and compared to the simulated and hence known value of the SOC for Behavioral models as shown in Figure 4.17 to Figure 4.22. The estimated SOC is initialized at 85% while the true SOC is at 95% (i.e. 10% error). For all models the EKF system and measurement noise covariance, and the SVSF ‘memory’ or convergence rate and smoothing boundary layers were obtained as in Table 4.6. The RMSE associated with SOC estimation using the EKF and the SVSF was obtained as in Table 4.5.

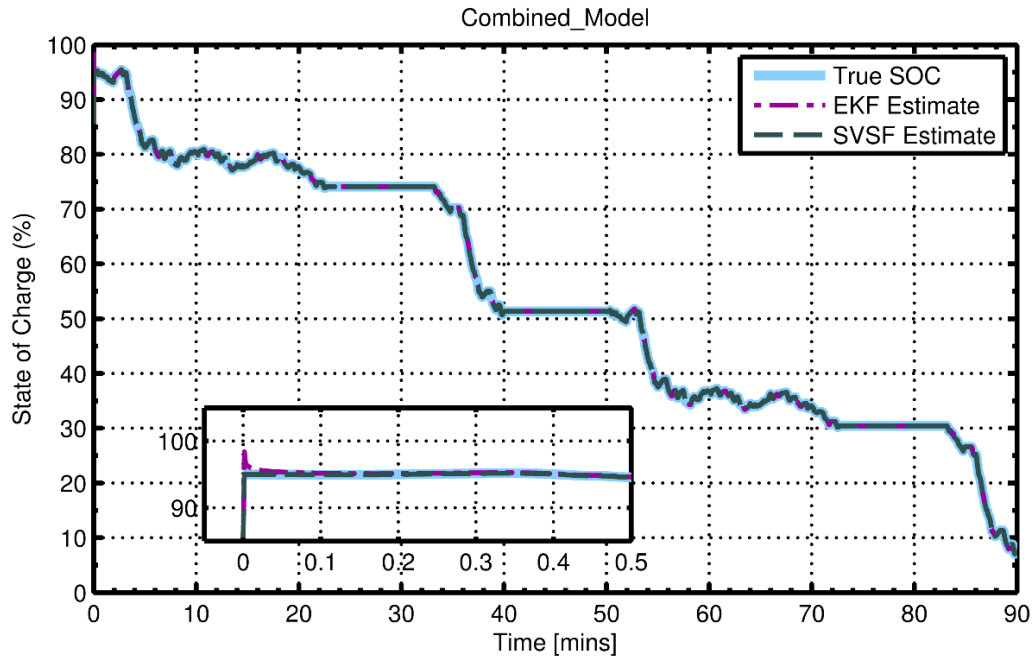


Figure 4.17 – Simulation results of SOC estimation with combined model showing the EKF and SVSF estimated versus model SOC.

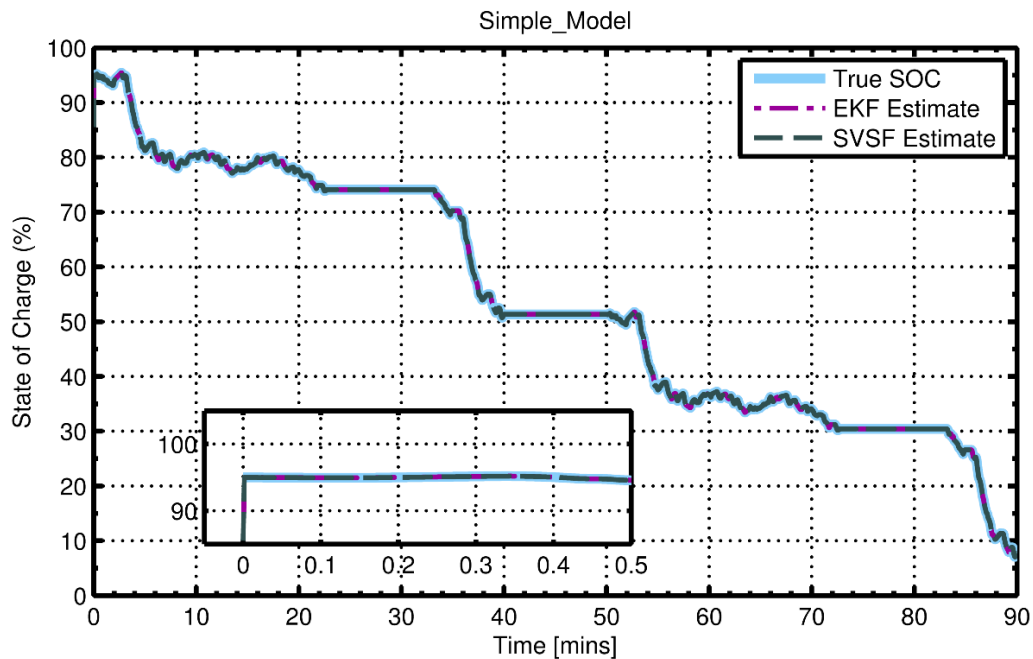


Figure 4.18 – Simulation results of SOC estimation with simple model showing the EKF and SVSF estimated versus model SOC.

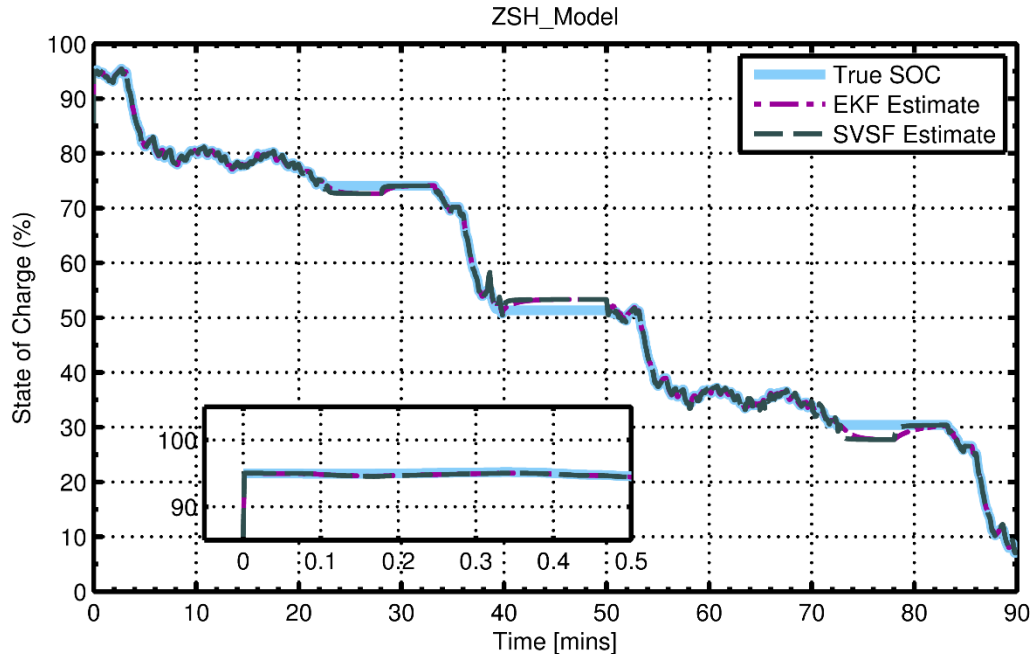


Figure 4.19 - Simulation results of SOC estimation with Zero State Hysteresis showing the EKF and SVSF estimated versus model SOC.

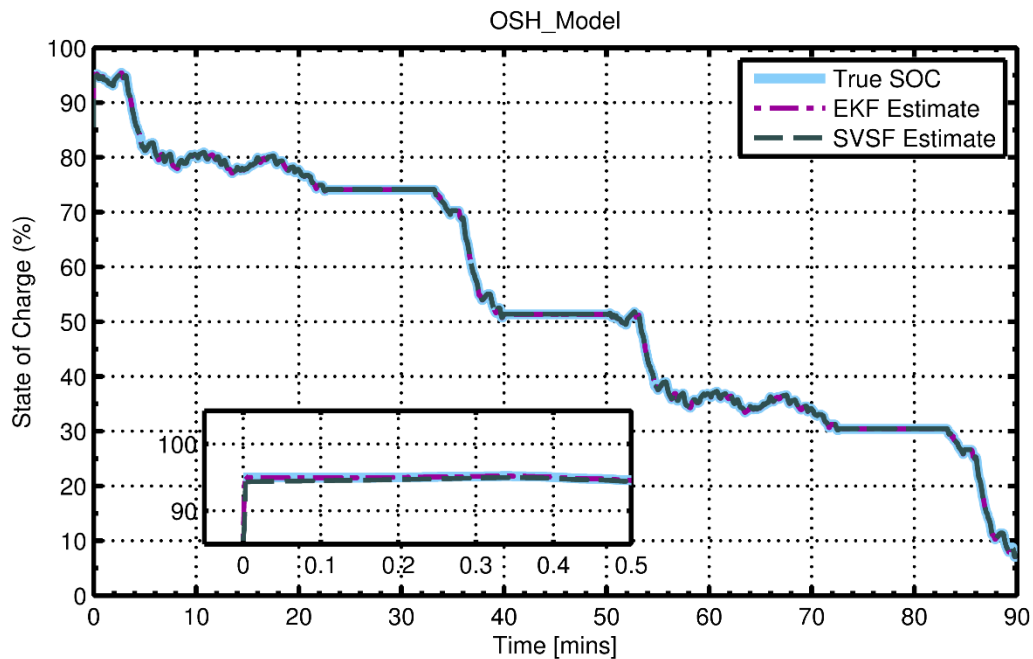


Figure 4.20 - Simulation results of SOC estimation with One State Hysteresis showing the EKF and SVSF estimated versus model SOC.

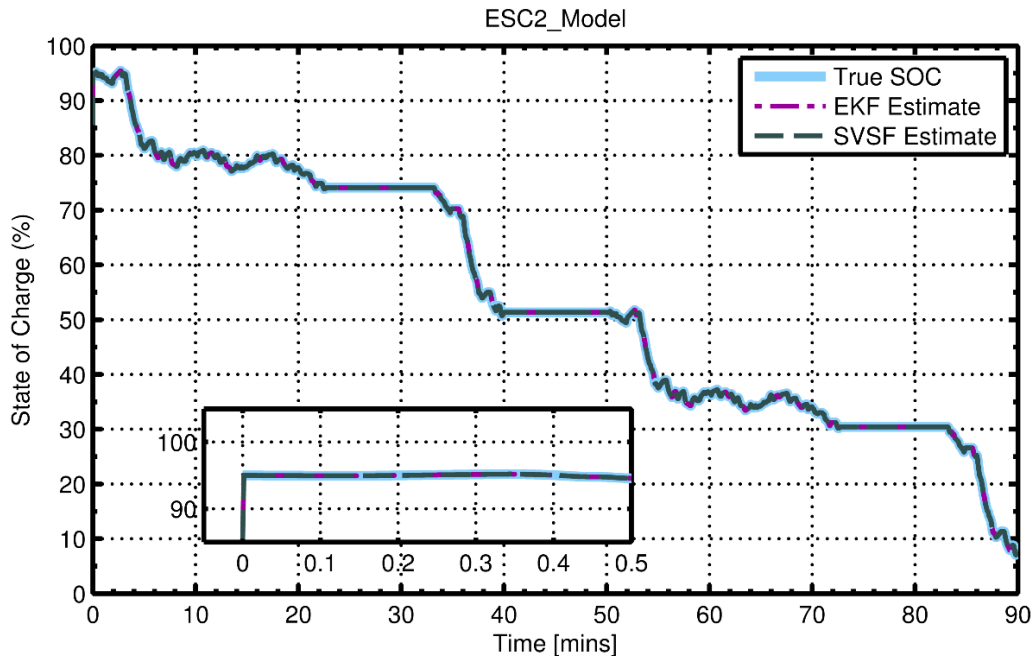


Figure 4.21 - Simulation results of SOC estimation with Enhanced Self Correcting model – 2 States showing the EKF and SVSF estimated versus model SOC.

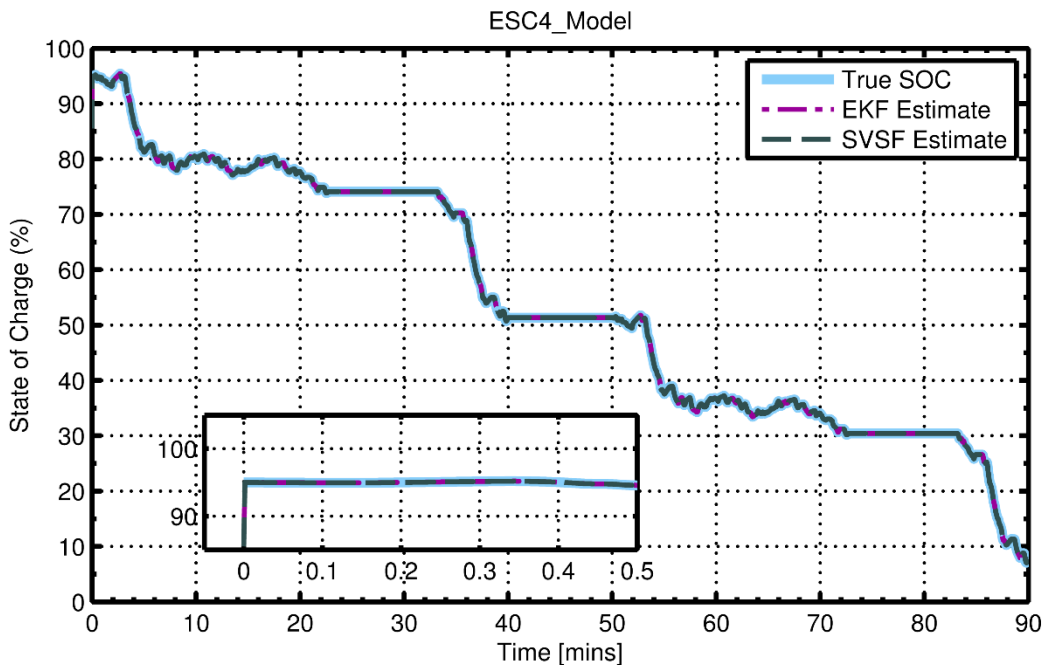


Figure 4.22 - Simulation results of SOC estimation with Enhanced Self Correcting model – 4  
States showing the EKF and SVSF estimated versus model SOC.

RMSE	Combined	Simple	Zero-State Hysteresis	One-State Hysteresis	ESC-2	ESC-4
EKF –SOC [%]	1.1	0.90	0.73	0.52	0.40	0.29
SVSF –SOC [%]	1.09	0.92	0.89	0.50	0.34	0.25

Table 4.5 – Root mean squared error (RMSE) for SOC using the EKF and the SVSF.

Filter Parameters		Combined	Simple	Zero-State Hysteresis	One-State Hysteresis	ESC-2	ESC-4
The Extended Kalman Filter (EKF)	$Q$	0.001	3.237e-2	6.293e-7	diag(1.522e-5, 14.365e-3)	diag(0.1374, 0.1867, 0.5204, 1.143e-6)	diag(0.2697, 0.1858, 0.3214, 0.18323, 0.184, 5.9e-7)
	$R$	0.0519	0.0519	0.0519	0.0519	0.0519	0.0519
The Smooth Variable Structure Filter (SVSF)	$\psi$	0.066	0.1003	0.684	4.12	0.0068	0.0075
	$\gamma$	0.305	0.932	0.99	0.99	0.97	0.91

Table 4.6 – The EKF system and measurement noise covariance, and the SVSF ‘memory’ or convergence rate and smoothing boundary layers.

#### 4.4.2. Experimental Results

In this section, the estimated EKF SOC and SVSF SOC will be presented and compared to the experimental SOC for Behavioral models as shown in Figure 4.23 to Figure 4.28. The estimated SOC is initialized at 90% while the true SOC is at 100% (10% error). For all models the EKF system and measurement noise covariance, and the SVSF ‘memory’ or convergence rate and smoothing boundary layers were obtained as in Table 4.8. The RMSE associated with SOC estimation using the EKF and the SVSF was obtained as in Table 4.7.

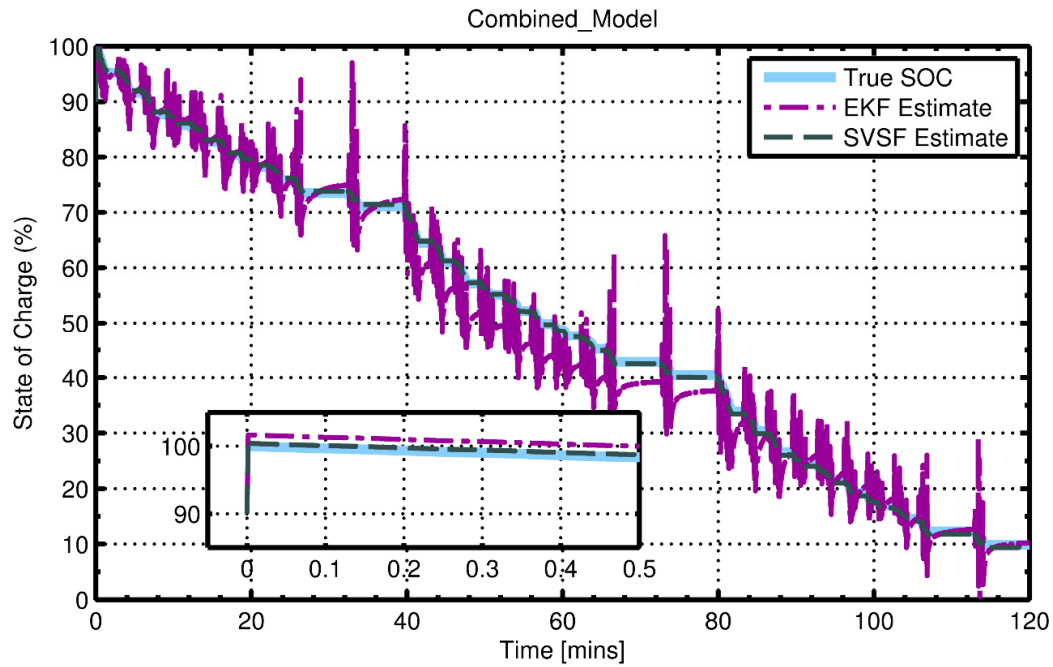


Figure 4.23 - Experimental results of SOC estimation with combined model showing the EKF and SVSF estimated versus model SOC.

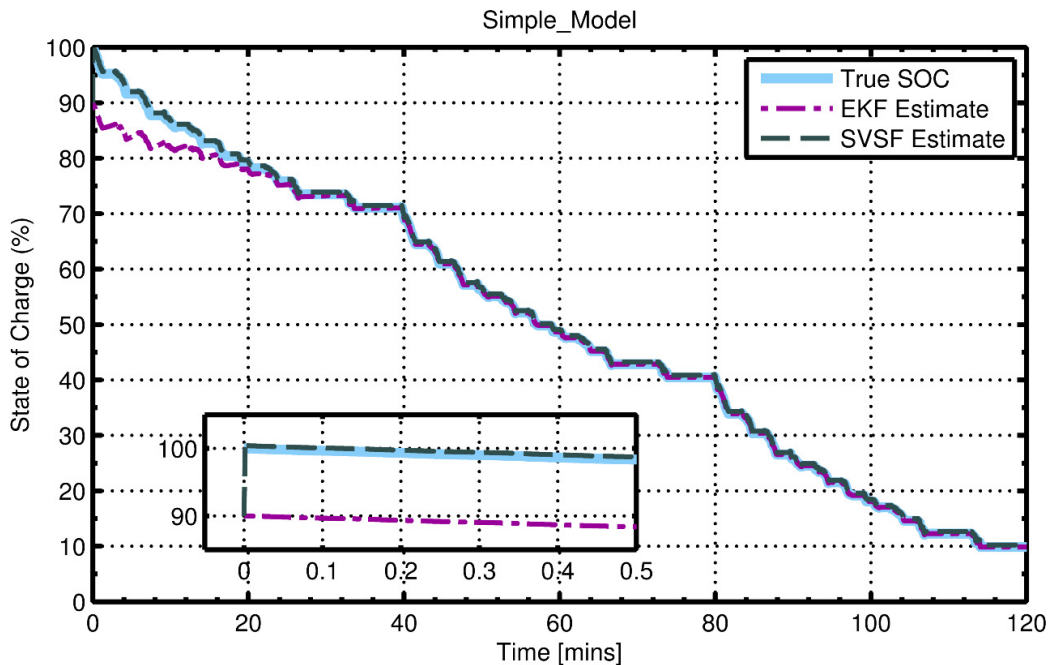


Figure 4.24 - Experimental results of SOC estimation with simple model showing the EKF and SVSF estimated versus model SOC.

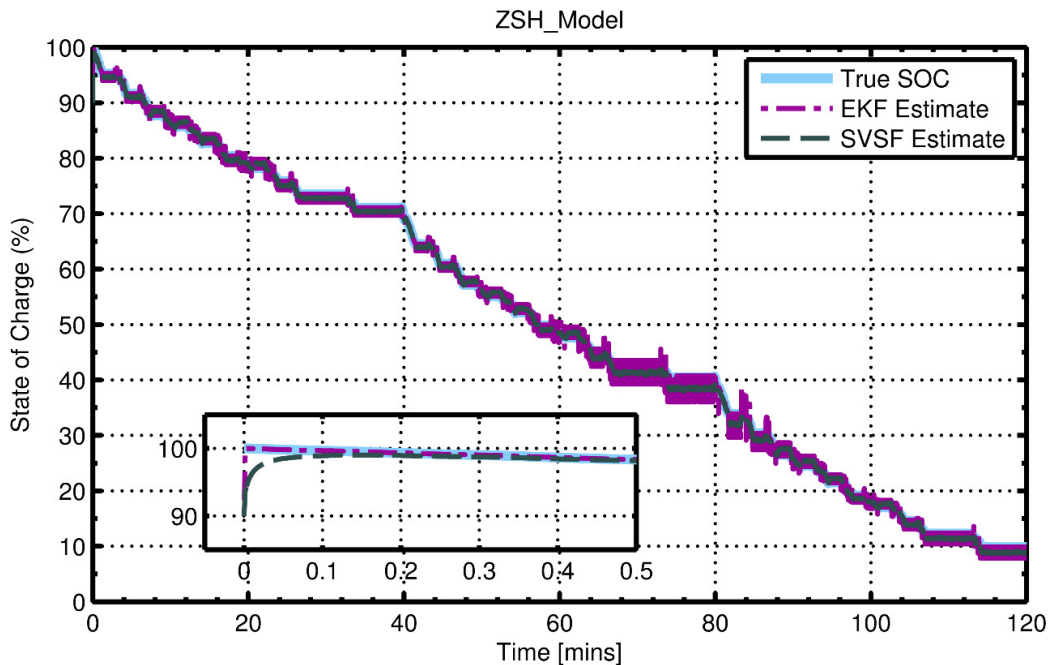


Figure 4.25 - Experimental results of SOC estimation with Zero State Hysteresis showing the EKF and SVSF estimated versus model SOC.

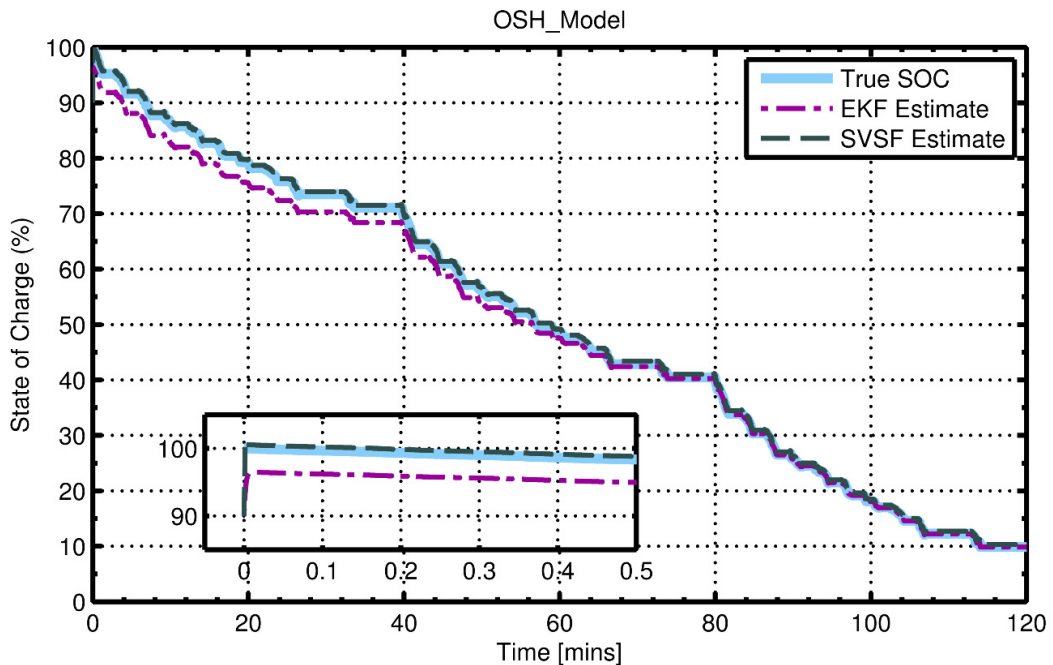


Figure 4.26 - Experimental results of SOC estimation with One State Hysteresis showing the EKF and SVSF estimated versus model SOC.

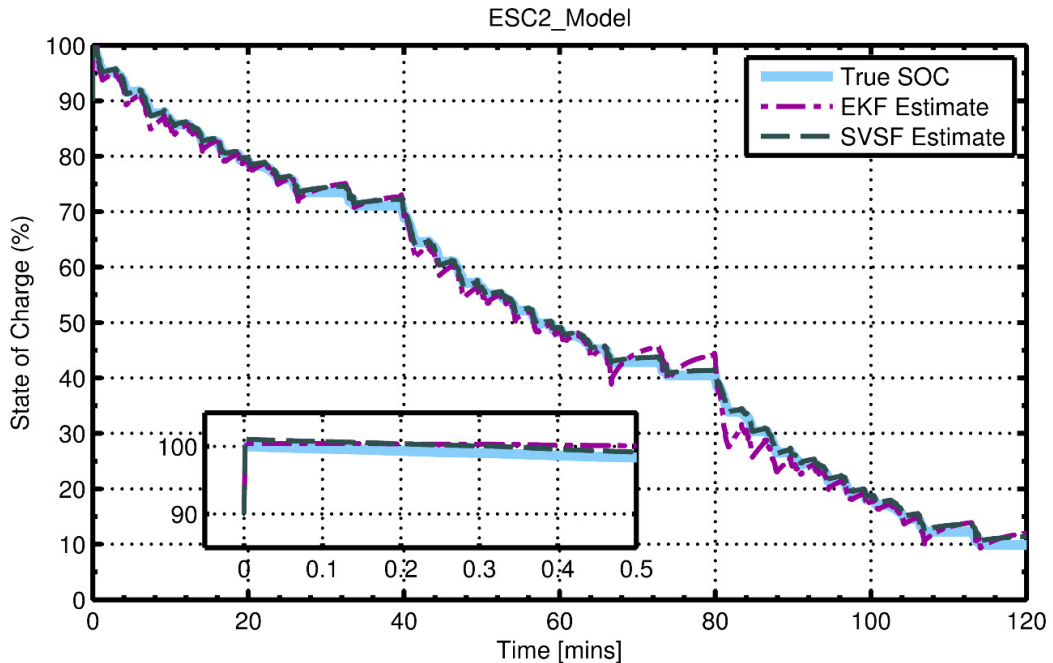


Figure 4.27 - Experimental results of SOC estimation with Enhanced Self Correcting model – 2 States showing the EKF and SVSF estimated versus model SOC.

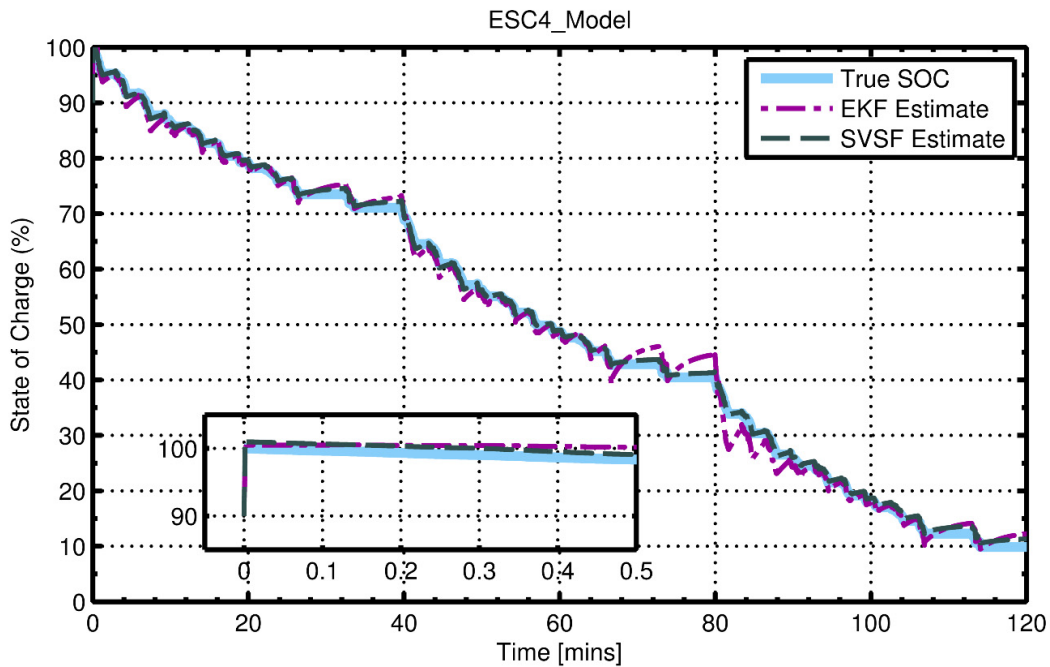


Figure 4.28 - Experimental results of SOC estimation with Enhanced Self Correcting model – 4  
States showing the EKF and SVSF estimated versus model SOC.

RMSE	Combined	Simple	Zero-State Hysteresis	One-State Hysteresis	ESC-2	Combined
EKF –SOC [%]	3.69	2.39	2.3	2.13	1.86	1.58
SVSF –SOC [%]	0.95	0.98	0.84	0.73	0.65	0.59

Table 4.7 – Root mean squared error (RMSE) for SOC using the EKF and the SVSF.

Filter Parameters		Combined	Simple	Zero-State Hysteresis	One-State Hysteresis	ESC-2	Combined
The Extended Kalman Filter (EKF)	$Q$	0.2753	4.692e-2	0.19865	diag(0.182, 0.223)	diag(0.963, 0.9624, 1.763e-6, 12.5)	diag(5.8e-7, 0.125e-4, 17.34, 1.1e-7, 1.6e-6, 40.40)
	$R$	0.065	0.065	0.065	0.065	0.065	0.065
The Smooth Variable Structure Filter (SVSF)	$\psi$	2.458	2.097	0.776	0.048	0.0041	0.0068
	$\gamma$	0.518	0.514	0.968	0.293	0.18	0.91

Table 4.8 – The EKF system and measurement noise covariance, and the SVSF ‘memory’ or convergence rate and smoothing boundary layers.

## 4.5. Summary

This chapter provided an overview about the Behavioral models and their implementation. These models simulate the terminal voltage behavior of the batteries without the need for the specification of the underlying physical or electrochemical behavior. The model parameters are tuned using numerical algorithms such as Globalized Pattern Search (GPS) Matlab toolbox.

In this chapter six different behavioral models were compared. Their Root Mean squared Error (RMSE) are shown in Figure 4.29 and Figure 4.30.

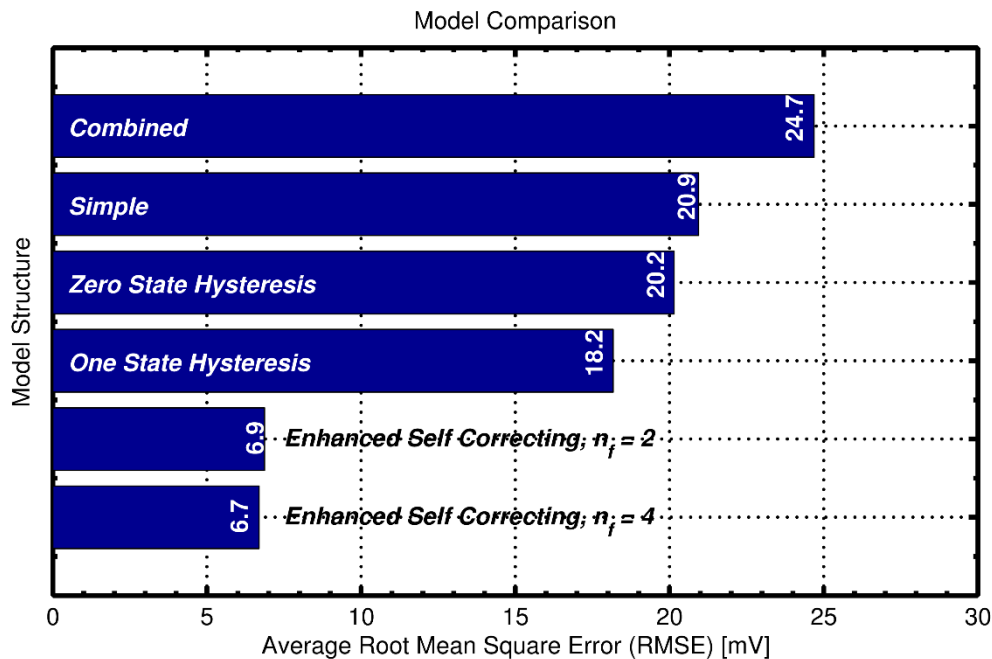


Figure 4.29 – Experimental Results for Behavioral Models comparison of average modeling results

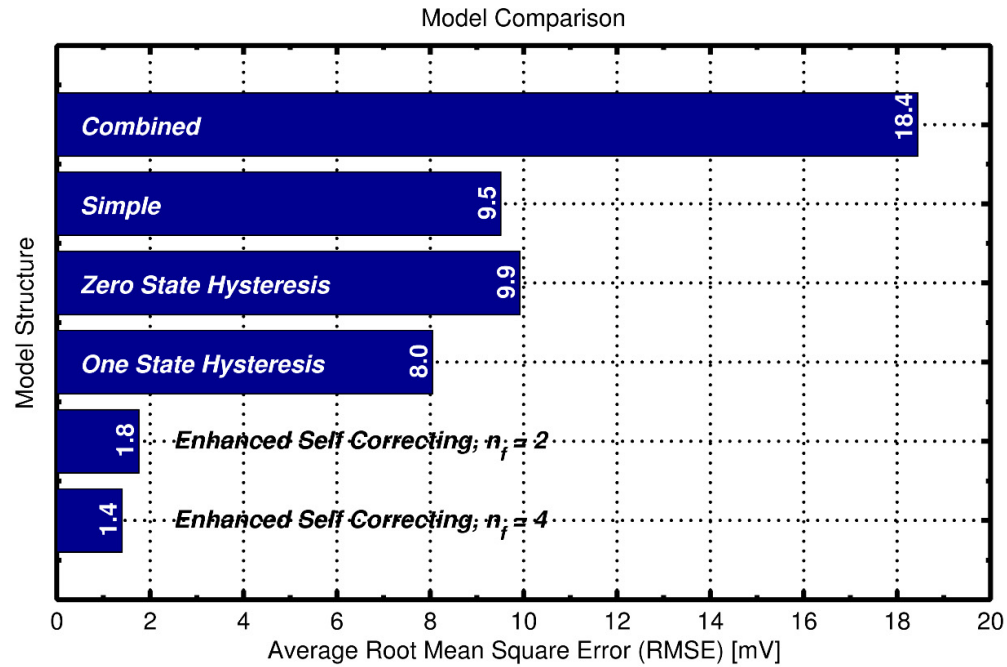


Figure 4.30 - Simulation Results for Behavioral Models comparison of average modeling results

As shown in Figure 4.29 and Figure 4.30, the model accuracy increases by increasing the number of states and parameters. Figure 4.31 and Figure 4.32 show the SVSF and the EKF state of charge estimation against simulation and experimental results respectively. The figures show SOC estimation results of the six model as discussed earlier. The SOC Root Mean squared Error (RMSE) percentage is shown as a measure of performance. According to Figure 4.31 and Figure 4.32, the SVSF has shown better results compared to the EKF.

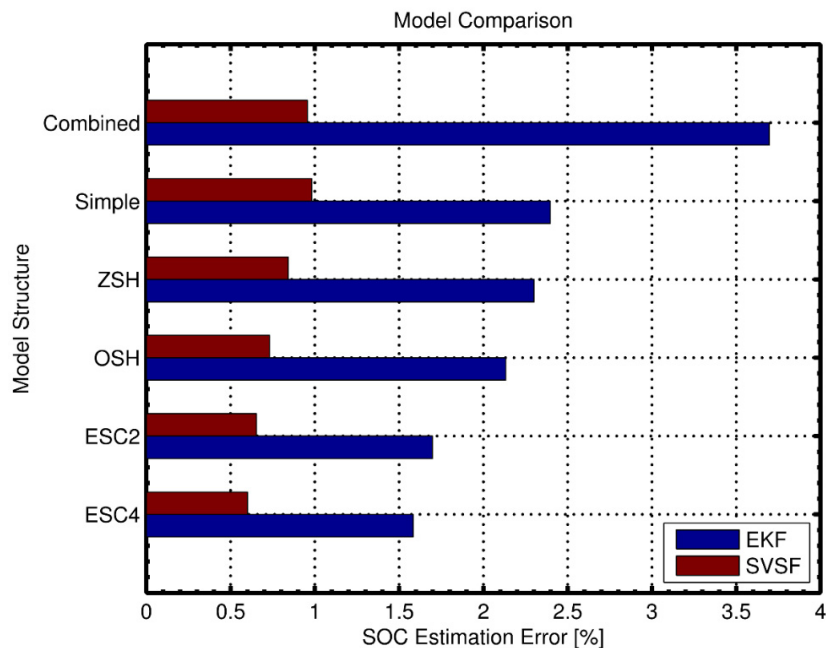


Figure 4.31 - Experimental results for Behavioral Models comparison of SOC Estimation Error using EKF and SVSF

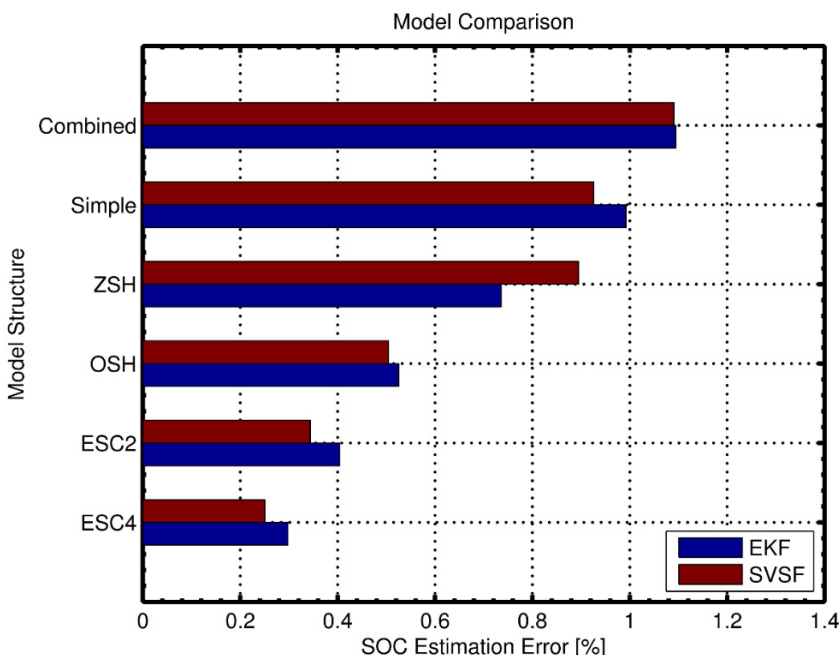


Figure 4.32 – Simulation results for Behavioral Models comparison of SOC Estimation Error using EKF and SVSF

---

# Equivalent Circuit Modelling

---

In this chapter, Lithium ion battery models based on first principal modelling approach (Equivalent Circuit Models) are reviewed. Introduction and a brief description of the advantages and disadvantages of this modelling approach is provided. It is followed by description of the evolution of the battery modelling techniques and implementation of six different models with various complexity. Summary and discussions are provided.

## 5.1. Introduction

The Equivalent Circuit Model approach in BMS has been extensively researched [100]. This choice is due to the early popularity of BMS for portable electronics, where the approximation of the battery model with an equivalent circuit model is adequate. This modelling approach has been extended to Li-ion batteries for automotive or similar energy storage applications. The circuit can be rather simple, e.g. only a voltage source and a variable resistance, or complex given local conditions in a spatially-resolved model.

Electrical impedance-based models can be treated as a group of resistances and capacitors, model parameters can be obtained similarly to Behavioral models using optimization. This leads to accurate models for the measured operating conditions. A disadvantage of equivalent circuit models is that these models are unable to measure underlying physical behavior like power fading, capacity fading and aging effect. Main advantage is the ability to be implemented in real-time application with acceptable range of performance.

## 5.2. Evolution of Equivalent Circuit Cell Models

### 5.2.1. The 1<sup>st</sup> Order RC Model

The OCV-R-RC model is the simplest equivalent circuit models and is selected to approximate the electrical performance of the battery as shown in Figure 5.1. It consists of 3 parts (1) Open Circuit Voltage OCV, (2) Internal Resistances representing the ohmic resistances, (3) Capacitors.

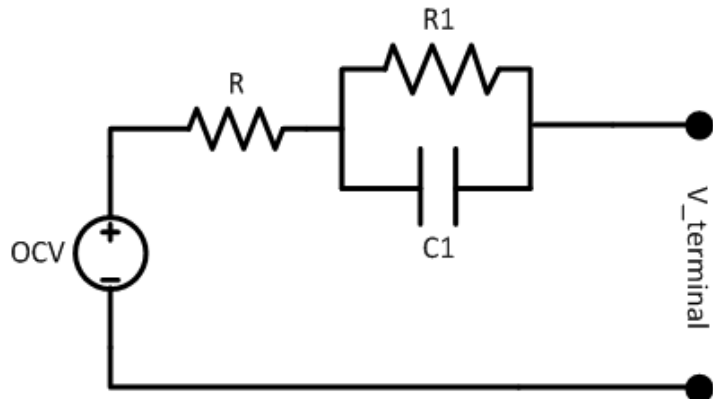


Figure 5.1 - Schematic Diagram for R-RC Battery Model

This model can capture the battery dynamics and can be easily implemented in a real-time application. The R-RC model can be represented as follows:

$$\begin{bmatrix} V_{1,k+1} \\ z_{k+1} \end{bmatrix} = \begin{bmatrix} 1 - \frac{\Delta t}{R_1 C_1} & 0 \\ 0 & 1 \end{bmatrix} \begin{bmatrix} V_{1,k} \\ z_k \end{bmatrix} + \begin{bmatrix} \frac{\Delta t}{C_1} \\ -\frac{\eta_i \Delta t}{C} \end{bmatrix} [i_k] \quad (5.1)$$

$$y_k = OCV(z_k) - Ri_k - V_{1,k} \quad (5.2)$$

where  $z_k$  is the state of charge,  $OCV$  is the open circuit voltage,  $C$  is the battery nominal capacity,  $R$  is the battery ohmic resistance,  $R_1 C_1$  are RC pair and they represent the polarization time constants,  $V_{1,k}$  is a state and represent the voltage across the capacitor. The states of the system are  $z_k, V_{1,k}$ . The model has one output  $y_k$ , which is the terminal voltage, the current  $i_k$  is the input.

### 5.2.2. The 1<sup>st</sup> Order RC Model with One-State Hysteresis

The OCV-R-RC-H model is the same as the OCV-R-RC except that it has an assed hysteresis state as shown in Figure 5.2. The model consists of 5 elements (1) Open Circuit Voltage OCV, (2, 3) Internal Resistances, (4) Capacitors, and (5) Hysteresis state to capture the battery charging and discharging hysteresis effect.

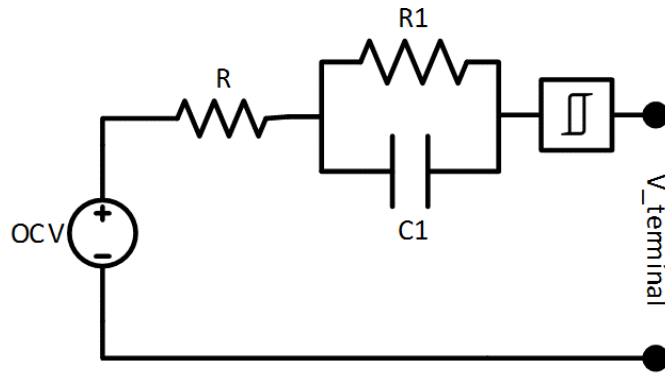


Figure 5.2 - Schematic Diagram for R-RC\_H Battery Model

The R-RC-H model can be represented as in Figure 5.2 and as follows:

$$\begin{bmatrix} V_{1,k+1} \\ h_{k+1} \\ z_{k+1} \end{bmatrix} = \begin{bmatrix} 1 - \frac{\Delta t}{R_1 C_1} & 0 & 0 \\ 0 & F(i_k) & 0 \\ 0 & 0 & 1 \end{bmatrix} \begin{bmatrix} V_{1,k} \\ h_k \\ z_k \end{bmatrix} + \begin{bmatrix} \frac{\Delta t}{C_1} & 0 \\ 0 & (1 - F(i_k)) \\ -\frac{\eta_i \Delta t}{C} & 0 \end{bmatrix} \begin{bmatrix} i_k \\ M(z, \dot{z}) \end{bmatrix} \quad (5.3)$$

$$y_k = OCV(z_k) - Ri_k - V_{1,k} + h_k \quad (5.4)$$

The states of the system are  $z_k, V_{1,k}, h_k$  representing the SOC, voltage drop across the RC pair, and hysteresis state respectively. The model has one output  $y_k$ , which is the terminal voltage, the current  $i_k$  is the input.

### 5.2.3. The 2<sup>nd</sup> Order RC Model

The OCV-R-RC-RC model is as shown in Figure 5.3, [100]. The model is able to imitate fast and slow time constants for the voltage recovery of the battery.

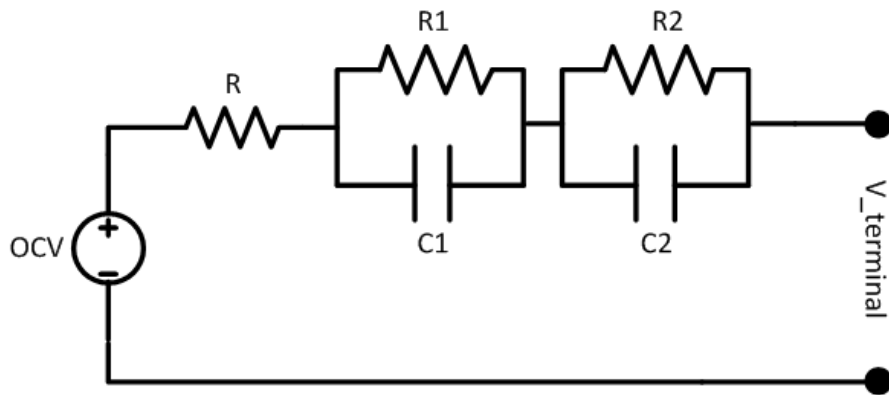


Figure 5.3 - Schematic Diagram for R-RC-RC Battery Model

This model can accurately capture the battery dynamics and can be easily implemented in a real-time application. The R-RC-RC model can be represented as follows:

$$\begin{bmatrix} V_{1,k+1} \\ V_{2,k+1} \\ z_{k+1} \end{bmatrix} = \begin{bmatrix} 1 - \frac{\Delta t}{R_1 C_1} & 0 & 0 \\ 0 & 1 - \frac{\Delta t}{R_2 C_2} & 0 \\ 0 & 0 & 1 \end{bmatrix} \begin{bmatrix} V_{1,k} \\ V_{2,k} \\ z_k \end{bmatrix} + \begin{bmatrix} \frac{\Delta t}{C_1} \\ \frac{\Delta t}{C_2} \\ -\frac{\eta_i \Delta t}{C} \end{bmatrix} [i_k] \quad (5.5)$$

$$y_k = OCV(z_k) - Ri_k - V_{1,k} - V_{2,k} \quad (5.6)$$

Where  $R_1 C_1$  represent the fast polarization time constants,  $R_2 C_2$  represent the slow polarization time constants,  $V_{1,k}$  is a state variable and represent the voltage across the first capacitor,  $V_{2,k}$  is a state variable and represent the voltage across the second capacitor. The state variables of the system are  $z_k, V_{1,k}, V_{2,k}$ . The model has one output  $y_k$ , which is the terminal voltage, the current  $i_k$  is the input. The parameters vector to be optimized for this model is  $\theta = [R^+, R^-, R_1, R_2, C_1, C_2]$ .

#### 5.2.4. The 2<sup>nd</sup> Order RC Model with One-State Hysteresis

The OCV-R-RC-RC-H model is the same as the OCV-R-RC-RC but with an added hysteresis state as shown in Figure 5.4. The model consists of 7 elements (1) Open Circuit Voltage OCV, (2, 3, 4) Internal Resistances, (5, 6) Capacitors, and (7) Hysteresis state to capture the battery charging and discharging dynamics.

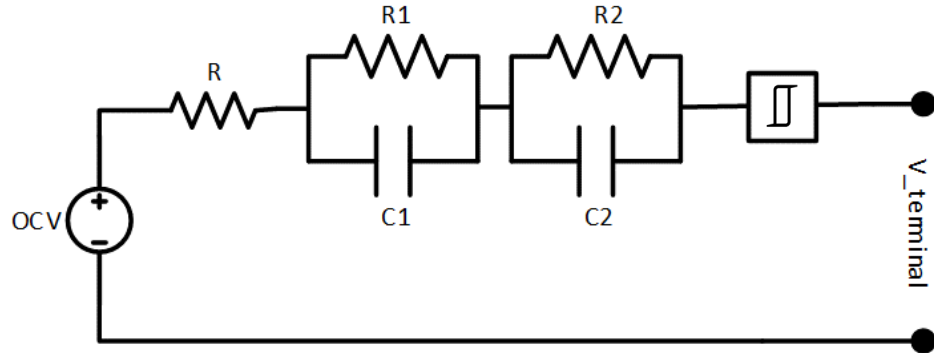


Figure 5.4 - Schematic Diagram for R-RC-RC\_H Battery Model

The R-RC-RC-H model can be represented as follows:

$$\begin{bmatrix} V_{1,k+1} \\ V_{2,k+1} \\ h_{k+1} \\ z_{k+1} \end{bmatrix} = \begin{bmatrix} 1 - \frac{\Delta t}{R_1 C_1} & 0 & 0 & 0 \\ 0 & 1 - \frac{\Delta t}{R_2 C_2} & 0 & 0 \\ 0 & 0 & F(i_k) & 0 \\ 0 & 0 & 0 & 1 \end{bmatrix} \begin{bmatrix} V_{1,k} \\ V_{2,k} \\ h_k \\ z_k \end{bmatrix} + \begin{bmatrix} \frac{\Delta t}{C_1} & 0 \\ \frac{\Delta t}{C_2} & 0 \\ 0 & (1 - F(i_k)) \\ -\frac{\eta_i \Delta t}{C} & 0 \end{bmatrix} \begin{bmatrix} i_k \\ M(z, \dot{z}) \end{bmatrix} \quad (5.7)$$

$$y_k = OCV(z_k) - Ri_k - V_{1,k} - V_{2,k} + h_k \quad (5.8)$$

The states of the system are  $z_k, V_{1,k}, V_{2,k}, h_k$  representing the SOC, voltage drop across the first RC pair, second RC pair, and hysteresis state respectively. The model has one output  $y_k$ , which is the terminal voltage, the current  $i_k$  is the input.

### 5.2.5. The 3<sup>rd</sup> Order RC Model

The OCV-R-RC-RC-RC model is as shown in Figure 5.5, [100]. The model is able to imitate the battery time constants for the battery voltage recovery from charge or discharge pulse.

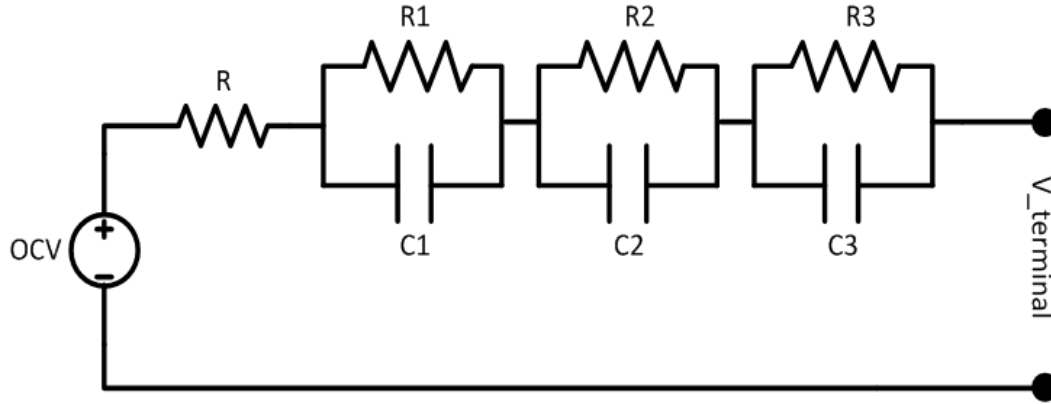


Figure 5.5 - Schematic Diagram for R-RC-RC-RC Battery Model

The R-RC-RC-RC model can be represented as follows:

$$\begin{bmatrix} V_{1,k+1} \\ V_{2,k+1} \\ V_{3,k+1} \\ z_{k+1} \end{bmatrix} = \begin{bmatrix} 1 - \frac{\Delta t}{R_1 C_1} & 0 & 0 & 0 \\ 0 & 1 - \frac{\Delta t}{R_2 C_2} & 0 & 0 \\ 0 & 0 & 1 - \frac{\Delta t}{R_3 C_3} & 0 \\ 0 & 0 & 0 & 1 \end{bmatrix} \begin{bmatrix} V_{1,k} \\ V_{2,k} \\ V_{3,k} \\ z_k \end{bmatrix} + \begin{bmatrix} \frac{\Delta t}{C_1} \\ \frac{\Delta t}{C_2} \\ \frac{\Delta t}{C_3} \\ -\frac{\eta_i \Delta t}{C} \end{bmatrix} [i_k] \quad (5.9)$$

$$y_k = OCV(z_k) - Ri_k - V_{1,k} - V_{2,k} - V_{3,k} \quad (5.10)$$

where  $R_1C_1$  represent polarization time constants,  $R_2C_2$  represent polarization time constants,  $R_3C_3$  are the third RC pair represent polarization time constants,  $V_{1,k}$  is a state and represents the voltage across the first RC pair,  $V_{2,k}$  is an internal state and represent the voltage across the second RC pair,  $V_{3,k}$  is a state in the system and represents the voltage across the third RC pair. The states of the system are  $z_k, V_{1,k}, V_{2,k}, V_{3,k}$ . The model has one output  $y_k$ , which is the terminal voltage, the current  $i_k$  is the input. The parameters vector to be optimized for this model is  $\theta = [R^+, R^-, R_1, R_2, R_3, C_1, C_2, C_3]$ .

### 5.2.6. The 3<sup>rd</sup> Order RC Model with One-State Hysteresis

The OCV-R-RC-RC-RC-H has an added hysteresis state over the OCV-R-RC-RC-RC as shown in Figure 5.6. The model consists of 9 elements (1) Open Circuit Voltage OCV, (2, 3, 4, 5) Internal Resistances, (6, 7, 8) Capacitors, and (9) Hysteresis state to capture the battery charging and discharging hysteresis effect.

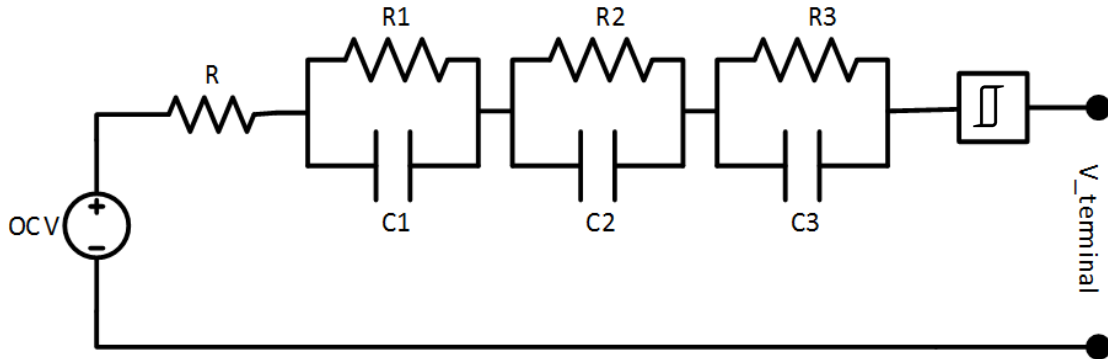


Figure 5.6 - Schematic Diagram for R-RC-RC-RC Battery Model

The R-RC-RC-RC-H model can be represented in a state space form as follows:

$$\begin{bmatrix} V_{1,k+1} \\ V_{2,k+1} \\ V_{3,k+1} \\ h_{k+1} \\ z_{k+1} \end{bmatrix} = \begin{bmatrix} 1 - \frac{\Delta t}{R_1 C_1} & 0 & 0 & 0 & 0 \\ 0 & 1 - \frac{\Delta t}{R_2 C_2} & 0 & 0 & 0 \\ 0 & 0 & 1 - \frac{\Delta t}{R_3 C_3} & 0 & 0 \\ 0 & 0 & 0 & F(i_k) & 0 \\ 0 & 0 & 0 & 0 & 1 \end{bmatrix} \begin{bmatrix} V_{1,k} \\ V_{2,k} \\ V_{3,k} \\ h_k \\ z_k \end{bmatrix} + \begin{bmatrix} \frac{\Delta t}{C_1} & 0 \\ \frac{\Delta t}{C_2} & 0 \\ \frac{\Delta t}{C_3} & 0 \\ 0 & (1 - F(i_k)) \\ -\frac{\eta_i \Delta t}{C} & 0 \end{bmatrix} \begin{bmatrix} i_k \\ M(z, \dot{z}) \end{bmatrix} \quad (5.11)$$

$$y_k = OCV(z_k) - Ri_k - V_{1,k} - V_{2,k} - V_{3,k} + h_k \quad (5.12)$$

The states of the system are  $z_k, V_{1,k}, V_{2,k}, V_{3,k}, h_k$  representing the SOC, voltage drop across the first RC pair, second RC pair, third RC pair and hysteresis state respectively. The model has one output  $y_k$ , which is the terminal voltage, the current  $i_k$  is the input.

Where the parameters vector to be optimized for this model is  $\theta = [R^+, R^-, R_1, R_2, R_3, C_1, C_2, C_3, M^+, M^-, \gamma]$ .

### 5.3. Model Parameter Tuning

The parametric vector  $\theta$  in each model is obtained by applying the same strategy as discussed in Chapter 4. The GPS optimization algorithm is used to tune the model parameters to fit the data shown in Figure 4.1 –Figure 4.4. These date are used for model parameter identification and represent approximately 25%, the renaming 75% are used for validating the model.

### 5.3.1. Simulation Results

The simulation data set of Figure 3.13 and Figure 3.14 were used as input to all models, the output of the models compared to the cell terminal voltage under UDDS cycle is shown in Figure 5.7 to Figure 5.12. The parametric vector  $\theta$  for all the models was obtained as in Table 5.2 using GPS optimization algorithm with data from Figure 4.1 and Figure 4.2.

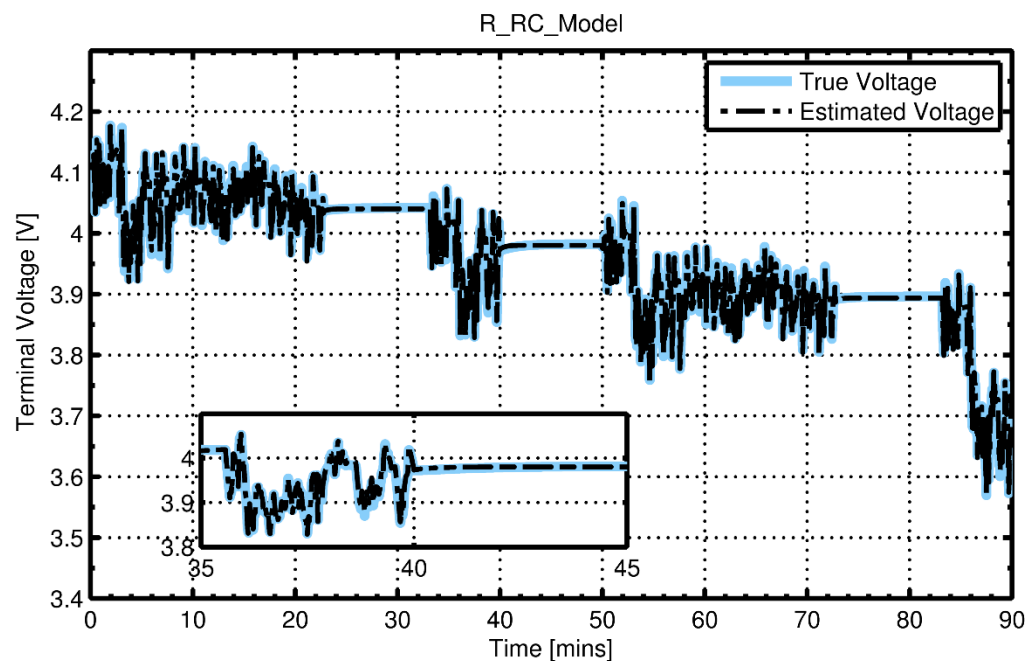


Figure 5.7 - Simulation results of cell modeling with R\_RC model showing the model terminal voltage versus simulated voltage

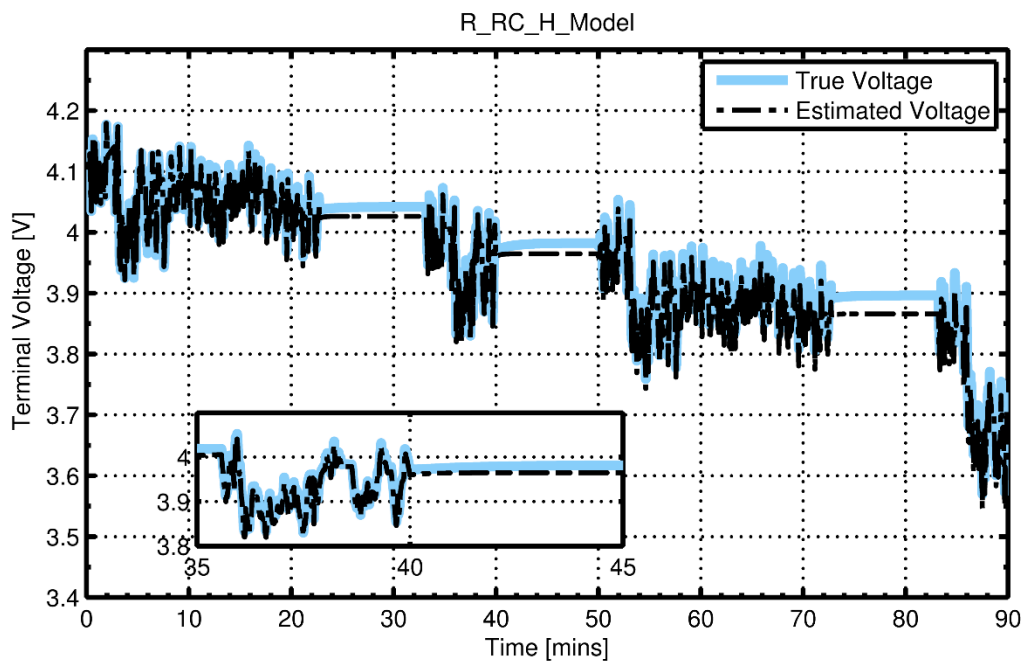


Figure 5.8 – Simulation results of cell modeling with R\_RC\_H model showing the model terminal voltage versus simulated voltage

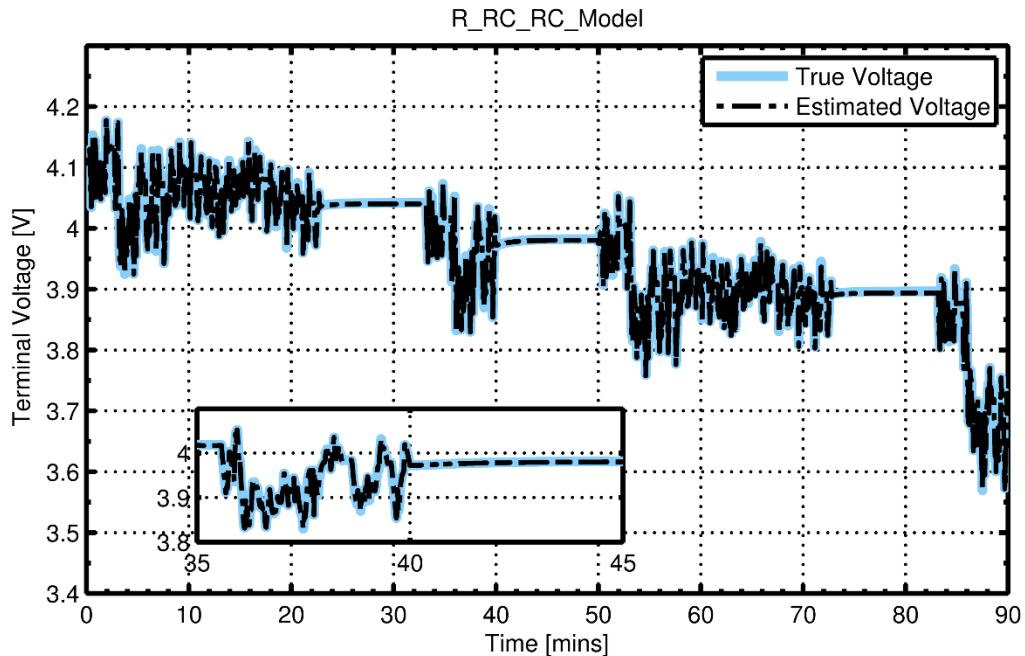


Figure 5.9 – Simulation results of cell modeling with R\_RC\_RC model showing the model terminal voltage versus simulated voltage

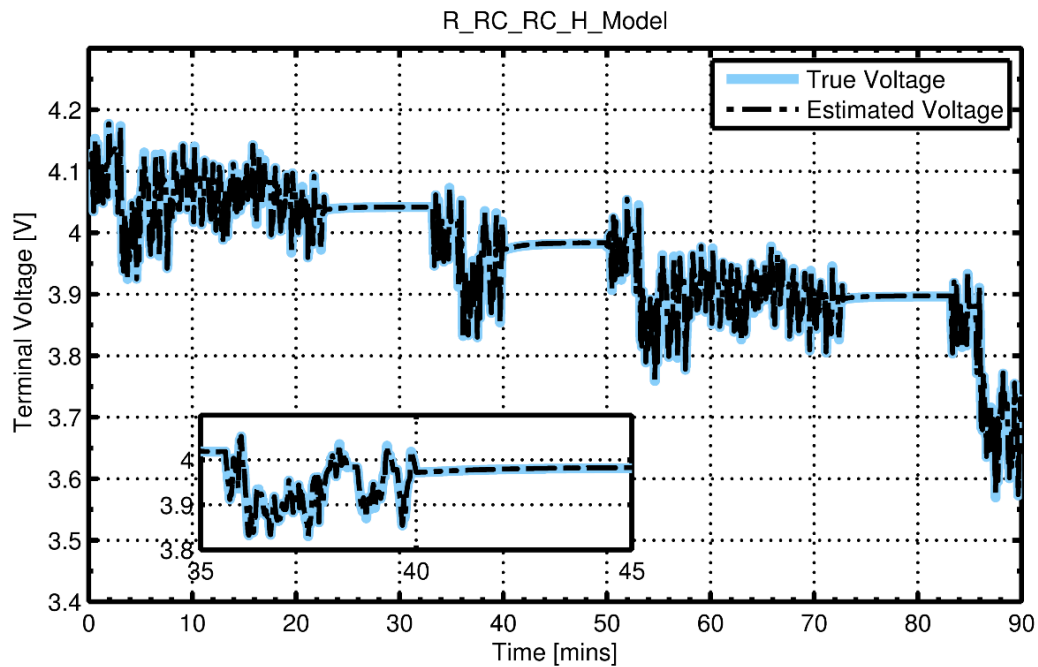


Figure 5.10 - Simulation results of cell modeling with R\_RC\_RC\_H model showing the model terminal voltage versus simulated voltage

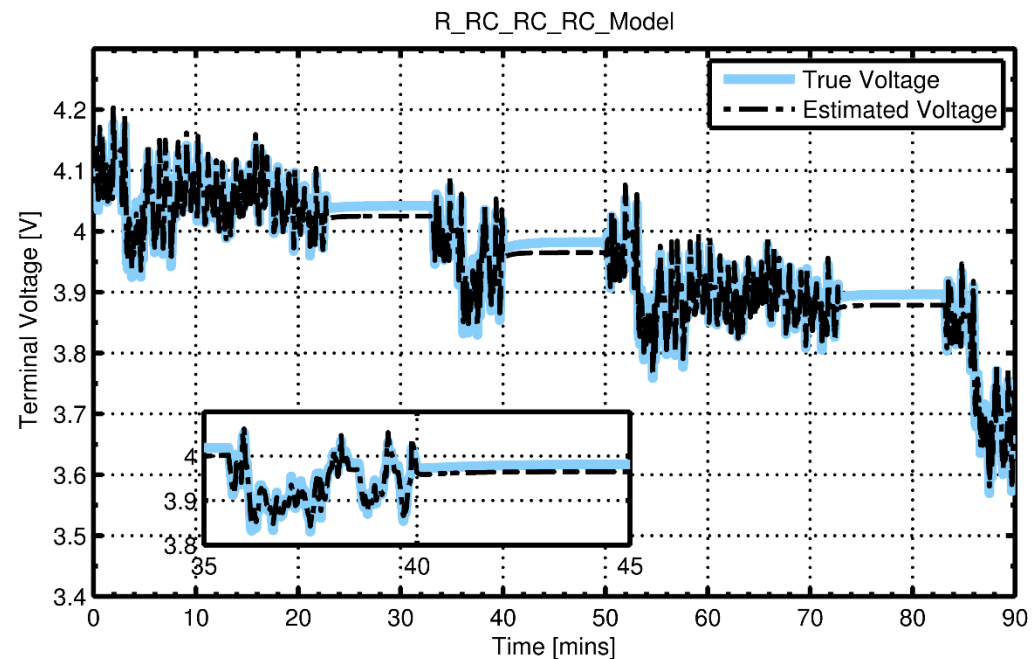


Figure 5.11 - Simulation results of cell modeling with R\_RC\_RC\_RC model showing the model terminal voltage versus simulated voltage

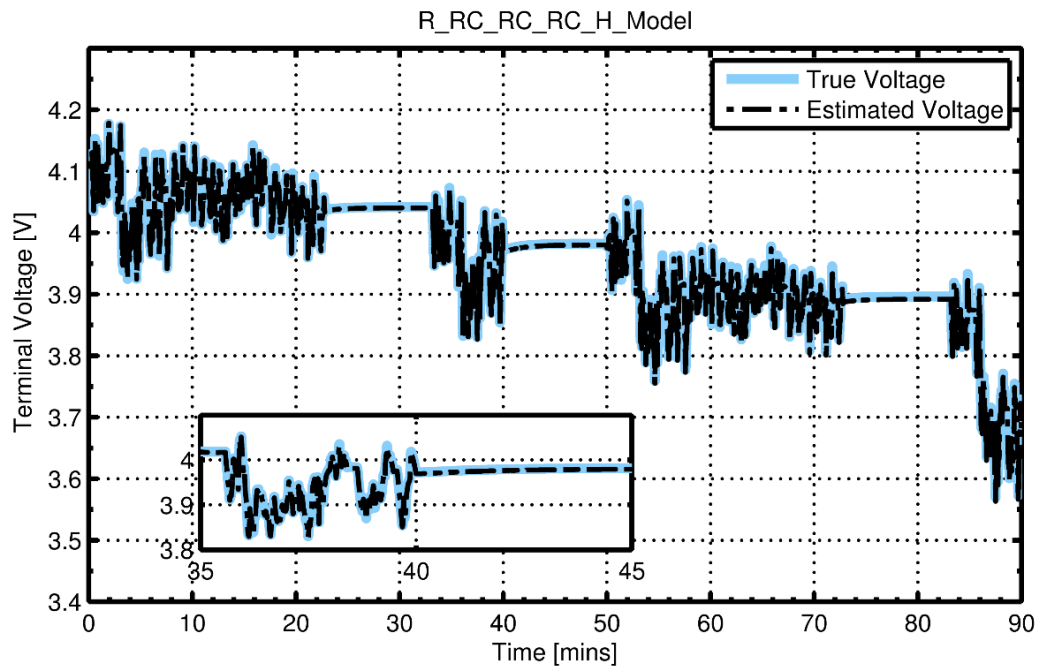


Figure 5.12 – Simulation results of cell modeling with R\_RC\_RC\_H model showing the model terminal voltage versus simulated voltage

The associated root mean squared error between the cell voltage and the simulated voltage is shown in Table 5.1.

Model Parameters	R_RC	R_RC_H	R_RC_RC	R_RC_RC_RC	R_RC_RC_RC_H	
RMSE	2.7	2.4	1.5	1.2	0.89	0.78

Table 5.1 – The RMSE for each model

Model Parameters	R_RC	R_RC_H	R_RC_RC	R_RC_RC_H	R_RC_RC_RC	R_RC_RC_RC_H
$R^+$	0.00182	0.00175	0.0017	0.0017	0.00104	0.0017
$R^-$	0.00173	0.00179	0.0017	0.0017	0.0024	0.0017
$R_1$	0.00124	0.00118	0.00062	0.00071	0.00065	0.00071
$C_1$	23691.5	20446.5	15397.04	14989.04	5847.08	14730.51
$R_2$	-	-	0.000935	0.00106	0.00106	0.00106
$C_2$	-	-	83763.66	101927.64	47719.07	100312.8
$R_3$	-	-	-	-	0.0002	0.0002
$C_3$	-	-	-	-	8.99E+09	8.99E+09
$M^+$	-	0.001	-	0.12	-	0.05915
$M^-$	-	-0.02	-	-0.19	-	-0.0499
$\gamma$	-	0.256	-	0.069	-	0.0693

Table 5.2 - The parametric Values for variable in all models

### 5.3.2. Experimental Results

The experimental data set of Figure 3.15 and Figure 3.17 were used as input to all models, the output of the models compared to the cell terminal voltage as shown in Figure 5.13 - Figure 5.18. The parametric vector  $\theta$  for all the models was obtained as in Table 5.4 using GPS algorithm with data from Figure 4.3 and Figure 4.4.

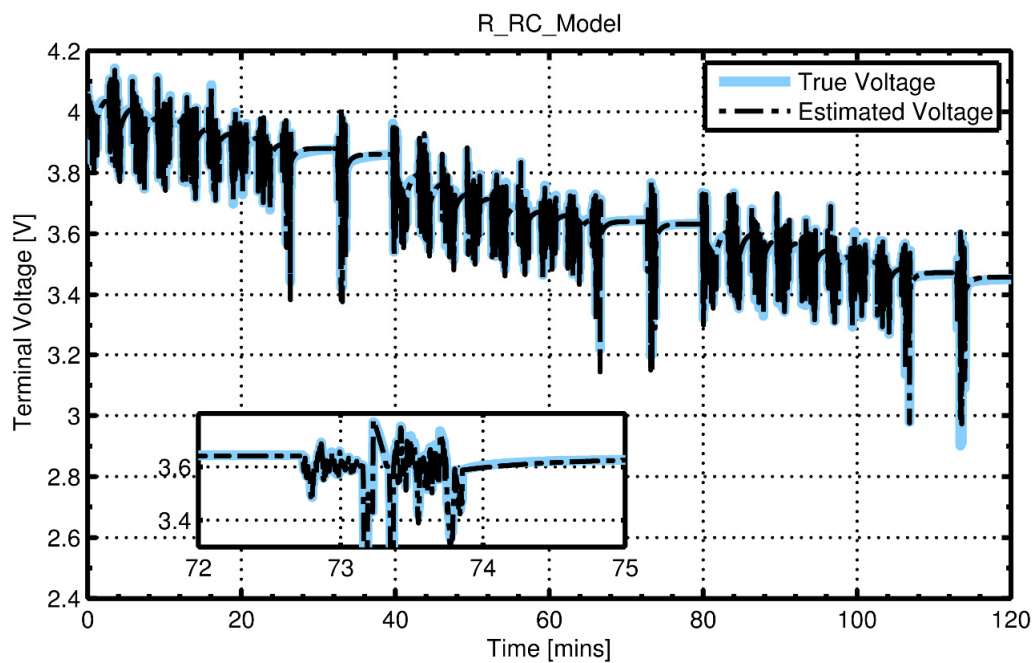


Figure 5.13– Experimental results of cell modeling with R\_RC model showing the model terminal voltage versus the true voltage

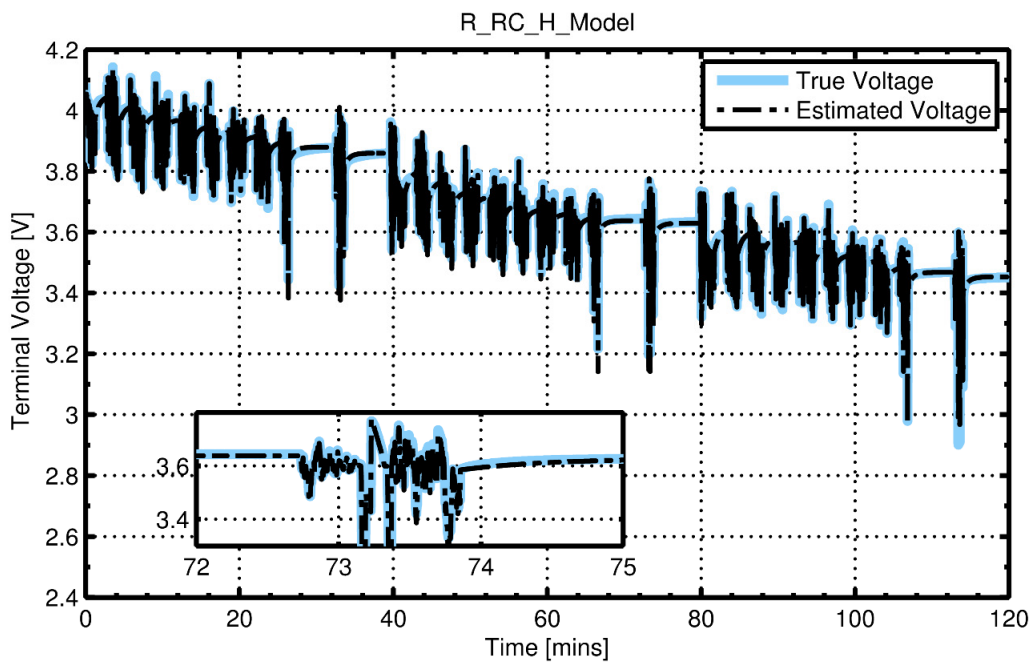


Figure 5.14– Experimental results of cell modeling with R\_RC\_H model showing the model terminal voltage versus the true voltage

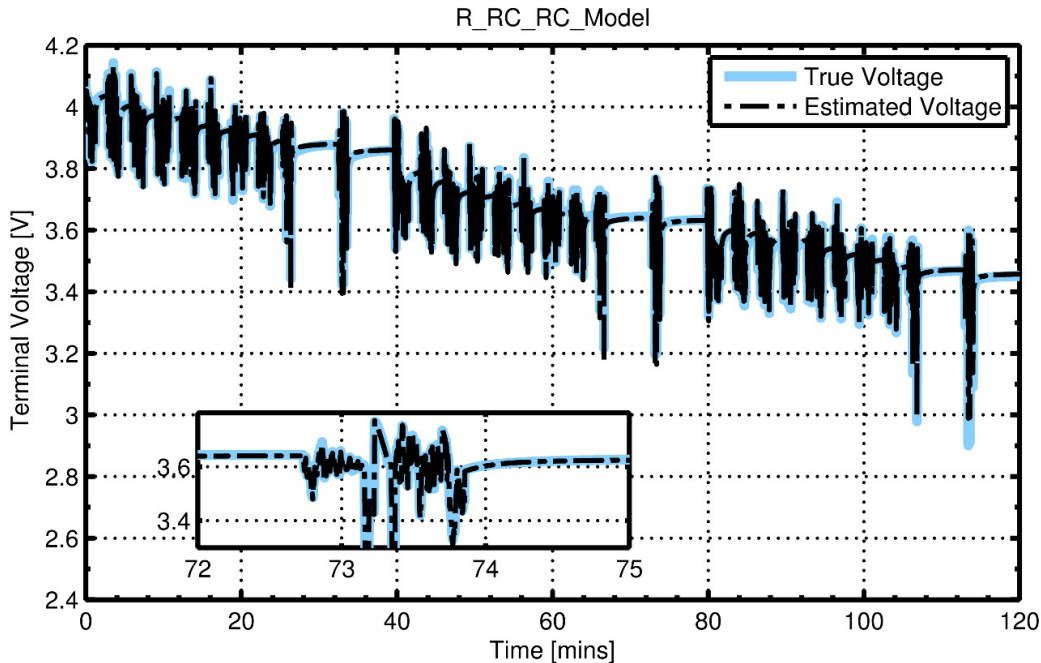


Figure 5.15– Experimental results of cell modeling with R\_RC\_RC model showing the model terminal voltage versus the true voltage

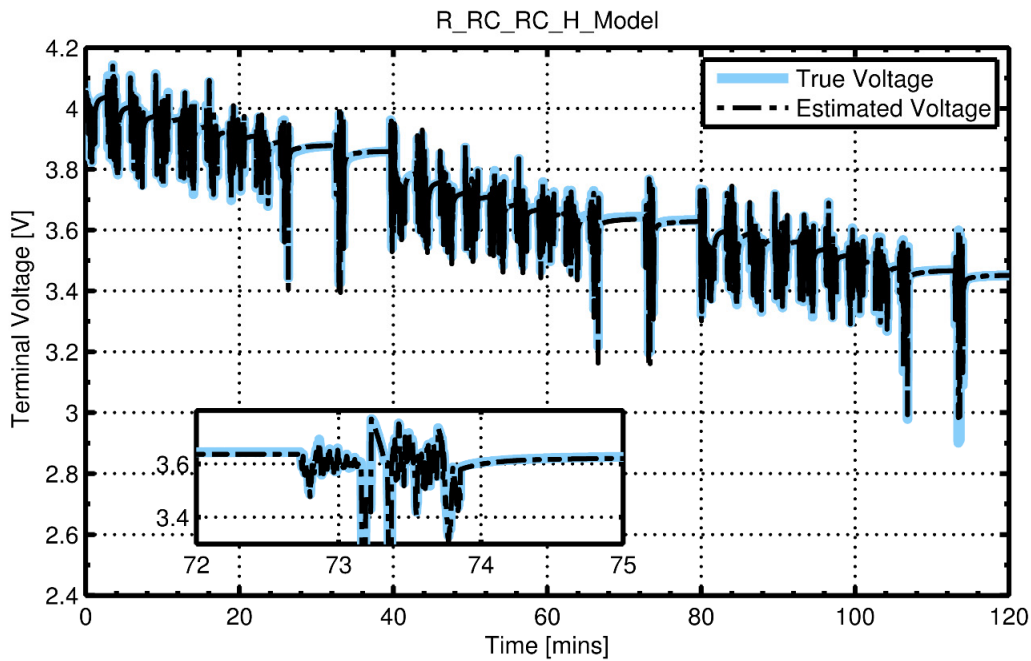


Figure 5.16– Experimental results of cell modeling with R\_RC\_RC\_H model showing the model terminal voltage versus the true voltage

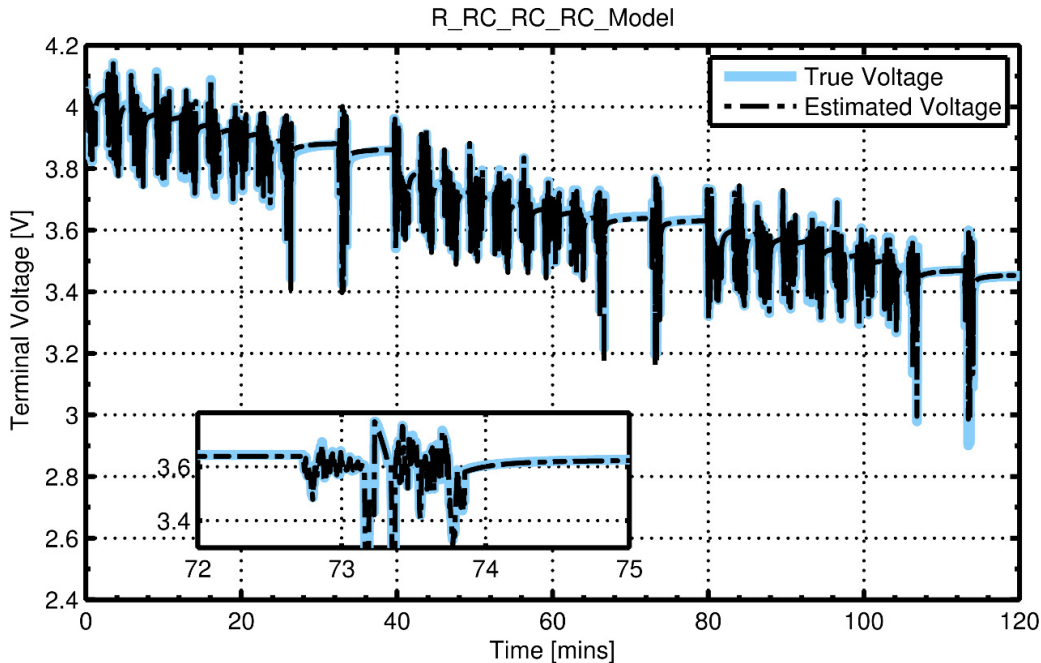


Figure 5.17 – Experimental results of cell modeling with R\_RC\_RC\_RC model showing the model terminal voltage versus the true voltage

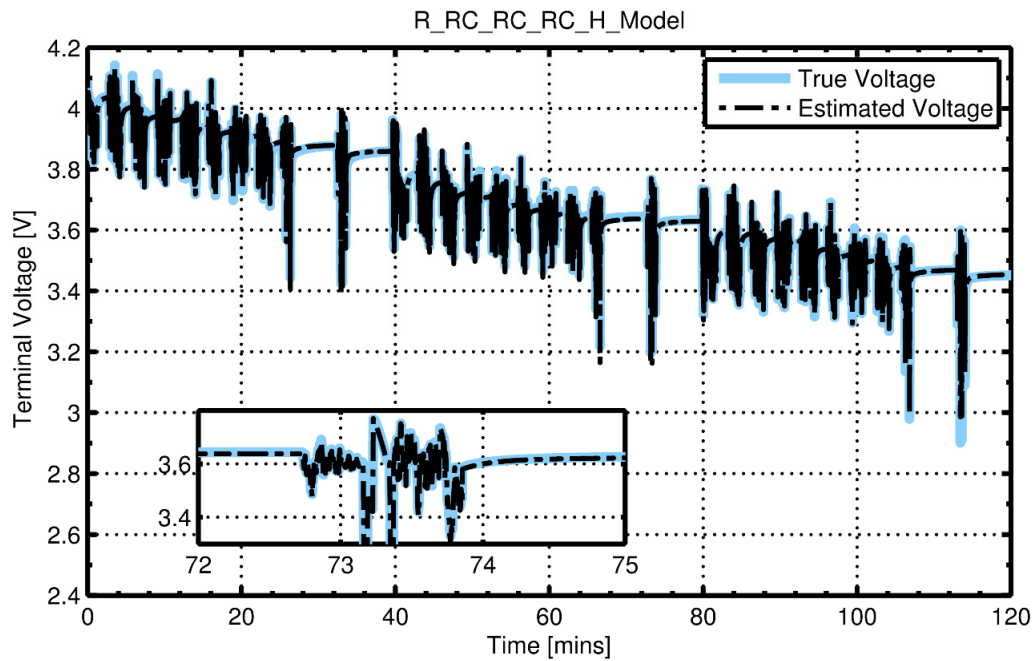


Figure 5.18 - Experimental results of cell modeling with R\_RC\_RC\_RC\_H model showing the model terminal voltage versus the true voltage

The associated root mean squared error between the cell voltage and the simulated voltage is shown in Table 5.3.

	R_RC	R_RC_H	R_RC_RC	R_RC_RC_H	R_RC_RC_RC	R_RC_RC_RC_H
RMSE	8.2	8	6.8	6.6	6.57	6.48

Table 5.3 – The RMSE for each model

Model Parameters	R_RC	R_RC_H	R_RC_RC	R_RC_RC_H	R_RC_RC_RC	R_RC_RC_RC_H
$R^+$	0.0014	0.0014	0.00132	0.00132	0.00131	0.00132
$R^-$	0.0012	0.0012	0.00132	0.00132	0.0013	0.00132
$R_1$	0.00175	0.0017	0.00077	0.00077	0.00077	0.00077
$C_1$	22310.6	22310.6	14475.24	14636.24	14466.37	14939.24
$R_2$	-	-	0.0011	0.0011	0.001178	0.0011
$C_2$	-	-	98246.01	98246.02	90704.65	95449.01
$R_3$	-	-	-	-	0.01057	6.49E-05
$C_3$	-	-	-	-	9745774.7	9.99E+09
$M^+$	-	0.0754	-	0.077	-	0.077065
$M^-$	-	-0.9153	-	-0.819	-	-0.8167
$\gamma$	-	0.04807	-	0.062	-	0.0425

Table 5.4 - The parametric Values for variable in all models

## 5.4. SOC Estimation

The SOC estimation results using the EKF and the SVSF for all of the six modeling techniques are presented in this section.

### 5.4.1. Simulation Results

In this section, the EKF SOC and SVSF SOC estimation results will be presented and compared to the simulated and hence known value of the SOC for Equivalent Circuit Models as shown in Figure 5.19 - Figure 5.24. The estimated SOC is initialized at 85% while the true SOC is at 95% (i.e. 10% error). For all models the EKF system and measurement noise covariance, and the SVSF ‘memory’ or convergence rate and smoothing boundary layers were obtained as in Table 5.6. The RMSE associated with SOC estimation using the EKF and the SVSF was obtained as in Table 5.5.

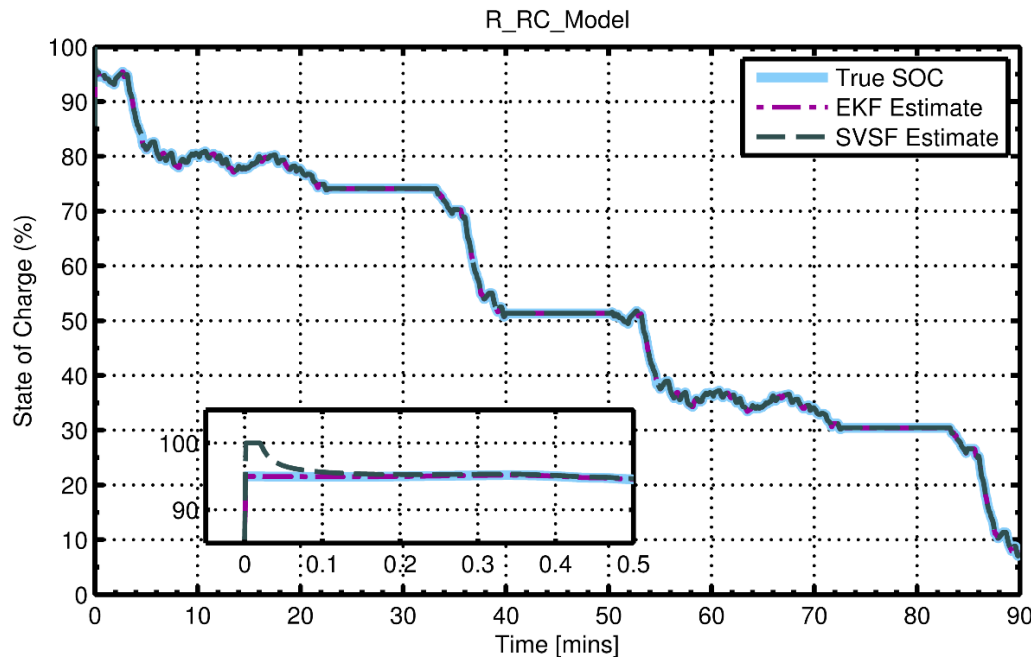


Figure 5.19 - Simulation results of SOC estimation with R\_RC model showing the EKF and SVSF estimated versus model SOC.

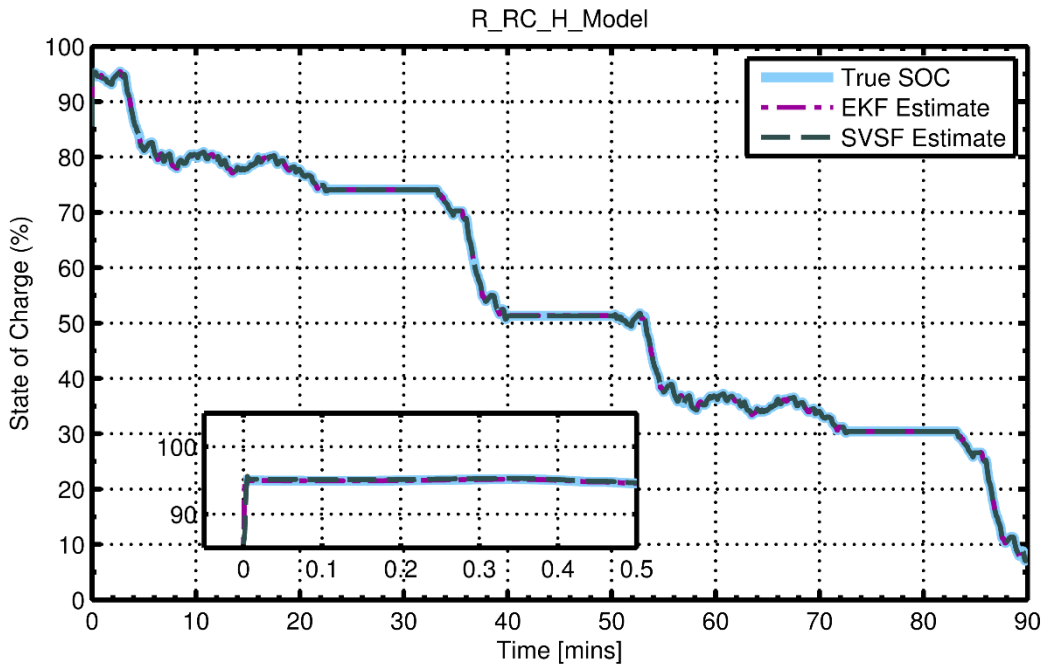


Figure 5.20 - Simulation results of SOC estimation with R\_RC\_H model showing the EKF and SVSF estimated versus model SOC.

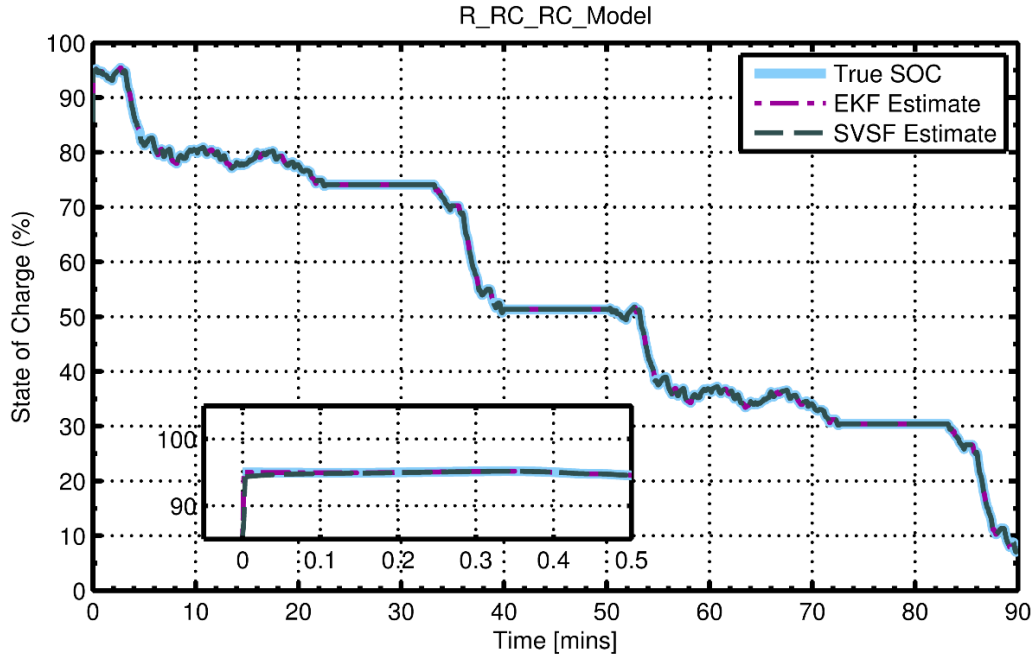


Figure 5.21 - Simulation results of SOC estimation with R\_RC\_RC model showing the EKF and SVSF estimated versus model SOC.

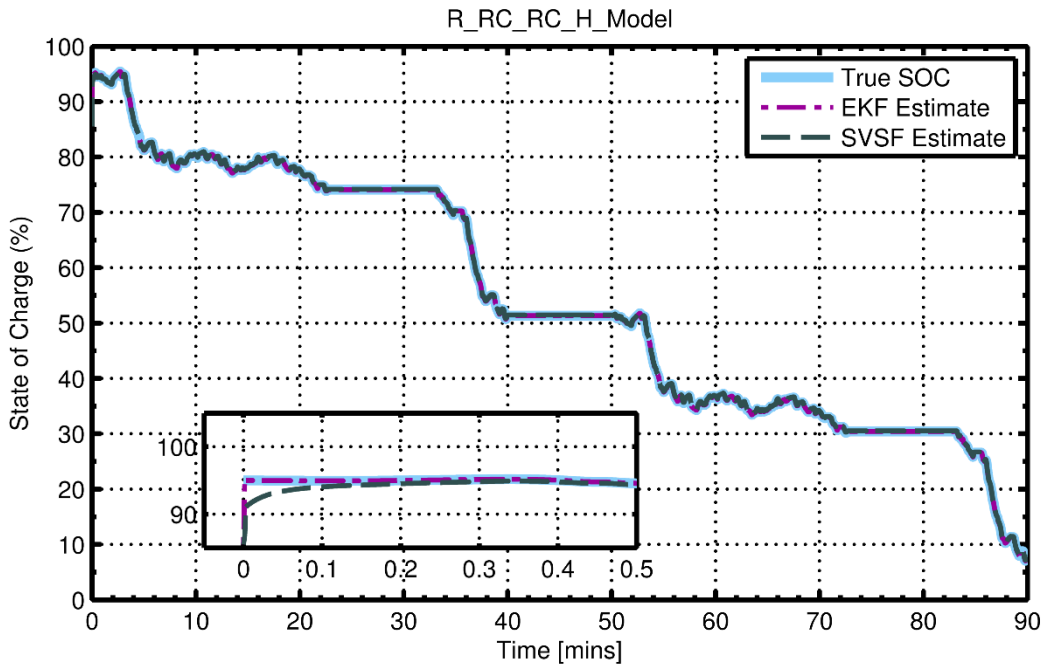


Figure 5.22 - Simulation results of SOC estimation with R\_RC\_RC\_H model showing the EKF and SVSF estimated versus model SOC.

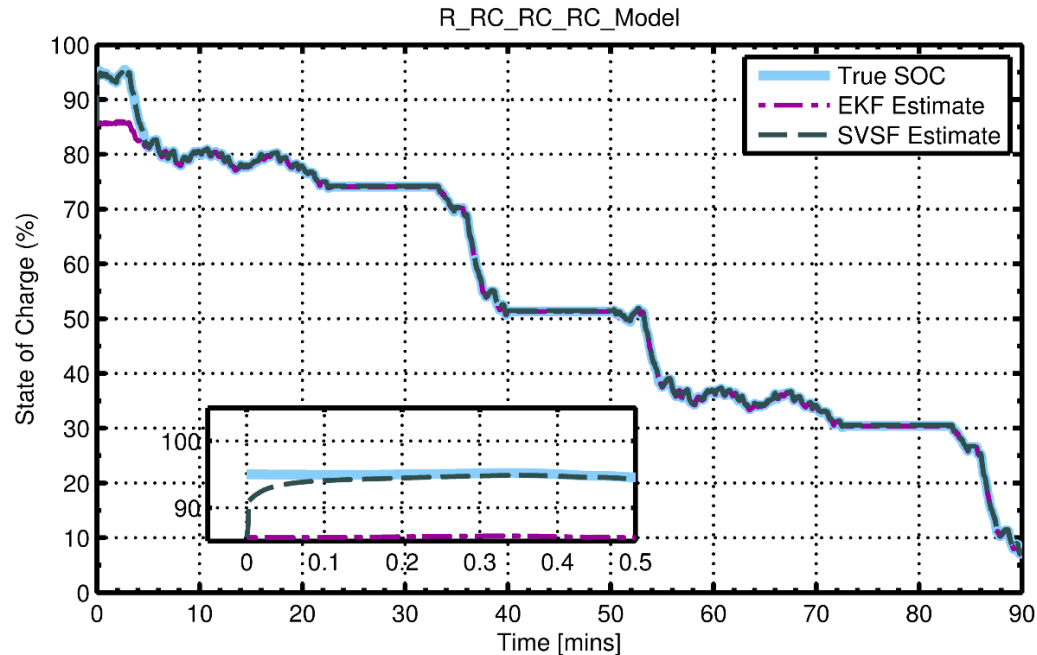


Figure 5.23 - Simulation results of SOC estimation with R\_RC\_RC\_RC model showing the EKF and SVSF estimated versus model SOC.

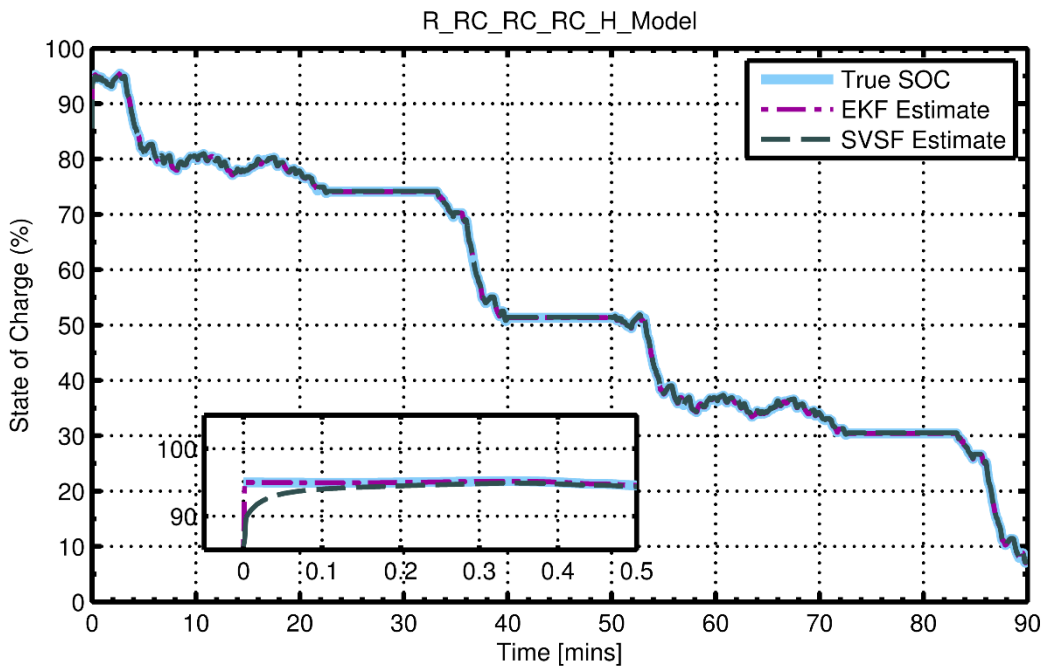


Figure 5.24 - Simulation results of SOC estimation with R\_RC\_RC\_RC\_H model showing the EKF and SSVF estimated versus model SOC.

RMSE	R_RC	R_RC_H	R_RC_RC	R_RC_RC_H	R_RC_RC_RC	R_RC_RC_RC_H
EKF -SOC [%]	0.47	0.39	0.31	0.24	0.16	0.12
SVSF -SOC [%]	0.48	0.37	0.34	0.2	0.14	0.12

Table 5.5 – Root mean squared error (RMSE) for SOC using the EKF and the SSVF.

Filter Parameters									
The Extended Kalman Filter (EKF)	$Q$	diag(0.00018, 86.73)		R_RC		R_RC_H			
	$R$	0.0519	0.0519	0.0519	0.0519	0.0519	0.0519	R_RC_RC	
The Smooth Variable Structure Filter (SVSF)	$\psi$	1.94	0.0105	3.058	4.043	4.02	4.038		
	$\gamma$	0.9	0.109	0.503	0.506	0.484	0.441		

Table 5.6 – The EKF system and measurement noise covariance, and the SVSF ‘memory’ or convergence rate and smoothing boundary layers.

### 5.4.2. Experimental Results

In this section, the EKF SOC and SVSF SOC estimation results will be presented and compared to the true SOC for Behavioral models as shown in the following figures () .

In this section, the estimated EKF SOC and SVSF SOC will be presented and compared to the experimental SOC for Equivalent Circuit Models as shown in Figure 5.25 - Figure 5.30. The estimated SOC is initialized at 90% while the true SOC is at 100% (i.e. 10% error). For all models the EKF system and measurement noise covariance, and the SVSF ‘memory’ or convergence rate and smoothing boundary layers were obtained as in Table 5.8. The RMSE associated with SOC estimation using the EKF and the SVSF was obtained as in Table 5.7.

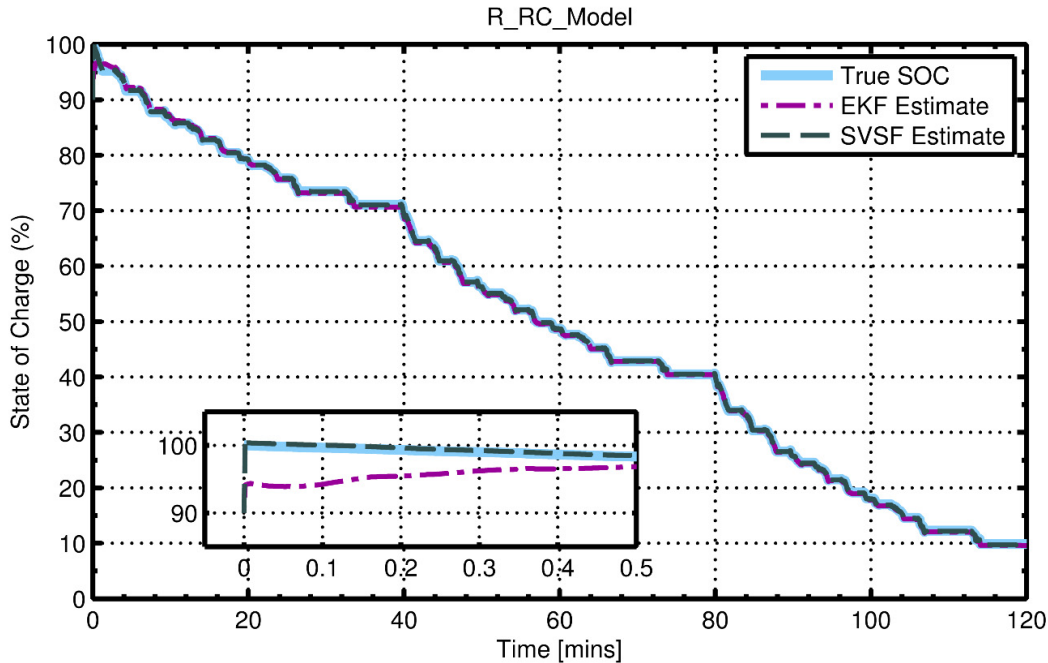


Figure 5.25 - Experimental results of SOC estimation with R\_RC model showing the EKF and SVSF estimated versus model SOC.

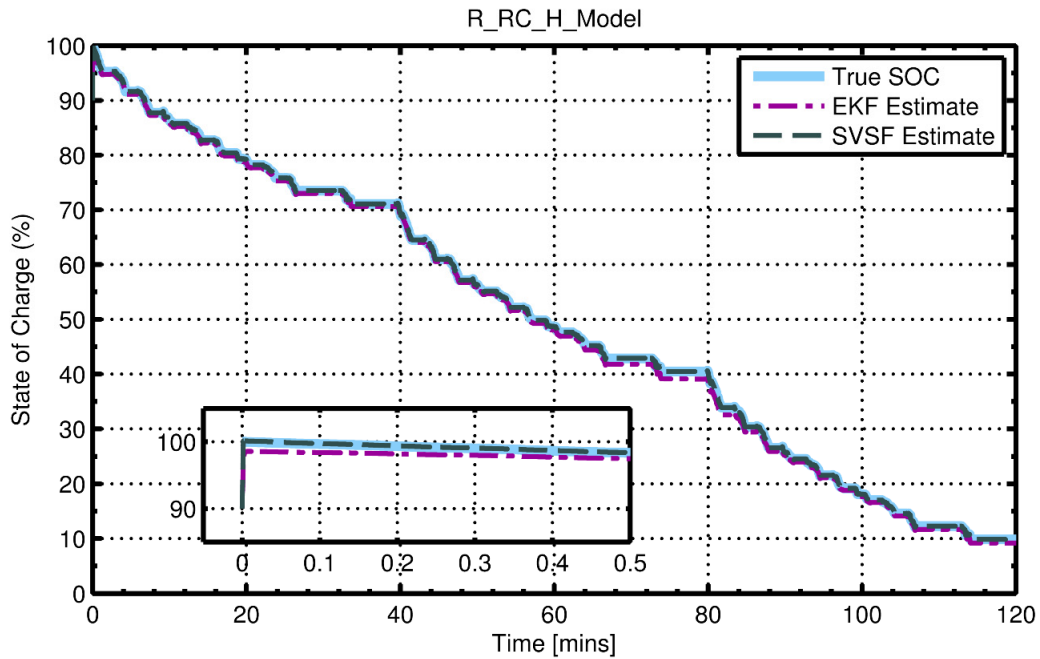


Figure 5.26 - Experimental results of SOC estimation with R\_RC\_H model showing the EKF and SVSF estimated versus model SOC.

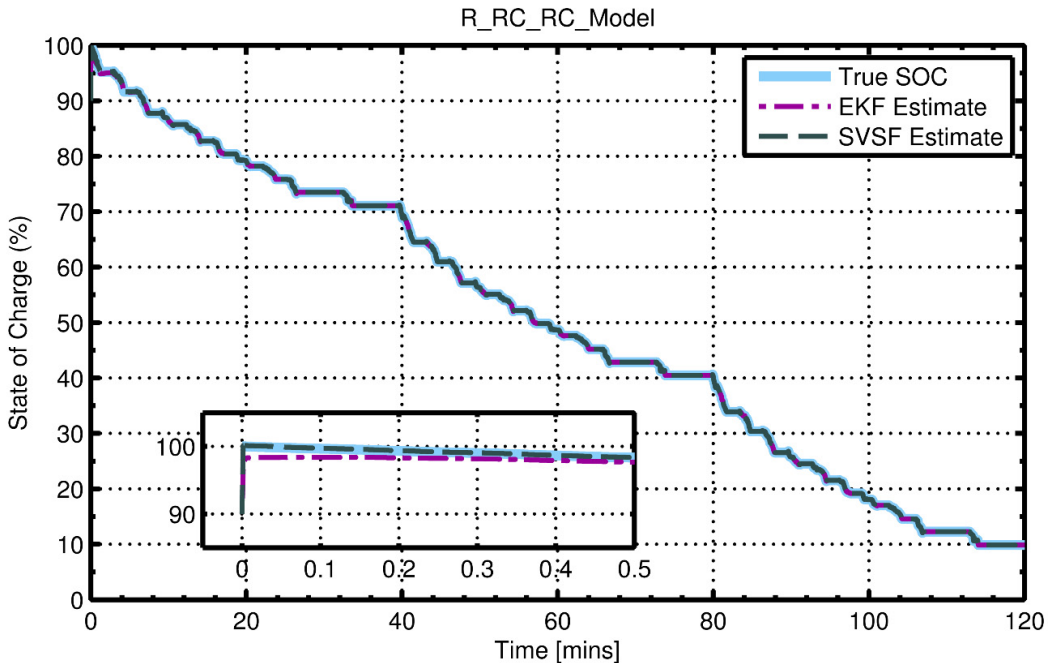


Figure 5.27 - Experimental results of SOC estimation with R\_RC\_RC model showing the EKF and SVSF estimated versus model SOC.

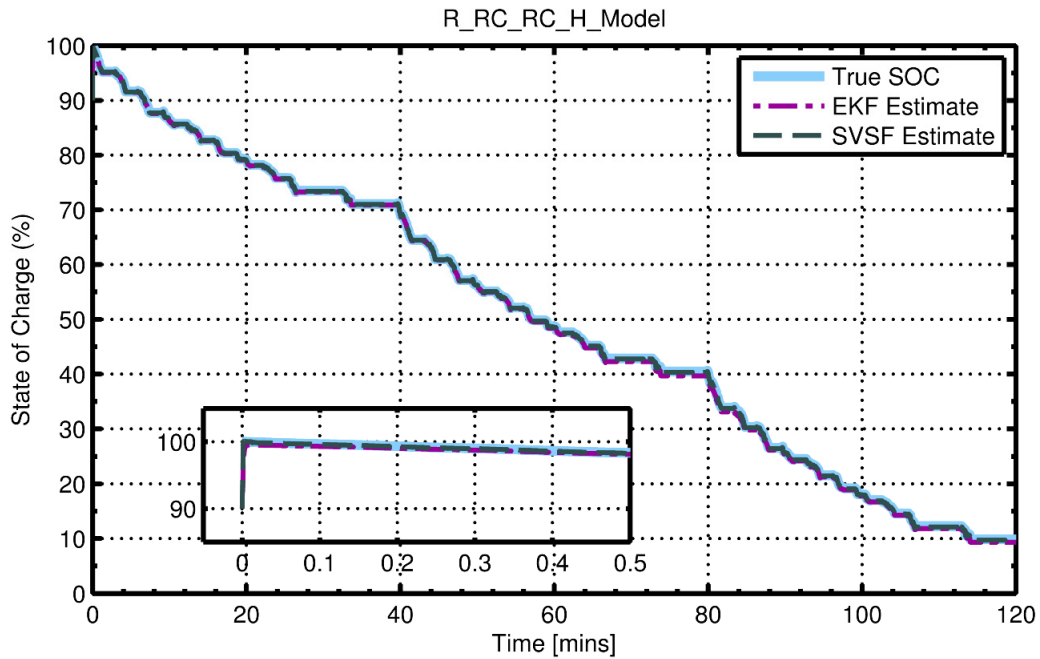


Figure 5.28 - Experimental results of SOC estimation with R\_RC\_RC\_H model showing the EKF and SVSF estimated versus model SOC.

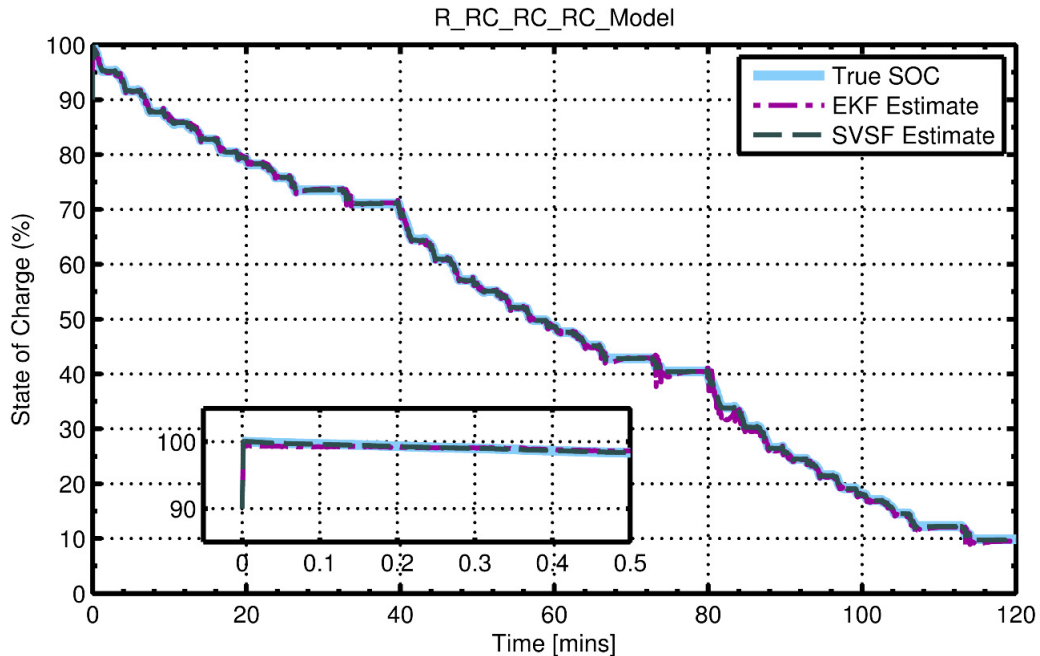


Figure 5.29 - Experimental results of SOC estimation with R\_RC\_RC\_RC model showing the EKF and SVSF estimated versus model SOC.

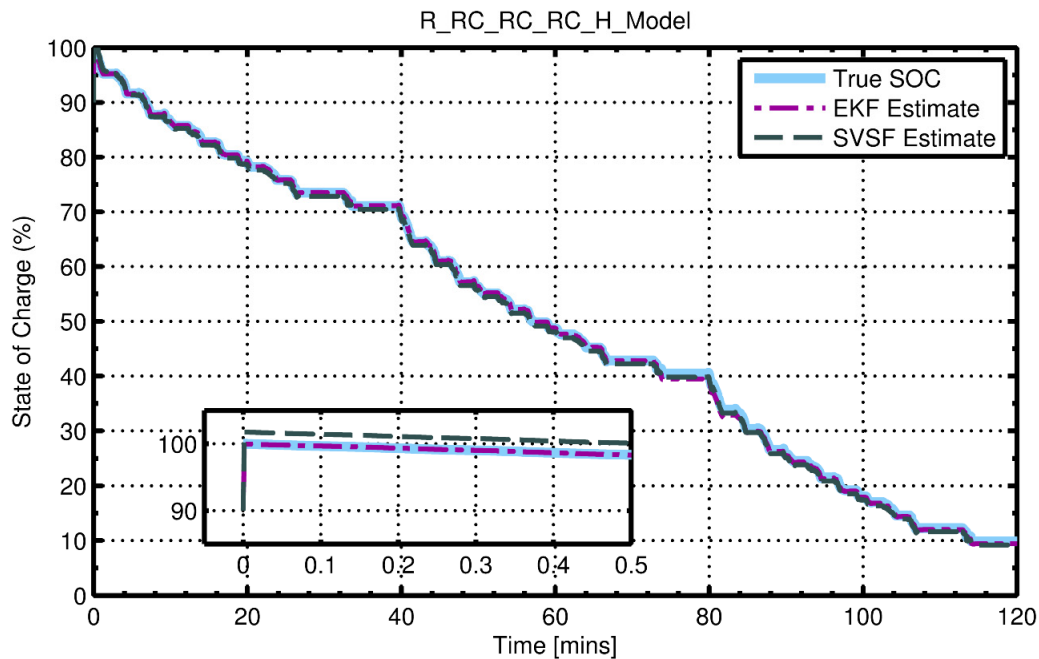


Figure 5.30 - Experimental results of SOC estimation with R\_RC\_RC\_RC\_H model showing the EKF and SVSF estimated versus model SOC.

RMSE	R_RC	R_RC_H	R_RC_RC	R_RC_RC_H	R_RC_RC_RC	R_RC_RC_RC_H
EKF -SOC [%]	0.76	0.70	0.56	0.44	0.42	0.36
SVSF -SOC [%]	0.61	0.36	0.30	0.22	0.14	0.14

Table 5.7 – Root mean squared error (RMSE) for SOC using the EKF and the SVSF for experimental data.

Filter Parameters									
The Extended Kalman Filter (EKF)	$Q$	diag(0.0151 , 0.0001 )		R_RC		R_RC_H			
	$R$	0.065	0.065	0.065	0.065	0.065	0.065	R_RC_RC	
The Smooth Variable Structure Filter (SVSF)	$\psi$	0.1356	0.1246	0.1424	0.0001	0.0677	0.0597		
	$\gamma$	0.7557	0.9979	0.8788	0.9659	0.4762	0.9936	R_RC_RC_RC	
		diag(0.0088 , 0.0001 , 0.0001 , 0.0053 , 5.4680)		R_RC_RC_RC_H					

Table 5.8 – The EKF experimental system and measurement noise covariance, and the SVSF ‘memory’ or convergence rate and smoothing boundary layers.

## 5.5. Summary

This chapter provided a description of Equivalent Circuit Models and their implementation. These models are widely used because they are simple, have less parameters to tune, and are easy to implement [35,36]. The Equivalent circuit models consist of first-order, second-order, or third-order RC models in addition to hysteresis effect [37]. The model parameters were optimized using Globalized Pattern Search Matlab toolbox.

A comparison of the model accuracies in capturing the measured terminal voltage for the six different models is shown in Figure 5.31 and Figure 5.32. The terminal voltage Root Mean squared Error (RMSE) is shown as a measure of performance. The error is the difference between the fitted models after parameter identification and the true voltage.

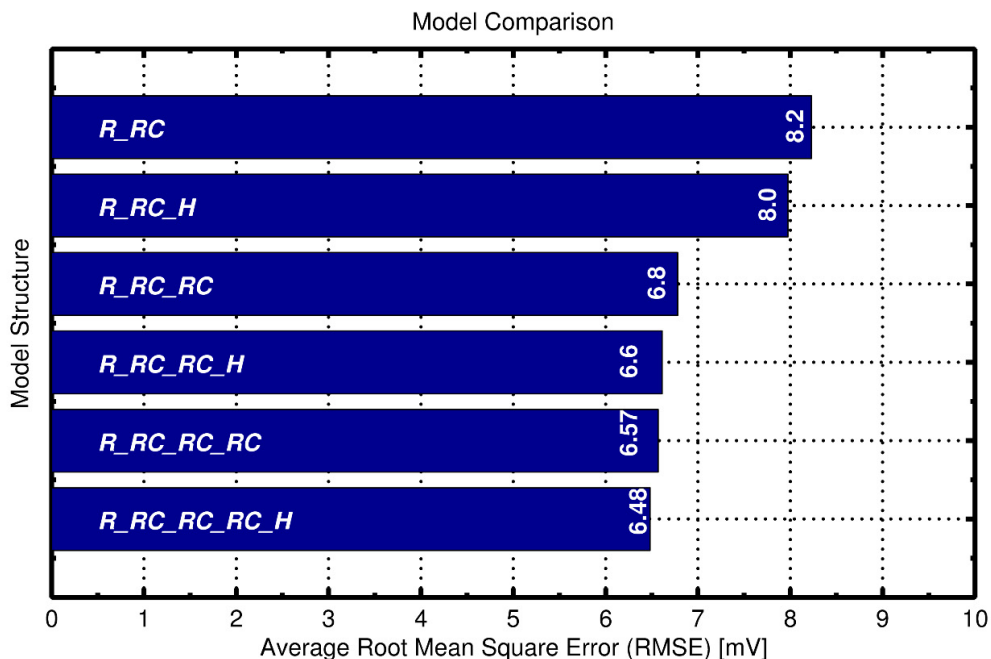


Figure 5.31– Experimental Results for Equivalent Circuit Models comparison of average modeling results

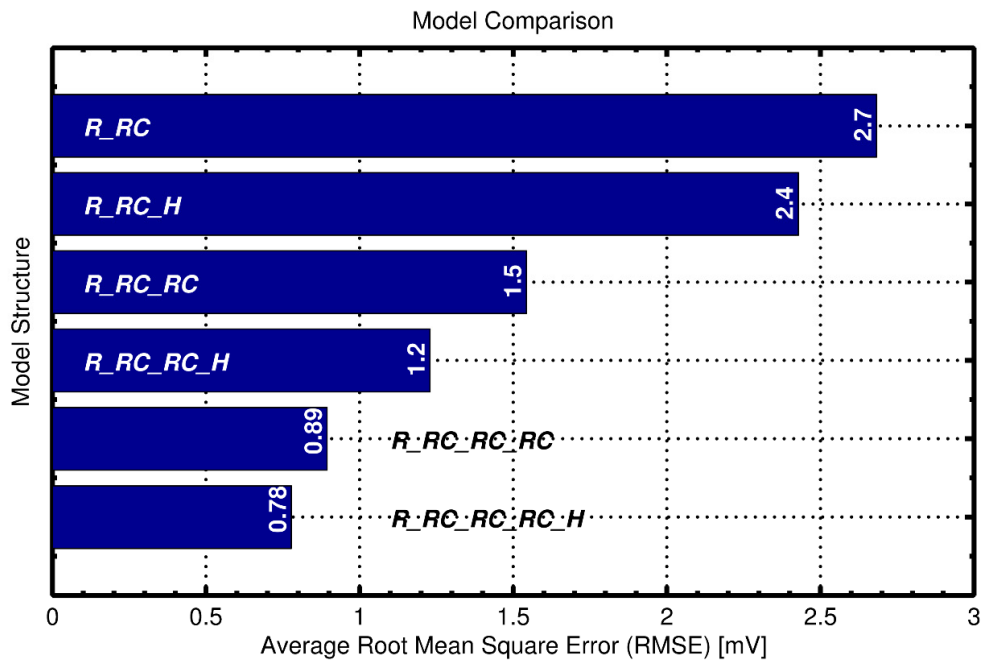


Figure 5.32 - Simulation Experimental Results for Equivalent Circuit Models comparison of average modeling results

As shown in Figure 5.31 and Figure 5.32. The model accuracy increase by increasing the number of states and parameters. Figure 5.33 and Figure 5.34 shows the SVSF and the EKF state of charge estimation against simulation and experimental results respectively. The figures show SOC estimation results of the six model as discussed earlier. The SOC Root Mean squared Error (RMSE) percentage is shown as performance measure. According to Figure 5.33 and Figure 5.34 the SVSF has shown better results compared to the EKF.

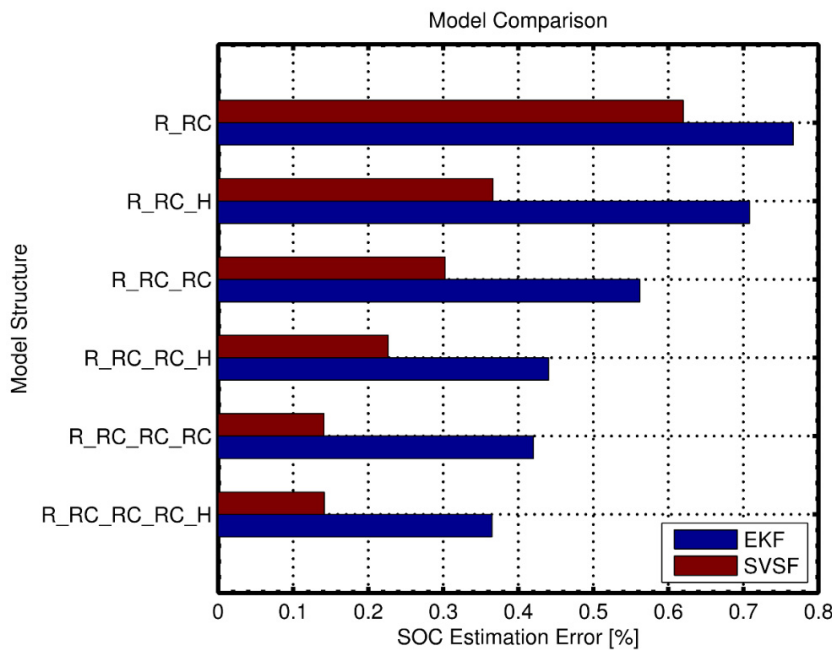


Figure 5.33 - Experimental Results for Equivalent Circuit Models comparison of SOC Estimation Error using EKF and SVSF

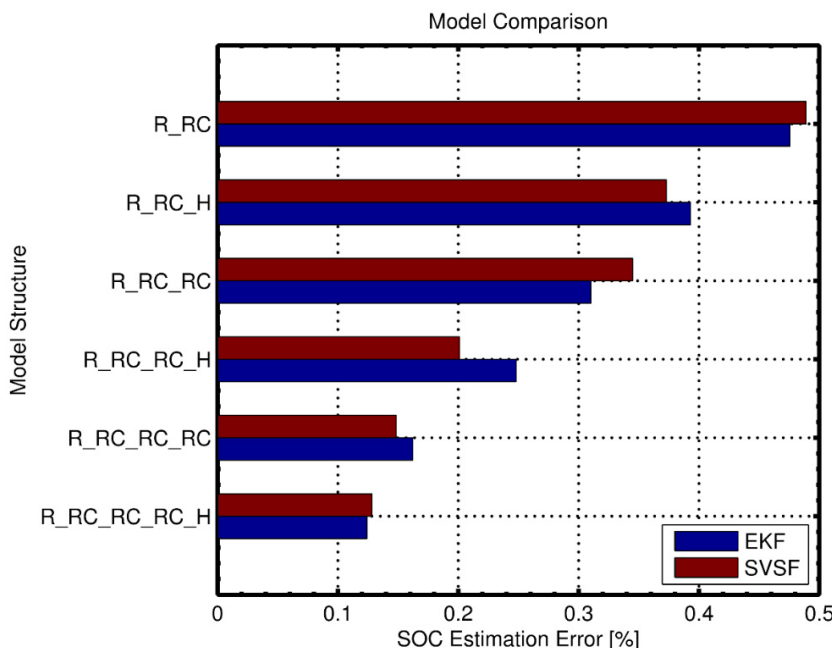


Figure 5.34 - Experimental Results for Equivalent Circuit Models comparison of SOC Estimation Error using EKF and SVSF

---

## Electro-Chemical Modelling

---

In this chapter, an electro-chemical model of the Lithium ion (Li-ion) cell using electrolyte is developed. The model is a spatially discretized partial differential equations (PDEs) in One Dimension (1D). In section 6.1, a general background and brief description of the working of the cell is discussed. In section 6.2 a full-order electro-chemical model with PDEs is described, the cell PDEs is discretized in one dimension resulting in a high order non-linear function. Simulation of such a high order model is slow, complex and computationally unpractical for real time implementation. In section 6.3, a Single Particle model is presented by simplifying the non-linear functions, then discretizing and rearranging them into a state-space form. In section 6.4, SOC estimation is presented using the Single Particle Model with SVSF and EKF. Conclusions are provided in section 6.5.

## 6.1. Overview of Li-Ion Battery Composition and Operation

The basic operation of the lithium ion batteries is discussed in Chapter 2. Here, an explanation of the mechanism associate with the charging and discharging of a cell is provided.

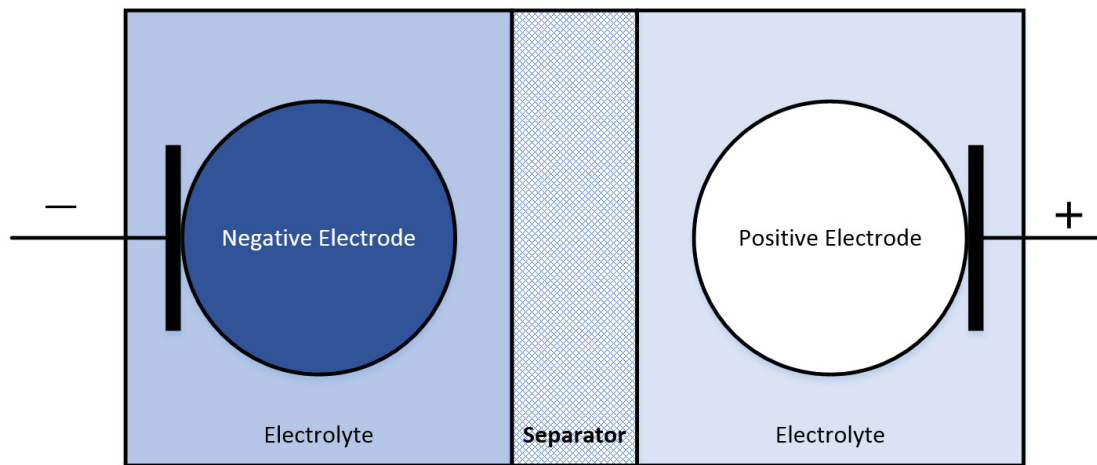


Figure 6.1 - Fully charged battery (100%)

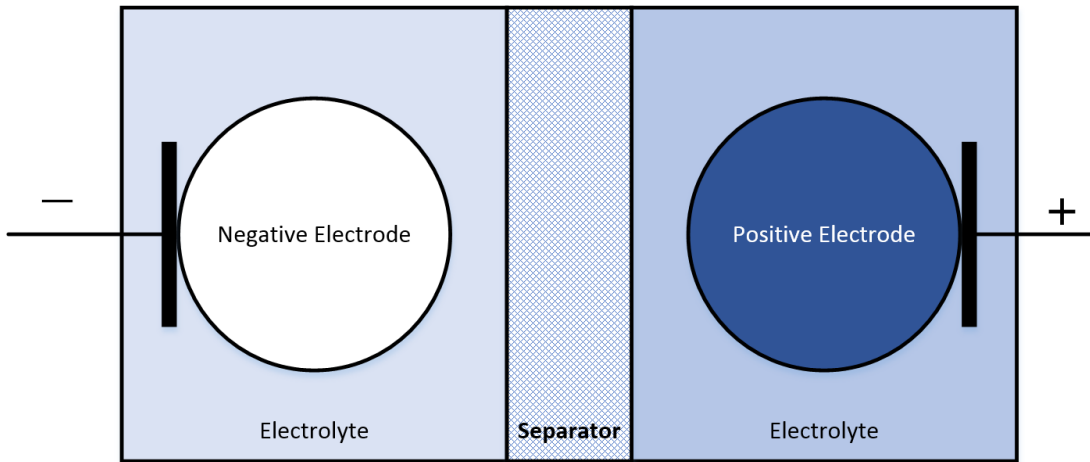


Figure 6.2 - Fully discharged battery (0%)

As shown in Figure 6.1 and Figure 6.2, the cell consists of a negative electrode and a positive electrode immersed in an electrolyte and a separator. A simplified approach involve treating the electrodes as a spherical particle.

When the cell is fully charged, the negative electrode is full with lithium ions i.e. the concentration of Lithium ions is at a maximum, as represented by a dark blue color in the Figure 6.1. The positive electrode is fully depleted of lithium ions. As the cell discharges, the Lithium ions moves from solid to liquid at the surface of the negative electrode. They travel through the electrolyte across the separator and reach the positive electrode. At the surface of the positive electrode, they again convert from liquid to solid and the positive electrode gets slowly charged with lithium ions. Thus during discharge, the concentration of Lithium ions decreases at the negative electrode while it increases at the positive electrode to finally reach a maximum. The exact opposite process happens during charging. End of discharge or charge is nothing but saturation or depletion of Lithium ion concentration at either electrode. These values of saturation or depletion of concentration can be considered as 0% and 100% of SOC and the intermediate range is a measure of SOC in percentage.

The concentration of Lithium ions cannot be measured so estimation techniques are used to infer its value from the Terminal Voltage of the cell. This terminal voltage is directly correlated to Lithium ion concentration at the surface of the electrodes. As can be seen from the Figure 6.1 and Figure 6.2, the terminal contacts can only give information of the surface concentration, not the bulk concentration. In case of low magnitude of charging and discharging currents, the surface concentration is almost equal to the bulk concentration and the terminal voltage can provide a measure of the SOC directly and without need of dynamic models. While, in case of high charging and discharging currents, gradients start forming in the electrodes as shown in Figure 6.4. This happens because the transport of Lithium ions from the inner regions to the surface occurs by diffusion and, if the current is high, the diffusion in both electrodes is not able to keep up

with the reaction rate at the electrode surface and the concentration of the lithium-ion at the electrode surface becomes lower compared to the inner regions at the anode. The exact opposite happens at the cathode. Moreover the transport of Lithium ions through the electrolyte again by diffusion can also prove to be sluggish resulting lithium-ion electrolyte gradients as shown in Figure 6.4.

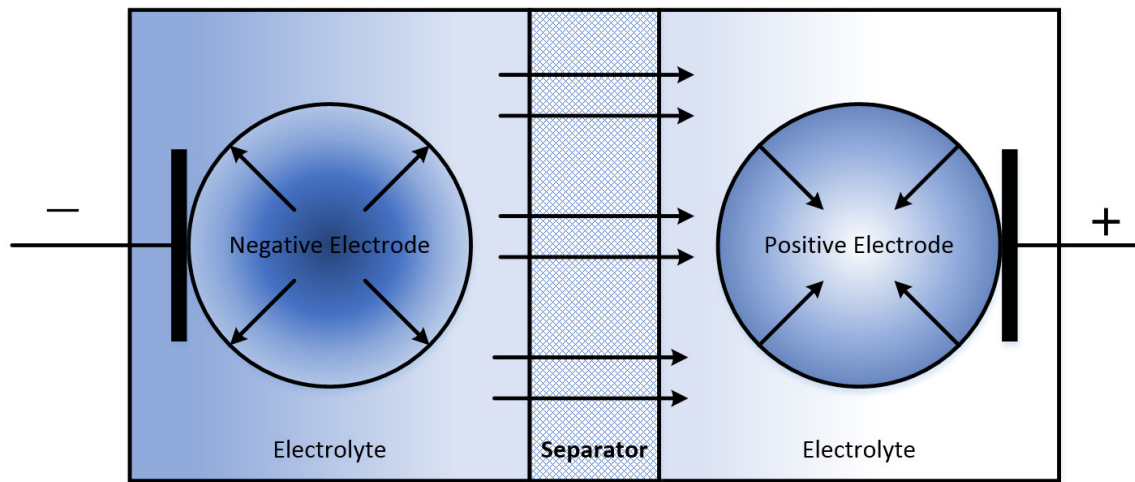


Figure 6.3 - Simplified schematic diagram showing concentration gradients during high rate discharge

The cell can be considered as a dynamic system, with current input, terminal voltage as its measurable output and the internal dynamics governed by the diffusion phenomena. The SOC can be considered as an internal state of the system which is the bulk concentration of the lithium-ions in the solid electrode particles that needs to be estimated using the terminal voltage. The terminal voltage is in turn correlated to the lithium-ion concentration in the electrode solid particles. Thus as a measure of the available SOC, the electrode average concentration of a single can be used as follows:

$$SOC(t) = \frac{c_{s,\text{avg}}(t) - c_{s,0\%}}{c_{s,100\%} - c_{s,0\%}} \quad (6.1)$$

Where  $c_{s,avg}(t)$  is the electrode average concentration at time  $(t)$ ,  $c_{s,0\%}$  and  $c_{s,100\%}$  are the reference values of concentration at 0% and 100% SOC respectively. This SOC definition is based on the fraction of concentration available in the solid phase. The concentration of lithium will be described using partial differential equations as will be explained in the next section.

## 6.2. The Full Order Electro-Chemical Model

In this section, the electrochemical model is considered. A one-dimensional (1D)-spatial model of the battery dynamics is developed along only one axis (the horizontal x-axis) while neglecting the dynamics in the other dimensions (Y-axis and Z-axis) [101,102] as shown in Figure 6.4

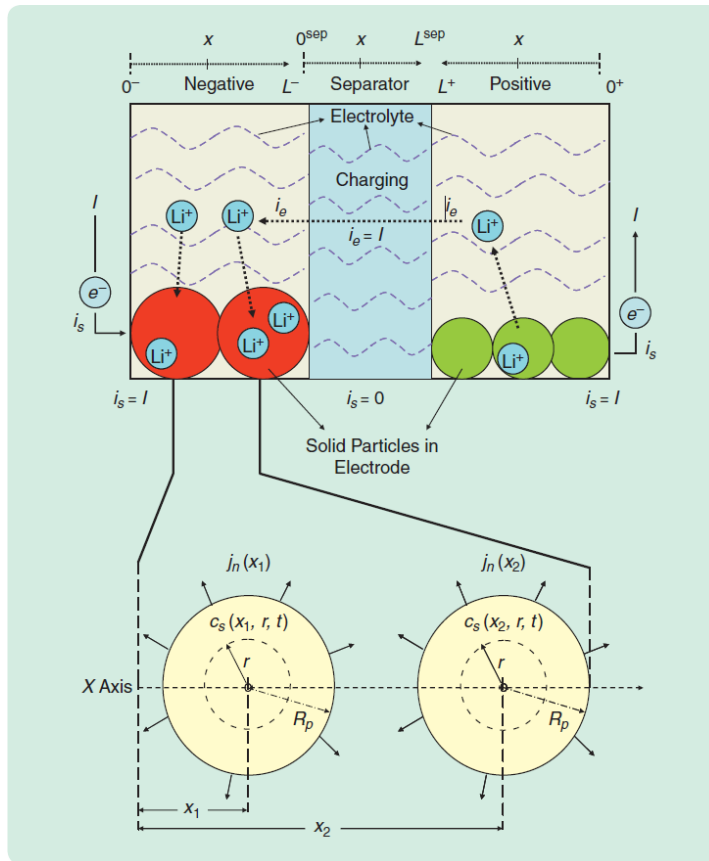


Figure 6.4 - Schematic diagram showing the intercalation approach for a battery cell [15]

The one-dimensional (1D)-spatial model can be described by four sets of equations:

- Lithium ion Conservation Equations
- Charge Conservation Equations
- Butler-Volmer Kinetics Equations
- Cell Potential Measurable Equations

The parameters for the cell and the model can be obtained from manufacturers, in the case of the cell considered in this research the parameters were obtained from [47] and can be found in Appendix A.

### 6.2.1. Lithium Ion Conservation Equations

These set of equations consider the change in concentration of the lithium ion in space and time inside both the electrodes solid spherical particles and the electrolyte.

*In case of electrodes*, equation (6.2) represents the conservation of Lithium ions in a single particle as described by Fick's law of diffusion, assuming it is a sphere of radius  $R_s$

$$\frac{\partial c_s(x, r, t)}{\partial t} = \frac{1}{r^2} \frac{\partial}{\partial r} \left( D_s r^2 \frac{\partial c_s(x, r, t)}{\partial r} \right) \quad (6.2)$$

Where  $c_s$  is the lithium ion concentration in the electrode solid particle,  $r$  is the particle radial radius,  $x$  is the particle location in  $x$  direction, and  $D_s$  is the solid phase diffusion coefficient. The boundary conditions for equation (6.2) are as follows:

$$\left. \frac{\partial c_s}{\partial r} \right|_{r=0} = 0 \quad (6.3)$$

$$D_s \left. \frac{\partial c_s}{\partial r} \right|_{r=R_s} = \frac{-j^{Li}}{a_s F} \quad (6.4)$$

Where  $a_s$  is the interfacial surface area,  $F$  is the Faraday's constant, and  $j^{Li}$  is the volumetric rate of chemical reaction. These equations reveals that at the surface of the

spherical particles, the rate at which ions exit the particle and enter the electrolyte is related to the volumetric rate of chemical reaction  $j^{Li}$ , and this rate is zero at the centre of the particle and is as  $\frac{-j^{Li}}{a_s F}$  at the interface of the electrode particle as shown in Figure 6.5 . Note that we neglect diffusion between adjacent particles due to the high solid phase diffusive impedance between particles.

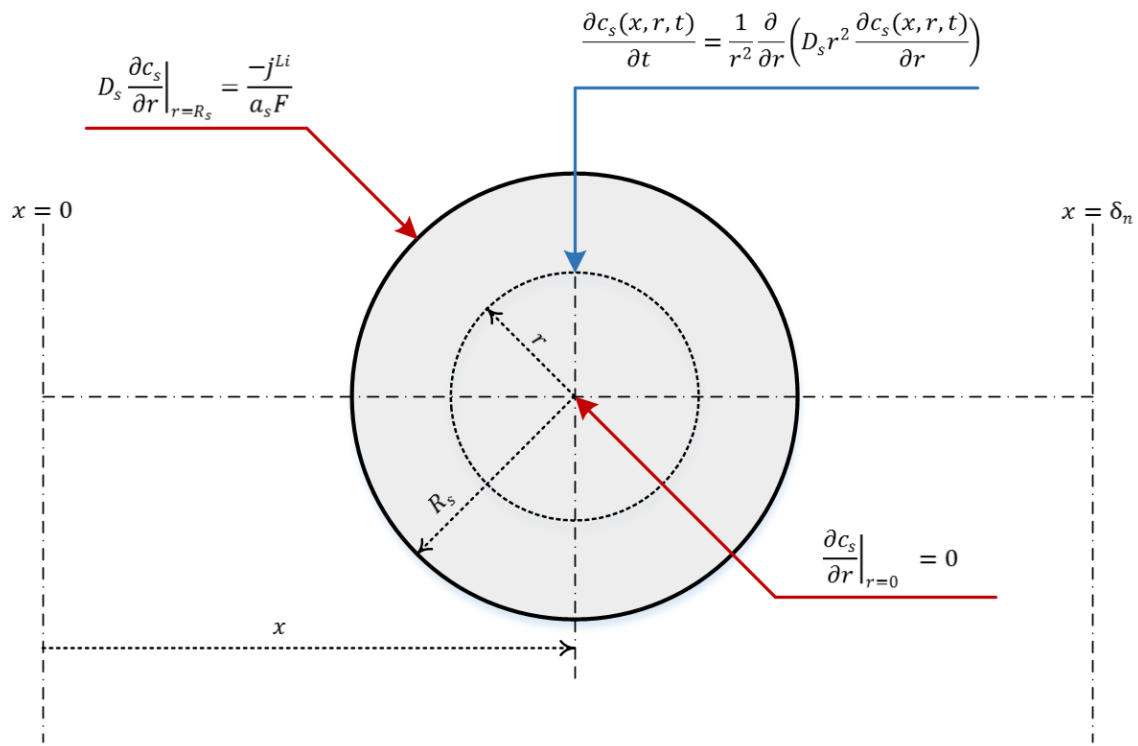


Figure 6.5 - Schematic simplification of lithium conservation equations in electrode spherical particle, red line equations represent boundary conditions, blue line represent the lithium ion governing equation

At the surface of the spherical particle  $c_s(x, r, t) = c_s(x, R_s, t)$ , and is equal to  $c_{se}(x, t)$  that describes the lithium concentration at the surface of the electrode spherical particle [17].

*In the case of Electrolyte*, the conservation of Lithium ions in the electrolyte phase is as follows [18]:

$$\frac{\partial \varepsilon_e c_e(x, t)}{\partial t} = \frac{\partial}{\partial x} \left( D_e^{eff} \frac{\partial c_e(x, t)}{\partial x} \right) + \frac{1 - t^0}{F} j^{Li} \quad (6.5)$$

Where  $c_e$  is the lithium concentration in the electrolyte,  $D_e^{eff}$  is the effective diffusion coefficient,  $\varepsilon_e$  is the volume fraction of the electrolyte (porosity), and  $t^0$  is the transference number<sup>4</sup> of the  $Li^+$  ions. The boundary conditions for equation (6.5) are as follows:

$$\left. \frac{\partial c_e}{\partial x} \right|_{x=0} = 0 \quad (6.6)$$

$$\left. \frac{\partial c_e}{\partial x} \right|_{x=L} = 0 \quad (6.7)$$

Which says that at the battery terminals the gradient of electrolyte concentration is zero as shown in Figure 6.6.

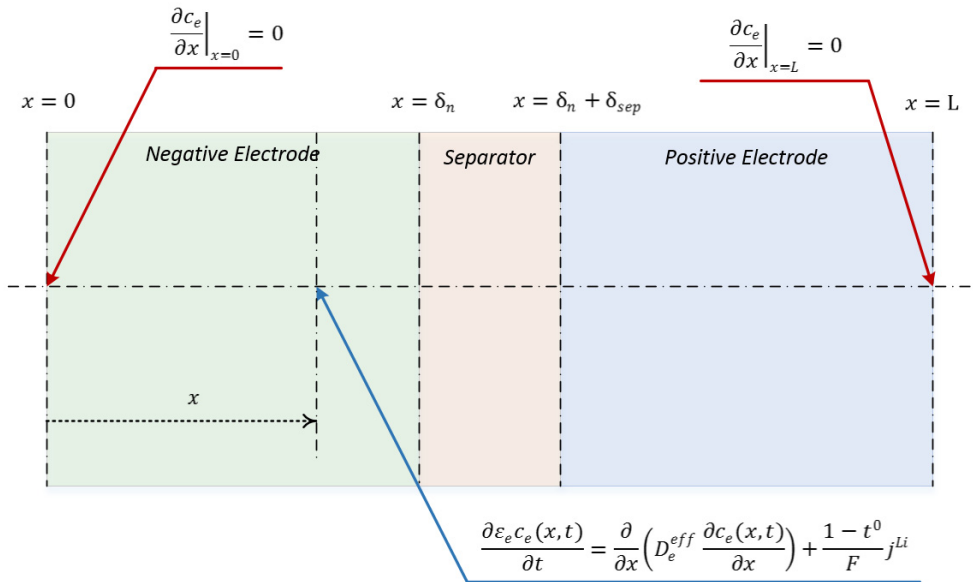


Figure 6.6 - Schematic simplification of lithium conservation equations in electrolyte, red line represent boundary conditions equations, blue line represent the governing equation

<sup>4</sup> Transference number is the fraction of the total electric current that anions and cations carry in passing through an electrolytic solution.

### 6.2.2. Charge Conservation Equations

These set of equations consider the relationship between the electrode potentials and currents inside the cell.

*In the case of electrodes*, the entire current leaves or enters the cell through the electrode spherical particles at the terminals. The current flowing in the electrode is governed by Ohm's law as [1]:

$$i_s(x) = -\sigma^{eff} \frac{\partial}{\partial x} \phi_s(x, t) \quad (6.8)$$

Where  $\sigma^{eff}$  is the solid phase effective conductivity,  $i_s$  is the solid phase current density, and  $\phi_s$  is the potential in the solid phase.

*In the case of electrolyte*, the current that flows through the electrolyte is also governed by Ohm's law, such that:

$$i_e(x) = -k^{eff} \frac{\partial}{\partial x} \phi_e(x, t) - k_D^{eff} \frac{\partial}{\partial x} \ln c_e \quad (6.9)$$

Where  $i_e$  is the electrolyte current density,  $k^{eff}$  is the effective electrolyte phase ionic conductivity,  $k_D^{eff}$  is the effective electrolyte phase diffusion conductivity,  $c_e$  is the electrolyte concentration and  $\phi_e$  is the potential in the electrolyte phase. Equation (6.9) follows a modified Ohm's law where the first term is Ohm's law, while the second term reflects the change in the electrolyte concentration across the electrolyte phase.

At electrode spherical particles, due to the reaction taking place between the electrode and the electrolyte there is an induced current. This current is in the form of lithium ions. The magnitude of the induced current is related to the volumetric rate of reaction taking place at the solid/electrolyte interface  $j^{Li}$  such that:

$$\frac{\partial}{\partial x} i_s(x) = -j^{Li} \quad (6.10)$$

This induced current is added to the current already flowing through the electrolyte at that point given by [33]:

$$\frac{\partial}{\partial x} i_e(x) = j^{Li} \quad (6.11)$$

The boundary conditions for equations (6.8), (6.9), (6.10) and (6.11) are [17]:

$$i_s(x)|_{x=0} = i_s(x)|_{x=L} = \frac{I}{A} \quad (6.12)$$

$$i_e(x)|_{x=0} = i_e(x)|_{x=L} = 0 \quad (6.13)$$

Where  $I$  is the cell current and  $A$  is the collector surface area. These equations indicate that the current flowing through the battery terminal is passing only through the solid active particles. Since there is no current flowing through the separator.

$$\left. \frac{\partial}{\partial x} \emptyset_s(x, t) \right|_{x=\delta_n} = \left. \frac{\partial}{\partial x} \emptyset_s(x, t) \right|_{x=\delta_n + \delta_{sep}} = 0 \quad (6.14)$$

Furthermore, there will be no current passing through the separator and all the input current  $I$  into the cell crosses the separator in the form of  $Li^+$  ions, and is governed by the following equations [1]:

$$\frac{\partial}{\partial x} i_e(x) = 0 \quad (6.15)$$

$$-k^{eff} \frac{\partial}{\partial x} \emptyset_e(x, t) - k_D^{eff} \frac{\partial}{\partial x} \ln c_e = \frac{I}{A} \quad (6.16)$$

These equation reveal that the electrolyte current density at the battery terminal is equal to zero while at the separator it is equal to  $\frac{I}{A}$  as shown in Figure 6.7. Where red line equations represent boundary conditions, blue line represents the charge conservation governing equation.

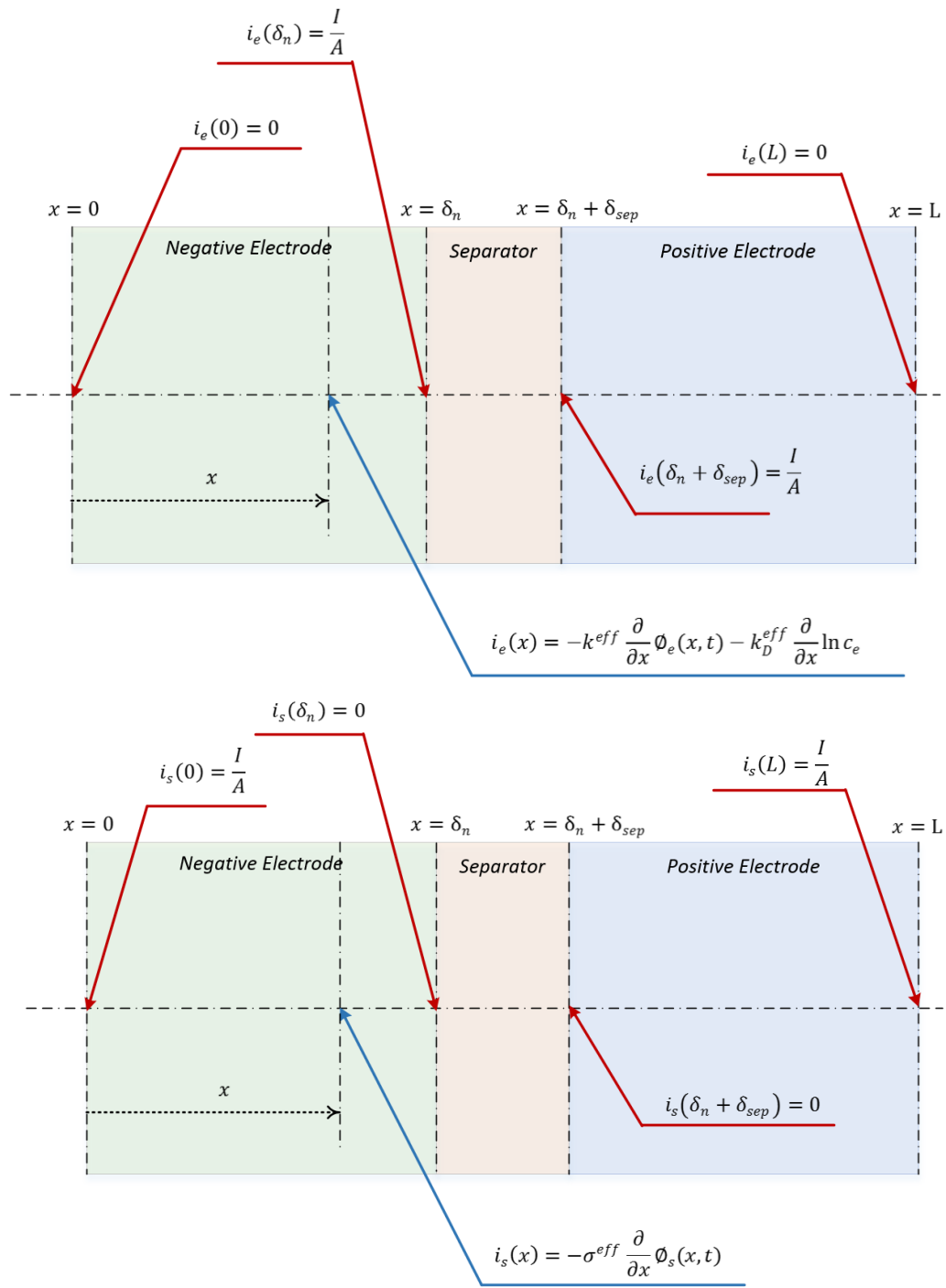


Figure 6.7 - Simplified schematic diagram showing all boundary conditions for Charge Conservation equations.

### 6.2.3. Butler-Volmer Kinetics Equations:

The volumetric rate of electrochemical reaction at the solid/electrolyte interface is governed by the Butler-Volmer current density equation. This equation links the Lithium ion conservation and charge conservation equations and is given by:

$$J^{Li} = a_s j_o \left[ \exp\left(\frac{\alpha_a F}{RT} \eta\right) - \exp\left(\frac{\alpha_c F}{RT} \eta\right) \right] \quad (6.17)$$

where  $\alpha_a$  is the anodic transfer coefficients of electrode reaction,  $\alpha_c$  is the cathodic transfer coefficients of electrode reaction,  $F$  is the Faraday's constant,  $R$  is the universal gas constant,  $T$  is the absolute temperature in Kelvin and  $a_s$  is the active surface area per electrode unit volume which is zero in the separator region (leads to no divergence of current). The overpotential  $\eta$  is defined as the difference between the battery's electromotive force (EMF) and its charge/discharge voltage. It is responsible for driving the electrochemical reaction, and can be calculated as follows, [21]:

$$\eta = \emptyset_s - \emptyset_e - U(c_{se}) \quad (6.18)$$

Where  $U(c_{se})$  is the open circuit voltage which relate the open circuit voltage to the normalized state of charge. The open circuit voltage varies from the cathode and the anode. An empirical relationship is used to calculate  $U(c_{se})$  which is given by [33]:

$$\begin{aligned} U_n(\theta_n) = & 8.0029 + 5.064\theta_n - 12.578\theta_n^{0.5} - 8.6322 \times 10^{-4}\theta_n^{-1} \\ & + 2.176 \times 10^{-5}\theta_n^{\frac{3}{2}} - 0.46016 \exp[15(0.06 - \theta_n)] \\ & - 0.55364 \exp[-2.4326(\theta_n - 0.92)] \end{aligned} \quad (6.19)$$

$$\begin{aligned} U_p(\theta_p) = & 85.681\theta_p^6 - 357.7\theta_p^5 + 613.89\theta_p^4 - 555.65\theta_p^3 \\ & + 281.06\theta_p^2 - 76.648\theta_p - 0.30987 \exp(5.657\theta_p^{115}) \\ & + 13.1983 \end{aligned} \quad (6.20)$$

Where  $\theta$  is the normalized solid-electrolyte concentration and can be obtained as follows, [17]:

$$\begin{aligned}\theta_p &= \frac{c_{se,p}}{c_{s,max,p}} \\ \theta_n &= \frac{c_{se,n}}{c_{s,max,n}}\end{aligned}\quad (6.21)$$

Where  $\theta_{0\%}$  and  $\theta_{100\%}$  are the normalized concentrations corresponding to 0% (fully discharged) and 100% (fully charged).  $\theta_{100\%}$  can be defined by obtaining the concentration corresponding to the maximum fully charged battery. Subsequently, the 0% reference value can be calculated by subtracting the battery capacity Q as in [33]:

$$\theta_{0\%} = \theta_{100\%} - \frac{Q}{\delta} \left( \frac{1}{AF\varepsilon c_{s,max}} \right) \quad (6.22)$$

The coefficient  $j_o$  in equation (6.17) depends on the solid and electrolyte concentrations according to the following equations [17]:

$$j_o = \kappa (c_e)^{\alpha_a} (c_{s,max} - c_{se})^{\alpha_a} (c_{se})^{\alpha_c} \quad (6.23)$$

Where  $\kappa$  is the electrolyte phase ionic conductivity. The lithium concentration at the solid electrolyte interface can be related to the Critical Surface Charge (CSC) as shown, [103]:

$$CSC(t) = \frac{\theta - \theta_{0\%}}{\theta_{100\%} - \theta_{0\%}} \quad (6.24)$$

#### 6.2.4. Cell Potential Measurable Equation:

The cell potential across the cell terminals is determined as follows [18]:

$$V = \phi_s(x = L) - \phi_s(x = 0) - \frac{R_f}{A} I \quad (6.25)$$

Where  $R_f$  is the film resistance at the electrode surface and its resistance increases after charging and discharging cycle (battery aging). Modelling the change in this value can give an indication about the current power fade and capacity fade.

### 6.3. Reduced Order Model - Single Particle Model (SPM)

It is clear from section 6.2, that our model can be represented by a set of high order non-linear equations making its real time implementation difficult. In this section, simplification are made to this model by spatially discretizing the PDEs in one dimension (1D) to obtain a set of Ordinary Differential Equations (ODE) and static relations as shown in Figure 6.8.

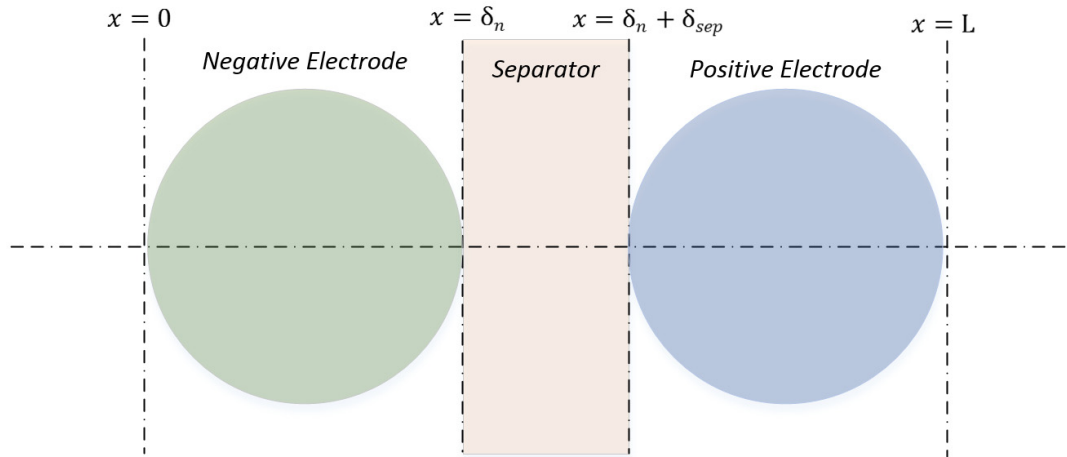


Figure 6.8 - Schematic representation of Single Particle Model

The full-order battery model of equations (6.2) to (6.25) are simplified in order to be implemented in real-time applications. The following assumptions are made [103,18,104] in relation to the schematic representation shown in Figure 6.8:

- The Lithium concentration in electrolyte  $c_e$  is assumed to be uniform, this simplifies equation (6.5) to a constant average.
- All model parameters are assumed to be constant.
- All thermal effects are ignored.
- No aging or capacity fade has been accounted for.
- The solid particle distribution along the electrode is neglected and is assumed to be a single sphere whose surface area is scaled to that of the porous electrode.
- These assumptions leads to the possibility of describing the diffusion sub-model of equation (6.2) to (6.7) with a single representative solid material particle for each electrode (anode and cathode) [104].

The simplified electrochemical model can be divided to four subsystems as shown in Figure 6.9, namely: (1) Butler–Volmer current calculation subsystem, (2) Spherical Particle Diffusion subsystem, (3) SOC Calculation subsystem, and (4) Voltage Calculation subsystem. These subsystems are discussed in details below.

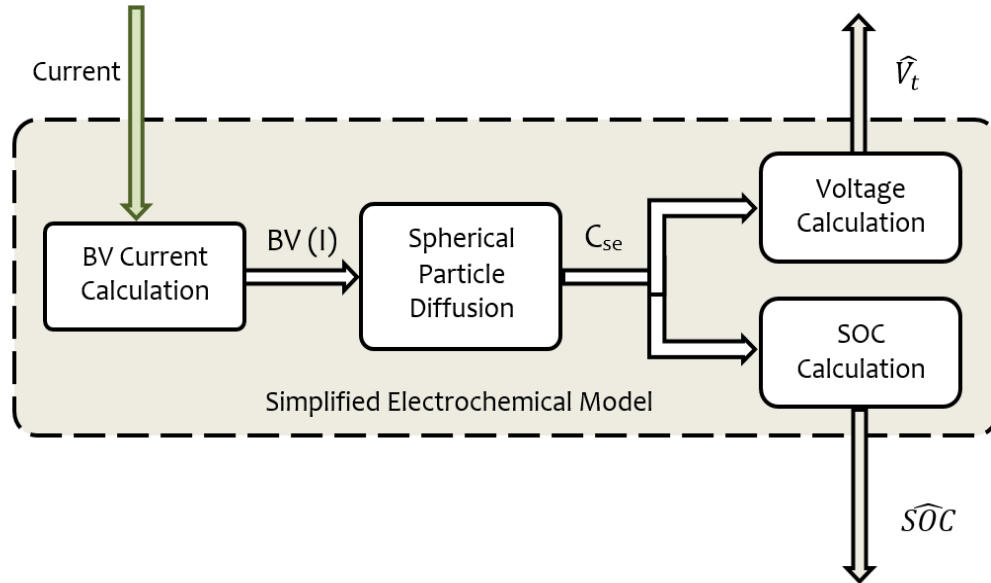


Figure 6.9 - Simplified reduced order model four main subsystems

### 6.3.1. Butler-Volmer Current Calculation Subsystem

The spatial dependence of the Butler-Volmer equation on the (x-direction) is ignored as shown below [18]:

$$\int_0^{\delta_n} j^{Li}(x)dx = \frac{I}{A} = \bar{j}_n^{Li} \delta_n \quad (6.26)$$

$$\int_{\delta_n + \delta_{sep}}^L j^{Li}(x)dx = \frac{I}{A} = \bar{j}_p^{Li} \delta_p \quad (6.27)$$

Where  $(\bar{j}^{Li})$  is a constant value that satisfy the integral and boundary conditions of equations (6.10) and (6.11).  $\delta_n, \delta_p$  are the anode and cathode electrode thicknesses, respectively as shown in Figure 6.8.

### 6.3.2. Spherical Particle Diffusion Sub-System

The mass conservation equation (6.2) describes the variations of the lithium ion concentration in the active spherical particle in any of the electrodes. It is discretized using a first order finite difference method (see Appendix B for more details). Each particle is discretized into  $M_r - 1$  regions along the radial dimension  $r$  and thus the diffusion phenomenon is approximated using discretized Fick's law of diffusion (see Appendix C for more details) [104]. Consider the spherical active material particle of the negative electrode, discretizing equation (6.2) and the boundary conditions (6.3) and (6.4) leads to:

$$\begin{aligned} \dot{c}_{s,(n,p)}(q) &= \frac{D_s}{\Delta r^2} \left[ \left( c_{s,(n,p)}(q+1) - 2c_{s,(n,p)}(q) + c_{s,(n,p)}(q-1) \right) \right. \\ &\quad \left. + \frac{\Delta r}{2r_q} \left( c_{s,(n,p)}(q+1) - c_{s,(n,p)}(q-1) \right) \right] \end{aligned} \quad (6.28)$$

Where  $q = 1, \dots, M_r - 1$  and  $r = q * \Delta r$ , substituting in equation (6.27)

$$\begin{aligned}\dot{c}_{s,(n,p)}(q) = & \frac{D_s}{\Delta r^2} \left[ \left(\frac{q-1}{q}\right) c_{s,(n,p)}(q-1) - 2c_{s,(n,p)}(q) \right. \\ & \left. + \left(\frac{q+1}{q}\right) c_{s,(n,p)}(q+1) \right]\end{aligned}\quad (6.29)$$

The boundary conditions equation (6.3) and (6.4) can be written as follows

$$c_{s,(n,p)}(0) = c_{s,(n,p)}(1) \quad (6.30)$$

For spherical particles in the negative electrode the lithium surface electrolyte concentration can be obtained as follows [47]:

$$c_{se} = c_s(M_r) = c_s(M_r - 1) + \Delta r \frac{-j^{Li}}{a_{s,n}FD_s} \quad (6.31)$$

While for spherical particles in the positive electrode:

$$c_{se} = c_s(M_r) = c_s(M_r - 1) + \Delta r \frac{-j^{Li}}{a_{s,p}FD_s} \quad (6.32)$$

With the above approximations for the mass conservation equation (6.2), a state space representation of the model can be obtained from equations (6.33) to (6.39) as:

$$\dot{c}_s = \mathbf{A}c_s + \mathbf{B}j^{Li} \quad (6.33)$$

$$c_{se} = \mathbf{C}c_s + \mathbf{D}j^{Li} \quad (6.34)$$

Where the state space matrices,  $\mathbf{A}$ ,  $\mathbf{B}$ ,  $\mathbf{C}$ ,  $\mathbf{D}$  are obtained as follows:

$$\mathbf{A} = \alpha \begin{bmatrix} -2 & \frac{q+1}{q} & 0 & \dots & \dots & 0 & 0 & 0 \\ \frac{q-1}{q} & -2 & \frac{q+1}{q} & \dots & \dots & 0 & 0 & 0 \\ 0 & \frac{q-1}{q} & -2 & \ddots & & 0 & 0 & 0 \\ \vdots & \vdots & \ddots & \ddots & \ddots & \vdots & \vdots & \vdots \\ \vdots & \vdots & & \ddots & \ddots & \ddots & \vdots & \vdots \\ 0 & 0 & 0 & \ddots & -2 & \frac{q+1}{q} & 0 & 0 \\ 0 & 0 & 0 & \dots & \dots & \frac{q-1}{q} & -2 & \frac{q+1}{q} \\ 0 & 0 & 0 & \dots & \dots & 0 & \frac{q-1}{q} & -\frac{q-1}{q} \end{bmatrix} \quad (6.35)$$

$$\mathbf{B} = \beta \begin{bmatrix} 0 \\ 0 \\ 0 \\ \vdots \\ \vdots \\ -\frac{q+1}{q} \end{bmatrix} \quad (6.36)$$

$$\mathbf{C} = [0 \ 0 \ \dots \ \dots \ 0 \ 1] \quad (6.37)$$

$$\mathbf{D} = -\frac{\beta}{\alpha} \quad (6.38)$$

Where,  $\alpha = \frac{D_s}{\Delta r^2}$  and  $\beta = \frac{1}{\Delta r * a_s * F}$

### 6.3.3. Calculate Terminal Voltage Subsystem:

The battery voltage is calculated by substituting equation (6.18) in equation (6.25) as follows:

$$V(t) = \eta(L, t) - \eta(0, t) - (\emptyset_e(L, t) - \emptyset_e(0, t)) + (U_p(c_{se}(L, t)) - U_n(c_{se}(0, t))) - \frac{R_f}{A} I \quad (6.39)$$

And by using the average simplifications values calculated above instead of using the boundary conditions the following equation is obtained

$$V(t) = (\bar{\eta}_p - \bar{\eta}_n) - (\bar{\emptyset}_{e,p} - \bar{\emptyset}_{e,n}) + (U_p(\bar{c}_{se,p}) - U_n(\bar{c}_{se,n})) - \frac{R_f}{A} I \quad (6.40)$$

The output voltage  $V(t)$  is calculated with 4 terms  $(\bar{\eta}_p - \bar{\eta}_n)$ ,  $(\bar{\emptyset}_{e,p} - \bar{\emptyset}_{e,n})$ ,  $(U_p(\bar{c}_{se,p}) - U_n(\bar{c}_{se,n}))$ ,  $\frac{R_f}{A} I$ , each of them will be obtained separately using the average current and the continuity at the interface and imposing the boundary conditions, as follows:

The term  $(\bar{\emptyset}_{e,p} - \bar{\emptyset}_{e,n})$ , is the difference between the electrolyte phase potential at the anode and cathode current collector and can be calculated using the following equation, [47]:

$$\bar{\emptyset}_{e,p} - \bar{\emptyset}_{e,n} = -\frac{I}{2Ak^{eff}}(\delta_n + 2\delta_{sep} + \delta_p) \quad (6.41)$$

The term  $(\bar{\eta}_p - \bar{\eta}_n)$ , is the difference between the anode and cathode over potentials can be calculated using the following equations [105]:

$$\bar{\eta}_n = \frac{RT}{\alpha_a F} \ln(\xi_n + \sqrt{\xi_n^2 + 1}) \quad (6.42)$$

$$\bar{\eta}_p = \frac{RT}{\alpha_a F} \ln(\xi_p + \sqrt{\xi_p^2 + 1}) \quad (6.43)$$

Where

$$\xi_n = \frac{\bar{J}_n^{Li}}{2a_s j_o} \quad (6.44)$$

$$\xi_p = \frac{\bar{J}_p^{Li}}{2a_s j_o} \quad (6.45)$$

Where,  $\bar{J}_n^{Li}$  and  $\bar{J}_p^{Li}$  are the Butler-Volmer currents defined as follows:

$$\bar{J}_n^{Li} = \frac{I}{A\delta_n} = a_s j_o \left[ \exp\left(\frac{\alpha_a F}{RT} \bar{\eta}_n\right) - \exp\left(\frac{\alpha_c F}{RT} \bar{\eta}_n\right) \right] \quad (6.46)$$

$$\bar{J}_p^{Li} = \frac{I}{A\delta_p} = a_s j_o \left[ \exp\left(\frac{\alpha_a F}{RT} \bar{\eta}_p\right) - \exp\left(\frac{\alpha_c F}{RT} \bar{\eta}_p\right) \right] \quad (6.47)$$

Finally, the battery output voltage equation can be obtained as a function of the average solid concentration and the battery current as:

$$V(t) = \frac{RT}{\alpha_a F} \ln \left( \frac{\xi_n + \sqrt{\xi_n^2 + 1}}{\xi_p + \sqrt{\xi_p^2 + 1}} \right) + \left( \frac{I}{2Ak^{eff}} (\delta_n + 2\delta_{sep} + \delta_p) \right) + \left( U_p(\bar{c}_{se,p}) - U_n(\bar{c}_{se,n}) \right) - \frac{R_f}{A} I \quad (6.48)$$

### 6.3.4. SOC Calculation

The  $c_{se,p}$  of the positive electrode is used to calculate the solid concentration at the solid electrolyte interface for the negative electrode  $c_{se,n}$  using the following equation:

$$\bar{c}_{se,n} = c_{s,max,n} \left( \theta_{n0\%} + \frac{\bar{c}_{se,p} - \theta_{p0\%} c_{s,max,p}}{(\theta_{p0\%} - \theta_{p0\%}) c_{s,max,p}} * (\theta_{n100\%} - \theta_{n0\%}) \right) \quad (6.49)$$

Where,  $\theta_{n0\%}$ ,  $\theta_{n100\%}$ ,  $\theta_{p0\%}$ ,  $\theta_{p100\%}$  are the stoichiometry reference points for the negative and positive electrodes [33]. The solid concentrations at the electrode-electrolyte interface for the positive and negative particles are obtained by dividing the current solid concentration with the maximum solid concentration to get  $\theta_n$ ,  $\theta_p$  as follows:

$$\theta_p = \frac{c_{se,p}}{c_{s,max,p}} \quad (6.50)$$

$$\theta_n = \frac{c_{se,n}}{c_{s,max,n}} \quad (6.51)$$

Concentration values in equations (6.50) and (6.51) are further used in equations (6.19) and (6.20) using the empirical relationship that relates the open circuit voltage to the normalized state of charge [106]. The Normalized solid-electrolyte concentration  $\theta$  is obtained first using equation (6.50) and (6.51); the State of Charge is calculated based on the positive electrode lithium concentration using the following equation [106]:

$$SOC = \frac{\theta_p - \theta_{p0\%}}{\theta_{p100\%} - \theta_{p0\%}} \quad (6.52)$$

The relation between SOC and solid surface concentration stoichiometry (also indicated as normalized concentration) is shown in Figure 6.10.

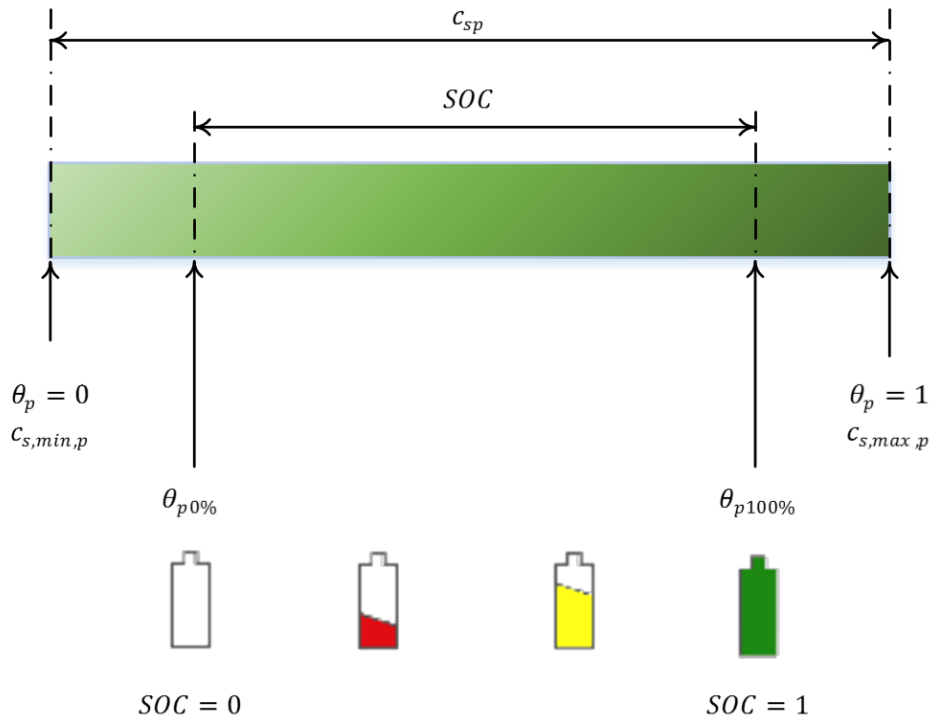


Figure 6.10 - Relation between SOC and solid surface concentration stoichiometry

## 6.4. SOC Estimation

The EKF and the SVSF were applied to the Single Particle Model (SPM) to estimate the battery SOC and the critical surface concentration (CSC). The overall model (4 subsystems) consists of a linear system equation (6.33) and a nonlinear measurement equation (6.34). The model has one input (demanded current), one output (measured terminal voltage), and  $M_r - 1$  states, the states represent the number of discretization along the radial dimension  $r$ . The SPM is considered to have 4 states (4 discretization along radial dimension). The Single Particle Model SPM battery terminal voltage is compared to the full order model terminal voltage as shown in Figure 6.11.

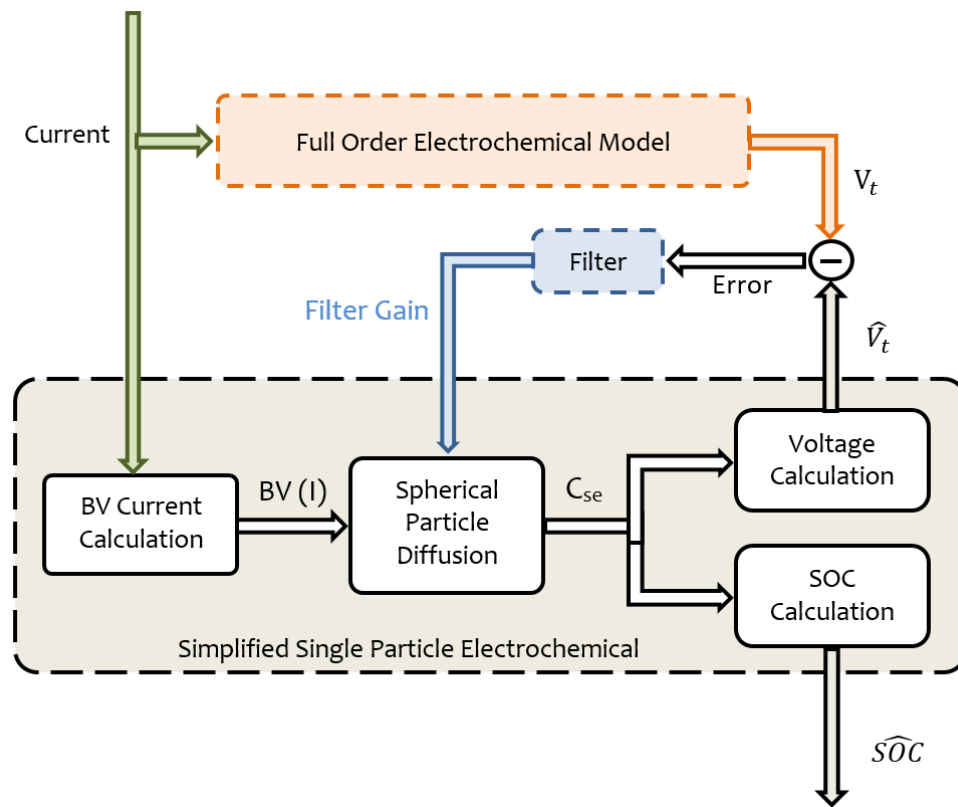


Figure 6.11 - SOC estimation using SVSF

The states are the solid concentration ( $C_s$ ) across various particle shells as in equation (6.35). The state space model is then obtained as:

$$\dot{x} = A_p x(t) + B_p u(t) \quad (6.53)$$

$$y = V(x, u) \quad (6.54)$$

The matrices  $A_p$  and  $B_p$  are defined in equations (6.35) and (6.36). The nonlinear output equation is linearized with respect to the latest estimate to obtain a linearized measurement equation using the following:

$$C = \left. \frac{\partial V}{\partial x} \right|_{x_k=\hat{x}_k} \quad (6.55)$$

The output C matrix has only one elements as follows, [18]:

$$\frac{\partial V}{\partial \bar{c}_{s,p(M_r-1)}} = \frac{\partial U_p}{\partial \bar{c}_{s,p(M_r-1)}} - \frac{\partial U_n}{\partial \bar{c}_{se,n}} \frac{\partial \bar{c}_{se,n}}{\partial \bar{c}_{s,p(M_r-1)}} \quad (6.56)$$

#### 6.4.1. Simulation Test Procedure and Results

SOC estimation algorithm used in the cell simulation is shown in Figure 6.11, where the Single particle model terminal voltage is compared with the full order model terminal voltage. The error signal is fed to the state estimator (EKF or SVSF). The filter gain is then used to adjust the a priori estimate of states, including SOC. The full order battery cell is of nominal capacity of 6 Ah. The parameters and constant values for this cell can be found in Appendix A.

##### *Simulation Driving Cycle*

In this section two driving cycles used in simulating the battery performance are presented. The first driving cycle is the Urban Dynamometer Driving Schedule (UDDS) discussed in Chapter 3. The vehicle speed profile is shown in Figure 3.9, and the battery current is shown in Figure 3.10. The second driving cycle is the Charging/discharging Pulse train cycle, where the battery current is shown in Figure 6.12.

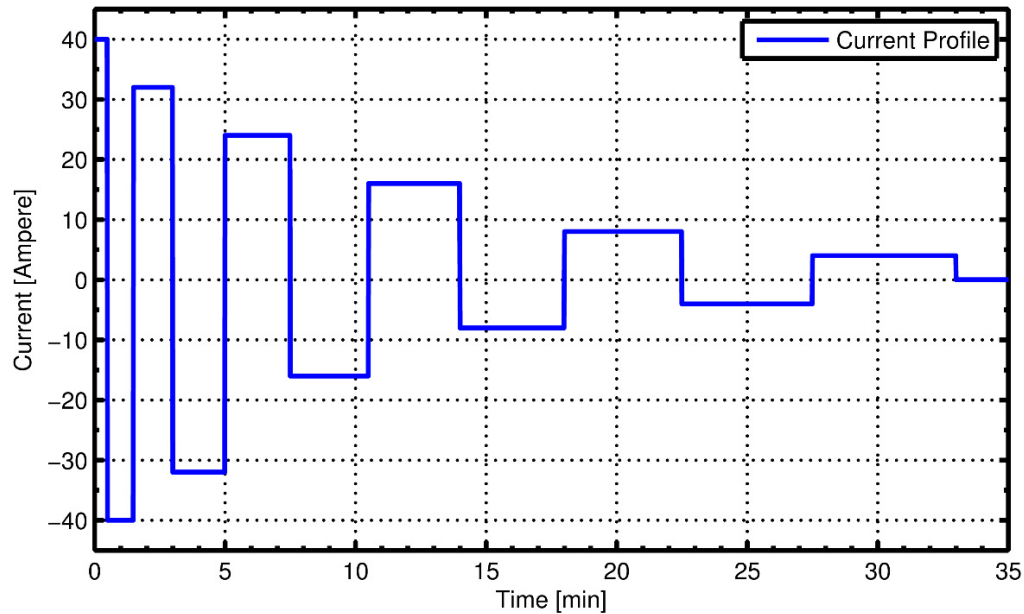


Figure 6.12 - Charging/discharging Pulse train cycle current profile

The full order model SOC using UDDS cycle is shown in Figure 6.13, and the cell terminal voltage is shown in Figure 6.14.

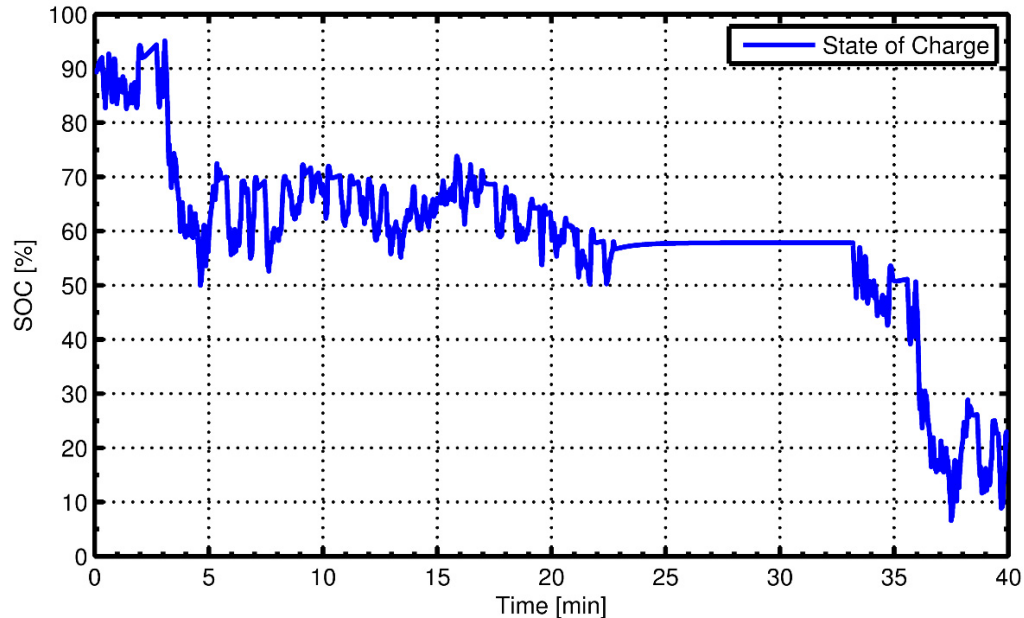


Figure 6.13 – Battery full order model SOC behavior [UDDS]

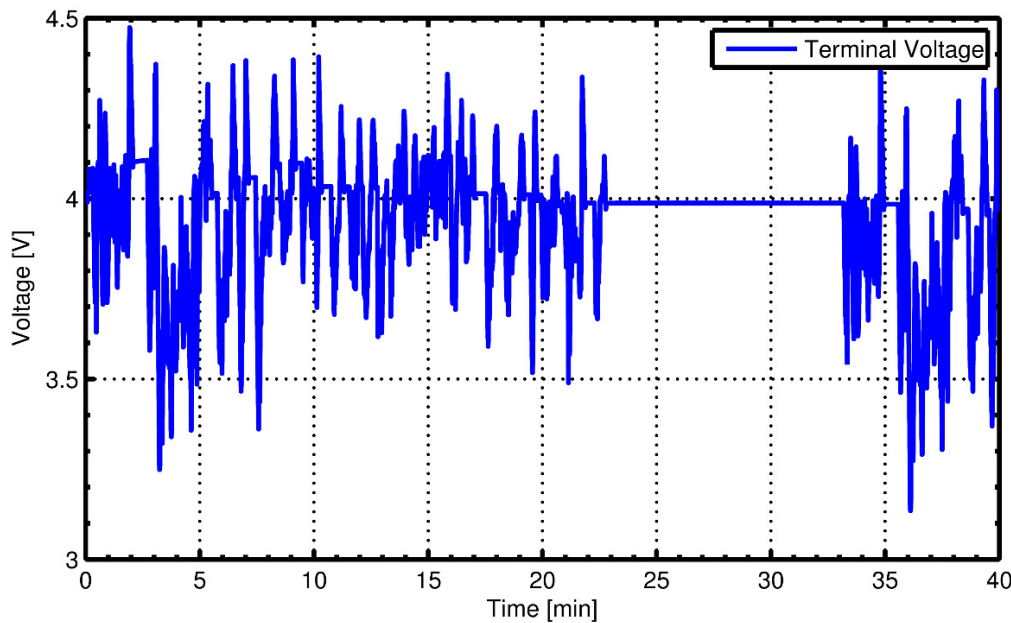


Figure 6.14 – Battery full-order model output voltage profile [UDDS]

While using the Charging/discharging Pulse train cycle the SOC behavior is shown in Figure 6.15, and the cell terminal voltage is shown in Figure 6.16.

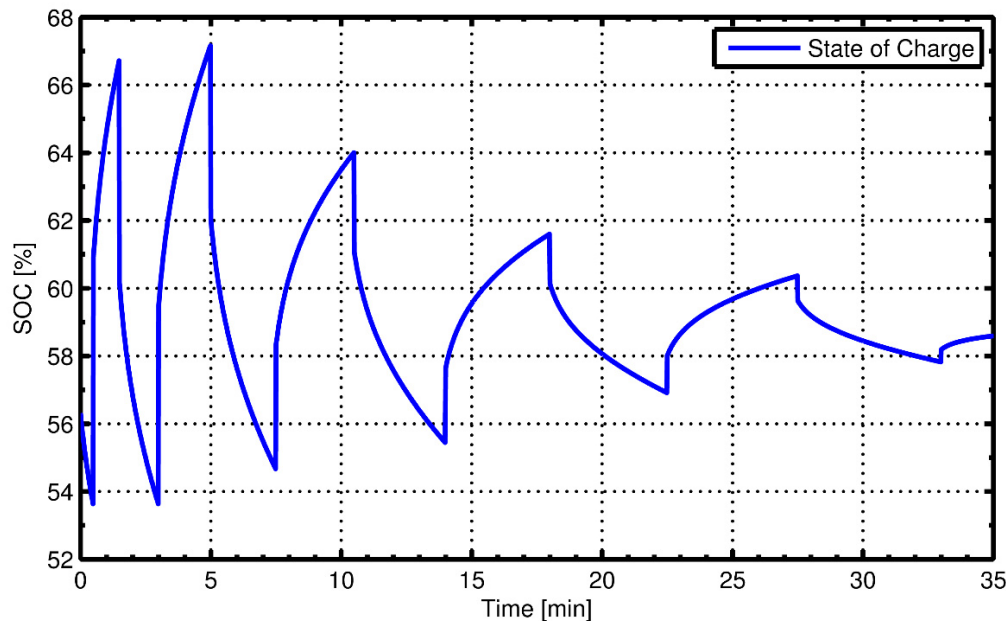


Figure 6.15 - Battery full order model SOC behavior [Pulse train cycle]

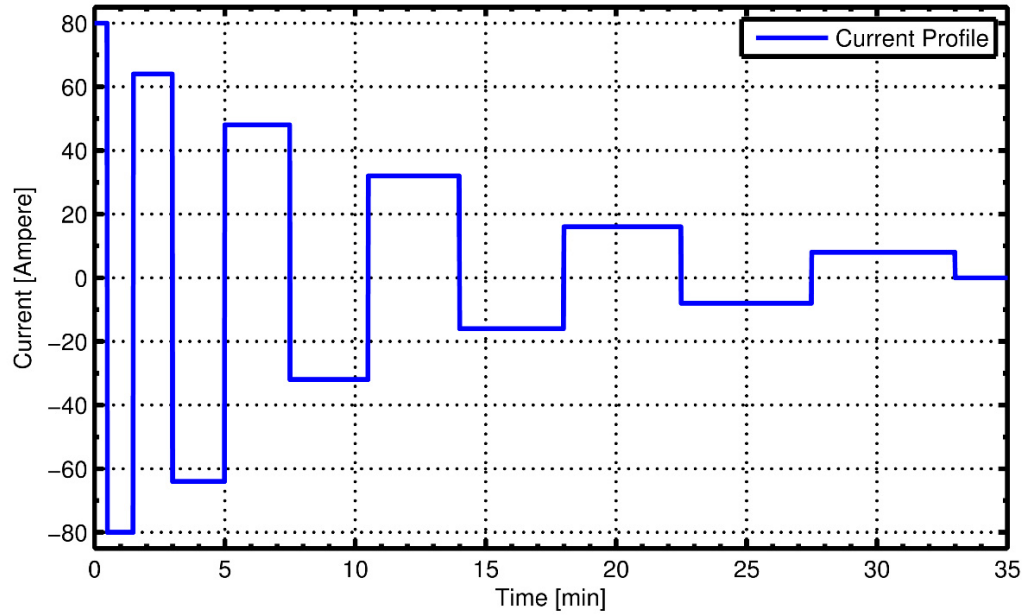


Figure 6.16 – Battery full-order model output voltage profile [Pulse train cycle]

## Results

In case of UDDS Cycle, the true SOC is 90% while the model is initialized at 75% (i.e. 15%), the system and measurement noise covariance for EKF were defined as follows:

$$Q = \text{diag}(0.01, \quad 0.01, \quad 0.01, \quad 0.01)$$

$$R = 0.1$$

The SVSF ‘memory’ or convergence rate and smoothing boundary layers were defined as follows:

$$\psi = 0.2$$

$$\gamma = 0.8$$

In case of Pulse train cycle, the true SOC is 60% while the model is initialized at 75%, the system and measurement noise covariance for EKF were defined as follows:

$$Q = \text{diag}(0.01, \quad 0.01, \quad 0.01, \quad 0.01)$$

$$R = 0.08$$

The SVSF ‘memory’ or convergence rate and smoothing boundary layers were defined as follows:

$$\psi = 0.25$$

$$\gamma = 0.8$$

- UDDS Cycle

In Figure 6.17, Figure 6.18, Figure 6.19, and Figure 6.20, the solid line represent the full-order model results, the dashed and dotted lines represent the EKF and the SVSF results respectively for the Single particle Model (SPM). Figure 6.17 shows the concentration variation in the electrode solid particle. Figure 6.18, shows the lithium concentration on the surface of spherical particle  $c_{se}$  known as critical surface concentration CSC, the four dashed and dotted lines represent the states estimated by the KF and the SVSF respectively. Figure 6.19 shows the estimated SOC using the EKF and the SVSF. Figure 6.20, shows the estimated terminal voltage and the EKF and the SVSF in comparison with full-order model terminal voltage.

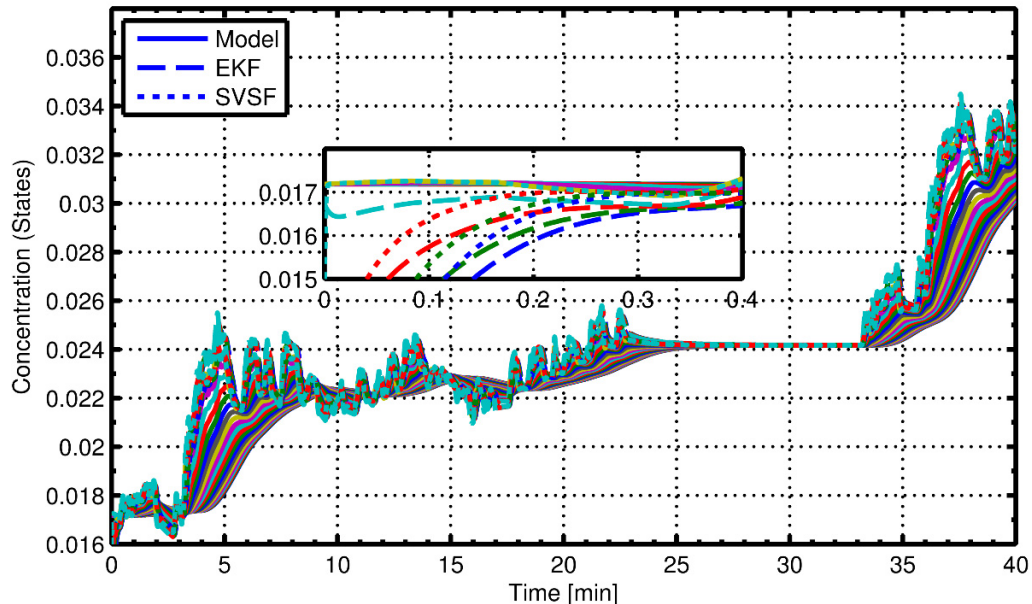


Figure 6.17 - Lithium concentration in solid particle Full-order model vs. SPM with EKF and SVSF

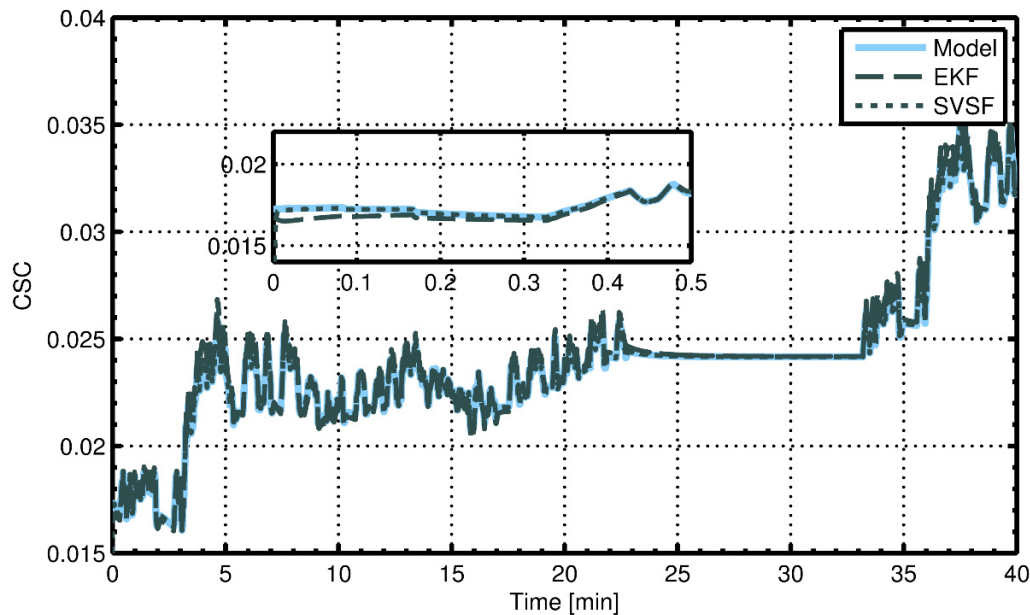


Figure 6.18 - Critical Surface Concentration in solid particle Full-order model vs. SPM with EKF and SVSF

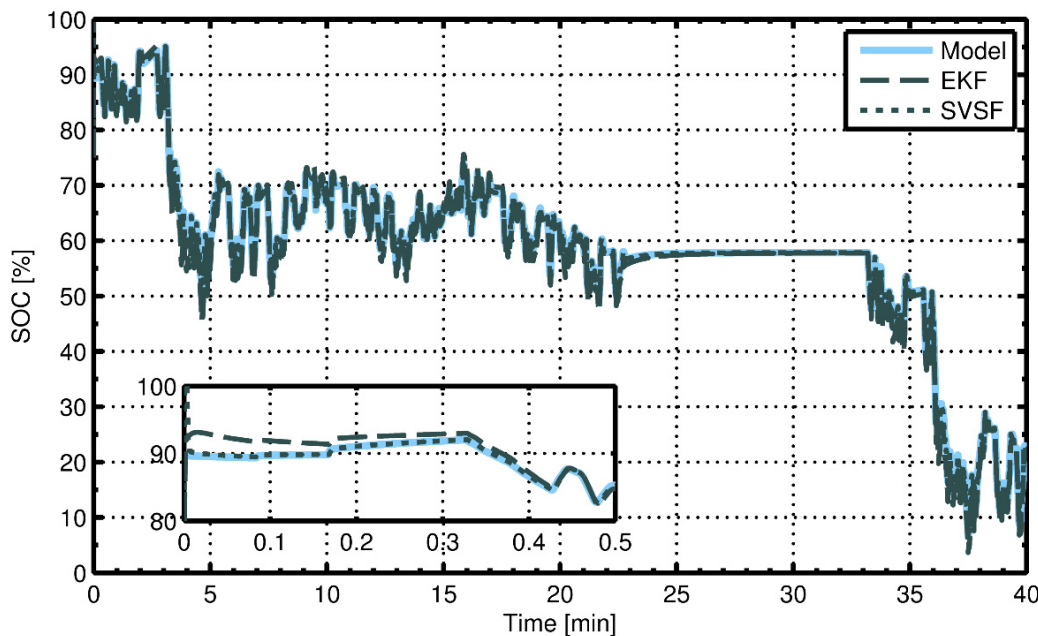


Figure 6.19 - SOC estimation using SPM with EKF and SVSF vs. full order model

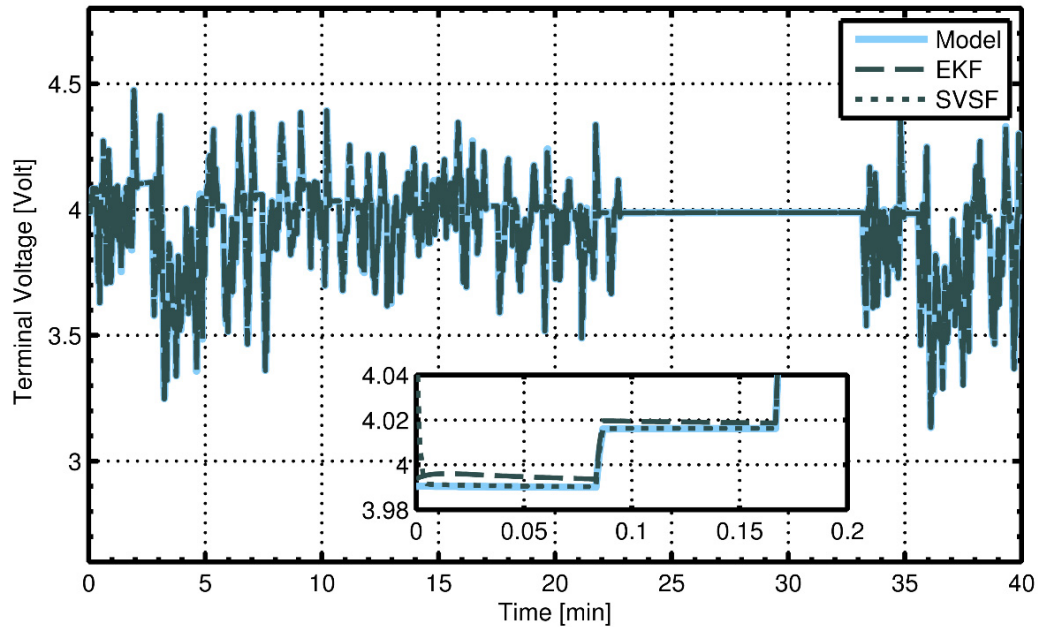


Figure 6.20 - Terminal Voltage comparison Full order Model vs. SPM with EKF and SVSF

- Pulse Cycle

In Figure 6.21 to Figure 6.24, the solid line represent the full-order model results, the dashed and dotted lines represent the EKF and the SVSF results respectively for the Single particle Model (SPM). Figure 6.21 shows the concentration variation in the electrode solid particle. Figure 6.22, shows the lithium concentration on the surface of spherical particle  $c_{se}$  known as critical surface concentration CSC, the four dashed and dotted lines represent the states estimated by the KF and the SVSF respectively. Figure 6.23, shows the estimated SOC using the EKF and the SVSF. Figure 6.24, shows the estimated terminal voltage and the EKF and the SVSF in comparison with full-order model terminal voltage.

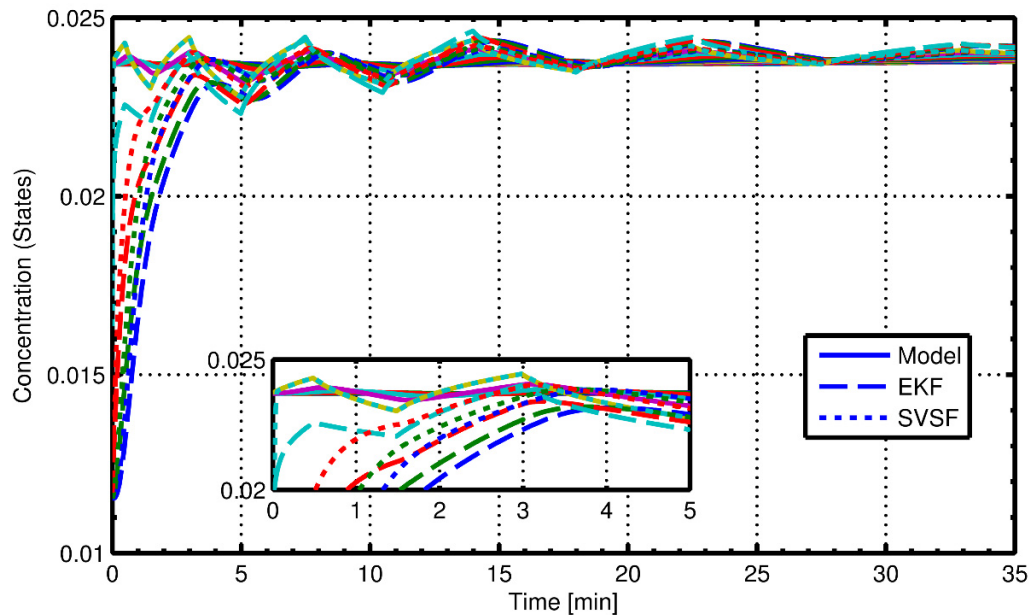


Figure 6.21 - Lithium concentration in solid particle Full-order model vs. SPM with EKF and SVSF [Pulse train Cycle]

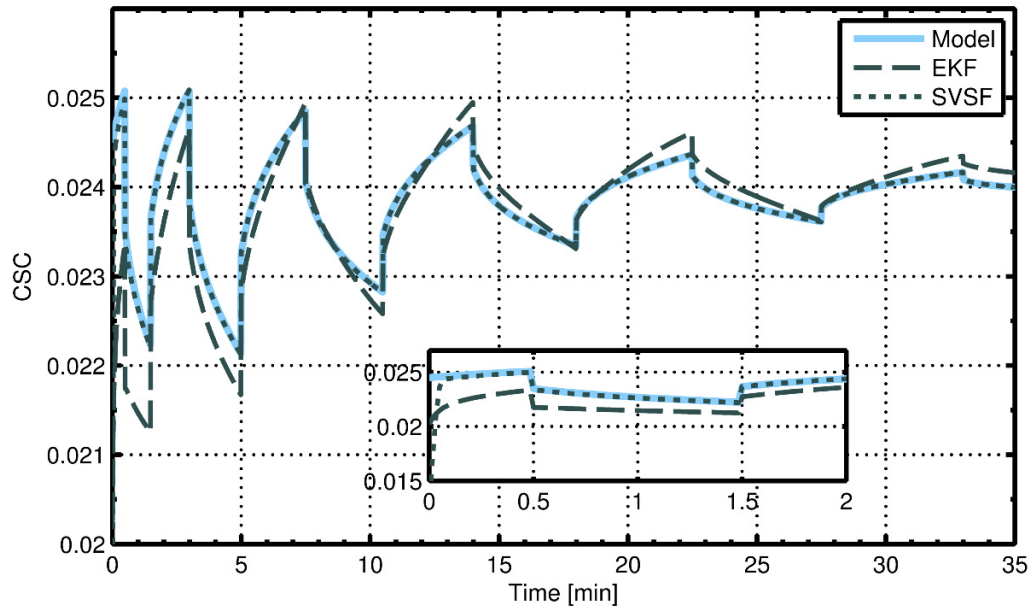


Figure 6.22- Critical Surface Concentration in solid particle Full-order model vs. SPM with EKF and SVSF [Pulse train cycle]

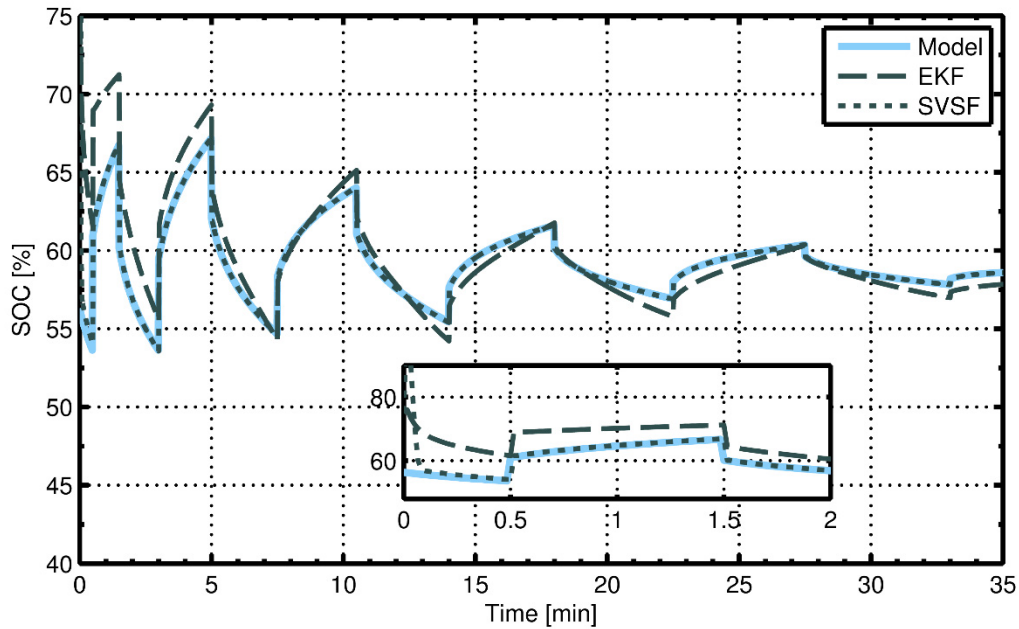


Figure 6.23 – SOC estimation using SPM with EKF and SVSF vs. full order model [Pulse train cycle]

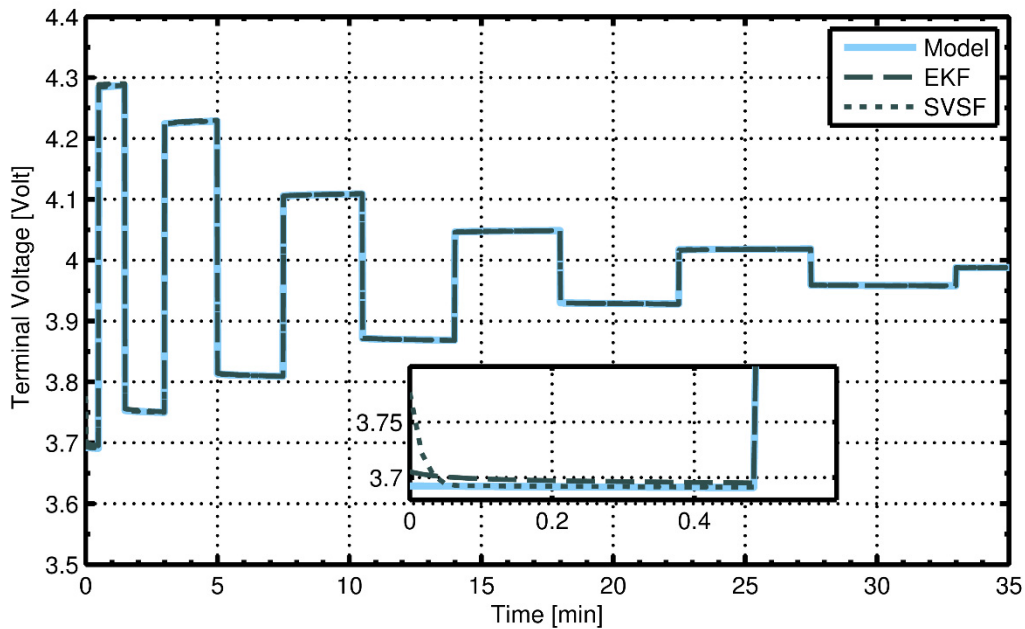


Figure 6.24 – Terminal Voltage comparison Full order Model vs. SPM with EKF and SVSF [Pulse train cycle]

## 6.5. Summary

This chapter provided a description of Electro-chemical Models (ECM) for lithium ion batteries and their implementation. These models are physics-based and capture the electrochemical reactions using partial differential equations (PDE). The models link physical parameters to internal electrochemical dynamics. The full order electro-chemical model provides a deep insight into the underlying physics. However, it is slow, complex, and computationally unfeasible for real time implementation. This chapter also provided the simplified Single Particle Model (SPM) that may be implemented in real time. The SPM was used for SOC estimation using both the EKF and the SVSF strategies. According to Figure 6.25 the SVSF shows a better performance compared to the EKF.

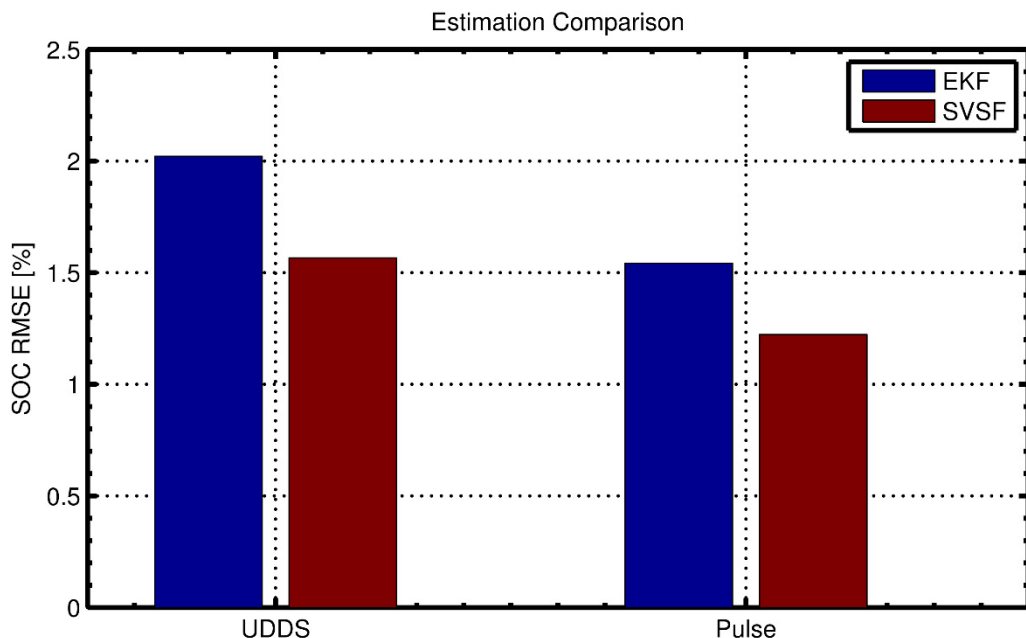


Figure 6.25 – Simulation Electro-Chemical Model estimation comparison of SOC Estimation Error using EKF and SVSF

---

# Conclusion and Recommendations

---

## 7.1. Summary of Research

A comparative study between different lithium-ion battery models and state of charge (SOC) estimation strategies was performed. Three categories of battery models were considered: Behavioral or Black-box models, equivalent circuit models, and electrochemical models. The SOC was estimated using two estimation strategies, namely the Extended Kalman filter (EKF) and the Smooth Variable Structure Filter (SVSF). The models and SOC estimation strategies were applied to experimental data provided by the BMW Electrical and Hybrid Research and Development Center. The results were validated using simulation models obtained from the AVL CRUISE software.

This thesis provided a detailed overview of Behavioral models and their implementation. The Behavioral models simulate the terminal voltage behavior of the batteries without the need for the specification of the underlying physical or electrochemical reactions. These models can be simple starting with one state to capture the SOC, and progressively

become more complex with more than one state used for to capture better the internal battery dynamics. The model parameters were optimized using the Globalized Pattern Search Matlab toolbox.

The EKF and SVSF were applied to six different Behavioral models, and the SOC was estimated. The results were compared based on the SOC root mean squared error (RMSE). It was discovered that the SVSF provided a more accurate estimation result, with an improvement of 30 to 60%. The greatest RMSE difference occurred when applying the estimation methods on the Combined Model. The SVSF estimation results were consistent throughout all 6 models (i.e., the SOC estimation error varied by under 0.5%). The EKF application results were less consistent; the SOC estimation error varied by upwards of 2.5%. The differences in consistency were likely due to the sensitivity of the EKF to modelling uncertainties. A comparison of results indicates that the SVSF is more robust to modelling uncertainties compared to the EKF.

Six Equivalent circuit models and their implementation were also considered. These models are widely used because they are relatively simple, have fewer parameters to tune, and are easy to implement. The Equivalent circuit models consist of first-order, second-order, or third-order resistance-capacitance (RC) models in addition to the hysteresis effect. The Equivalent circuit model parameters were also optimized using Globalized Pattern Search Matlab toolbox.

The results of applying both the EKF and SVSF estimation methods on the Equivalent circuit models were shown and discussed. The SVSF SOC strategy yielded the best performance in terms of estimation accuracy. Similar to the Behavioral models, the SOC estimation RMSE was improved by 15 to 60%, depending on the model used. The worst model for both estimation methods was the first-order RC model; whereas the most accurate model was the third-order RC model which included hysteresis. This was to be

expected, as the RC model was unable to capture the nonlinear battery dynamics compared to the third-order RC model with hysteresis.

Electro-chemical models (ECM) and their corresponding implementation were also considered. These models are physics-based and capture electrochemical reactions using partial differential equations (PDE). This type of models links physical parameters to internal electrochemical dynamics. It was concluded that the full order electro-chemical model provides a comprehensive insight to battery physical parameters and underlying physics. However, it was found to be slow, complex, and computationally unpractical for real time implementations. A detailed description for the simplified Single Particle Model (SPM) was also described, which may be implemented to improve the full order model's computational performance. The EKF and SVSF estimation strategies were applied to an ECM model. It was found that the SOC estimation using the SVSF was significantly better than results obtained by using the EKF and improve RMSE by 60 to 80% compared to EKF.

## 7.2. Recommendations and Future Work

A trade-off exists between model complexity, accuracy, and parameterization. It is recommended that the selection of a battery model should be made based on the required accuracy and the available computation power. For example, in some situations a simple RC model may suffice; such as in simple, low current operating conditions. However, a more complicated model is required to capture nonlinearities present in environments involving fast transients.

The first recommendation for new research involves further study of electro-chemical models. In most cases, the ECM is considered to be one dimensional. This can be extended to higher dimensions (2 or 3) by using finite element analysis (FEA). An FEA strategy could be developed to create more accurate ECM models.

It is important to note that the temperature dependence of model parameters were not considered in this work. Future studies can include energy balance equations in the models to incorporate temperature information and its effects on the system. Additionally, a temperature sensor can be proposed for the cell along with a sensor for terminal voltage. This will add more information to the experimental setup, which can be used in modelling and SOC estimation. Furthermore, the aging effect of the cell was ignored in this work. A very important recommendation for future work includes the study of aging and its effects on a battery cell. This work is important because it may yield more accurate estimation for battery state of health (SOH).

---

# APPENDIX A

---

## Model Parameters for Electro-chemical Li-Ion Cell

*Universal Constants:*

---

Parameter	Value
Faraday's number, $F$ (C mol <sup>-1</sup> )	96,487
Universal Gas constant, $R$ (J K <sup>-1</sup> mol <sup>-1</sup> )	8.3143

*Discretization, Geometry and Volume Fractions:*

---

Parameter	Negative electrode	Separator	Positive electrode
Thickness (cm)	$\delta_n = 50 \times 10^{-4}$	$\delta_{sep} = 25.4 \times 10^{-4}$	$\delta_p = 36.4 \times 10^{-4}$
Particle radius $R_s$ (cm)	$1 \times 10^{-4}$	-	$1 \times 10^{-4}$
Active material volume fraction $\varepsilon_s$	0.580	-	0.500
Electrolyte phase volume fraction (porosity) $\varepsilon_e$	0.332	0.5	0.330
Active surface area per electrode unit volume	$a_{sn} = \frac{3\varepsilon_e}{R_s}$	-	$a_{sp} = \frac{3\varepsilon_e}{R_s}$

***Plate Area-Specific Parameters and Temperature:***

Parameter	Value
Electrode plate area A (cm <sup>2</sup> )	10,452
Current collector contact resistance, $R_f$ (Ωcm <sup>2</sup> )	20
Temperature, T(K)	298

***Kinetic and Transport Properties:***

Parameter	Negative electrode	Separator	Positive electrode
Change transfers coefficient $\alpha_a, \alpha_c$	0.5,0.5	-	0.5,0.5
Solid phase diffusion coefficient $D_s$	$2.0 \times 10^{-12}$	-	$3.7 \times 10^{-12}$
Conductivity of solid active material $\sigma$	1	-	0.1
Electrolyte phase diffusion coefficient $D_e$	$2.6 \times 10^{-6}$	$2.6 \times 10^{-6}$	$2.6 \times 10^{-6}$
Transference number	0.363	0.363	0.363
Electrolyte phase ionic conductivity $\kappa$ ( $\Omega^{-1} cm^{-1}$ )	$\kappa = 0.0158 c_e * e^{(0.85 c_e^{1.4})}$	$\kappa = 0.0158 c_e * e^{(0.85 c_e^{1.4})}$	$\kappa = 0.0158 c_e * e^{(0.85 c_e^{1.4})}$
Effective conductivity of solid active material	$\sigma^{eff} = \varepsilon_s \sigma$	-	$\sigma^{eff} = \varepsilon_s \sigma$
Effective electrolyte phase diffusion coefficient	$D_e^{eff} = (\varepsilon_e)^{1.5} D_e$	$D_e^{eff} = (\varepsilon_e)^{1.5} D_e$	$D_e^{eff} = (\varepsilon_e)^{1.5} D_e$
Effective electrolyte phase ionic conductivity	$\kappa^{eff} = (\varepsilon_e)^{1.5} \kappa$	$\kappa^{eff} = (\varepsilon_e)^{1.5} \kappa$	$\kappa^{eff} = (\varepsilon_e)^{1.5} \kappa$
Effective electrolyte phase diffusion conductivity	$\kappa_D^{eff} = \frac{2RT\kappa^{eff}}{F} * (t_+^0 - 1)$	$\kappa_D^{eff} = \frac{2RT\kappa^{eff}}{F} * (t_+^0 - 1)$	$\kappa_D^{eff} = \frac{2RT\kappa^{eff}}{F} * (t_+^0 - 1)$

***Lithium Ion Concentrations:***

Parameter	Negative electrode	Separator	Positive electrode
Maximum solid-phase concentration $C_{s,max}$	$1.61 \times 10^{-3}$	-	$23.9 \times 10^{-3}$
Stoichiometry at 0% $\theta_0\%$	0.26	-	0.936
Stoichiometry at 100% $\theta_{100\%}$	0.676	-	0.442
Average electrolyte concentration $\bar{c}_e$ (mol cm <sup>-3</sup> )	$1.2 \times 10^{-3}$	$1.2 \times 10^{-3}$	$1.2 \times 10^{-3}$

---

## APPENDIX B

---

### Fick's Law of Diffusion

Diffusion refers to the phenomenon of elements moving from a region of high concentration to one of low concentration, thus minimizing the concentration gradient in time. This effect is clearly visible in lithium diffusion batteries, where lithium ions transfer from high concentration areas to low concentrations during charging and discharging.

Adolf Fick was a German physiologist who proposed two laws of diffusion named after him. The two laws describe solid state diffusion in one dimension, such as the concentration of one species in another over time. Fick's first law describes diffusion at steady state, where the source concentration never changes. The concentration gradient is constant and linear between the high and low concentration sides, as shown below:

$$J = -D \left( \frac{\partial c}{\partial x} \right) \quad \text{B.1}$$

Where  $J$  is the flux,  $D$  is the diffusion coefficient, and  $\frac{\partial c}{\partial x}$  is the change in concentration with distance as shown in Figure Appendix B.1

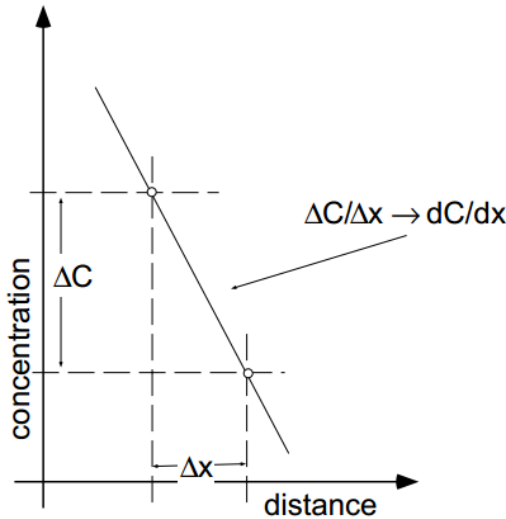


Figure Appendix B.1 – Concentration gradient (Constant in X-direction) [107].

Fick's second law describes the non-steady state diffusion, where the concentration gradient will not be linear as shown below:

$$\frac{\partial c}{\partial x} = D \left( \frac{\partial^2 c}{\partial x^2} \right) \quad \text{B.2}$$

The difference between the steady state diffusion and non-steady state diffusion is shown in Figure Appendix B.2 [107].

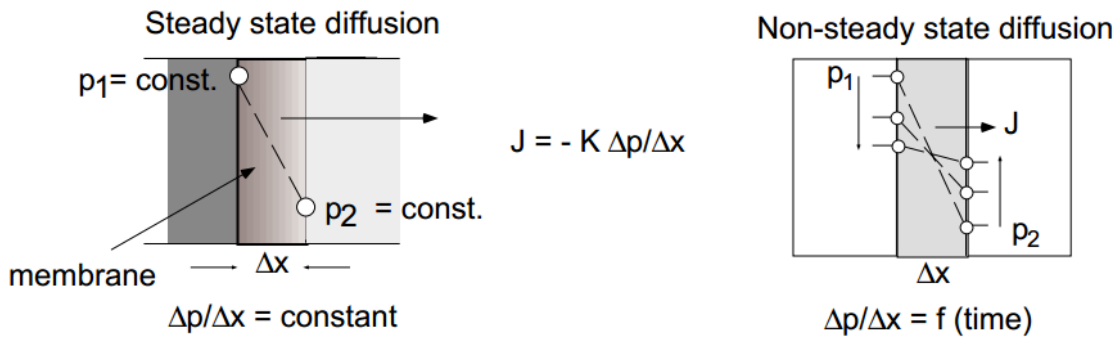


Figure Appendix B.2 - Steady state and non-steady state diffusion

---

## BIBLIOGRAPHY

---

- [1] Nimit Bhatt, "Model-based Estimation of State of Charge of Lithium Cells," Delft University of Technology, Delft, Netherlands, Master of Science Thesis 2011.
- [2] B. Pattipati, C. Sankavaram, and K.R. Pattipati, "System Identification and Estimation Framework for Pivotal Automotive Battery Management System Characteristics," *IEEE Trans. on SMC: Part C*, vol. 41, no. 6, pp. 869–884, November 2011.
- [3] Matteo Muratori, "Thermal Characterization of Lithium-Ion," Facoltà di Ingegneria Industriale, Milan, Italy, Corso di Laurea in Ingegneria energetica 2009.
- [4] C.J. Campbell. (2004) ASPO International. [Online].  
<http://www.peakoil.net/>
- [5] Thomas Reddy, *Handbook of batteries.*: McGraw-Hill Professional; 4th edition,

2010.

- [6] Scott J. Moura, Jason B. Siegel, Donald J. Siegel, Hosam K. Fathy, and Anna G. Stefanopoulou, "Education on vehicle electrification: Battery Systems, Fuel Cells, and Hydrogen," in *IEEE Vehicle Power and Propulsion Conference*, 2010.
- [7] Bruce Dunn, Haresh Kamath, and Jean-Marie Tarascon, "Electrical Energy Storage for the Grid: A Battery of Choices," *Science*, vol. 334, pp. 928-935, 2011.
- [8] Christopher Suozzo, "Lead-Acid Battery Aging And State Of Health Diagnosis," Columbus, Ohio, USA, 2008.
- [9] Venkat Srinivasan, "Batteries for Vehicular Applications," in *Physics of Sustainable Energy*, Berkeley, California, 2008.
- [10] MIT Electric Vehicle Team. (2008, December) A Guide to Understanding Battery Specifications. [Online].  
[http://mit.edu/evt/summary\\_battery\\_specifications.pdf](http://mit.edu/evt/summary_battery_specifications.pdf)
- [11] Ahmed Fasih, "Modeling and Fault Diagnosis of Automotive Lead-Acid Batteries," Columbus, Ohio, USA, April 2006.
- [12] J. Chiasson and B. Vairamohan, "Estimating the state of charge of a battery," *Proceedings of the 2003 American Control Conference*, vol. 4, no. 2, pp. 2863-2868, 2003.
- [13] V. Pop, H.J. Bergveld, D. Danilov, P.P.L. Regtien, and P.H.L. Notten, *Battery Management Systems.*: Springer, 2008.
- [14] Long Lam, "A Practical Circuit-based Model for State of Health Estimation of Li-ion Battery Cells in Electric Vehicles," Delft, Netherlands, August 2011.
- [15] Gholam-Abbas Nazri and Gianfranco Pistoia, *Lithium Batteries: Science and Technology.*: Springer, 2009.
- [16] P. Arora and Z. Zhang, "Battery Separators," *Chem. Rev.*, vol. 104, pp. 4419-4468, 2004.

- [17] Domenico Di Domenico, Anna Stefanopoulou, and Giovanni Fiengo, "Lithium-Ion Battery State of Charge and Critical Surface Charge Estimation Using an Electrochemical Model-Based Extended Kalman Filter," *Journal of Dynamic Systems, Measurement, and Control*, vol. 132, no. 6, p. 061302, 2010.
- [18] K. Smith and Chao-Yang Wang, "Solid-state diffusion limitations on pulse operation of a lithium ion cell for hybrid electric vehicles," *Journal of Power Sources*, vol. 161, no. 1, pp. 628–639, 2006.
- [19] M. Barak, *Electrochemical Power Sources: Primary and Secondary Batteries*. Stevenage, UK: IET, 1980.
- [20] A.J. Bard and L.R. Faulkner, *Electrochemical Methods: Fundamentals and Applications*. New York, USA: John Wiley&Sons, 1980.
- [21] H.J. Bergveld, W.S Kruijt, and P.H.L Notten, *Battery Management Systems: Design by Modelling*.: Springer, 2002.
- [22] W. Peukert, *Über die Abhängigkeit der Kapazität von der Entladestromstärke bei Bleiakkumulatoren*.: ETZ 18, 1897.
- [23] Dennis Doerffel and Suleiman Abu Sharkh, "A critical review of using the Peukert equation for determining the remaining capacity of lead-acid and lithium-ion batteries," vol. 155 , no. 395–400, 2006.
- [24] C. M. Shepherd, "Design of Primary and Secondary Cells, Part II. An Equation Describing Battery Discharge," *Journal of the Electrochemical Society*, vol. 112, no. 7, pp. 657-664, 1965.
- [25] Stephan Buller, "Impedance-Based Simulation Models for Energy Storage Devices in Advanced Automotive Power Systems," Aachen, North Rhine-Westphalia, Germany, 2003.
- [26] G. Plett, "Extended Kalman filtering for battery management systems of LiPB-based HEV battery packs," *Journal of Power Sources*, pp. 252–261, 2004.

- [27] Richard L. Hartmann II, "An Aging Model for Lithium-Ion Cells," December, 2008.
- [28] G. Plett, "Extended Kalman Filtering for Battery Management Systems of LiPB-Based HEV Battery Packs - Part 1: Background," *Journal of Power Sources*, vol. 134, no. 2, pp. 252-261, 2004.
- [29] G. Plett, "Extended Kalman Filtering for Battery Management Systems of LiPB-Based HEV Battery Packs - Part 2: Modeling and Identification," *Journal of Power Sources*, vol. 134, no. 2, pp. 262-276, 2004.
- [30] G. Plett, "Extended Kalman Filtering for Battery Management Systems of LiPB-Based HEV Battery Packs - Part 3: State and Parameter Estimation," *Journal of Power Sources*, vol. 134, no. 2, pp. 277-292, 2004.
- [31] M.S. Farag, R. Ahmed, S.A. Gadsden, S.R. Habibi, and J. Tjong, "A comparative study of Li-ion battery models and nonlinear dual estimation strategies," in *IEEE - Transportation Electrification Conference and Expo (ITEC)*, Dearborn, MI, USA, 2012.
- [32] A.J. Salkind, C. Fennie, P. Singh, T. Atwater, and D.E. Reisner, "Determination of state-of-charge and state-of-health of batteries by fuzzy logic methodology," *Journal of Power Sources*, vol. 80, no. 1-2, pp. 293–300, 1999.
- [33] Domenico Di Domenico, Giovanni Fiengo, and Anna Stefanopoulou, "Lithium-Ion battery State of Charge estimation with a Kalman Filter based on a electrochemical model," in *IEEE Interantional Conference on control Applications (CCA)*, San Antonio, TX, USA, 2008.
- [34] V. Pop et al., "Modeling Battery Behavior for Accurate State-of-Charge Indication," *Journal of Electrochemical Society*, vol. 153, no. 11, pp. A2013-A2022, 2006.
- [35] Antoni Szumanowsk and Yuhua Chang, "Battery Management System Based on Battery Nonlinear Dynamics Modeling," *IEEE Transaction on Vehicular*

*Technology*, vol. 57, no. 3, pp. 1425-1432, 2008.

- [36] N.A. Windarko, Jaeho Choi, and Gyo-Bum Chung, "Improvement of electrical modeling of NiMH battery for application of Microgrid System," in *Energy Conversion Congress and Exposition (ECCE)*, Atlanta, GA, USA, 2010.
- [37] Mark Verbrugge and Edward Tate, "Adaptive state of charge algorithm for nickel metal hydride batteries including hysteresis phenomena," *Journal of Power Sources*, vol. 126, no. 1-2, pp. 236-249, 2004.
- [38] Hector E Perez, Jason B Siegel, Xinfan Lin, and Yi Ding, "Parameterization and Validation of an Integrated Electro-Thermal Cylindrical LFP Battery Model," in *ASME Dynamic Systems Control Conference*, Fort Lauderdale, Florida, USA, 2012.
- [39] Marc Doyle, Thomas F Fuller, and John Newman, "Modeling of Galvanostatic Charge and Discharge of the Lithium / Polymer / Insertion Cell," *Journal of The Electrochemical Society*, vol. 140, no. 6, pp. 1526-1533, 1993.
- [40] Thomas F Fuller, Marc Doyle, and John Newman, "Simulation and Optimization of the Dual Lithium Ion Insertion Cell," *Journal of The Electrochemical Society*, vol. 141, no. 1, pp. 1-10, 1994.
- [41] James L. Lee, Andrew Chemistruck, and Gregory L. Plett, "One-dimensional physics-based reduced-order model of lithium-ion dynamics," *Journal of Power Sources*, vol. 220, no. 0, pp. 430-448, 2012.
- [42] Joel C. Forman, Saeid Bashash, Jeffrey L. Stein, and Hosam K. Fathy, "Reduction of an Electrochemistry-Based Li-Ion Battery Model via Quasi-Linearization and Padé Approximation," *Journal of The Electrochemical Society*, vol. 158, no. 2, pp. A93-A101, 2010.
- [43] C. Y. Wang, W. B. Gu, and B. Y. Liaw, "Micro-Macroscopic Coupled Modeling of Batteries and Fuel Cells Part I. Model Development," *Journal of The Electrochemical Society*, vol. 145, no. 10, pp. 3407-3417, 1998.

- [44] Venkat R. Subramanian, Vinten D. Diwakar, and Deepak Tapriyal, "Efficient Macro-Micro Scale Coupled Modeling of Batteries," *Journal of The Electrochemical Society*, vol. 152, no. 10, pp. A2002-A2008, 2005.
- [45] Long Cai and Ralph E. White, "Reduction of Model Order Based on Proper Orthogonal Decomposition for Lithium-Ion Battery Simulations," *Journal of The Electrochemical Society*, vol. 156, no. 3, pp. A154-A161, 2009.
- [46] Smith Kandler, "Electrochemical Modeling, Estimation and Control of Lithium Ion Batteries," Altoona, PA, USA, 2006.
- [47] Smith Kandler, D. Rahn Christopher, and Wang Chao-Yang, "Control oriented 1D electrochemical model of lithium ion battery," *Energy Conversion and Management*, vol. 48, pp. 2565-2578, 2007.
- [48] Smith Kandler, "Electrochemical Control of Lithium-Ion Batteries," in *IEEE Control Systems Magazine*, 2010.
- [49] W. B. Gu and C. Y. Wang, "Thermal-electrochemical modeling of battery systems," *Journal of The Electrochemical Society*, vol. 147, no. 8, pp. 2910-2922, 2000.
- [50] Kumaresan Karthikeyan, Sikha Godfrey, and E. White Ralph, "Thermal Model for a Li-Ion Cell," *Journal of the Electrochemical Society*, vol. 155, no. 2, pp. A164-A171, 2008.
- [51] Ramadesigan Venkatasailanathan et al., "Modeling and Simulation of Lithium-Ion Batteries from a Systems Engineering Perspective," *Journal of The Electrochemical Society*, vol. 159, no. 3, pp. R31-R45, 2012.
- [52] S.J. Moura, N.A. Chaturvedi, and M. Krstic, "PDE estimation techniques for advanced battery management systems — Part II: SOH identification," in *American Control Conference (ACC)*, Montréal, Quebec, Canada, 2012, pp. 566 - 571.
- [53] N. Fouquet, C. Doulet, C. Nouillant, G. Dauphin-Tanguy, and B. Ould-

- Bouamama, "Model based PEM fuel cell state-of-health monitoring via ac impedance measurements," *Journal of Power Sources*, vol. 159, no. 2, pp. 905-913, September 2006.
- [54] Sabine Piller, Marion Perrin, and Andreas Jossen, "Methods for state-of-charge determination and their applications," *Journal of Power Sources*, vol. 96, no. 1, pp. 113-120, 2001.
- [55] J. Alzieu, H. Smimite, and C. Glaize, "Improvement of intelligent battery controller: state-of-charge indicator and associated functions," *Journal of Power Sources*, vol. 67, no. 1-2, pp. 157-161, 1997.
- [56] Hans-Peter Hönes, "Electrochemical energy storage in photovoltaic systems," Stuttgart, Germany, 1994.
- [57] Suleiman Abu-Sharkh and Dennis Doerffel, "Rapid test and non-linear model characterisation of solid-state lithium-ion batteries," *Journal of Power Sources*, vol. 130, no. 1-2, pp. 226-274, 2004.
- [58] T. Weigert, Q. Tianb, and K. Lianb, "State-of-charge prediction of batteries and battery-supercapacitor hybrids using artificial neural networks," *Journal of Power Sources*, vol. 196, no. 8, pp. 4061-4066, 2011.
- [59] N. Abolhassani Monfared et al., "Prediction of state-of-charge effects on lead-acid battery characteristics using neural network parameter modifier," *Journal of Power Sources*, vol. 158, no. 2, pp. 932-935, 2006.
- [60] M. Charkhgard and M. Farrokhi, "State-of-Charge Estimation for Lithium-Ion Batteries Using Neural Networks and EKF," *IEEE Transactions on Industrial Electronics*, vol. 57, no. 12, pp. 4178-4187, 2010.
- [61] Chrislb. [www.wikibooks.org](http://www.wikibooks.org). [Online].  
[http://en.wikibooks.org/wiki/Artificial\\_Neural\\_Networks/Print\\_Version](http://en.wikibooks.org/wiki/Artificial_Neural_Networks/Print_Version)
- [62] Olivier Gérard, Jean-Noël Patillon, and Florence d'Alché-Buc, "Neural network adaptive modeling of battery discharge behavior," *Artificial Neural Networks —*

*ICANN'97*, vol. 1327, pp. 1095-1100, 1997.

- [63] S. Grewal and D.A. Grant, "A novel technique for modelling the state of charge of lithium ion batteries using artificial neural networks," in *Telecommunications Energy Conference, 2001. INTELEC 2001. Twenty-Third International*, Edinburgh, UK, 2001.
- [64] N. Watrin, B. Blunier, and A. Miraoui, "Review of adaptive systems for lithium batteries State-of-Charge and State-of-Health estimation," in *IEEE, Transportation Electrification Conference and Expo (ITEC), 2012*, Dearborn, MI, USA, 2012.
- [65] K. Takano et al., "Simulation study of electrical dynamic characteristics of lithium-ion battery," *Journal of Power Sources*, vol. 90, no. 2, pp. 214-223, 2000.
- [66] E. Barsoukov, J. Kim, C. Yoon, and H. Lee, "Universal battery parameterization to yield a non-linear equivalent circuit valid for battery simulation at arbitrary load," *Journal of Power Sources*, vol. 83, no. 1 - 2, pp. 61-70, 1999.
- [67] S. Rodrigues, N. Munichandraiah, and A. Shukla, "A review of state- of-charge indication of batteries by means of ac impedance measurements," *Journal of Power Sources*, vol. 87, no. 1-2, pp. 12-20, 2000.
- [68] A. Salkind, C. Fennie, P. Singh, T. Atwater, and D. Reisner, "Determination of state-of-charge and state-of-health of batteries by fuzzy logic methodology," *Journal of Power Sources*, vol. 80, no. 1-2, pp. 293-300, 1999.
- [69] P. Singh, C. Fennie, D. Reisner, and A. Salkind, "Fuzzy logic-enhanced electrochemical impedance spectroscopy (fleéis) to determine battery state of charge," in *Proceedings of the 15th Annual Battery Conference on Applications and Advances*, Long Beach, CA, USA, 2000, pp. 199-204.
- [70] Xinfan Lin et al., "Parameterization and Observability Analysis of Scalable Battery Clusters for Onboard Thermal Management," in *Les Rencontres Scientifiques d'IFP Energies nouvelles – Int. Scient. Conf. on hybrid and electric*

*vehicles*, December 2011.

- [71] Richard L. Hartmann II, "AN AGING MODEL FOR LITHIUM-ION CELLS," The Graduate Faculty of The University of Akron, Ph.D. Thesis, Akron, Ohio, USA, 2008.
- [72] K. Amine et al., "Factors responsible for impedance rise in high power lithium ion batteries," *Journal of Power Sources*, vol. 97-98, pp. 684-687, July 2001.
- [73] I Bloom et al., "An accelerated calendar and cycle life study of Li-ion cells," *Journal of Power Sources*, vol. 101, no. 2, pp. 238-247, October 2001.
- [74] M. Broussely et al., "Main aging mechanisms in Li ion batteries," *Journal of Power Sources*, vol. 146, no. 1-2, pp. 90-96, August 2005.
- [75] J. Vetter et al., "Ageing mechanisms in lithium-ion batteries," *Journal of Power Sources*, vol. 147, no. 1-2, pp. 269-281, September 2005.
- [76] R. Spotnitz, "Simulation of capacity fade in lithium-ion batteries," *Journal of Power Sources*, vol. 113, no. 1, pp. 72-80, January 2003.
- [77] J Li, E Murphy, J Winnick, and P.A Kohl, "Studies on the cycle life of commercial lithium ion batteries during rapid charge–discharge cycling," *Journal of Power Sources*, vol. 102, no. 1-2, pp. 294-301, December 2001.
- [78] F. Savoye, P. Venet, M. Millet, and J. Groot, "Impact of Periodic Current Pulses on Li-Ion Battery Performance," , St. Priest, France, 2012, pp. 3481-3488.
- [79] Jens Groot, "State-of-Health Estimation of Li-ion Batteries: Cycle Life Test Methods," Chalmers University of Technology, Division of Electric Power Engineering, Licentiate's degree, Göteborg, Sweden, 2012.
- [80] Yaakov Bar-Shalom, X. Rong Li, and Thiagalingam Kirubarajan, *Estimation with Applications to Tracking and Navigation*, 139780471416555th ed.: Wiley-Interscience, 2001.
- [81] R. E. Kalman, "A New Approach to Linear Filtering and Prediction Problems,"

*Transactions of the ASME--Journal of Basic Engineering*, vol. 82, pp. 35-45, 1960.

- [82] P. S. Maybeck, *Stochastic models, estimation and control*, Academic Press, Ed., 1979, vol. 1.
- [83] Greg Welch and Gary Bishop, "An Introduction to the Kalman Filter," Department of Computer Science, University of North Carolina at Chapel Hill, Chapel Hill, North Carolina, USA, TR 95-041, 2006.
- [84] S. A. Gadsden, "Smooth Variable Structure Filtering: Theory and Applications," Hamilton, ON, Canada, 2011.
- [85] R. E. Kalman and R. S. Bucy, "New Results in Linear Filtering and Prediction Theory," *J. Fluids Eng*, vol. 83, no. 1, pp. 95-108, 1961.
- [86] S. Haykin, *Kalman Filtering and Neural Networks*.: Wiley, 2001.
- [87] S. Julier, J. Uhlmann, and H.F. Durrant-White, "A New Method for Nonlinear Transformation of Means and Covariances in Filters and Estimators," *IEEE Trans. Aut. Cont.*, vol. 45, no. 3, pp. 477-482, 2000.
- [88] D. Simon, *Optimal State Estimation: Kalman, H [infinity] And Nonlinear Approaches*. 2006: Wiley-Interscience.
- [89] S. R. Habibi, "The Smooth Variable Structure Filter," *Proceedings of the IEEE*, vol. 95, no. 5, pp. 1026-1059, 2007.
- [90] V. Utkin, *Sliding Modes in Control Optimization*.: New York: Springer-Verlag, 1992.
- [91] J. J. E. Slotine, "Sliding Controller Design for Nonlinear Systems," *International Journal of Control*, vol. 40, pp. 421-434, 1984.
- [92] J. J. E. Slotine, "The Robust Control of Robot Manipulators," *International Journal of Robotic Research*, vol. 4, no. 2, pp. 49-64, 1985.
- [93] S. R. Habibi and R. Burton, "The Variable Structure Filter," *Journal of Dynamic Systems, Measurement, and Control (ASME)*, vol. 125, pp. 287-293, September

2003.

- [94] Mohammed Sayed Farag, Ryan Ahmed, S. A. Gadsden, S. R. Habibi, and J. Tjong, "A Comparative Study of Li-ion Battery Models and Nonlinear Dual Estimation Strategies," in *IEEE Transportaion Electrificaion Conference and Expo (ITEC'12)*, Dearborn, Michigan, USA, 2012.
- [95] M. Al-Shabi, "The General Toeplitz/Observability SVSF," Department of Mechanical Engineering, McMaster University, Hamilton, Ontario, Canada, Ph.D. Thesis 2011.
- [96] Bogdan Ovidiu Varga, "Electric vehicles, primary energy sources and CO<sub>2</sub> emissions: Romanian case study," *Energy*, vol. 49, pp. 61-70, January 2013.
- [97] G. L. Plett, "Extended Kalman Filtering for Battery Management Systems of LiPB-Based HEV Battery Packs: Part 2. Modeling and Identification," *Journal of Power Sources*, vol. 134, no. 2, pp. 262-276, 2004.
- [98] K. Sakurai, K. I. Muramoto, and T. Yamazaki, "Estimation of the Recharge Capacity of Sealed Lead-Acid Batteries by Neural Network," in *IEEE ITEC*, San Francisco, CA, 1998, pp. 210-214.
- [99] Battery modeling for HEV simulation by ThermoAnalytics. [Online].  
<http://www.thermoanalytics.com/docs/batteries.html>
- [100] W.Y. Sean, J.C. Ke Y.H. Chiang, "A comparative study of equivalent circuit models for Li-ion batteries," *J. Power Sources*, pp. 3921–3932, 2011.
- [101] John Newman and William Tiedemann, "Porous-electrode theory with battery applications," *AICHE Journal*, vol. 21, no. 1, pp. 25-41, 1975.
- [102] Allen J. Bard and Larry R. Faulkner, *Electrochemical Methods: Fundamentals and Applications.*, 2002, vol. 38.
- [103] Domenico Di Domenico, Giovanni Fiengo, Anna Stefanopoulou, and Carmelo Speltino, "Comparison of reduced order lithium-ion battery models for control applications," , Shanghai, 2009.

- [104] Spelton C., Stefanopoulou A., and Fiengo G., "Parameterization and Estimation of Surrogate Critical Surface," MI, USA, March 2011.
- [105] A.P. Schmidt, M. Bitzer, A.W. Imre, and L. Guzzella, "Experimental driven electrochemical modeling and systematic paramterization of a Li-Ion Battery Cell," *Journal of Power Sources*, vol. 195, no. 15, pp. 5071–5080, 2010.
- [106] M. Doyle and Y. Fuentes, "Computer Simulations of a Lithium-Ion Polymer Battery and Implications for Higher Capacity Next-Generation Battery Designs," *Journal of Electrochemistry Soc.*, pp. A706–A713, 2003.
- [107] "3.091 – Introduction to Solid State Chemistry," MIT,.

---

## GLOSSARY

---

---

---

### List of Acronyms

---

$\mu$ C	Microcontrollers
1D	One Dimension
AC	Alternative Current
Ah	Ampere-hour
ANN	Artificial Neural Networks
ASPO	Association for the Study of Peak Oil and Gas
BEV	Battery Electric Vehicles
BMS	Battery Management System

BOL	Beginning of Life
CCCV	Constant Voltage Constant Current
CPU	Central Processing Unit
DOD	Depth of Discharge
DSP	Digital Signal Processing
EAM	Electrode Averaged Model
EIS	Electrochemical Impedance Spectroscopy
EKF	Extended Kalman Filter
EOL	End of Life
ESC	Enhanced Self Correcting
EV	Electric Vehicles
GHG	Green House Gas
GPS	Generalized Pattern Search
HEV	Hybrid Electric Vehicles
KF	Kalman Filter
Li-ion	Lithium ion
LTI	Linear Time Invariant
LTV	Linear Time Varying

MMSE	Minimum Mean Square Error
MSE	Mean Square Error
OCV	Open Circuit Voltage
ODE	Ordinary Differential Equation
PDE	Partial Differential Equation
PHEV	Plug-in Hybrid Electrical Vehicles
RBS	Regenerative Braking System
RMS	Root Mean Square
RMSE	Root Mean Square Error
ROM	Reduced Order Model
RUL	Remaining Useful Life
SMC	Sliding Mode Control
SOC	State of Charge
SOH	State of Health
SVSF	Smooth Variable Structure Filter
VSC	Variable Structure Control
VSF	Variable Structure Filter